Lateral-Torsional Buckling Instability Caused by Individuals Walking on Wood Composite I-Joists

Jose Maria Villasenor Aguilar

Dissertation submitted to the faculty of the Virginia Polytechnic Institute and State University in partial fulfillment of the requirements for the degree of

Doctor of Philosophy

In

Wood Science and Forest Products

Daniel P. Hindman, Chair

Maury A. Nussbaum

Joseph R. Loferski

Norman E. Dowling

Surot Thangjitham

December 11, 2012

Blacksburg, Virginia

Keywords: Falls from Elevation, Wood Composite I-Joist, Lateral Bending Stiffness, Torsional Rigidity, Lateral Hanger Stiffness, Lean-on Bracing System, Lateral-Torsional Buckling Instability, Lateral Bending Motion.

Lateral-Torsional Buckling Instability Caused by Individuals Walking on Wood Composite I-Joists

Jose Maria Villasenor Aguilar

Abstract

Recent research has shown that a significant number of the falls from elevation occur when laborers are working on unfinished structures. Workers walking on wood I-joists on roofs and floors are prone to fall hazards. Wood I-joists have been replacing dimension lumber for many floor systems and a substantial number of roof systems in light-frame construction. Wood I-joists are designed to resist axial stresses on the flanges and shear stresses on the web while minimizing material used. However, wood I-joists have poor resistance to applied lateral and torsional loads and are susceptible to lateral-torsional buckling instability. Workers walking on unbraced or partially braced wood I-joists can induce axial and lateral forces as well as twist. Experimental testing demonstrated that workers cause lateral-torsional buckling instability in wood I-joists. However, no research was found related to the lateral-torsional buckling instability induced by individuals walking on the wood I-joists. Furthermore, no research was found considering the effects of the supported end conditions and partial bracing in the lateral-torsional buckling instability of wood I-joists.

The goal of this research was to derive mathematical models to predict the dynamic lateral-torsional buckling instability of wood composite I-joists loaded by individuals walking considering different supported end conditions and bracing system configurations. The dynamic lateral-torsional buckling instability was analyzed by linearly combining the static lateral-torsional buckling instability with the lateral bending motion of the wood I-joists. Mathematical models were derived to calculate the static critical loads for the simply supported end condition and four wood I-joist hanger supported end conditions. Additionally, mathematical models were derived to calculate the dynamic maximum lateral displacements and positions of the individual walking on the wood I-joists for the same five different supported end conditions. Three different lean-on bracing systems were investigated, non-bracing, one-bracing, and two-bracing systems. Mathematical models were derived to calculate the amount of constraint due to the lean-on bracing system. The derived mathematical models were validated by comparison to data from testing for all supported end conditions and bracing systems.

The predicted critical loads using the static buckling theoretical models for the non-bracing system and the static buckling theoretical models combined with the bracing theoretical models for the simply and hanger supported end conditions agreed well with the critical loads obtained from testing for the two wood I-joist sizes investigated.

The predicted maximum lateral displacements and individual positions using the bending motion theoretical models for the simply and hanger supported end conditions agreed well with the corresponding maximum lateral displacements and individual positions obtained from testing for both wood I-joist sizes. Results showed that; a) the supported end condition influenced the critical loads, maximum lateral displacements and individual positions, b) the bracing system increased the critical loads and reduced the maximum lateral displacements, c) the critical load increased as the load position displaced away from the wood I-joist mid-span, d) the critical load reduced as the initial lateral displacement of the wood I-joist increased and e) the wood I-joist mid-span was the critical point in the dynamic lateral-torsional buckling instability.

Acknowledgements

It is a pleasure to thank those who made this Dissertation possible.

I am deeply thankful to my advisor, Daniel P. Hindman, whose guidance, encouragement and assistance allowed me to successfully achieve my Research Project.

I am also sincerely grateful for all support from the members of my committee, Maury A. Nussbaum, Joseph R. Loferski, Norman E. Dowling and Surot Thangjitham.

Lastly, I honestly offer my affections and blessings to Rick A. Caudill, Angela G. Riegel and David Jones who supported me in any manner during the completion of my Dissertation.

This work was supported by an award (R21OH008902) from the Centers for Disease Control and Prevention (CDC). Its contents are solely the responsibility of the authors and do not necessarily represent the official views of the CDC.

Jose Maria Villasenor Aguilar

Table of Contents

List of Figures

List of Tables

Notation

a = distance from the neutral axis of the cross-section to the loading point

$b_{(2n-1)}$ = coefficients in the angle of twist function

d_{tf} = lateral displacement of the top flange of the wood I-joist

d_{bf} = lateral displacement of the bottom flange of the wood I-joist

f = dynamic force

f_d = walking frequency

$g(t)$ = adjusting function

h = depth of the I-beam

h_i = i^{th} observation of the cross-section height of the wood I-joist

k = lateral bending stiffness of the wood I-joist hanger

k_i = i^{th} observation of the lateral bending stiffness of the wood I-joist hanger

l_e = effective wood I-joist length

l_u = un-braced wood I-joist length

m = mass of the wood I-joist

m_{bi} = mass of the wood I-joists braced to the loaded wood I-joist

m_i = i^{th} observation of the mass of the wood I-joist

m_{Ad} = adjusted mass

m_L = mass of the loaded wood I-joist

n_s = sample size

q = constant for the load eccentricity factor equation

s = distance from the end of the wood I-joist to the loading point

s_{cr_i} = i^{th} observation of the dynamic critical lateral-torsional buckling position

t_T = total time to transverse the wood I-joist

u = wood I-joists lateral displacement

v = wood I-joist axial displacement

w = distance from the end of the wood I-joist to the bracing point

$x[w]$ = lateral deflection of the loaded wood I-joist at the bracing point

$x[z]$ = lateral deflection of the loaded wood I-joist at the loading point

z = number of standard deviations away from the mean of the normal distribution

B = wood I-joist hanger bearing constant

C_b = equivalent moment factor

C_e = load eccentricity factor

C_w = warping constant

E = modulus of elasticity

EI_x = axial bending stiffness

EI_y = lateral bending stiffness

$EI_{y_{bi}}$ = lateral bending stiffness of the wood I-joists braced to the loaded wood I-joist

EI_{y_i} = i^{th} observation of the lateral bending stiffness of the wood I-joist

$EI_{y_{Ad}}$ = adjusted lateral bending stiffness

EI_{y_L} = lateral bending stiffness of the loaded wood I-joist

F_d = function of the force of the dynamic loading due to an individual walking

F_{dL} = function of the lateral component of the force of the dynamic loading due to an individual walking

G = shear modulus

GJ = torsional rigidity

GJ_{bi} = torsional rigidity of the wood I-joists braced to the loaded wood I-joist

G_w = weight of the individual walking

GJ_{Ad} = adjusted torsional rigidity

GJ_L = torsional rigidity of the loaded wood I-joist

G_{WL} = lateral component of the weight of the individual walking

H = total response of the walking surface to the force imposed by the individual walking

I_y = centroidal area moment of inertia

L = wood I-joist length

M = bending moment

M_{cr} = critical lateral-torsional buckling moment

M_{max} = absolute value of the maximum moment

M_{ocr} = critical lateral-torsional buckling moment for the fundamental case

M_A = absolute value of the moment at $\frac{l_u}{4}$

M_B = absolute value of the moment at $\frac{l_u}{2}$

M_C = absolute value of the moment at $\frac{3l_u}{4}$

$M(\zeta)$ = moment with respect to the ζ axis

$M(\eta)$ = moment with respect to the η axis

$M(\xi)$ = moment with respect to the ξ axis

P = load applied to the wood I-joist

P_{cr} = static critical lateral-torsional buckling load

P_{cr_i} = i^{th} observation of the static critical lateral-torsional buckling load

Q = shear force

T = torsional moment

T_e = width of the tolerable error

U_B = strain energy increase in the wood I-joist due to lateral deflection

U_T = strain energy increase in the wood I-joist due to torsion

V = spatial domain to time domain transformation constant

W_{LD} = work done by the system due to the lateral bending deflection

W_s = work done by the spring

α = probability of committing a Type I error

α_n = dynamic load factor of the n^{th} harmonic of the weight of the individual walking

α_w = elastic warping stiffness at the end of the I-beam

β = wood I-joist angle of torsion

γ = axial displacement

δ = lateral deflection of the wood I-joist

$\delta(z)$ = spatial Dirac Delta function

ε_i = i^{th} observation of the random error

$\mu_{1,2,3}$ = regression analysis model parameters

σ = standard deviation of the population

φ_n = n^{th} harmonic phase angle of the weight of the individual walking

$\chi_{r,s}$ = wood I-joist profile under the action of dynamic loading

ψ_r = variation of the wood I-joist profile

ω_r = frequency of oscillation of the wood I-joist

$\Theta(t)$ = temporal Heaviside Theta function

1: Introduction

Workers in the residential construction industry may need to walk on unfinished structures such as floors or roofs constructed with wood composite I-joists, or simply wood I-joists, to perform construction tasks. When workers walk on wood I-joists, the wood I-joists deform and move, creating difficult walking conditions. Wood I-joists commonly have long spans and large depth to width ratios. Under these geometric characteristics and the worker's weight, the wood I-joist may develop lateral-torsional buckling instability. During construction, the end fixity of the wood I-joists vary according with the type of wood I-joist hanger and may not have bracing installed. Poor end fixity installations and a lack of a bracing system increase the risk of lateral-torsional buckling instability (Kirby and Nethercot 1979). Lateral-torsional buckling instability causes loss of balance of the worker walking on the wood I-joist and may cause the worker to fall. After the fall, there is little to no evidence of the cause, because the wood I-joist returns to its original unloaded form. Currently, there is a lack of research on lateral-torsional buckling instability in wood I-joists under several end conditions and bracing systems including those found in construction sites. Falls from elevation are a cause of fatal work injures on construction sites in the residential construction industry (Suruda et al. 1995). Falls from the same level most commonly result in sprains or contusions, but falls from elevation more often result in fractures and multiple injuries (Lipscomb et al. 2003). Fatal falls were the second most frequent work-related fatal event in the United States from 1999 through 2010 only under highway accidents (Bureau of Labor Statistics 2011). Costs associated with a fatal fall could be economically disastrous to small or medium sized construction industries (Bobick 2004). Personal fall-arrest protection systems can be effective to prevent serious injuries; however, the worker may still suffer injures and loss of personal reliability (Huang and Hinze 2003). Thus the importance in reducing potential fall hazards in construction sites, such as lateral-torsional buckling instability. Recently, wood I-joists have replaced dimension lumber for many floor systems and a significant number of roof systems in light-frame construction (Leichti et al. 1990). Wood I-joists are designed to resist axial stresses on the flanges and shear stresses on the web while minimizing material used. However, wood I-joists have poor resistance to applied lateral and torsional loads (Hindman et al. 2005a). Lateral-torsional buckling instability is a critical condition in which the wood I-joist deflects axially and laterally as well as twist with respect to the neutral axis when a gradually increasing load is applied to the vertical plane of the wood I-joist. The axial load at which lateral-torsional buckling instability occurs is known as the critical lateral-torsional buckling load (Kirby and Nethercot 1979). Two main methods have been used to analyze lateral-torsional buckling instability in wood I-joists; the differential equations of equilibrium method, and the strain energy method. The principles of the strain energy method are based on the equalization of the loss of energy in the system to the work done by the system.

The goal of this research was to derive mathematical models to predict the lateral-torsional buckling instability of wood I-joists focused on loads caused by individuals walking on the wood I-joists for different supported end conditions and bracing systems.

Specific objectives included:

- Develop a testing setup to measure the lateral stiffness of four different types of wood I-joist hangers for two different wood I-joist sizes.
- Derive theoretical models for simply, fixed and hanger supported end conditions to predict the static critical lateral-torsional buckling loads in wood I-joists.
- Derive theoretical models for simply, fixed and hanger supported end conditions to predict the maximum lateral displacements and the positions of the individual walking on the wood I-joists.
- Derive theoretical models for simply, fixed and hanger supported end conditions to predict the bracing restraint in the lateral-torsional buckling instability and lateral bending motion due to a bracing system in the wood I-joists.
- Validate with testing the static lateral-torsional buckling theoretical models and bracing theoretical models for all supported end conditions and wood I-joist sizes.
- Validate with testing the lateral bending motion theoretical models and bracing theoretical models for all supported end conditions and wood I-joist sizes.
- Develop regression analysis models for three different bracing systems to predict the static critical lateral-torsional buckling loads in wood I-joists.

Three different supported end conditions were used in this research. A simply supported end condition, a fixed supported end condition and a hanger supported end condition. The hanger supported end condition was modeled using a lateral spring support analogy. The hanger supported end condition used the axial and the torsional restrictions from the simply supported end condition while the lateral restriction is modeled as a spring support. The hanger supported end condition can be used for several wood I-joist hangers by substituting the lateral stiffness of the hanger. Four wood I-joist hangers were tested to calculate the lateral hanger stiffness. Three bracing systems were used in this research. A non-bracing system, a one-bracing system and a two-bracing system. Theoretical Models to calculate the amount of bracing restraint due to the bracing system in the lateral-torsional buckling instability were derived. The three bracing systems were tested under five different supported end conditions, the simply supported and four hanger supported end conditions.

Two different loading conditions were used in this research to develop the theoretical models, static loading and dynamic loading. The static loading which was a gradually increasing load was applied to the wood I-joist at the mid-span top flange using a universal testing machine. The dynamic loading which was a constant load (individual's weight) was applied to the wood I-joist using a single individual walking across the wood I-joist span. The static lateral-torsional buckling models were derived based on the strain energy method. The static

lateral-torsional buckling models were compared when possible to the models found in the *Designing for Lateral-Torsional Stability in Wood Members Technical Report 14* (TR-14) (AF&PA 2003), which were derived using the differential equations of equilibrium method and adjusting factors. The adjusting factors were used to account for different loading conditions and loading positions with respect to the neutral axis. The dynamic lateral-torsional buckling instability was analyzed by linearly combining the static lateral-torsional buckling models with the lateral bending motion models of the wood I-joists. The bending motion equations used the lateral component of the force imposed by the individual walking on the wood I-joists. The dynamic lateral-torsional buckling instability equations were used to find the critical lateral-torsional buckling position of the individual walking on the wood I-joist considering the individual's weight large enough to cause lateral-torsional buckling instability.

Regression analysis models were developed to be compared with the theoretical static lateral-torsional buckling models. The regression analysis models were developed using the measurements of the critical lateral-torsional buckling loads, the lateral bending stiffness of the wood I-joists, the amount of bracing restraint due to the bracing system and the wood I-joist depths as input parameters. The following chapter discusses the research problem and its effects in the residential construction industry, the wood I-joist materials and characteristics, the static lateral-torsional buckling instability and the lateral bending motion of the wood I-joists.

2: Literature Review

The main goal of this research was to derive mathematical models to predict the lateral-torsional buckling instability caused by individuals walking on the wood I-joists. Workers in the residential construction industry may walk on wood I-joists in unfinished floors and roofs. In these structures, the end fixity of the wood I-joists may vary according with the type of wood I-joist hanger used or may not be braced along their spans. Long un-braced or partially braced wood I-joists may develop lateral-torsional buckling instability under the worker's weight. The weight necessary to cause lateral-torsional buckling instability is called the critical lateral-torsional buckling load and is a function of the wood I-joist un-braced span and the wood I-joist supported end fixity. Lateral-torsional buckling instability may lead workers to lose their balance and fall. Falls from elevation are a major cause of fatal work injures in the construction sites. This chapter discusses falls from elevation in the residential construction industry, wood I-joists and lateral-torsional buckling instability under static and dynamic loading conditions.

2.1: Falls on Construction Sites

Floor and roof assembly in the residential construction industry involves tasks where workers may need to traverse from one side of the structure to the other across the wood I-joists. The wood I-joists may not have braces installed and the end fixity of the wood I-joist ends vary according with the type of wood I-joist hanger used. Under these conditions, the wood I-joists may undergo lateral-torsional buckling instability caused by the worker's weight when the worker is walking on the wood I-joist. Lateral-torsional buckling instability is a condition in which the wood I-joist deflects axially, deflects laterally and rotates with respect to its neutral axis. Lateral-torsional buckling instability may lead workers to lose their balance and fall.

Construction workers are among the most likely workers to experience serious occupational injuries (Suruda et al. 1995). Falls from the same level most commonly result in sprains or contusions, but falls from elevation more often result in fractures and multiple injuries (Lipscomb et al. 2003). Huang and Hinze (2003) found that fall accidents are most frequent on projects involving commercial buildings and single family or duplex dwellings and that in high-rise buildings more fall-related hazards exist. Single residential buildings are frequently constructed by small contractors who often provide inadequate personal protective equipment and informal safety training (Huang and Hinze 2003). Falls from elevation most frequently occur when laborers are working on roofing, erecting structural steel, and exterior carpentry (Webster 2003). These tasks are conducted at elevation or on temporary scaffolding structures. From 1992 to 2002, roofing, siding and sheet metal workers had the most fall-related deaths, an average of 64 worker fatalities per year related to falls occurred while working on high-rise buildings (Bobick 2004).

According to the Bureau of Labor Statistics (2011), fatal falls were the second most frequent work-related fatal event from 1999 through 2010 with only highway accidents having more fatal events. Averaging the number of fatal falls from 2004 through 2010 the approximate mean number of fatal falls totals 737 per year, thus fatal falls is a major problem for the construction industry in the United States.

More than one half of the total falls were related to environmental factors involving surfaces or layout conditions. One third of falls involving roofing tasks were caused by misjudgment of hazardous situations (Huang and Hinze 2003). Thus, elevated projects may underestimate or ignore hazards not observed at lower elevations in the residential construction industry. When a fatal fall does occur, costs associated with the incident could be economically disastrous to small or medium sized construction businesses (Bobick 2004).

Personal fall-arrest protection systems (PFAS) can be effective to reduce serious injuries from a fatal fall. However these systems serve as a fall-protection measure, not as a fall-prevention device (Bobick 2004). Even if the worker is using a PFAS system, a potential fall risk is always present. If a fall does occur when the worker is using the PFAS, the worker still may suffer injuries and loss of personal reliability. Huang and Hinze (2003) found that prevention was the most promising method to avert falls. Personal protective technology (PPT) such as guardrails, safety nets, and PFAS may provide insufficient protection under certain worker's tasks (Huang and Hinze 2003), for instance, when the worker needs to carry oversized materials or when the worker must perform complicate tasks in a places of difficult access. Suruda et al. (1995) found that workers believe that productivity is reduced when the used of safety devices is increased.

Recent research has shown that many of the falls from elevation occur when laborers are working on unfinished structures. Workers walking on wood I-joists on roofs and floors structures are prone to fall hazards. Recently, wood I-Joists have replaced dimension lumber for floor systems and a significant number of roof systems in light-frame construction. Wood I-joists have poor resistance to applied lateral and torsional loads. Workers walking on unbraced wood I-joists can induce axial and lateral forces as well as twist. Current research has demonstrated that workers may cause lateral-torsional buckling instability in wood I-joists. To effectively prevent fatal falls in the residential construction industry caused by lateral-torsional buckling instability of the wood I-joists, the response behavior of the wood I-joists to the workers walking over the wood I-joists must be understood. This response behavior depends on the intensive properties of the wood I-joist composition materials as well as on the wood I-joist geometric characteristics. The next section describes the wood I-joists used as structural members and the lateral-torsional buckling instability of the wood I-joists.

2.2: Wood I-Joists

Wood I-joists or wood composite I-joists are structural members used in the residential construction industry as alternative to traditional solid sawn lumber. Wood I-joists are manufactured using both solid sawn lumber or structural composite lumber (SCL) materials in the flanges and plywood or oriented strand board (OSB) in the web (Leichti et al. 1990). The preferred materials for manufacturing wood I-joists are laminated veneer lumber

(LVL) in the flanges and OSB in the web. LVL is a composite of wood veneer sheet elements with wood fibers primarily oriented along the length of the member bonded with an exterior type adhesive (ASTM 2005a). LVL is more consistent and has higher bending strength compared to solid-sawn lumber of equal dimension and species (Leichti et al. 1990). OSB is a structural sheathing panel commonly used in light-frame construction and is manufactured from layers of strands with the face layers parallel to the length of the panel and the core layer perpendicular that provides panel dimensional stability. Wood I-joist flanges and web are bonded together with exterior-type adhesives forming the cross-sectional shape of an "I" (Leichti et al. 1990).

Wood I-joists replace solid sawn lumber joists in floor and roof applications where longer length and greater load capacity are needed (USDA 1999). In carrying the same load wood I-joists use less material compared to rectangular wood beams (Leichti et al. 1990). Builders choose wood I-joists over rectangular solid sawn beams because they are stiff, lightweight and are manufactured in long spans. Important advantages of wood I-joists compared to rectangular solid sawn beams include; greater dimensional stability, better elimination of floor noise, fewer field modifications and rejections in the field (AF&PA 1999).

Wood I-joists use less material at the neutral axis and more material at the upper and lower flanges. Flanges in wood I-joists are designed to resist bending moments while the web is designed to resist shear forces. Web design requires that the wood I-joist does not buckle axially under design loads (USDA 1999). The bending moment of the wood I-joist flanges is calculated using simple bending theory, while the shear stress of the web is most often calculated based on experimental results (Leichti et al. 1990).

Wood I-joists are available throughout the United States in several sizes and materials. Flanges range from $1^{5}/_{16}$" to $1^{1}/_{2}$" thick and from $1^{1}/_{2}$" to $3^{1}/_{2}$" wide. Webs in wood I-joists used in typical residential applications are either $^{3}/_{8}$" or $^{7}/_{16}$" thick. For residential spans, wood I-joists depths from $9^{1}/_{2}$" to 16" are typically used (AF&PA 2006). Wood I-joists in used must be designed for serviceability considerations including; deflection, vibration, creep, lateral torsional buckling instability and strength retention under normal load conditions (AF&PA 2006).

The wood I-joist is a complex assembly of orthotropic and anisotropic materials (Leichti et al. 1990). Anisotropic materials are directionally dependent having different physical properties in all directions (Singer and Pytel 1980). If a material possesses symmetry about three orthogonal planes in which the elastic material quantities are independent of each other the material is orthotropic (USDA 1999). The stress-strain constitutive equations for orthotropic and anisotropic materials under the action of complicated loading conditions have in the most cases overall complex solutions. In these cases, the elastic material quantities can be found by testing since the response of the materials to the applied loading already accounts for the orthotropic and anisotropic behavior.

2.3: Lateral-Torsional Buckling Instability

The fundamental definition of stability involves structural integrity of the elements of a given system. A particular solution of a dynamic system is stable if all possible small perturbations of the initial conditions permit only small changes in the solution. Under certain minor restrictions stability can be decided by analyzing linear systems

(Bažant 2000). Elastic stability must satisfy two basic criteria, the ability of the structure to support the imposed loading (strength) and the capacity of the structure to resist distortions (stiffness) (Kirby and Nethercot 1979). In contrast, inelastic instability is the condition where the structure does not return to its initial position when slightly disturbed, even when the yield stress is assumed to be infinitely large (Kirby and Nethercot 1979). Elastic buckling instability is frequently associated with large changes of geometry which often occur quickly as the structural member moves from one geometrical position of equilibrium to another (Kirby and Nethercot 1979).

When a wood I-joist is loaded in the plane of its web by a gradually increasing load, an axial deflection is the first wood I-joist response to the applied load. This axial deflection lasts until a particular load is reached. Any further increase on the applied load will cause wood I-joist instability. This instability is characterized by the presence of additional wood I-joists responses to the applied load, including a lateral wood I-joist deflection and rotation of the wood I-joist with respect to its neutral axis. This condition of instability is called lateral-torsional buckling instability. The load at which lateral-torsional buckling instability occurs is known as the critical lateral-torsional buckling load (Kirby and Nethercot 1979).

Two different theoretical methods have been used to calculate the critical lateral-torsional buckling load for I-beams; the differential equations of equilibrium method and the strain energy method. The differential equations of equilibrium method for lateral-torsional buckling instability in I-beams is based on the elastic bending theory of beams. The problem to mathematically define the critical lateral torsional buckling load using the differential equations of equilibrium method is non-linear for large deflections, but linearization for small deflections is possible (Bažant 2000). The linearization process develops a linear fourth-order ordinary differential equation for deflections. The critical lateral-torsional buckling load is found by solving the linear fourth-order ordinary differential equation using the supported end conditions as boundary conditions. The strain energy method uses the equilibrium of the overall energy of the system. When an I-beam experiences lateral-torsional buckling instability, the strain energy increases as the applied load is transformed into axial deflection, lateral deflection and rotation of the I-beam. The point of load application moves downwards and laterally producing work in the system. The critical lateral-torsional buckling load is found by equating the increase of the strain energy in the system to the work done by the system (Timoshenko 1936). The strain energy method uses an approximate function for the angle of twist of the I-beam that must satisfy the boundary conditions defined by the supported end conditions (Timoshenko 1936). Thus, the two methods, the differential equation of equilibrium method and the strain energy method use the boundary conditions to mathematically define the critical lateral-torsional buckling load. Besides of the boundary conditions, stiffness properties including the lateral bending stiffness of the I-beam and the torsional rigidity of the I-beam are needed to calculate the critical lateral-torsional buckling load.

The present research is focused on the study of the lateral-torsional buckling instability of wood I-joists. The lateral bending stiffness of the wood I-joists was calculated using simple bending theory. The derivation of the equations to calculate the torsional rigidity of the wood I-joists was based on the analysis of torsion. The next

sections discuss the boundary conditions generally used on the development of the lateral-torsional buckling instability equations, the lateral bending stiffness theory and the torsional rigidity theory focused on wood I-joists. Lateral-torsional buckling behavior in wood members has been studied in the *Designing for Lateral-Torsional Stability in Wood Members Technical Report 14* (TR-14) (AF&PA 2003), research was derived using the differential equations of equilibrium method and adjusting factors to account for different loading and supported end conditions. Research developed in the TR-14 was used to support and compare the work developed in the current paper. Most of the lateral-torsional buckling research in the literature has been conducted on steel I-beams and it was used for comparison with the current research on wood I-joists.

2.3.1: Supported End Conditions

To obtain the equations to calculate the critical lateral-torsional buckling load for either the differential equations of equilibrium method or the strain energy method, it is necessary to take into account the mathematical relations of the boundary conditions. Solutions of the differential equations of equilibrium for wood I-joists found in the TR-14 were derived using a simply supported end condition as boundary conditions (AF&PA 2003). In the simply supported end condition, the ends of the wood I-joist are free to rotate with respect to the principal axes of inertia normal to the plane of the web and parallel to the plane of the web and load application, while rotation with respect to the axis parallel to the plane of the web but perpendicular to the load application is not allowed (Timoshenko 1936). The simply supported end condition was used in the TR-14 to analyze different loading conditions, including the case in which the load is not applied at the neutral axis of the wood I-joist as considered in the derivation of the differential equations of equilibrium and the case when the load is not applied at the mid-span of the wood I-joist.

Maljaars et al. (2005) investigated lateral-torsional buckling instability in steel I-beams for several real supported end conditions found on structural applications. Real supported end conditions differ from the simply supported end condition and consequently the solutions of the differential equations of equilibrium for the critical lateral-torsional buckling load are also different. These solutions are more complex, exact solutions are available only for few cases, for the most cases numerical solutions are necessary. The difference between the simply supported case and the real supported end conditions in research and design recommendations has been largely ignored in spite of its importance (Maljaars et al. 2005). In a similar research, Wang et al. (1987) found that geometrical imperfections and residual stress have significant influence on the lateral-torsional buckling instability especially for beams in the region of medium slenderness, and that this influence may be reduced applying proper restraints at the ends of the I-beam. The supported end conditions also affected the maximum elastic deformations and post-buckling behavior of the I-beams (Wang et al. 1987).

Timoshenko (1936) and Kirby and Nethercot (1979) proved theoretically that warping stresses have important influence at the ends of the I-beams in lateral-torsional buckling instability. Pi and Trahair (2000) noted that the supported end conditions may induce flange moments that oppose the warping stresses modifying the elastic

lateral-torsional buckling response of the I-beam. Hence, to correctly determine the elastic lateral-torsional buckling response of the I-beams the warping effects at the ends of the I-beam must be estimated. Pi and Trahair (2000) proposed the following differential equation to account for the warping effects at the ends of the I-beam.

$$\alpha_w = -\frac{EC_w\frac{d^2\beta(z)}{dz^2}}{\frac{d\beta(z)}{dz}} \tag{2-1}$$

Where, α_w is the elastic warping stiffness at the end of the I-beam, E is the modulus of elasticity, C_w is the warping constant of the cross-section of the I-beam, and β is the angle of torsion at the end of the I-beam. Equation 2-1 was derived for steel I-beams but can be used to compare results obtained in wood I-joists. Equation 2-1 cannot be applied directly to wood I-joists since wood I-joists are manufacture using composite wood materials and consequently the modulus of elasticity of the wood I-joists as an entire entity cannot be directly calculated.

Kirby and Nethercot (1979) stated that the influence of the supported end conditions in the elastic lateral-torsional buckling instability for I-beams can be approximated by using effective length factors. However, under complicated loading conditions the problem of determining the effective length factors are frequently not constant but vary with the length to depth ratio of the I-beam (Kirby and Nethercot 1979). Thus, the importance of deriving the critical lateral-torsional buckling loads for the supported end conditions under consideration.

For the case of wood I-joists, two different approaches to account for the effects of the supported end conditions have been used; the effective length approach and the equivalent moment factor approach (AF&PA 2003). The two approaches were derived to account for both the loading position and the supported end conditions. The effective length approach adjusts the un-braced length of the wood I-joists to account for the supported end conditions (AF&PA 2003). However, tabulated values to account for real supported end conditions in wood I-joists used in the residential construction industry were not found in design literature. Based on the current design methods, all wood I-joist supported end conditions were assumed to be the simply supported case. The equivalent moment factor approach adjusts the simply supported end condition to other supported end conditions using a factor (AF&PA 2003). The equivalent moment factor is an approximate value to the critical lateral-torsional buckling moment calculated from the moment equations derived according to the loading and boundary conditions (Kirby and Nethercot 1979). To calculate the moment equation for given supported end conditions, the differential equations of equilibrium must be solved. Differential equations of equilibrium derived from real supported end conditions found in practice in the residential construction industry are complex and in the most cases, a closed-form solution does not exist (AF&PA 2003).

2.3.2: Lateral Bending Stiffness in Wood I-Joists

The lateral bending stiffness of the wood I-joist (EI_y) is the capacity of the wood I-joist to resist normal to the plane of the web deformations when a normal to the plane of the web loading is applied to the wood I-joist. In the general case and for anisotropic materials the lateral bending stiffness is determined by elastic material properties of the beam such as elastic moduli and shear moduli, by geometric properties of the beam such as the moment of

inertia of the cross-section and the length of the beam and by the loading and end supported conditions of the beam. Lateral bending stiffness for wood I-joists in this research was analyzed using linear elastic beam analysis and simple bending theory.

Hindman et al. (2005a) and Burow et al. (2006) reported lateral bending stiffness values for several types of wood I-joists shown in Table 2-1. The height of the all wood I-joists was 9.50 inches. Wood I-joist flanges were composed of LVL and laminated strand board (LSL) materials while the web was composed of OSB for all wood I-joists tested. LVL and OSB materials were composed of southern pine (*Pinus spp*) veneer and flakes, and LSL was composed of yellow poplar (*Liriodendron tulipifera*) flakes. The difference between Hindman et al. (2005a) and Burow et al. (2006) lateral bending stiffness was most likely due to manufacturing differences between the two sets of composite wood I-joists as well as small differences in the moisture content of the specimens (Burow et al. 2006).

Table 2-1: Lateral Bending Stiffness of Wood I-Joists Hindman et al. (2005a) and Burow et al. (2006).

	Flanges			Web		Wood I-joists	
	Material	**Width (in.)**	**Depth (in.)**	**Material**	**Thickness (in.)**	**Height (in.)**	***EI*$_y$ (lb. in.^{2})**
Sample 1 Hindman et al. (2005a)	LVL	$1^1/_2$	$1^1/_2$	OSB	$^3/_8$	$9^1/_2$	1.90×10^6
Sample 2 Hindman et al. (2005a)	LSL	$1^3/_4$	$1^1/_2$	OSB	$^3/_8$	$9^1/_2$	2.14×10^6
Sample 3 Burow et al. (2006)	LVL	$1^1/_2$	$1^1/_2$	OSB	$^3/_8$	$9^1/_2$	1.83×10^6

2.3.3: Torsion in Wood I-Joists

An I-beam subjected to torsional moments undergoes warping longitudinal stresses, pure torsional shear stresses and warping shear stresses due to torsion of the cross-section as shown in Figure 2-1. Warping longitudinal stresses are developed in the flanges, which are constant across the thickness of the flanges but vary in the transverse directions with respect to the applied moments from zero at the mid-point to maximum at the peripheries. When I-beams have a large span to depth ratio and narrow flanges like wood I-joists, warping longitudinal stresses have very little effect and can be safely neglected (Timoshenko 1936). Warping longitudinal stresses in this research were not included in the derivation of the torsional rigidity equations or in the derivation of the lateral-torsional buckling equations. Pure torsional shear stresses in I-beams vary across the thickness of each element linearly. These stresses have their maximum effects at the outside peripheries of the I-beam. Warping shear stresses in I-beams are parallel to the edge of the elements. These stresses are constant across the thickness of the flanges but vary in the lateral directions from the maximum effects at the mid-point to zero at the peripheries (Yu 2000). Torsion in I-beams is determined by elastic material properties such as elastic moduli and shear moduli, by geometric properties such as the warping static moment, the St. Venant torsion constant, the warping torsion constant of the cross-section and derivatives of the angle of twist. Torsional properties of I-beams vary from the neutral axis to the top and bottom surfaces and the derivatives of the angle of rotation change along the length of the member (Yu 2000).

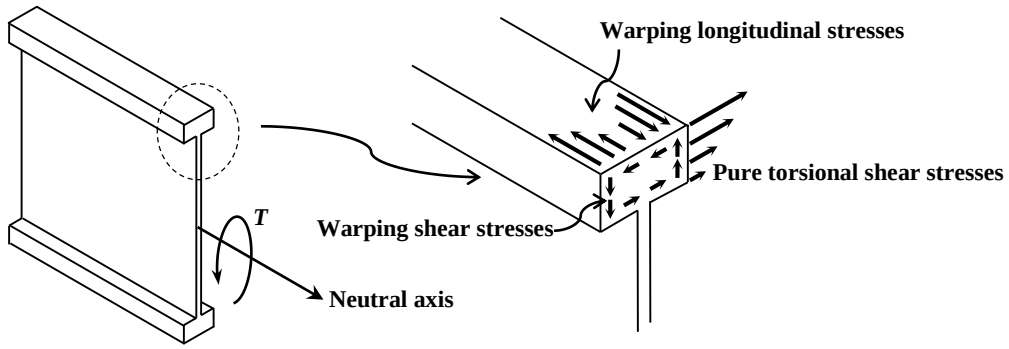

Figure 2-1: Stresses in wood I-joist flanges due to torsion.

Since wood I-joists are composed of anisotropic materials, the calculation of torsional properties is a complex task and can be obtained only approximately. Pure torsional shear stresses and warping shear stresses have important effects on the lateral-torsional buckling instability in wood I-joists and must be included in the calculations of both the torsional rigidity of the wood I-joists and the critical lateral-torsional buckling load (Timoshenko 1936). Although the wood I-joist web may experience warping shear stresses, these stresses are usually small compared to the warping shear stresses of the wood I-joist flanges and can be safety neglected. Warping shear stresses in wood I-joists may be interpreted as bending of the flanges in opposite directions about a vertical axis that crosses the shear center of the wood I-joists, shown in Figure 2-2.

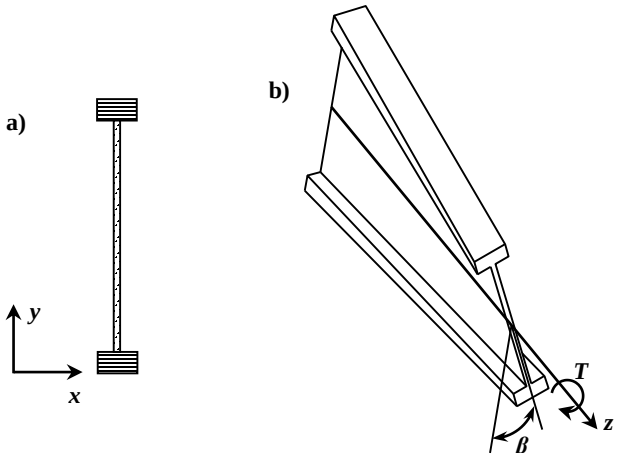

Figure 2-2: Torsion of a wood I-joist, a) cross-section, b) isometric view.

Kirby and Nethercot (1979) presented the following differential equation for an I-beam loaded by a torsional moment with both pure torsional shear stresses and warping shear stresses included.

$$T = GJ\frac{d\beta(z)}{dz} - \frac{EI_y h^2}{4}\frac{d^3\beta(z)}{dz^3} \tag{2-2}$$

Where, T is the applied torsional moment, GJ is the torsional rigidity, β is the angle of torsion, EI_y is the lateral bending stiffness and h is the depth of the I-beam.

Torsional rigidity in this research is the capacity of the wood I-joist to resist angular deformations when a torsional moment is applied to the wood I-joist through the neutral axis parallel to the plane of the web. The calculation of

the torsional rigidity in wood I-joist is greatly influence by the cross-section shape and the boundary conditions (Kirby and Nethercot 1979). Equation 2-2 can be solved for the case of a fixed wood I-joist to calculate the torsional rigidity as shown in Equation 2-3.

$$T = \frac{GJ\beta}{L}\left(\frac{1}{1-\frac{h}{L}\sqrt{\frac{EI_y}{GJ}}\tanh\left(\frac{L}{h}\sqrt{\frac{GJ}{EI_y}}\right)}\right) \tag{2-3}$$

Where, L is the wood I-joist length. It is not possible to solve Equation 2-3 explicitly for the torsional rigidity and therefore is necessary to use numerical solutions. Numerical solutions can reach any degree of accuracy needed in real assembling situations.

Hindman et al. (2005b) and Burow et al. (2006) tested several types of wood I-joists to measure their torsional rigidity. The height of all wood I-joists was 9.50 inches. Wood I-joist flanges were composed of LVL and LSL materials while the web was composed of OSB for all wood I-joists tested. LVL and OSB materials were composed of southern pine (*Pinus spp*) veneer and flakes, and LSL was composed of yellow poplar (*Liriodendron tulipifera*) flakes. Results are shown in Table 2-2. The difference between Hindman et al. (2005b) and Burow et al. (2006) torsional rigidities is most likely due to differences in the manufacturing process or materials used when constructing the two different sets of test specimens, sampling error, or to the differences in specimen rotation measurement (Burow et al. 2006).

Table 2-2: Torsional Rigidity of Wood I-Joists Hindman et al. (2005b) and Burow et al. (2006).

	Flanges			Web		Wood I-joists	
	Material	**Width (in.)**	**Depth (in.)**	**Material**	**Thickness (in.)**	**Height (in.)**	***EI*$_y$ (lb. in.^{2})**
Sample 1 Hindman et al. (2005b)	LVL	1 1/2	1 1/2	OSB	3/8	9 1/2	2.22 x 10^6
Sample 2 Hindman et al. (2005b)	LSL	1 3/4	1 1/2	OSB	3/8	9 1/2	2.27 x 10^6
Sample 3 Burow et al. (2006)	LVL	1 1/2	1 1/2	OSB	3/8	9 1/2	1.83 x 10^6

2.3.4: Static Lateral-Torsional Buckling Instability, Differential Equations of Equilibrium Method

In deriving the differential equations of equilibrium for the lateral-torsional buckling instability in I-beams, the following assumptions are made. The I-beam is initially straight without distortions, the I-beam behaves elastically, loading is strictly applied in the plane of the web (no lateral or torsional forces are applied), and the I-beam is initially unstressed. The case of a simply supported I-beam loaded by equal and opposite moments about the neutral axis parallel to the plane of the web known as the fundamental case was investigated, shown in Figure 2-3. In the simply supported end condition the ends of the wood I-joist are free to rotate with respect to the principal axes of inertia normal to the plane of the web (x axis) and parallel to the plane of the web and load application (y axis), while rotation with respect to the axis parallel to the plane of the web but perpendicular to the load application (z axis) is not allowed (Timoshenko 1936). The fundamental case is widely used in the literature with correction factors applied to account for different loading and supported end conditions.

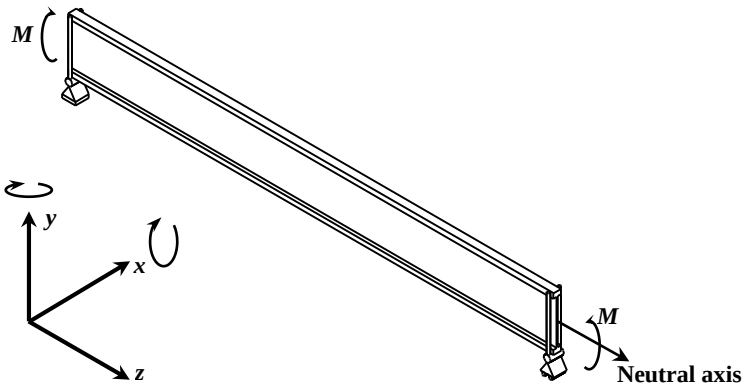

Figure 2-3: Simply supported I-beam loaded by equal and opposite moments.

Lateral-torsional buckling instability is accompanied by an axial displacement *v*, a lateral displacement *u* and a twist β about the neutral axis parallel to the *z*-axis. The general coordinate system of the un-deformed wood-I-joist is defined as *x*-*y*-*z*, and is fixed at the centroid of any cross-section. The coordinate system which rotates with the wood I-joist when it undergoes lateral-torsional buckling instability is defined as ξ-η-ζ. Both coordinate systems are shown in Figure 2-4.

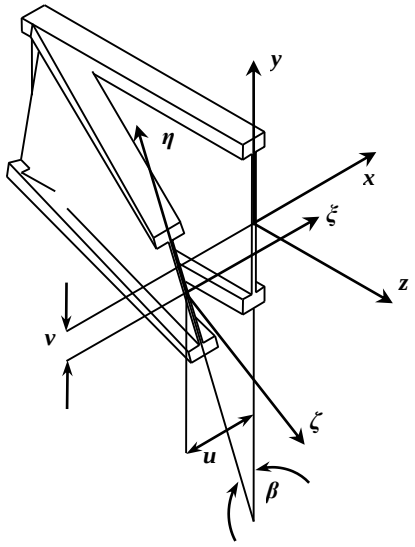

Figure 2-4: Coordinate systems before and after lateral-torsional buckling instability.

Equations 2-4 and 2-5 are the governing bending equations in the planes ξ-ζ and η-ζ, describing the axial displacement *v*, and the lateral displacement *u* (Kirby and Nethercot 1979).

$$EI_x \frac{d^2v(z)}{dz^2} = M(\xi) \tag{2-4}$$

$$EI_y \frac{d^2u(z)}{dz^2} = M(\eta) \tag{2-5}$$

Where, EI_x is the axial bending stiffness, $M(\xi)$ is the moment with respect to the ξ axis, EI_y is the lateral bending stiffness and $M(\eta)$ is the moment with respect to the η axis. The governing equation for twisting β, from Equation 2-2 is given below.

$$GJ\frac{d\beta(z)}{dz} - \frac{EI_y h^2}{4}\frac{d^3\beta(z)}{dz^3} = M(\zeta) \tag{2-6}$$

Where, $M(\zeta)$ is the moment with respect to the ζ axis. The quantities $M(\xi)$, $M(\eta)$ and $M(\zeta)$ are related to the projection of the applied moments onto the ξ, η and ζ axes, as shown in Figure 2-4. Linearization of the system assumes that the quantities *v*, *u* and β are very small. Also neglecting quantities of higher order, the following relations are obtained (Timoshenko 1936).

$$M(\xi) = -M \tag{2-7a}$$

$$M(\eta) = \beta(z)M \tag{2-7b}$$

$$M(\zeta) = -\frac{du(z)}{dz}M \tag{2-7c}$$

Where M are the applied moments about the neutral axis parallel to the plane of the web, see Figure 2-3. Substituting the values from Equations 2-7 into Equations 2-4, 2-5 and 2-6, the following set of differential equations of equilibrium defining the axial deflection *v*, the lateral deflection *u* as well as the angle of twist β are obtained.

$$EI_x\frac{d^2v(z)}{dz^2} = -M \tag{2-8a}$$

$$EI_y\frac{d^2u(z)}{dz^2} = \beta(z)M \tag{2-8b}$$

$$GJ\frac{d\beta(z)}{dz} - \frac{EI_y h^2}{4}\frac{d^3\beta(z)}{dz^3} = -\frac{du(z)}{dz}M \tag{2-8c}$$

The axial displacement *v* from Equation 2-8a is mathematically independent of the lateral displacement *u* and the angle of twist β from Equations 2-8b and 2-8c. In practice, the effect of the axial deflection *v* is very small for wood I-joists with narrow flanges. This effect is beneficial (tending to provide a conservative result) and can be safely neglected (Timoshenko 1936). Differentiating Equation 2-8c with respect to *z* and eliminating the differential term $\frac{d^2u(z)}{dz^2}$ by using Equation 2-8b, the following differential equation describing the angle of twist was obtained.

$$\frac{d^4\beta(z)}{dz^4} - \frac{4GJ}{EI_y h^2}\frac{d^2\beta(z)}{dz^2} - \frac{4M^2}{EI_y^2 h^2}\beta(z) = 0 \tag{2-9}$$

Equation 2-9 is a linear fourth-order differential equation with constant coefficients. The generalized solution can be represented by a linear combination of four exponential functions. Equation 2-9 has innumerable solutions for the applied moment M. The smallest solution corresponds to the critical lateral-torsional buckling moment M_{cr} represented by Equation 2-10.

$$M_{cr} = \frac{\pi}{L}\sqrt{EI_y GJ + \frac{\pi^2 EI_y^2 h^2}{4L^2}} \tag{2-10}$$

The first term inside the square root symbol of Equation 2-10 corresponds to the critical lateral-torsional buckling moment for rectangular beams with the same loading and boundary conditions. The second term inside the square root symbol of Equation 2-10 is the wood I-joist response to the warping effects. Warping effects become progressively more important as the I-beam depth increases and as the I-beam length decreases. In this research the wood I-joists are considered deep. Thus, it is important to consider warping effects. According to Equation 2-10, warping effects are affected by the lateral bending stiffness of the wood I-joists, but not the torsional rigidity of the wood I-joist.

Yin et al. (2004) tested steel and aluminum I-beams to measure the elastic-plastic response of these beams to the lateral-torsional buckling instability under cyclic pure bending. Structural degradation in I-beams was greatly influence by the progressive growth of the flange lateral deflections. Compressive strains at the mid-span point of the I-beams due to deflections in the compression flange (upper flange) became progressively greater causing wrinkles and buckling failures. Initial lateral-torsional buckling failures modes appeared in some cases after the 12^{th} to the 16^{th} cycle. Yin et al. (2004) emphasized the importance that warping shear stresses have in the lateral-torsional buckling instability.

Lateral-torsional buckling instability in wood I-joists is influenced by several factors including loading conditions, supported end conditions, member cross-section, un-braced length and loading relative to the neutral axis (AF&PA 2003). Loading relative to the neutral axis effects are more significant in cases where warping effects are important such as in I-beams (Kirby and Nethercot 1979). Loading applied to positions above the neutral axis reduces the critical lateral-torsional buckling load, while loading applied to positions below the neutral axis increases the critical lateral-torsional buckling load (Helwig et al 1997). Equation 2-10 applies exclusively for loading and boundary conditions according to the fundamental case shown in Figure 2-3. For loading and boundary conditions different to those of the simply supported case loaded by equal and opposite moments through the neutral axis parallel to the plane of the web, a closed form-solution was not available and the differential equations of equilibrium describing these cases must be solved by numerical methods or infinite series approximations (AF&PA 2003). In the *Designing for Lateral-Torsional Stability in Wood Members Technical Report 14* (AF&PA 2003) the following closed form solution for the fundamental case for wood I-joists is presented.

$$M_{ocr} = \frac{\pi}{l_u}\sqrt{EI_yGJ + \left(\frac{\pi E}{l_u}\right)^2 I_y C_w} \tag{2-11}$$

Where, M_{ocr} is the critical lateral-torsional buckling moment, l_u is the un-braced wood I-joist length, I_y is the centroidal area moment of inertia with respect to the parallel axis to the load application and C_w is the warping constant.

Warping shear stresses due to torsion of the cross-section in Equation 2-11 are expressed by the warping constant C_w. TR-14 does not address the problem of determining the warping constant so equation 2-11 cannot be applied

directly to wood I-joists (AF&PA 2003). For rectangular cross-section beams Equation 2-11 can be simplified to Equation 2-12 which ignores the increased resistance providing by warping shear stresses.

$$M_{ocr} = \frac{\pi}{l_u}\sqrt{EI_y GJ} \tag{2-12}$$

For rectangular beams undergoing loading conditions and supported end conditions different than those of the fundamental case Equation 2-12 can be readjusted. TR-14 presents the effective length approach and the equivalent moment factor approach for adjusting Equation 2-12 (AF&PA 2003). The effective length approach replaced the un-braced length l_u with an "effective length" l_e shown in Equation 2-13.

$$M_{ocr} = \frac{\pi}{l_e}\sqrt{EI_y GJ} \tag{2-13}$$

For a concentrated load applied at the mid-span of the wood beam and at the neutral axis of the cross-section with no lateral support the effective length l_e is 1.35 (AF&PA 2003). The case of a concentrated load applied away from mid-span of the wood beam is not discussed in the TR-14. The equivalent moment factor approach uses a factor C_b for adjusting the critical moment of Equation 2-12 to other loading and supported end conditions. The equivalent moment factor C_b is given by Equation 2-14 (AF&PA 2003).

$$C_b = \frac{12.5M_{max}}{2.5M_{max}+3M_A+4M_B+3M_C} \tag{2-14}$$

Where, M_{max} is the absolute value of the maximum moment, M_A is the absolute value of the moment at $\frac{l_u}{4}$, M_B is the absolute value of the moment at $\frac{l_u}{2}$, and M_C is the absolute value of the moment at $\frac{3l_u}{4}$. Equation 2-14 is applicable to linear and nonlinear moment diagrams and also it can be applied to wood beams with bracing points. TR-14 uses the load position relative to the neutral axis equation 2-15 to adjust loading applied at the neutral axis to loading applied above or below from the neutral axis(AF&PA 2003).

$$C_e = \sqrt{\left(\frac{qh}{2L}\right)^2 \frac{EI_y}{GJ} + 1} - \frac{qh}{2L}\sqrt{\frac{EI_y}{GJ}} \tag{2-15}$$

Where, C_e is the load eccentricity factor and q is a constant based on the loading conditions and supported end conditions. For a simply supported beam with a concentrated load applied at the top surface of the mid-span, TR-14 uses a constant q equals to 1.72 (AF&PA 2003). No values are given for the case when loading is not applied at the mid-span or for cases when the beam is supported by different supported end conditions. For all loading cases, q can be conservatively taken as 1.72 (AF&PA 2003), and consequently in this research the value of 1.72 was used for the constant q for all cases under investigation. Using the 1.72 value for q, the minimum value for the load eccentricity factor C_e becomes 0.27 (AF&PA 2003).

Hindman et al. (2005a) tested wood I-joists to investigate the lateral-torsional buckling instability of an un-braced cantilever wood I-joist. Results shown that the *Load and Resistance Factor Design* (AF&PA 1996) equations were overly conservative and predicted values in some cases over 70.3 % less than the measured wood I-joist

critical lateral-torsional buckling loads. Theoretical models for the critical lateral-torsional buckling loads did not use warping effects of the torsion section. The difference between theoretical predictions and measurements of the critical lateral-torsional buckling loads mainly resulted from the composite construction of the wood I-joists (Hindman et al. 2005a).

Burow et al. (2006) applied three different mathematical models combined with the *Load and Resistance Factor Design* (AF&PA 1996) to study the lateral-torsional buckling instability of wood I-joists in cantilever and simply supported configurations under a concentrated load. Burow et al. (2006) used Equation 2-16 by replacing the elastic buckling moment equation of the *Load and Resistance Factor Design* (AF&PA 1996) by the equivalent moment factor C_b from Equation 2-14 to calculate the critical lateral-torsional buckling loads.

$$M_e = C_b \left(\frac{4.013}{l_u} \sqrt{EI_y GJ + \left(\frac{\pi E}{l_u}\right)^2 I_y C_w} \right) \tag{2-16}$$

Equation 2-16 was found to be the best predictor model of the three mathematical models of the expected critical lateral-torsional buckling load for the simply supported configuration when loading was applied away from the neutral axis (Burow et al. 2006).

2.3.5: Static Lateral-Torsional Buckling Instability, Strain Energy Method

The differential equations of equilibrium describing the lateral-torsional buckling instability for I-beams have a closed-form solution only for few cases found in practice. Another approach, the strain energy method can be used to investigate the lateral-torsional buckling instability of wood I-joists by replacing complicated solutions of the differential equations of equilibrium with the calculation of integrals with available solutions (Timoshenko 1936). The strain energy method is widely used in lateral-torsional buckling instability in research rather than in practice where higher degree of accuracy is necessary (Robert 2002).

In the equations derived using the strain energy method, small change in stored energy due to axial deflection in the plane of the web was neglected. Using the differential equations of equilibrium method, the axial deflection is also neglected since the axial deflection governing equation has no mathematical relation with the lateral deflection and angle of twist governing equations. The results obtained neglecting the loss of energy from axial deflection are sufficiently correct for research applications when the rigidity of the wood I-joist in the plane of the web is large in comparison with the rigidity in the lateral direction (Timoshenko 1936).

The increase in the strain energy in the wood I-joist due to the lateral deflection U_B is Equation 2-17 (Singer and Pytel 1980).

$$U_B = \int_0^L \frac{\left(M\beta(z)\right)^2}{2EI_y} dz \tag{2-17}$$

The lateral component of the applied moment to the wood I-joist by the load P is expressed by Equation 2-8b.

$$EI_y \frac{d^2u(z)}{dz^2} = M\beta(z) \tag{2-18}$$

Inserting Equation 2-18 into Equation 2-17, Equation 2-19 is obtained, which provides the increase in the strain energy in the wood I-joist due to the lateral deflection U_B.

$$U_B = \frac{EI_y}{2}\int_0^L \left(\frac{d^2u(z)}{dz^2}\right)^2 dz \tag{2-19}$$

The increase in the strain energy in the wood I-joist due to torsion U_T is equal to the product of one half of the torsional moment multiplied by the angle of torsion as function of the wood I-joist length (Singer and Pytel 1980).

$$U_T = \frac{1}{2}T\beta(z) \tag{2-20}$$

An important assumption made when deriving Equation 2-20 is that the torsional moments are applied through the neutral axis of the wood I-joist. The torsional moment for wood I-joist which includes warping shear stresses is taken from Equation 2-2.

$$U_T = \frac{1}{2}\left(GJ\frac{d\beta(z)}{dz} - \frac{EI_y h^2}{4}\frac{d^3\beta(z)}{dz^3}\right)\beta(z) \tag{2-21}$$

Integrating Equation 2-21, Equation 2-22 is obtained. This equation provides the increase in the strain energy in the wood I-joist due to torsion.

$$U_T = \frac{GJ}{2}\int_0^L \left(\frac{d\beta(z)}{dz}\right)^2 dz - \frac{EI_y h^2}{8}\int_0^L \left(\frac{d^3\beta(z)}{dz^3}\frac{d\beta(z)}{dz}\right) dz \tag{2-22}$$

The expression of the work done by the applied load *P* during lateral-torsional buckling instability can be derived by integrating the infinitely small elements ds of the curvature of the wood I-joist due to lateral and vertical displacements as shown in Figure 2-5. The curvature of the wood I-joist depicted in Figure 2-5 is considered to be the curvature of its neutral axis.

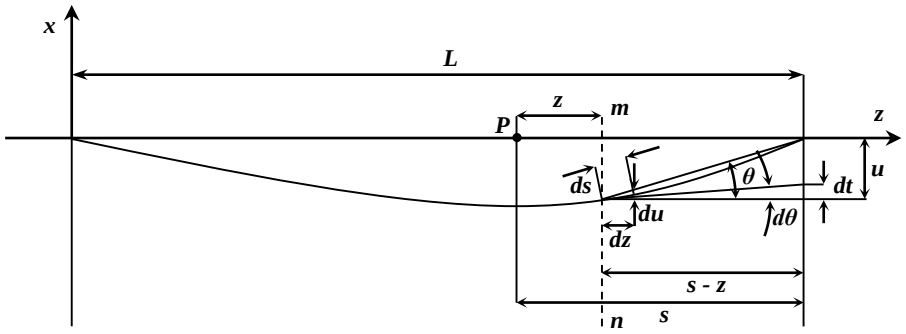

Figure 2-5: Displacement of the load *P* during lateral-torsional buckling instability. Top view.

Considering the cross section *m-n* as fixed in Figure 2-5, the total angle θ representing the lateral displacement of the wood I-joists under the action of the applied force can be approximately taken for small deflections as shown in Equation 2-23.

$$\theta = \frac{du(z)}{dz} \tag{2-23}$$

Deriving Equation 2-23 with respect to the *z* variable, Equation 2-24 is obtained.

$$d\theta = \frac{d^2u(z)}{dz^2}dz \tag{2-24}$$

From Figure 2-5 and Equation 2-24 the differential lateral component dt of the total lateral displacement of the wood I-joist due to the applied load P is shown in Equation 2-25.

$$dt = (s - z)d\theta = \frac{d^2u(z)}{dz^2}(s - z)dz \tag{2-25}$$

The total differential displacement of the load P can be obtained by multiplying Equation 2-25 by the angle of torsion $\beta(z)$. See Figures 2-4 and 2-5.

$$\beta(z)\frac{d^2u(z)}{dz^2}(s - z)dz \tag{2-26}$$

The total displacement of the load P during lateral-torsional buckling instability is consequently given by the sum of all infinitely small elements ds and can be calculated by integrating Expression 2-26 from one end of the wood I-joist to the load application point s.

$$\int_0^s \beta(z)\frac{d^2u(z)}{dz^2}(s - z)\,dz \tag{2-27}$$

The equation to calculate the critical lateral-torsional buckling load was deduced from the condition that the total increase in the strain energy in the wood I-joist is equal to the work done by the system. The work done by the system is given by Expression 2-27 multiplied by the applied load P, while the total increase in the strain energy in the wood I-joist is given by the sum of the strain energy increase due to lateral deflection U_B, Equation 2-19, and the strain energy increase due to torsion U_T, Equation 2-22.

$$P\int_0^s \beta(z)\frac{d^2u(z)}{dz^2}(s - z)\,dz =$$

$$\frac{EI_y}{2}\int_0^L \left(\frac{d^2u(z)}{dz^2}\right)^2 dz + \frac{GJ}{2}\int_0^L \left(\frac{d\beta(z)}{dz}\right)^2 dz - \frac{EI_y h^2}{8}\int_0^L \left(\frac{d^3\beta(z)}{dz^3}\frac{d\beta(z)}{dz}\right) dz \tag{2-28}$$

Two variables related to the lateral-torsional buckling instability are present in Equation 2-28, the lateral deflection of the wood I-joist $u(z)$ and the torsion of the wood I-joist $\beta(z)$. These two variables are related (see Equation 2-8b) as shown in Equation 2-29.

$$\frac{d^2u(z)}{dz^2} = \frac{\beta(z)M}{EI_y} \tag{2-29}$$

The flexural moment M in the lateral direction of Equation 2-29 was calculated from geometrical considerations and the reaction at the ends of the wood I-joist to the loading conditions. For a wood I-joist loaded by a concentrated force P applied at a distance s from one of the wood I-joist ends, the corresponding flexural moment is shown in Equation 2-30.

$$M = \frac{P(L-s)(s-z)}{L} \tag{2-30}$$

Inserting Equation 2-30 into Equation 2-29 a differential equation associating the lateral deflection of the wood I-joist $u(z)$ with the torsion of the wood I-joist $\beta(z)$ is obtained as shown in Equation 2-31.

$$\frac{d^2u(z)}{dz^2} = \frac{\beta(z)P(L-s)(s-z)}{EI_yL} \tag{2-31}$$

Now, inserting Equation 2-31 into Equation 2-28, the following equation to calculate the critical lateral-torsional buckling load is obtained.

$$\frac{P^2(L-s)}{EI_yL}\left(\int_0^s\left(\beta(z)(s-z)\right)^2 dz - \frac{L-s}{2L}\int_0^L\left(\beta(z)(s-z)\right)^2 dz\right) =$$

$$\frac{GJ}{2}\int_0^L\left(\frac{d\beta(z)}{dz}\right)^2 dz - \frac{EI_yh^2}{8}\int_0^L\left(\frac{d^3\beta(z)}{dz^3}\frac{d\beta(z)}{dz}\right)dz \tag{2-32}$$

Since it was assumed that the torsional moments applied to the wood I-joist to derive the equation for the increase in the strain energy in the wood I-joist were applied through the neutral axis, and that the curvature of the wood I-joist used to develop the expressions for the work done by the applied load to the wood I-joist was the curvature of the neutral axis, Equation 2-32 can only be correctly used for loads applied at the neutral axis of the wood I-joists. Equation 2-32 is widely used in the literature along with adjusting factors to research different loading and supported end conditions on I-beams composed of different structural materials (Timoshenko 1936). However, in this research, loading was not applied at the neutral axis, instead it was applied at the top surface of the top flange of the wood I-joist and therefore the effects of applying the load in a higher position relative to the neutral axis must be investigated (Timoshenko 1936 and Kirby and Nethercot 1979). The effects of applying the load in a higher position relative to the neutral axis are more important for wood I-joists with large depth to width ratio than for shorter wood I-joists (Timoshenko 1936).

Calling a the distance from the neutral axis of the wood I-joist to the point of the applied load, an approximate expression for the work done by the additional displacement that the load undergoes can be obtained by considering the rotation of the cross-section during lateral-torsional buckling instability of the wood I-joist. By geometry considerations from Figure 2-4, Equation 2-33 was derived to account for the effects of applying the load away from the neutral axis.

$$\frac{Pa}{2}(1-\cos\beta(z)) \approx \frac{Pa\left(\beta(z)\right)^2}{4} \tag{2-33}$$

Inserting Equation 2-33 into Equation 2-32, Equation 2-34 was obtained to calculate the critical lateral-torsional buckling load when the load is applied at the top flange of the wood I-joist and at any point along the wood I-joist span.

$$\frac{Pa\left(\beta(z)\right)^2}{4} + \frac{P^2(L-s)}{EI_yL}\left(\int_0^s\left(\beta(z)(s-z)\right)^2 dz - \frac{L-s}{2L}\int_0^L\left(\beta(z)(s-z)\right)^2 dz\right) =$$

$$\frac{GJ}{2}\int_0^L\left(\frac{d\beta(z)}{dz}\right)^2 dz - \frac{EI_yh^2}{8}\int_0^L\left(\frac{d^3\beta(z)}{dz^3}\frac{d\beta(z)}{dz}\right)dz \tag{2-34}$$

To calculate the critical lateral-torsional buckling load using equation 2-34 the function for the angle of torsion $\beta(z)$ must be known, however this function is unknown for the majority of the loading and supported end condition cases encountered in real structural situations and therefore this function must be approximated. Several methods for approximating an arbitrary function to the function for the angle of torsion $\beta(z)$ had been developed. The arbitrary function can be approximated to the real function with any degree of accuracy needed. Arbitrary functions regularly are constructed by superimposing trigonometry functions. The arbitrary function must satisfy the supported end conditions of the loaded wood I-joist under consideration. Particular solutions of Equation 2-34 along with the required functions for the angle of torsion $\beta(z)$ are analyzed in the Theoretical Models Chapter of this research.

The strain energy method has been used widely in the literature to investigate lateral-torsional buckling instability in beams manufactured from several different construction materials and cross-section shapes and for several applications under diverse loading and supported end conditions. Roberts (2002) derived equations using the strain energy method to calculate the influence of shear deformation on the flexural buckling, torsional buckling and lateral buckling of pultruded fiber reinforced plastic I-profiles. Testing performed on a simply supported test configuration shown that shear deformation reduced the pure torsional buckling loads by up to approximately 9% and the lateral buckling moment by up to approximately 1% for narrow flange profiles.

Qiao et al. (2002) studied lateral-torsional buckling instability of pultruded fiber-reinforced plastics in an un-braced cantilever test configuration. Analytical formulations were developed to compare the strain energy methods with plate theory methods. An assumption included in the formulation was that the lateral deflection and rotation of the web were coupled. Results from testing proved that the analytical solutions from both the strain energy method and the plate theory method had good agreement with the experimental data.

Pi and Trahair (1992) performed an analytical comparison between the differential equations of equilibrium method and the strain energy method for lateral-torsional buckling instability of steel I-beams. Pre-buckling deformations and second order moments due to axial loads were considered in both methods. Results verified that the strain energy method provides values for the lateral-torsional buckling instability with a higher degree of accuracy compare to the differential equations of equilibrium method even when effects from pre-buckling deformations were included in the mathematical formulations.

Kitipornchai and Trahair (1980) tested mono-symmetric steel I-beams and proved that calculations on the elastic critical lateral-torsional buckling loads derived from the differential equations of equilibrium give only approximate solutions compared to the test results. Design codes either avoid these calculations or replace then by simplifications mainly because the effort required is prohibitive in routine designs (Kitipornchai and Trahair 1980).

The strain energy method is always conservative, and provides values for the critical lateral-torsional buckling loads slightly less than the loads obtained from testing. The conservatism of the strain energy method can be

reduced to at any degree of accuracy needed. The limit of this reduction is the value of the critical-lateral torsional buckling loads obtained by exact methods derived from the differential equations of equilibrium method (Timoshenko 1936). However, only a few loading and supported end conditions cases can be solved exactly by using the differential equations of equilibrium method. When numerical solutions of approximate solutions are performed to solve the differential equations of equilibrium, generally the strain energy method is more accurate (Pi and Trahair 1992). The strain energy method simplifies considerably the calculations in obtaining the lateral-torsional buckling loads and gives accuracy sufficient for practical applications (Timoshenko 1936). Energy methods are also useful as the basis of approximate solutions of critical lateral-torsional loads in post buckling instability (Bažant 2000). The strain energy method proved to be an alternative to the differential equations of equilibrium method in studying lateral-torsional buckling instability in wood I-joists.

2.3.6: Dynamic Lateral-Torsional Buckling Instability

Dynamic lateral-torsional buckling instability was investigated in this research by linearly combining the static lateral-torsional buckling models with the bending motion of the wood I-joists caused by individuals walking over them. The load used in the static lateral-torsional buckling models was the weight of one individual walking on the wood I-joists while the load used in the bending motion equations of the wood I-joists was the lateral component of the weight of the same individual walking on the wood I-joists. The goal of the dynamic lateral-torsional buckling models was to predict the position along the wood I-joist length in which the lateral-torsional buckling instability occurs considering the individual's weight large enough to cause lateral-torsional buckling instability. Dynamic instability in beams is typically caused by vibrations of increasing amplitude, during which the beam moved to absorb unbounded energy from the load (Bažant 2000). Dynamic lateral-torsional buckling instability in this research refers to loading applied due to individuals walking on wood I-joists that cause lateral-torsional buckling instability. In the next section, the forces caused by people walking and the bending motion of the wood I-joist under the action of these forces are described.

2.3.7: Forces Caused by People Walking

Forces imposed by individuals walking under normal conditions at a regular pace can be mathematically described as a function of time. Single footstep forces are mathematically expressed using descriptive parameters including; the dynamic load factor, the pacing rate and the phase angle (Ebrahimpour et al. 1996). Dynamic loading due to pedestrians walking on structures is considered as a periodic excitation and it is modeled by a Fourier series with the fundamental harmonic frequency equal to the pace of the pedestrian. Higher harmonics have frequencies that are integer multiples of the fundamental frequency (Pimentel et al. 2001). The intensity of the dynamic force induced by individuals walking varied with the pace. Pedestrians normally walk with a pace rate between 1.6 Hz (slow pace) through 2.4 Hz (brisk pace), with a mean of approximately 2.0 Hz. The dynamic load from each footstep is approximately the same. The summation of the load produced by continuous footsteps is simulated by

creating pulse trains of single footstep loads. Pimentel et al. (2001) described the force of the dynamic loading due to an individual walking $F_d(t)$, (H = 1) as Equation 2-35.

$$F_d(t) = G_w(H + \sum_{n=1}^{m} \alpha_n \sin(2n\pi f_d t + \varphi_n)) \quad (2\text{-}35)$$

Where G_w is the weight of the individual, H is the total response of the walking surface to the force imposed by the individual walking for a given particular direction, α_n is the dynamic load factor of the n^{th} harmonic of the weight of the individual walking, f_d is the pacing rate of the individual walking and φ_n is the n^{th} harmonic phase angle of the weight of the individual walking. The dynamic load factors $\alpha_1, \alpha_2, \alpha_3, \ldots, \alpha_n$ are generally derived from the analysis of the response signals in the frequency domain where the contribution of each harmonic is identified and isolated. About 10% of the vertical dynamic loading from an individual walking is applied laterally (Nakamura and Kawasaki 2006). The center of gravity of the body moves laterally with the individual footsteps when walking this movement induces the laterally force.

Figure 2-4 depicts a graph of the dynamic loading from an individual walking as a function of time (Equation 2-35). The graph considers only the first two harmonics. The weight of the person G_w and the constant H were normalized, the dynamic load factors $\alpha_1 = 0.33$ and $\alpha_1 = 0.15$ were averaged values from Ebrahimpour et al. (1996), Pimentel et al. (2001), and Figueiredo et al. (2008), the pacing rate $f_d = 1.80\,Hz$ was an averaged frequency from pace on platforms (Ebrahimpour et al. 1996), the phase angles were $\varphi_1 = 0$ and $\varphi_2 = \frac{\pi}{2}$. In Figure 2-4 the loading from a single footstep was outlined.

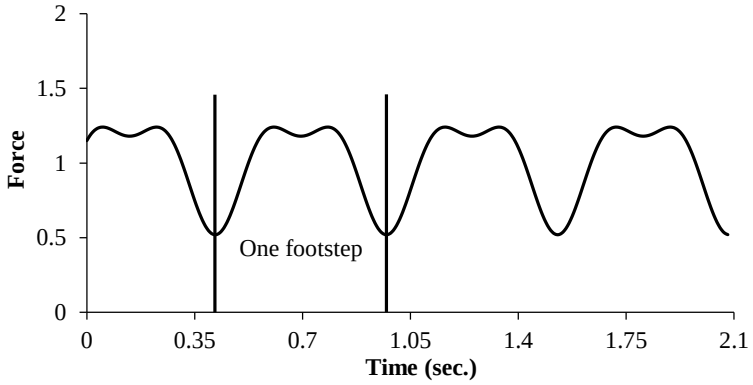

Figure 2-6: Dynamic loading of one individual walking.

The dynamics of the human body when walking is an organized leg movement that causes an ascending and descending movement of the effective center of mass of the human body at each step. When walking the human body mass accelerations are associated to the floor reactions which are approximately periodic to the step frequency (Figueiredo et al 2008). Structural response to dynamic loading depends on factors such as stiffness and damping of the floor system as well as on the relationship of the excitation forces to the natural frequencies of the floor system. Since wood I-joists are used to assemble the floor system, the wood I-joists must have a response behavior to the individuals walking somewhat similar to the floor system.

Workers walking on wood I-joists in bending configurations induce axial and lateral vibrations. The level of these vibrations is unlikely to be sufficient to cause structural damage to the system. However, the human body is very sensitive to vibrations and these vibrations can cause disturbance to the workers (Pimentel et al. 2001). Disturbance of the individual walking on the wood I-joists intensifies the threat of lateral-torsional buckling instability since the center of mass of the human body moves erratically increasing the lateral component of the dynamic force. When the position of the dynamic loading corresponds to the excitation induced by the individual walking there is a substantial increase in the structural dynamic response (Figueiredo et al 2008). This response increases the risk of lateral-torsional buckling instability and therefore it must be taken into consideration in investigating the bending movement of the wood I-joists under loading by individuals walking.

2.3.8: Bending Motion of Beams

Lateral dynamic loading from individuals walking on the wood I-joists generates lateral bending motion in the wood I-joist with their corresponding lateral deflections. Wood I-joist lateral deflections are initial conditions that modify the static critical lateral-torsional buckling loads since the response capacity of the wood I-joist have been altered. Because the lateral deflections increase and decrease according with the bending motion of the wood I-joist the corresponding critical lateral-torsional buckling loads increase and decrease under the same pattern. Thus the importance of studying the lateral bending motion of the wood I-joist in order to fully understand the lateral-torsional buckling instability of the wood I-joist triggered by workers walking on the wood I-joists.

Elementary beam theory assumptions applied to the bending motion of the wood I-joist include: rotation of the differential elements is negligible compared to translation, angular distortion due to shear is small in relation to bending deformation, the length to depth ratio of the wood I-joist is relatively large, and the wood I-joist does not wrinkle due to flexure. Considering that the bending motion equations are conservative and linear, the partial differential equation for bending motion of the wood I-joist under dynamic loading is given in Equation 2-36 (Meirovitch 2001).

$$-\frac{\partial^2}{\partial z^2}\left(EI_y(z)\frac{\partial^2 x(z,t)}{\partial z^2}\right) + f(z,t) = m(z)\frac{\partial^2 x(z,y)}{\partial t^2} \tag{2-36}$$

Where, f is the dynamic force applied to the wood I-joist and m is the mass of the wood I-joist. Assuming that the lateral bending stiffness EI_y and the mass m of the wood I-joist are constants throughout the wood I-joist length, Equation 2-36 can be simplified to Equation 2-37.

$$-EI_y\frac{\partial^4 x(z,t)}{\partial z^4} + f(z,t) = m\frac{\partial^2 x(z,t)}{\partial t^2} \tag{2-37}$$

The partial differential Equation 2-37 has a closed-form solution only under special loading and motion cases, so alternative solutions are needed. Wood I-joists under the action of the dynamic loading from the individual walking undergo synchronous motion (every point of the wood I-joist executes the same motion with respect to the other points in time, passing through equilibrium and reaching the maximum displacements at the same time). During synchronous motion, the wood I-joist exhibits a certain unique profile, and this profile does not change

with time, only the amplitude of the profile changes. The profile is defined by the static bending equations according with the loading and supported end conditions. In mathematical sense, the last assumption implies that the solution $x(z,t)$ from Equation 2-37 is separable in the spatial *z*, and the temporal *t* variables. Equation 2-37 is a linear time invariant system, hence the solution of this equation can be performed in two steps, solving the wood I-joist response to initial excitations, and then solving the wood I-joist response to the applied forces. Linearly combining these two solutions the complete general solution of the motion of the wood I-joist is obtained. The solution $x(z,t)$ is expressed by Equation 2-38 (Meirovitch 2001).

$$x(z,t) = \sum_{r=1}^{\infty} \chi_r(z)\psi_r(t) \tag{2-38}$$

Where, $\chi_r(z)$ represents the wood I-joist profile as a function of the spatial variable z alone, while $\psi_r(t)$ represents the variation of the profile with respect to the temporal variable t alone. Inserting Equation 2-38 into Equation 2-37 and simplifying produces Equation 2-39.

$$-EI_y\psi_r(t)\frac{d^4}{dz^4}\sum_{r=1}^{\infty}\chi_r(z) + f(z,t) = m\chi_r(z)\frac{d^2}{dt^2}\sum_{r=1}^{\infty}\psi_r(t) \tag{2-39}$$

Integrating Equation 2-39 over the wood I-joist length and multiplying the solution by a spatial function $\chi_s(z)$ to transform the system into an orthogonal system and normalizing the final solutions Equation 2-40 is achieved.

$$m\frac{d^2}{dt^2}\psi_r(t)\int_0^L \chi_s(z)\chi_r(z)dz - EI_y\psi_r(t)\int_0^L \chi_s(z)\frac{d^4}{dz^4}\chi_r(z)dz = \int_0^L f(z,t)\chi_r(z)dz \tag{2-40}$$

The two terms of the left side of Equation 2-40 represent the wood I-joist response to the initial excitations and are related for linear systems by Equation 2-41 (Meirovitch 2001).

$$m\int_0^L \chi_r(z)\chi_s(z)dz = \delta_{rs} \tag{2-41a}$$

$$EI_y\int_0^L \chi_s(z)\frac{d^4}{dz^4}\chi_r(z)dz = \omega_r^2\delta_{rs} \tag{2-41b}$$

Where, ω_r is the frequency of oscillation of the wood I-joist. The general solution to Equation 2-40 is found by using convolution integrals and is shown in Equation 2-42 (Meirovitch 2001).

$$x(z,t) = \sum_{r=1}^{\infty}\frac{\chi_r(z)}{\omega_r}\int_0^t\left(\int_0^L f(z,t)\chi_r(z)dz\right)\sin(\omega_r\tau)\,d\tau \tag{2-42}$$

In Equation 2-42 the wood I-joist profile $\chi_r(z)$ and the frequency of oscillation ω_r remain undetermined. These two parameters can be obtained at the same time by equating both terms of Equation 2-41 as in Equation 2-43.

$$\frac{d^4}{dz^4}\chi_r(z) - \omega_r^2\frac{m}{EI_y}\chi_r(z) = 0 \tag{2-43}$$

Equation 2-43 is a fourth order linear homogeneous differential equation. The solution of this equation will contain four constants of integration in addition to the frequency of oscillation ω_r. To solve Equation 2-43, the supported end conditions of the wood I-joist must be considered.

The solution of the bending motion of the wood I-joist Equation 2-43 in addition with the solution of the static critical lateral-torsional buckling load, Equation 2-34, permits the calculation of the critical lateral-torsional buckling position of the individual walking on the wood I-joist. It is assumed that the weight of the individual walking on the wood I-joist is large enough to cause lateral-torsional buckling instability.

2.3.9: Bracing Systems

Bracing systems applied to the wood I-joists in this research were intended to reduce the possibility of lateral-torsional buckling instability. When lateral-torsional buckling instability occurs due to the action of an applied load, the wood I-joists experience axial deflection, lateral deflection and twist. Bracing systems are intended to increase the wood I-joist response to the lateral deflection as well to the twist of the wood I-joist by transmitting part of the applied loading to the braced wood I-joist through the bracing system. A bracing system with infinity stiffness and enough strength to support all applied loads was assumed.

The primary purpose of any bracing system in structural construction is the transference of loads between individual beams and the increase of resistance of individual beams to out of plane loads. The structural bracing system compels higher modes of deformation in the principal members (beams, I-joists, etc.) by providing resistance to lateral or rotational displacements through axial, shear or flexural deformations in the bracing members (Chen and Yura 2005). Structural bracing systems to control stability can be classified into two general categories: lateral bracing systems, and torsional bracing systems. Lateral bracing systems are used to prevent or minimize lateral displacements of the principal members. Lateral bracing systems can be classified into four subcategories: relative, nodal, continuous and lean-on. Torsional bracing systems are employed to prevent or minimize rotation of the cross-section of the principal members. Torsional bracing systems can be classified into two subcategories: nodal and continuous.

Relative lateral bracing systems such as diagonal bracing or shear walls prevent relative lateral movements of adjacent points along the length of the principal members. Relative lateral bracing systems are identified when a cut at any location along the length of the principal member passes through the bracing member itself. Nodal lateral and torsional bracing systems control the movement only in the points where they are attached to the principal member and do not directly interact with adjacent bracing points. Continuous lateral and torsional bracing systems provide uninterrupted support along the entire length of the principal member. Lean-on bracing systems rely on adjacent principal members to provide support. Lean-on lateral and torsional bracing links together adjacent principal members in such a way that lateral-torsional buckling of one member requires all members in the system to buckle with the same lateral and torsional displacements (Chen and Yura 2005). To investigate lateral-torsional buckling instability in wood I-joists in this research a lean-on lateral-torsional bracing system was used in the form of cross-frames interconnecting adjacent wood I-joists.

The primary factors influencing the effectiveness of the lateral bracing systems are; the number of bracing members, space between bracing members, vertical position of the bracing members with respect to the neutral

axis, vertical position of the applied loading with respect to the neutral axis, type of loading and supported end conditions (Chen and Yura 2005). Lateral bracing is more effective to reduce lateral-torsional buckling instability when positioned at the compression flange (top flange) of the wood I-joist. Lateral bracing applied at the neutral axis of the principal members was not recommended due to effects of cross-section and web distortion (Chen and Yura 2005).

The effectiveness of torsional bracing systems depends upon the resistance of the cross-section of the principal members to twist. The resistance of the cross-section of the principal members to twist is primarily affected by the number of bracing members, the space between bracing members, the vertical position of the bracing members with respect to the neutral axis, the type of loading and supported end conditions (Chen and Yura 2005). Torsional bracing systems can be designed to effectively control twisting of the beam and reduce lateral-torsional buckling instability (AF&PA 2003). A torsional bracing member is equally effective if attached to the top or bottom flange of the wood I-joists.

A combination of lateral and torsional bracing system is more effective than either lateral or torsional bracing systems acting alone. An effective bracing system must prevent both relative displacements in the top and in the bottom of the beam (Chen and Yura 2005). When lateral deflections in addition to torsional deflections are prevented, the part of the beam between intermediate bracing members can be considered as a simply supported beam under the action of unequal end moments and a superimposed load (Hooley and Madsen 1964).

The bracing system must have sufficient stiffness to limit movement at the bracing point to the specified permissible deflections, thereby ensuring that lateral-torsional buckling instability occurs only between bracing members. The bracing system must also have sufficient strength to withstand the transmitted forces (Zahn 1984). The calculation of the required strength of the bracing members cannot be uniquely determined since it depends on both the magnitude of the stiffness of the bracing member and the out-of-straightness of the principal member (Chen and Yura 2005).

Complex analyses based on the bracing configuration, the bracing strength and the bracing stiffness as well as on the loading and supported end conditions of the wood I-joist are necessary to derive the exact magnitude of the critical lateral-torsional buckling load when a bracing system is installed. Since, it is not possible to exactly calculate the induced forces in the bracing members, the required stiffness and strength are found approximately (Kirby and Nethercot 1979). Testing has confirmed that comparatively light bracing systems provide substantial increment in the lateral-torsional buckling stability of the principal members (Kirby and Nethercot 1979). An approximate solution for the bracing system in wood I-joists requires the bracing members to be capable of resisting a lateral force of at least 2.5% of the maximum force in the compression flange of the principal member and a stiffness of at least 25 times the lateral bending stiffness of the principal member to be braced (Kirby and Nethercot 1979).

Bamberg (2009) investigated lateral displacements on wood I-joists under dynamic loading from individuals walking on the wood I-joists using two different bracing patterns with five different values on the stiffness. The braces were placed at two different positions along the wood I-joists length, spaced out 60 inches and 80 inches from each end. The braces were placed exclusively at the top flange of the wood I-joists. The stiffness of the braces was $0.0\frac{lbs}{in}$, $1.2\frac{lbs}{in}$, $8.5\frac{lbs}{in}$, $14.0\frac{lbs}{in}$, and approximately 400,000.0 $\frac{lbs}{in}$ considered as infinite stiffness. Results shown that, increasing the amount of bracing reduced the lateral displacement of the wood I-joists. The increase of the amount of bracing had a greater effect at low stiffness values compared with high stiffness values. Increasing the bracing stiffness the lateral displacement is reduced. The stiffness of the braces controlled the magnitude of the lateral displacements.

2.4: Conclusion of Literature Review

Falls from elevation are an essential cause of fatal work injures as well as excessive costs in the construction sites. In the residential construction industry workers are in risk of a fall when they traverse wood I-joists. Wood I-joist may undergo lateral-torsional buckling instability under the worker's weight. Lateral-torsional buckling instability is a condition in which the wood I-joist deflects axially and laterally as well as twist with respect to the neutral axis losing its steadiness. Static lateral-torsional buckling models from two different methods, the differential equations of equilibrium method and the strain energy method were analyzed. Dynamic lateral-torsional buckling models were developed by linearly combining the static lateral-torsional buckling models with the bending motion of the wood I-joists. The bending motion of the wood I-joists was analyzed using the lateral component of the force imposed by the individual walking on the wood I-joist. The final goal of the dynamic lateral-torsional buckling models was to calculate the critical lateral-torsional buckling position of the individual walking on the wood I-joist. To reduce potential lateral-torsional buckling instability problems in wood I-joist structures, the improvement of the end fixity of the wood I-joist as well as the installation of bracing systems is recommended.

3: Theoretical Models

The derivation of mathematical models to predict lateral-torsional buckling instability focused on loads from individuals walking on wood I-joists for different supported end conditions and bracing systems was the goal of this research. Lateral-torsional buckling instability in wood I-joists is influenced by the supported end conditions, bracing systems as well as loading conditions (Kirby and Nethercot 1979). Three different supported end conditions were analyzed in this research: simply, fixed and hanger supported. The hanger supported end condition was modeled using a lateral spring analogy. Numerical values for the lateral spring analogy were obtained by testing the wood I-joist hanger on their lateral stiffness. Differences between hangers were incorporated into the diverse models by their lateral spring stiffness values. Additionally, three different lean-on cross bracing systems were analyzed throughout all supported end conditions: Non-bracing, one mid-span brace, and two quarter-span braces. Equations for the amount of bracing restrain due to the bracing system were derived for the one mid-span brace and two quarter-span braces. Two different lateral-torsional buckling models were developed for each of the three supported end conditions, a static lateral-torsional buckling model, and a dynamic lateral-torsional buckling model. The static lateral-torsional buckling models were developed using the strain energy method. The dynamic lateral-torsional buckling models were developed by linearly combining the static lateral-torsional buckling models with the lateral bending motion of the wood I-joists. The bending motion of the wood I-joists was analyzed using the lateral component of the force imposed by an individual walking on the wood I-joists and an adjusting function to simulate the average variation of the response of the wood I-joists to the individual walking. A different adjusting function was proposed for each of the three supported end conditions.

3.1: Supported End Conditions

The equations for lateral-torsional buckling instability derived based on the differential equations of equilibrium method as well as the strain energy method used the supported end conditions as boundary conditions. In the strain energy method, the function $\beta(z)$ for the angle of twist must satisfy the supported end conditions. Supported end conditions are vital since poor end fixity configurations reduce the critical lateral-torsional buckling loads while strong end fixity configurations have the opposite behavior (Timoshenko 1936). Three different supported end conditions were used in this research to analyze the lateral-torsional buckling instability in wood I-joists, simply, fixed and hanger supported end conditions.

3.1.1: Simply Supported End Condition

In the simply supported end condition, the ends of the wood I-joists can rotate freely with respect to the principal axes of inertia parallel to the *x*-axis and *y*-axis, while rotation about the *z*-axis is prevented. The simply supported

end condition is often used in the literature since this condition can be approximated in practice. More complicated supported end conditions are often compared to the simply supported end condition (Kirby and Nethercot 1979). When the simply supported end condition cannot be reached in practice, adjusting factors can be applied to approximate other supported end conditions (AF&PA 2003). In research, a simply supported wood I-joist loaded by equal and opposite moments about its neutral axis is considered the fundamental case. Figure 3-1 is a diagram of the simply supported end condition.

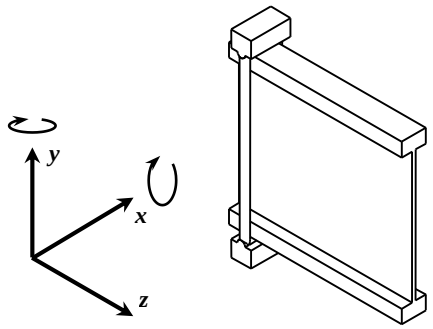

Figure 3-1: Simply supported end condition.

Physically in the simply supported end condition, the wood I-joist flanges are supported at the bottom and laterally by round bars that allow rotation. The wood I-joist web is not supported and is assumed to undergo zero lateral displacement. Displacements and moments at the ends of the wood I-joist for the *x*-axis and *y*-axis equal zero. Mathematically the simply supported end conditions are expressed by the following equations.

$$x(z,t) = 0 \quad \text{and} \quad \frac{\partial^2 x(z,t)}{\partial z^2} = 0 \quad \text{for} \quad z = 0 \quad \text{and} \quad z = L \tag{3-1a}$$

$$y(z,t) = 0 \quad \text{and} \quad \frac{\partial^2 y(z,t)}{\partial z^2} = 0 \quad \text{for} \quad z = 0 \quad \text{and} \quad z = L \tag{3-1b}$$

3.1.2: Fixed Supported End Condition

The fixed supported end condition has no rotation at the ends of the wood I-joist in any direction. This condition is the strongest end fixity that can be reached in theoretical analysis and practical circumstances. The fixed supported end condition is difficult to attain with wood I-joists. However, this supported end condition can be approximated in practice when strong end fixity hangers are used. The fixed supported end condition is shown in Figure 3-2.

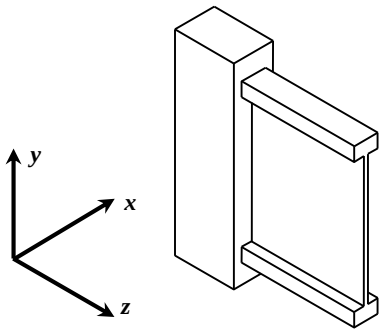

Figure 3-2: Fixed supported end condition.

In the fixed supported end condition, displacements and deflections at the ends of the wood I-joist for the *x*-axis and *y*-axis equal zero. The wood I-joist web is fully supported and is assumed to undergo zero displacement and deflection. Mathematically the fixed end supported conditions are expressed by the following equations.

$$x(z,t) = 0 \quad \text{and} \quad \frac{\partial x(z,t)}{\partial z} = 0 \quad \text{for} \quad z = 0 \quad \text{and} \quad z = L \tag{3-2a}$$

$$y(z,t) = 0 \quad \text{and} \quad \frac{\partial y(z,t)}{\partial z} = 0 \quad \text{for} \quad z = 0 \quad \text{and} \quad z = L \tag{3-2b}$$

3.1.3: Hanger Supported End Condition

The hanger supported end condition is a model of real supported end conditions found in practice in the residential construction industry when wood I-joist hangers are used. Hanger supported end condition allows the ends of the wood I-joist to rotate freely with respect to the principal axis of inertia parallel in the *x*-axis and *y*-axis directions. Lateral displacements at the ends of the wood I-joist in the direction normal to the *y*-*z* plane are restored by springs. Rotation in the *z*-axis is prevented. A physical model of the hanger supported end condition is shown in Figure 3-3. The model uses a spring with a stiffness constant *k* in the lateral direction. The axial support was assumed to be the same as the simply supported end condition. Differences between end fixity from several wood I-joist hangers were incorporated into the diverse models by adjusting the spring stiffness constant *k*. Numerical values for the constant *k* were determined by testing the wood I-joist hangers on their lateral stiffness.

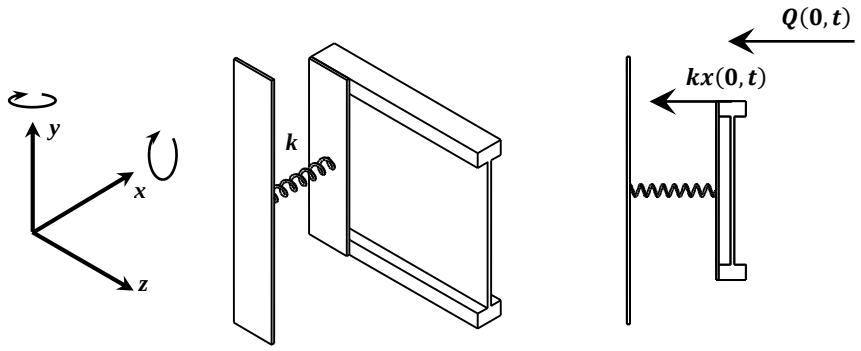

Figure 3-3: Model of a hanger supported end condition.

The reaction force in the spring is $kx(0,t)$. This reaction equals the lateral shear force produced by the wood I-joist. Assuming that the lateral bending stiffness EI_y has a constant value throughout the wood I-joist, the shear force can be expressed with the following equation.

$$Q(z,t) = -EI_y \frac{\partial^3 x(z,t)}{\partial z^3} = kx(z,t) \tag{3-3}$$

In the hanger supported end condition, displacements in the axial direction and moments at the ends equal zero. Mathematically, the hanger fixed end supported condition is expressed by the following equations.

$$\begin{aligned} -EI_y \frac{\partial^3 x(z,t)}{\partial z^3} &= kx(z,t) \quad and \quad \frac{\partial^2 x(z,t)}{\partial z^2} = 0 \quad for \quad z = 0 \\ -EI_y \frac{\partial^3 x(z,t)}{\partial z^3} &= -kx(z,t) \quad and \quad \frac{\partial^2 x(z,t)}{\partial z^2} = 0 \quad for \quad z = L \end{aligned} \tag{3-4a}$$

$$y(z,t) = 0 \quad and \quad \frac{\partial^2 y(z,t)}{\partial z^2} = 0 \quad for \quad z = 0 \quad and \quad z = L \tag{3-4b}$$

3.2: Static Lateral-Torsional Buckling Models

Static loading refers to a gradually increasing load applied at a single point over the top flange of the wood I-joist until lateral-torsional buckling instability occurs. The static lateral-torsional buckling models were developed using the strain energy method. The strain energy method uses approximate functions $\beta(z)$ for the angle of twist that the wood I-joist undergoes under the action of the applied loading. The static lateral-torsional buckling models along with the dynamic bending movement models of the wood I-joists were used to develop the dynamic lateral-torsional buckling models. Assumptions made in the development of the static lateral-torsional buckling models included, the loading was applied at the top flange of the wood I-joist, and small change of energy from axial deflections was neglected.

3.2.1: Static Lateral-Torsional Buckling Model for a Simply End Supported Wood I-Joist

To calculate the static critical lateral-torsional buckling load for a simply supported wood I-joist Equation 2-34 was used. The function $\beta(z)$ for the angle of twist for a simply supported beam was described by Timoshenko (1936).

$$\beta(z) = \sum_{n=1}^{\infty} b_{(2n-1)} \cos\left(\frac{(2n-1)\pi z}{L}\right) \tag{3-5}$$

The best approximation for the static critical lateral-torsional buckling load is obtained by adjusting the coefficients $b_1, b_2, b_3, \ldots$ to minimize Function 3-5. However, by using a single term in Function 3-5, the accuracy of the solution is suitable for practical applications (Timoshenko 1936). Solving Equation 2-34 by considering that the load is applied at the mid-span $\left(s = \frac{L}{2}\right)$ and using a single term for $\beta(z)$ from Function 3-5, the following equation for the static critical lateral-torsional buckling load is obtained for a simply supported wood I-joist.

$$P_{cr} = \left(\left(\frac{24\pi^2 a E I_y}{(6+\pi^2)L^3}\right)^2 + \frac{EI_y GJ + \left(\frac{\pi h E I_y}{2L}\right)^2}{\frac{(6+\pi^2)L^4}{48\pi^4}} \right)^{\frac{1}{2}} - \frac{24\pi^2 a E I_y}{(6+\pi^2)L^3} \tag{3-6}$$

Where a is the distance from the neutral axis of the cross-section to the point in which the load is being applied. If the load is applied at the neutral axis (a equals zero) the accuracy of the remaining equation is 1.0135 greater compared to the solution obtained by solving the system of differential equations of equilibrium. This accuracy is satisfactory for practical applications (Timoshenko 1936). In this research the load was applied at the top flange of the wood I-joist so that a equals $\frac{h}{2}$. Equation 3-6 accounts for the effects of the warping shear stresses. When the warping shear stresses from Equation 3-6 equals zero the remaining equation equals the static critical lateral-torsional buckling load equation for a simply supported rectangular cross-section beams with the load applied at the top surface.

3.2.2: Static Lateral-Torsional Buckling Model for a Fixed End Supported Wood I-Joist

No research was found in the literature for the function $\beta(z)$ for the angle of twist for a fixed supported wood I-joist. Function 3-7 was derived in this research to mathematically describe the torsion that wood I-joist undergoes under the influence of lateral-torsional buckling instability. Function 3-7 was derived by considering the supported end conditions from Equations 3-2.

$$\beta(z) = \sum_{n=1}^{\infty} b_{(2n-1)} \cos\left(\frac{(2n-1)\pi z}{L}\right)^2 \tag{3-7}$$

Function 3-7 can be minimized in the same form as Function 3-5. Solving Equation 2-34 by considering that the load is applied at the mid-span $\left(s = \frac{L}{2}\right)$ and using a single term for $\beta(z)$ from Function 3-7, the following equation shows the static critical lateral-torsional buckling load obtained for a fixed supported wood I-joist.

$$P_{cr} = \left(\left(\frac{64\pi^2 a E I_y}{(17+2\pi^2)L^3} \right)^2 + \frac{E I_y G J + \left(\frac{\pi h E I_y}{L}\right)^2}{\frac{(17+2\pi^2)L^4}{128\pi^4}} \right)^{\frac{1}{2}} - \frac{64\pi^2 a E I_y}{(17+2\pi^2)L^3} \tag{3-8}$$

Comparing Equation 3-6 with Equation 3-8, the warping shear stresses are greater for the simply supported wood I-joist compared to the fixed supported wood I-joist. Solutions derived from the differential equations of equilibrium method for the case of a fixed wood I-joist were not found in the literature. Therefore, Equation 3-8 cannot be compared with exact solutions. When the warping shear stress term from Equation 3-8 equals zero, the remaining equation becomes the static critical lateral-torsional buckling load equation for fixed supported rectangular cross-section beams with the load applied at the top surface.

3.2.3: Static Lateral-Torsional Buckling Model for a Hanger End Supported Wood I-Joist

No research was found in the literature for the function $\beta(z)$ for the angle of twist for a hanger fixed supported wood I-joist. Instead of deriving a new function for $\beta(z)$, Equation 2-34 was modified to account for the effects of the lateral deflections of the wood I-joist hangers modeled by restoring springs placed at the ends of the wood I-joist and Equation 3-5 was used for the function $\beta(z)$. The increase in the wood I-joist strain energy due to lateral deflection and torsion remains the same as for the case of the simply supported wood I-joist since the wood I-joist response to the applied loads does not change. The wood I-joist response to the applied loading is a function of the intensive properties of the wood I-joist including the lateral bending stiffness (EI_y) and torsional rigidity (GJ), which do not change when the specimen is tested under different loading and supported end conditions. So, the only quantity that needs to be readjusted is the work done by the applied load. The work done by the springs W_s can be found using Equation 3-3 and the reaction at the end of the wood I-joist.

$$W_s = \frac{P^2(L-s)^2}{kL^2} \tag{3-9}$$

Incorporating the work done by the springs W_s from Equation 3-9 into Equation 2-34, the following equation to calculate the critical lateral-torsional buckling load for a hanger supported end wood I-joist is obtained.

$$\frac{P^2(L-s)^2}{kL^2}+\frac{Pa\left(\beta(z)\right)^2}{4}+\frac{P^2(L-s)}{EI_yL}\left(\int_0^s\left(\beta(z)(s-z)\right)^2dz-\frac{L-s}{2L}\int_0^L\left(\beta(z)(s-z)\right)^2dz\right)=$$

$$\frac{GJ}{2}\int_0^L\left(\frac{d\beta(z)}{dz}\right)^2dz-\frac{EI_yh^2}{8}\int_0^L\left(\frac{d^3\beta(z)}{dz^3}\frac{d\beta(z)}{dz}\right)dz \tag{3-10}$$

Solving Equation 3-10 by considering that the load is applied at the mid-span $\left(s=\frac{L}{2}\right)$ and using a single term for $\beta(z)$ from Function 2-5, the following equation for the static critical lateral-torsional buckling load is obtained for a hanger fixed supported wood I-joist.

$$P_{cr}=\left(\left(\frac{24\pi^2aEI_y}{(6+\pi^2)L^3+\frac{48\pi^2EI_y}{k}}\right)^2+\frac{EI_yGJ+\left(\frac{\pi hEI_y}{2L}\right)^2}{\frac{(6+\pi^2)L^4}{48\pi^4}+\frac{LEI_y}{\pi^2k}}\right)^{\frac{1}{2}}-\frac{24\pi^2aEI_y}{(6+\pi^2)L^3+\frac{48\pi^2EI_y}{k}} \tag{3-11}$$

Where k is the stiffness constant of the spring. As k approaches infinity, the spring becomes a rigid body and a simply supported wood I-joist is Equation 3-6 is attained. Equation 3-11 was developed to be applied to different hanger supported end conditions by modifying the stiffness constant k of the hanger in the lateral direction.

3.3: Dynamic Lateral-Torsional Buckling Models

In this research dynamic loading refers to the loading applied by an individual walking on the wood I-joist under normal walking. Normal human walking is characterized by a smooth vertical rise and fall of the trunk, occurring once with each step or twice during a gait cycle (Gard and Childress 2001). In a normal human walking only one foot at a time leaves contact with the ground and there is a period of double-support (Pimentel et al. 2001).

The dynamic lateral-torsional buckling models were derived by linearly combining the static lateral-torsional buckling models with the bending motion equations of the wood I-joists. The static lateral torsional buckling models used the total lateral displacement of the wood I-joist generated by the bending motion as initial conditions to find the critical lateral-torsional buckling position of the individual walking on the wood I-joists. The bending motion equations used the lateral component of the force G_{WL} imposed by the individual walking to calculate the total lateral displacement of the wood I-joists. Nakamura and Kawasaki (2006) found that the lateral component of the force G_{WL} imposed by an individual walking under normal walking was of 10% of the vertical component while Huang et al. (2007) found that the same lateral component of the force was 4% of the vertical component. In Equation 2-35 the individual's weight G_W walking on the wood I-joists was substituted by the lateral component of the force G_{WL} to account for the lateral dynamic loading on the wood I-joist.

$$F_{dL}(t)=G_{WL}(H+\textstyle\sum_{n=1}^{m}\alpha_n\sin(2n\pi f_dt+\varphi_n)) \tag{3-12}$$

The bending motion of the wood I-joist was investigated by using Equation 2-42 which was developed for a distributed uniform load, therefore the lateral dynamic loading in Equation 3-12 must be converted to a distributed load. The conversion can be carried out by multiplying Equation 3-12 by the spatial Dirac Delta $\delta(z)$ function and the temporal Heaviside Theta $\Theta(t)$ function as shown in Equation 3-13.

$$f(z,t) = F_{dL}(t)\delta(z-s)\Theta(t) \tag{3-13}$$

When an individual walks on a wood I-joist, the lateral dynamic component of the loading is a discrete loading in which the loading points correspond to the footsteps given by the individual walking. When this discrete loading is applied to Equation 2-42, it produces a unique solution for the wood I-joist bending motion for each footstep given by the individual walking. Consequently, the mathematical description of the response of the wood I-joist to walking would require separate solutions from each footstep from Equation 2-42 that must be summed. This summation creates a complicated and cumbersome solution for the bending motion of the wood I-joist that is challenging for practical applications. Also, the risk of making mistakes when using this solution is increased since a large amount of mathematical information needs to be processed. In this research, a different approach was proposed and developed. The lateral dynamic loading (Equation 3-13) was applied to the wood I-joist at the mid-span and was adjusted by a function $g(t)$ in the time domain. This function simulated the average variation of the response of the wood I-joist to the individual walking. Adjusting functions were developed by taking the ratio of the mid-span wood I-joist response to the wood I-joist response position of the individual walking from the deflection curves of Equation 3-14. To obtain the adjusting functions, the spatial solutions of Equation 3-14 were converted to the time domain. The adjusting functions were derived solving Equation 3-14 for each of the three supported end conditions given by Equations 3-1, 3-2 and 3-4.

$$EI_y \frac{d^2x(z)}{dz^2} - M(z) = 0 \tag{3-14}$$

The adjusting functions comply with the physical characteristics of the response of the wood I-joist to the individual walking. The adjusting functions are zero at the ends, and gradually increase until a maximum value at the mid-span.

3.3.1: Dynamic Lateral-Torsional Buckling Model for a Simply End Supported Wood I-Joist

The dynamic lateral-torsional buckling model for a simply supported wood I-joist was derived by solving Equation 2-42 to find the wood I-joist lateral deflections produced by the individual walking. The lateral dynamic loading $f(z,t)$ was applied from Equation 3-13. The spatial function $\chi_r(z)$ and the frequency of oscillation ω_r were calculated by solving Equation 2-43. The adjusting function $g(t)$ was derived by solving Equations 3-14 using the supported end conditions from Equations 3-1. A normalized solution of Equation 2-43 for a simply supported wood I-joist and for the first natural mode is shown.

$$\chi_r(z) = \sqrt{\frac{2}{mL}} \sin\left(\frac{\pi z}{L}\right) \tag{3-15}$$

The natural frequency of oscillation is shown in Equation 3-16.

$$\omega_r = \pi^2 \sqrt{\frac{EI_y}{mL^4}} \tag{3-16}$$

The adjusting function for a simply supported wood I-joist was derived from Equations 3-14.

$$g(t) = \frac{t\left(3t_T^2 - 4t^2\right)}{t_T^3} \qquad 0 \le t \le \frac{t_T}{2}$$
$$g(t) = \frac{(t_T - t)\left(3t_T^2 - 4(t_T - t)^2\right)}{t_T^3} \qquad \frac{t_T}{2} \le t \le t_T \tag{3-17}$$

Where t_T is the total time needed for the individual walking on the wood I-joist to transverse the wood I-joist from one end to the other.

Figure 3-4 shows the adjusting function from Equation 3-17 and the lateral dynamic load history produced by an individual walking on a simply supported wood I-joist from Equation 3-12 modified by the adjusting function from Equation 3-17. The lateral component of the individual's weight G_{WL} was normalized to a maximum lateral dynamic loading of one pound. All other input parameters were the same than those used in Section 2.3.7. The total time shown in the graph corresponded to the necessary time for the individual walking on the wood I-joist to reach the mid-span of the wood I-joist. Figure 3-4 can be compared with Figure 2-4 which shows the dynamic load history for one individual walking on a common surface.

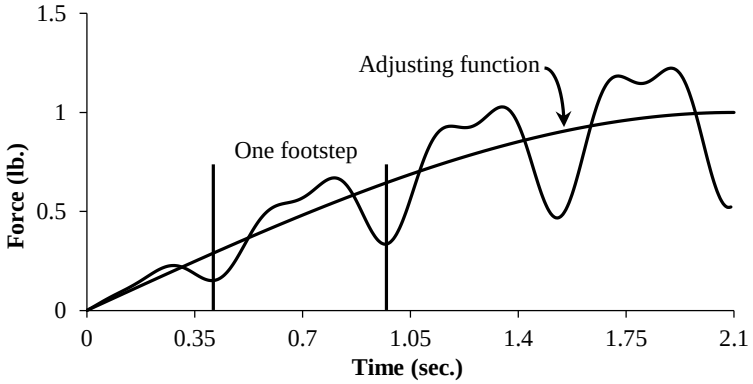

Figure 3-4: Vertical dynamic load history for an individual walking on a simply supported wood I-joist modified by an adjusting function.

For a simply supported wood I-joist the bending motion equation was developed by solving Equation 2-42. The lateral dynamic loading $f(z,t)$ was substituted from Equation 3-13. The spatial function $\chi_r(z)$ was substituted from Equation 3-15. The frequency of oscillation ω_r was substituted from Equation 3-16. The adjusting function $g(t)$ was substituted from Equation 3-17. The bending motion equation for a simply supported wood I-joist is shown in Equation 3-18.

$$x(z,t) = \frac{L^3\sqrt{2mL}\left(1-\cos\left(\pi^2 t\sqrt{\frac{EI_y}{mL^4}}\right)\right)g(t)F_{dL}(t)\chi_r(z)}{\pi^4 EI_y} \tag{3-18}$$

Equation 3-18 permits the calculation of the wood I-joist lateral deflections when an individual is walking on the wood I-joist for simply supported end conditions. The work done to produce the wood I-joist lateral deflection at the point in which the individual walking is positioned along the wood I-joist span was inserted into Equation 2-34 to calculate the dynamic critical lateral-torsional buckling position of the individual walking on a simply supported wood I-joist.

3.3.2: Dynamic Lateral-Torsional Buckling Model for a Fixed End Supported Wood I-Joist

The dynamic lateral-torsional buckling model for a fixed wood I-joist was derived by solving Equation 2-42 to find the wood I-joist deflections produced by the individual walking. The lateral dynamic loading $f(z,t)$ was applied from Equation 3-13. The spatial function $\chi_r(z)$ and the frequency of oscillation ω_r were calculated by solving Equation 2-43. The adjusting function $g(t)$ was derived by solving Equation 3-14 using the supported end conditions from Equations 3-2. A normalized solution of Equation 2-43 for a fixed wood I-joist and for the first natural mode is Equation 3-19.

$$\chi_r(z) = \frac{\cosh\left(\frac{4.730z}{L}\right) - \cos\left(\frac{4.730z}{L}\right) - 0.982\left(\sinh\left(\frac{4.730z}{L}\right) - \sin\left(\frac{4.730z}{L}\right)\right)}{\sqrt{mL}} \tag{3-19}$$

The natural frequency of oscillation is given by Equation 3-20.

$$\omega_r = 22.375\sqrt{\frac{EI_y}{mL^4}} \tag{3-20}$$

The adjusting function was derived by solving Equation 3-14 for a fixed wood I-joist.

$$\begin{aligned} g(t) &= \frac{t^2(12t_T - 16t)}{t_T^3} \qquad 0 \le t \le \frac{t_T}{2} \\ g(t) &= \frac{(t_T - t)^2(16t - 4t_T)}{t_T^3} \qquad \frac{t_T}{2} \le t \le t_T \end{aligned} \tag{3-21}$$

Figure 3-5 is a graph of the adjusting function from Equation 3-21 and the lateral dynamic load history produced by an individual walking on a fixed supported wood I-joist from Equation 3-12 modified by the adjusting function from Equation 3-21. The lateral component of the individual's weight G_{WL} was normalized to a maximum lateral dynamic loading of one pound. All other input parameters were the same than those used in Section 2.3.7. The total time shown in the graph corresponded to the necessary time for the individual walking on the wood I-joist to reach the mid-span of the wood I-joist. Figure 3-5 can be compared with Figure 2-4, which shows the dynamic load history for one individual walking on a common surface.

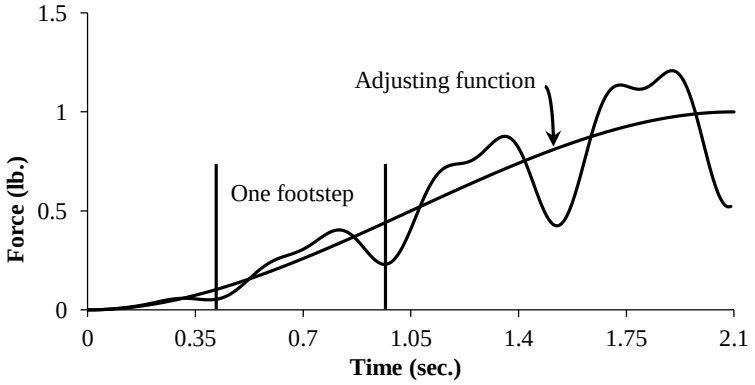

Figure 3-5: Vertical dynamic load history for an individual walking on a fixed supported wood I-joist modified by an adjusted function.

For a fixed supported wood I-joist the bending motion equation was developed by solving Equation 2-42. Equation 3-13 was inserted into Equation 2-42 to account for the lateral dynamic loading $f(z,t)$ from the individual walking on the wood I-joist. The spatial function $\chi_r(z)$ was substituted from Equation 3-19. The frequency of oscillation ω_r was substituted from Equation 3-20. The adjusting function $g(t)$ was substituted from Equation 3-21. The bending motion equation for a fixed supported wood I-joist is shown in Equation 3-22.

$$x(z,t) = \frac{0.00318L^3\sqrt{mL}\left(1-\cos\left(22.375t\sqrt{\frac{EI_y}{mL^4}}\right)\right)g(t)F_{dL}(t)\chi_r(z)}{EI_y} \tag{3-22}$$

Equation 3-22 permits the calculation of the wood I-joist deflections when an individual is walking on a fixed supported wood I-joist. The work done to produce the wood I-joist lateral deflection at the point in which the individual walking is positioned along the wood I-joist span was inserted into Equation 2-34 to calculate the dynamic critical lateral-torsional buckling position of the individual walking on a fixed supported wood I-joist.

Figure 3-6 is a comparison graph between the adjusting functions from the simply and the fixed supported end conditions. The lateral component of the dynamic force imposed by the individual walking on the wood I-joist was normalized to one pound for both functions. All other input parameters were the same than those used in Section 2.3.7. The total time shown in the graph corresponded to the necessary time for the individual walking on the wood I-joist to reach the mid-span of the wood I-joist. The adjusting function and consequently the lateral dynamic load history for the individual walking on the wood I-joist for the fixed supported end condition are more constricting showing smaller effects at the beginning of the graph than the simply supported end condition. The adjusting functions of Figure 3-6 are not intended to show the wood I-joist deflections rather, the graph shows how the lateral component of the individual walking is applied to the wood I-joist depending upon of the wood I-joist supported end conditions.

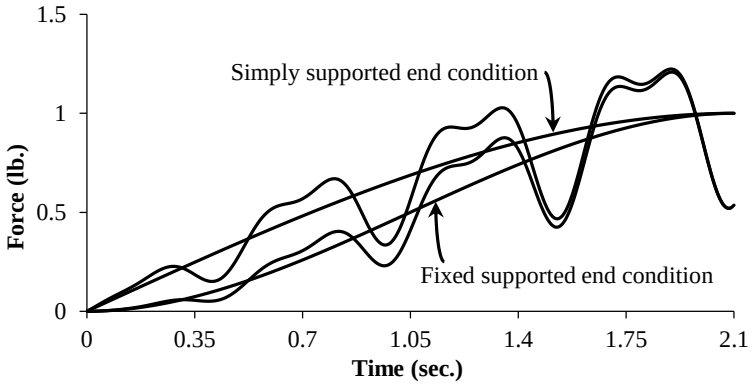

Figure 3-6: Adjusting functions comparing the simply and the fixed supported end conditions.

Figure 3-7 is a graph of the hypothetical oscillations of the wood I-joist lateral deflection and the adjusting function under lateral dynamic loading from an individual walking on the wood I-joist. The wood I-joist response to the dynamic loading increases as the lateral deflection of the wood I-joist increases. The wood I-joist lateral deflection increases as the individual walking on the wood I-joists approaches to the wood I-joists mid-span.

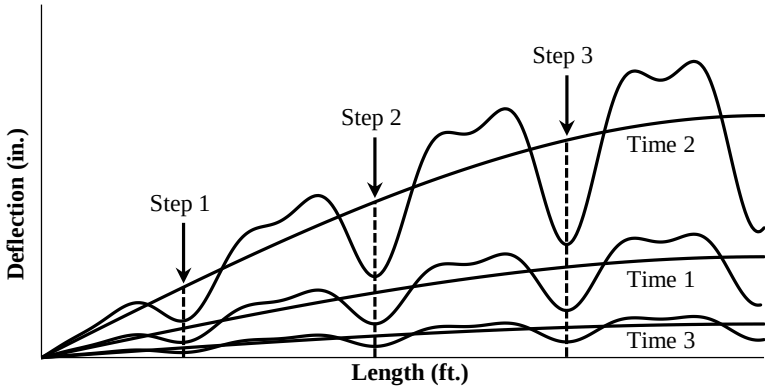

Figure 3-7: Hypothetical oscillations of the wood I-joist lateral deflection and the adjusting function.

According to Equations 3-18 and 3-22, the wood I-joist deflections depend on both the position of the footsteps given by the individual and the weight of the individual, so heavier individuals not necessarily produce larger wood I-joist deflections. Individual deflections for each given footstep are linearly added to each other.

3.3.3: Dynamic Lateral-Torsional Buckling Model for a Hanger End Supported Wood I-Joist

The dynamic lateral-torsional buckling model for a hanger fixed wood I-joist was derived by solving Equation 2-42 to find the wood I-joist deflections produced by the individual walking. The lateral dynamic loading $f(z,t)$ was applied from Equation 3-13. The spatial function $\chi_r(z)$ and the frequency of oscillation ω_r were calculated by solving Equation 2-43 applying the supported end conditions given by Equation 3-4. The stiffness constant k of the spring remained unspecified in the spatial function $\chi_r(z)$ and in the frequency of oscillation ω_r. The adjusting function $g(t)$ was derived by solving Equation 3-14 using the supported end conditions from Equations 3-4. Similarly, the stiffness constant k of the spring remained unspecified in the adjusting function $g(t)$. A solution of Equation 2-43 for a hanger fixed wood I-joist is shown.

$$\chi_r(z) = \frac{2Ak(\sinh L\psi \sin z\psi + \sin L\psi \sinh z\psi)}{2k \sinh L\psi + (\cos L\psi - \cosh L\psi)\psi^3 EI_y} +$$

$$\frac{A\big((\sinh L\psi - \sin L\psi)\cos z\psi + (\sinh L\psi - \sin L\psi)\cosh z\psi + (\cos L\psi - \cosh L\psi)\sin z\psi + (\cos L\psi - \cosh L\psi)\sinh z\psi\big)\psi^3 EI_y}{2k \sinh L\psi + (\cos L\psi - \cosh L\psi)\psi^3 EI_y} \quad (3\text{-}23)$$

The constant A is to be determined when normalizing Equation 3-23 to satisfy conditions of Equation 2-41. To calculate the term ψ the transcendental equation for ψ in Equation 3-24 must be solved. Equation 3-24 needs to be solved after determining the value for both, the stiffness constant k of the spring and the lateral bending stiffness of the wood I-joist.

$$\psi^6(\cos L\psi \cosh L\psi - 1)EI_y^2 + 2k\psi^3(\cosh L\psi \sin L\psi - \cos L\psi \sinh L\psi)EI_y - 2k^2 \sin L\psi \sinh L\psi = 0 \quad (3\text{-}24)$$

The frequencies of oscillation for a hanger fixed wood I-joist are given in Equation 3-25. The variation of oscillations between wood I-joist hangers is involved in the constant ψ which is different for different values of the stiffness constant k of the spring according with Equation 3-24.

$$\omega_r = (L\psi)^2 \sqrt{\frac{EI_y}{mL^4}} \quad (3\text{-}25)$$

The adjusting function was derived by solving Equation 3-14 for a hanger fixed wood I-joist. The boundary conditions were taken from Equations 3-4.

$$g(t) = \frac{t\left(3t_T^2 - 4t^2\right) + \frac{24EI_y}{kV^3}}{t_T^3 + \frac{24EI_y}{kV^3}} \qquad 0 \le t \le \frac{t_T}{2}$$
$$g(t) = \frac{(t_T - t)\left(3t_T^2 - 4(t_T - t)^2\right) + \frac{24EI_y}{kV^3}}{t_T^3 + \frac{24EI_y}{kV^3}} \qquad \frac{t_T}{2} \le t \le t_T \tag{3-26}$$

Where V is a constant used to transform Equation 3-26 from the spatial domain to the time domain. The constant V always equals one and has units of length divided by units of time (e.g. m/s, in/s). When the lateral stiffness of the wood I-joist hanger k of Equation 3-26 approaches infinite the equation becomes Equation 3-17 which is the adjusting function for the simply supported wood I-joist. Equation 3-26 shows that the adjusting functions for the hanger supported wood I-joist depend on both the lateral stiffness of the wood I-joist EI_y and the lateral stiffness of the wood I-joist hanger k.

For a hanger fixed wood I-joist, the bending motion equation was developed by solving Equation 2-42. Equation 3-13 was substituted into Equation 2-42 to account for the lateral dynamic loading $f(z,t)$. The spatial function $\chi_r(z)$ was substituted from Equation 3-23. The frequency of oscillation ω_r was substituted from Equation 3-25. The adjusting function $g(t)$ was substituted from Equation 3-26. The bending motion equation for a hanger fixed wood I-joist is shown in Equation 3-27.

$$x(z,t) = \frac{L^4 m\left(1 - \cos\left((L\psi)^2 t\sqrt{\frac{EI_y}{mL^4}}\right)\right)\left(\frac{2A\left(\cos\frac{L\psi}{2} + \cosh\frac{L\psi}{2}\right)\left(\left(EI_y\psi^3\cos\frac{L\psi}{2} + 2k\sin\frac{L\psi}{2}\right)\sinh\frac{L\psi}{2} - EI_y\psi^3\cosh\frac{L\psi}{2}\sin\frac{L\psi}{2}\right)}{EI_y\psi^3(\cos L\psi - \cosh L\psi) + 2k\sinh L\psi}\right) g(t)F_{dL}(t)\chi_r(z)}{(L\psi)^4 EI_y} \tag{3-27}$$

Equation 3-27 permits the calculation of the wood I-joist deflections when an individual is walking on a hanger supported wood I-joist. The work done to produce the wood I-joist lateral deflection at the point in which the individual walking is positioned along the wood I-joist span was inserted into Equation 2-34 to calculate the dynamic critical lateral-torsional buckling position of the individual walking on a hanger supported wood I-joist. When the lateral stiffness constant k of the wood I-joist hangers approaches infinity, Equations 3-23, 3-25 and 3-27 approximate Equations 3-15, 3-16 and 3-18 respectively demonstrating that when k approaches infinity, the hanger fixed supported end condition becomes the simply supported end condition.

3.4: Bracing Systems

Three different cross bracing systems in a lean-on configuration were used in this research: non-bracing, one mid-span bracing, and two quarter-span bracing (Figure 3-4). Mathematical bracing models were developed to calculate the static critical lateral-torsional buckling loads and the bending motion of the wood I-joists when a particular bracing system in a lean-on configuration is applied to the assembly. The static lateral-torsional buckling models were derived by adjusting in the previous models derived in Section 3.2 the lateral bending

stiffness and the torsional rigidity of the wood I-joist. The bending motion of the wood I-joist models were derived by adjusting in the previous models derived in section 3.3 the lateral bending stiffness and the mass of the wood I-joist. The wood I-joist length, the cross-section of the wood I-joist and the loading position with respect to the wood I-joist depth were not adjusted since in this research they are constant (in this research the main wood I-joist is of the same type than the braced wood I-joists). As before, the dynamic critical lateral-torsional buckling models for the position of an individual walking on the wood I-joist was calculated by linearly combining the bending motion of the wood I-joist models with the static lateral-torsional buckling models when a cross bracing system in a lean-on configuration was used. Mathematical models were derived for each one of the three supported end conditions under investigation: simply supported, fixed supported and hanger fixed supported.

No research was found in the literature to mathematically describe the brace reactions that lean-on systems have on the loaded wood I-joist. Assumptions for the bracing models include: buckling of the loaded wood I-joist required all braced wood I-joists to buckle with the same lateral displacement and rotation, all loads were within the elastic range of the materials, the bracing members were perfectly rigid and stiff, reactions at the bracing points were fully transmitted from the loaded wood I-joist through the braces to the other wood I-joists, reactions transmitted through the braces were zero at the ends of the wood I-joist and had the maximum effect at the loading point, the supported end conditions were the same for all wood I-joists in the bracing system, all wood I-joists in the system had the same length and the bracing system was symmetric with respect to the mid-span of the wood I-joists.

The adjusted lateral bending stiffness $EI_{y_{Ad}}$, the adjusted torsional rigidity GJ_{Ad} and the adjusted mass m_{Ad} of the wood I-joist when a bracing system is installed in a lean-on configuration were derived in this research as Equations 3-28.

$$\begin{aligned} EI_{y_{Ad}} &= EI_{y_L} + \frac{x[w]}{x[z]}\left(\sum_{i=1}^{n} EI_{y_{bi}}\right) \\ GJ_{Ad} &= GJ_L + \frac{x[w]}{x[z]}\left(\sum_{i=1}^{n} GJ_{bi}\right) \\ m_{Ad} &= m_L + \frac{x[w]}{x[z]}\left(\sum_{i=1}^{n} m_{bi}\right) \end{aligned} \tag{3-28}$$

Where, EI_{y_L}, GJ_L, and m_L are the lateral bending stiffness, torsional rigidity and mass of the wood I-joist in which the load is being applied and $EI_{y_{bi}}$, GJ_{bi} and m_{bi} are the lateral bending stiffness, torsional rigidity and mass of the wood I-joists braced to the wood I-joist in which the load is being applied. The ratio $\frac{x[w]}{x[z]}$ is composed by the lateral deflection of the wood I-joist at the bracing point in which the load is being applied $x[w]$ and the lateral deflection of the same wood I-joist but at the loading point $x[z]$ (Figure 3-8).

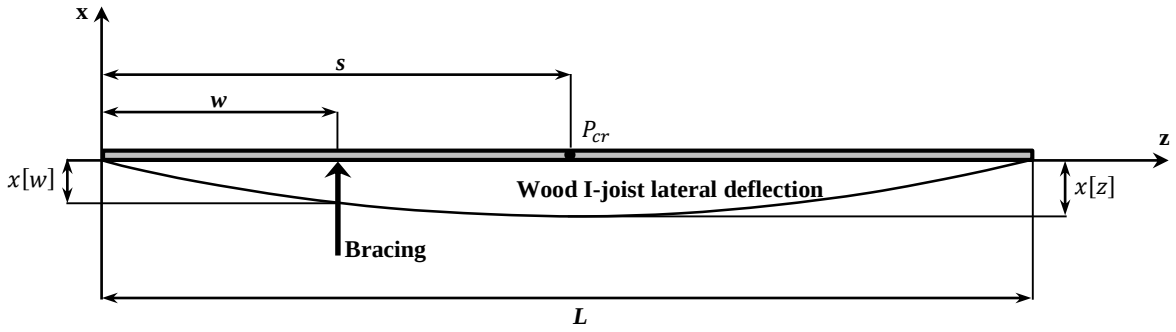

Figure 3-8: Lateral deflection of a lateral-torsional buckled wood I-joist. Top view.

The $x[w]$ and $x[z]$ lateral deflections of the wood I-joist can be calculated by solving the following differential equations.

$$x[w] = EI_{y_L} \frac{d^2x(w)}{dw^2} - M(w) = 0 \tag{3-29a}$$

$$x[z] = EI_{y_L} \frac{d^2x(z)}{dz^2} - M(z) = 0 \tag{3-29b}$$

In this research, bending lateral deflections from the lateral-torsional buckled wood I-joist are used to adjust the lateral bending stiffness, torsional rigidity and mass of the wood I-joist when a bracing system in a lean-on configuration is used, so it is assumed that the ratio of the lateral deflection at the bracing point to the lateral deflection at the loading point is approximately equal to the ratio of the torsional displacement at the bracing point to the torsional displacement at the loading point and also it is approximately equal to the ratio of the second derivative of the lateral deflection at the bracing point (lateral acceleration of a differential element of the wood I-joist at the bracing point) to the second derivative of the lateral deflection at the loading point (lateral acceleration of a differential element of the wood I-joist at the loading point). Taking the lateral deflection ratio instead of the torsional displacement ratio simplifies considerably the calculations otherwise the final models describing the lateral-torsional buckling behavior of a wood I-joist with a bracing system would be cumbersome and difficult to be applied in practical circumstances. The ratio of the lateral deflection at the bracing point to the lateral deflection at the loading point of the wood I-joist in which the load is being applied is used in this research since these lateral deflections are mathematical functions of the wood I-joist reactions at the bracing and loading points. Equations 3-29 must be solved along with the supported end conditions for each case, simply supported, fixed supported and hanger fixed supported for the current research.

3.4.1: Lateral-Torsional Buckling Bracing Models for Simply End Supported Wood I-Joists

Solving Equations 3-29 along with the supported end conditions given by Equations 3-1 the following equations were obtained to adjust the lateral bending stiffness, the torsional rigidity and the mass of a simply supported wood I-joist when a bracing system in a lean-on configuration is applied to it.

$$EI_{y_{Ad}} = EI_{y_L} + \frac{w(2sL - w^2 - s^2)\left(\sum_{i=1}^{n} EI_{y_{bi}}\right)}{2(L-s)s^2} \qquad w \leq s$$

$$GJ_{Ad} = GJ_L + \frac{w(2sL - w^2 - s^2)\left(\sum_{i=1}^{n} GJ_{bi}\right)}{2(L-s)s^2} \qquad w \leq s \tag{3-30}$$

$$m_{Ad} = m_L + \frac{w(2sL - w^2 - s^2)\left(\sum_{i=1}^{n} m_{bi}\right)}{2(L-s)s^2} \qquad w \leq s$$

In Equations 3-30, w is the distance from the end of the wood I-joist to the bracing point and s is the distance from the end of the wood I-joist to the loading point. In Figure 3-9 is observed that the distance w is always smaller or equal to the distance s. The term $\frac{w(2sL-w^2-s^2)}{2(L-s)s^2}$ from Equations 3-30 equals 1.0 for the one mid-span brace configuration as expected since the load and braces are applied at the mid-span. The term $\frac{w(2sL-w^2-s^2)}{2(L-s)s^2}$ equals $\frac{11}{16}$ for the two quarter-span braces configuration. Equations 3-30 demonstrates that a bracing system is more effective when applied at the mid-span compared to bracing applied away from the mid-span. For the one mid-span brace configuration and assuming that the lateral bending stiffness, the torsional rigidity and the mass of the three wood I-joists have the same value respectively, the term $\frac{w(2sL-w^2-s^2)}{2(L-s)s^2}$ proves that the static critical lateral-torsional buckling load for simply supported wood I-joists is three times larger compared with the static critical lateral-torsional buckling load for the same wood I-joist without the bracing system, for the two quarter-span braces configuration the difference was around two times larger.

When the distance from the end of the wood I-joist to the bracing point w equals zero in equations 3-30, the bracing points are localized at the end supports and the term $\frac{w(2sL-w^2-s^2)}{2(L-s)s^2}$ becomes zero. The result obtained in this way from Equations 3-30 equals the lateral bending stiffness, the torsional rigidity and the mass of the wood I-joists without the bracing respectively.

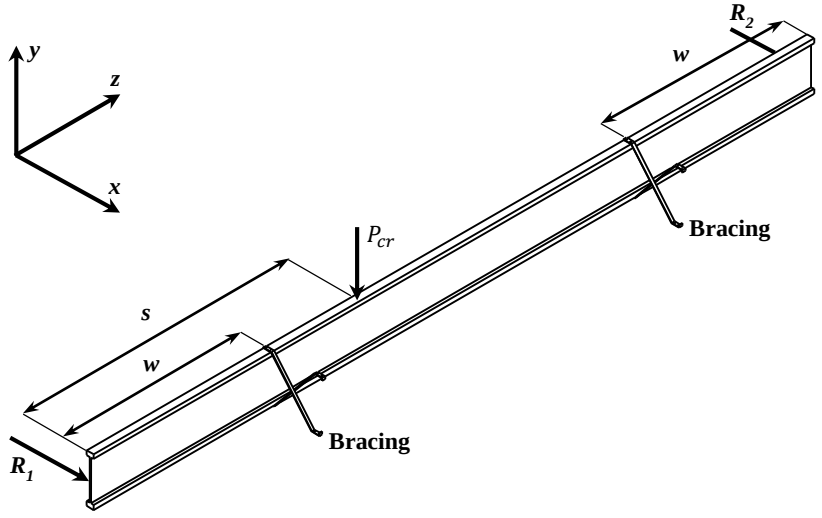

Figure 3-9: Wood I-joist with a bracing system in a lean-on configuration.

To calculate the static critical lateral-torsional buckling load at the mid-span for a simply supported wood I-joist with a bracing system, Equation 3-6 is used in which the lateral bending stiffness and the torsional rigidity are replaced for the adjusted lateral bending stiffness and the adjusted torsional rigidity from Equations 3-30. To calculate the static critical lateral-torsional buckling load at any point along the wood I-joist span for a simply supported wood I-joist with a bracing system, Equation 2-34 is used in which the lateral bending stiffness and the torsional rigidity are replaced for the adjusted lateral bending stiffness and the adjusted torsional rigidity from Equations 3-30, and the function $\beta(z)$ for the angle of twist is taken from Equation 3-5. To calculate the bending motion of the wood I-joist with a bracing system, Equation 3-18 is with the lateral bending stiffness and the mass replaced by the adjusted lateral bending stiffness and the adjusted mass from Equations 3-30. The calculation of the critical lateral-torsional buckling position of an individual walking on the wood I-joist with a bracing system is carried out by linearly combining the static lateral-torsional buckling equation with the lateral deflection from bending motion equation, both equations must describe the same bracing system.

3.4.2: Lateral-Torsional Buckling Bracing Models for Fixed End Supported Wood I-Joists

Solving Equations 3-29 according with the supported end conditions given by Equations 3-2 and inserting the solutions into Equations 3-28, the following equations for the adjusted lateral bending stiffness, the adjusted torsional rigidity and the adjusted mass for a fixed wood I-joist with a bracing system in a lean-on configuration were obtained.

$$\begin{aligned} EI_{y_{Ad}} &= EI_{y_L} + \frac{w^2(3sL-wL-2ws)\left(\sum_{i=1}^{n} EI_{y_{bi}}\right)}{2(L-s)s^3} \qquad w \le s \\ GJ_{Ad} &= GJ_L + \frac{w^2(3sL-wL-2ws)\left(\sum_{i=1}^{n} GJ_{bi}\right)}{2(L-s)s^3} \qquad w \le s \\ m_{Ad} &= m_L + \frac{w^2(3sL-wL-2ws)\left(\sum_{i=1}^{n} m_{bi}\right)}{2(L-s)s^3} \qquad w \le s \end{aligned} \tag{3-31}$$

The term $\frac{w^2(3sL-wL-2ws)}{2(L-s)s^3}$ from Equations 3-31 equals 1.0 for the one mid-span brace configuration as expected since the load and braces are applied at the mid-span. The term $\frac{w^2(3sL-wL-2ws)}{2(L-s)s^3}$ equals $\frac{1}{2}$ for the two quarter-span braces configuration. For the one mid-span brace configuration assuming that the lateral bending stiffness, the torsional rigidity and the mass of the three wood I-joists in the bracing system have the same value respectively the term $\frac{w^2(3sL-wL-2ws)}{2(L-s)s^3}$ proves that the static critical lateral-torsional buckling load for simply supported wood I-joists is three times larger compared with the static critical lateral-torsional buckling load for the same wood I-joist without the bracing system. For the two quarter-span braces configuration, the difference was 1.5 times larger. Lean-on bracing systems are more restrictive for simply supported wood I-joists compared to fixed wood I-joists.

When the distance from the end of the wood I-joist to the bracing point *w* equals zero in equations 3-31, the bracing points are localized at the end supports and the term $\frac{w^2(3sL-wL-2ws)}{2(L-s)s^3}$ becomes zero, and the result obtained

from Equations 3-31 equals the lateral bending stiffness, the torsional rigidity and the mass of the wood I-joists without the bracing respectively.

To calculate the static critical lateral-torsional buckling load at the mid-span for a fixed wood I-joist with a bracing system, Equation 3-8 is used in which the lateral bending stiffness and the torsional rigidity are replaced for the adjusted lateral bending stiffness and the adjusted torsional rigidity from Equations 3-31. To calculate the static critical lateral-torsional buckling load at any point along the wood I-joist length for a fixed wood I-joist with a bracing system, Equation 2-34 is used in which the lateral bending stiffness and the torsional rigidity are replaced for the adjusted lateral bending stiffness and the adjusted torsional rigidity from Equations 3-31, and the function $\beta(z)$ for the angle of twist is taken from Equation 3-7. To calculate the bending motion of the wood I-joist with a bracing system Equation, 3-22 is used in which the lateral bending stiffness and the mass are replaced by the adjusted lateral bending stiffness and the adjusted mass from Equations 3-31.

3.4.3: Lateral-Torsional Buckling Bracing Models for Hanger End Supported Wood I-Joists

Solving Equations 3-29 according with the supported end conditions given by Equations 3-4 and inserting the solutions into Equations 3-28, the following equations for the adjusted lateral bending stiffness, the adjusted torsional rigidity and the adjusted mass for a hanger fixed wood I-joist with a bracing system in a lean-on configuration were obtained.

$$EI_{y_{Ad}} = EI_{y_L} + \frac{\left(kwL(L-s)(2sL-w^2-s^2)+6EI_{y_L}(L^2+2ws-wL-sL)\right)\left(\sum_{i=1}^{n} EI_{y_{bi}}\right)}{2\left(ks^2L(L-s)^2+3EI_{y_L}(2s^2-2sL+L^2)\right)} \qquad w \le s$$

$$GJ_{Ad} = GJ_L + \frac{\left(kwL(L-s)(2sL-w^2-s^2)+6EI_{y_L}(L^2+2ws-wL-sL)\right)\left(\sum_{i=1}^{n} GJ_{bi}\right)}{2\left(ks^2L(L-s)^2+3EI_{y_L}(2s^2-2sL+L^2)\right)} \qquad w \le s \qquad (3\text{-}32)$$

$$m_{Ad} = m_L + \frac{\left(kwL(L-s)(2sL-w^2-s^2)+6EI_{y_L}(L^2+2ws-wL-sL)\right)\left(\sum_{i=1}^{n} m_{bi}\right)}{2\left(ks^2L(L-s)^2+3EI_{y_L}(2s^2-2sL+L^2)\right)} \qquad w \le s$$

The term $\frac{\left(kwL(L-s)(2sL-w^2-s^2)+6EI_{y_L}(L^2+2ws-wL-sL)\right)}{2\left(ks^2L(L-s)^2+3EI_{y_L}(2s^2-2sL+L^2)\right)}$ from Equation 3-32 equals 1.0 for the one mid-span lean-on brace configuration as expected since the load and brace are applied at the mid-span. The term $\frac{\left(kwL(L-s)(2sL-w^2-s^2)+6EI_{y_L}(L^2+2ws-wL-sL)\right)}{2\left(ks^2L(L-s)^2+3EI_{y_L}(2s^2-2sL+L^2)\right)}$ equals $\frac{11}{16}+\frac{15EI_{y_L}}{48EI_{y_L}+2kL^3}$ for the two quarter-span braces. Results show that when the stiffness constant k of the spring approaches infinity, the term $\frac{\left(kwL(L-s)(2sL-w^2-s^2)+6EI_{y_L}(L^2+2ws-wL-sL)\right)}{2\left(ks^2L(L-s)^2+3EI_{y_L}(2s^2-2sL+L^2)\right)}$ approaches $\frac{11}{16}$ which is the case for simply supported wood I-joists. Thus, the hanger fixed supported end condition can be bounded by the simply supported end condition.

When the distance from the end of the wood I-joist to the bracing point *w* equals zero in equations 3-32, the bracing points are localized at the end supports of the wood I-joist and the term

$\frac{\left(kwL(L-s)(2sL-w^2-s^2)+6EI_{y_L}(L^2+2ws-wL-sL)\right)}{2\left(ks^2L(L-s)^2+3EI_{y_L}(2s^2-2sL+L^2)\right)}$ should become zero. However, the fact that having the braces at the ends of the wood I-joist the lateral hanger stiffness k becomes inevitably infinity (in this research the braces were considered and modeled as having infinity stiffness) and therefore the physical test loses any tangible sense. In the same way, the mathematical relationship of the term $\frac{\left(kwL(L-s)(2sL-w^2-s^2)+6EI_{y_L}(L^2+2ws-wL-sL)\right)}{2\left(ks^2L(L-s)^2+3EI_{y_L}(2s^2-2sL+L^2)\right)}$ in Equation 3-32 remains indeterminate when w equals zero and k reaches the infinity value. Thus, the physical conditions correspond to the mathematical relationships.

To calculate the static critical lateral-torsional buckling load at the mid-span for a hanger fixed wood I-joist with a bracing system, Equation 3-11 is used in which the lateral bending stiffness and the torsional rigidity are replaced for the adjusted lateral bending stiffness and the adjusted torsional rigidity from Equations 3-32. To calculate the static critical lateral-torsional buckling load at any point along the wood I-joist length for a fixed wood I-joist with a bracing system, Equation 3-10 is used in which the lateral bending stiffness and the torsional rigidity are replaced for the adjusted lateral bending stiffness and the adjusted torsional rigidity from Equations 3-32, and the function $\beta(z)$ for the angle of twist is taken from Equation 3-5. To calculate the bending motion of the wood I-joist with a bracing system Equation 3-27 is used in which the lateral bending stiffness and the mass are replaced by the adjusted lateral bending stiffness and the adjusted mass from Equations 3-32.

3.5: Conclusion to Theoretical Models

Static lateral-torsional buckling models were developed for each one of the three supported end conditions under investigation: simply supported, fixed supported and hanger fixed supported. The hanger fixed supported condition was derived to include various wood I-joist hangers found in practical circumstances in the residential construction industry. The dynamic lateral-torsional buckling models were developed by linearly combining the static lateral-torsional buckling models with the lateral deflection of the wood I-joist from the bending motion equations. The bending motion equations used the lateral component of the force imposed by an individual walking on the wood I-joists to calculate the lateral deflection of the wood I-joists. The static and dynamic lateral-torsional buckling models were applied to three different bracing systems: no-bracing, one mid-span brace and two quarter-span braces. The bracing models describe the amount of bracing restrain on the lateral-torsional buckling instability. The bracing models were developed for each of the three supported end conditions.

4: Materials and Methods

This chapter describes the materials and testing protocols used in this research. Tests conducted included: lateral bending stiffness tests, torsional rigidity tests, lateral hanger stiffness tests, static lateral-torsional buckling tests and dynamic lateral-torsional buckling tests. Static and dynamic lateral-torsional buckling tests were conducted on five different supported end conditions with three different bracing systems. The lateral bending stiffness and the torsional rigidity of the wood I-joists were used as input parameters to calculate the static critical lateral-torsional buckling loads. The lateral bending stiffness of the wood I-joists was also used to calculate the lateral wood I-joist deflections under dynamic loading. The lateral hanger stiffness was used as the value of the constant k of the spring supports in the theoretical models. Static and dynamic lateral-torsional buckling regression analysis models were derived using the data from the different tests.

4.1: Wood I-Joists

Wood I-joists used in this research were composed of solid sawn lumber (SSL) flanges and oriented strand board (OSB) webs. Two different cross-section wood I-joist sizes were used as shown in Table 4-1 and Figure 4-1. The length of the wood I-joists was of 240 inches for both cross-section sizes. The installation of the wood I-joists for testing followed the manufacturer published instructions when information was available.

Table 4-1: Wood I-Joist Compound Materials and Dimensions.

	Flanges			Web		Wood I-joists	
	Material	**Width (in.)**	**Depth (in.)**	**Material**	**Thickness (in.)**	**Height (in.)**	**Length (in.)**
Sample 1	SSL	2 7/16	1 1/2	OSB	7/16	11 7/8	240
Sample 2	SSL	2 7/16	1 1/2	OSB	7/16	16	240

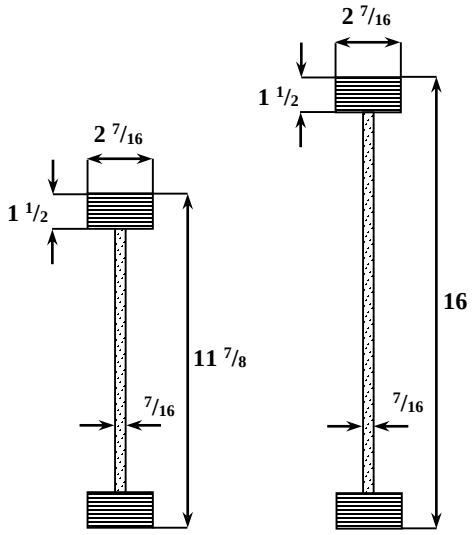

Figure 4-1: Cross section dimensions of the wood I-joists (inches).

4.2: Wood I-Joists Hangers

To investigate various supported end conditions, four different types of wood I-joist hangers were used. Wood I-joists hangers were ITS hanger series, ITT hanger series, IUS hanger series and IUT hanger series all of them from Simpson Strong-Tie Company, Inc. Wood I-joist hangers are shown in Figure 4-2. All wood I-joist hangers were die-formed from 18 gage galvanized steel. All wood I-joist hangers were meant to connect wood I-joists to supporting wood beams. The ITS hanger has a top flange depth of $1^{7}/_{16}$ inches and two large prongs at the seat that are used to resist uplift forces (ESR-2615 2008). The ITT hanger has a top flange depth of $1^{3}/_{8}$ inches and two bend tabs at the seat that are used to fasten the hanger to the wood I-joist. The bend tabs are bent over and nailed into the wood I-joist bottom flange when web stiffeners are not used. Alternatively, the bend tabs may remain unbent when used with web stiffeners and nails are installed directly into the web stiffeners (ESR-2615 2008). The IUS hanger has two large prongs at the seat that are used to resist uplift forces (ESR-2552 2008). The IUT hanger has two steel tabs located at the bottom flange of an installed wood I-joist that are bent over and nailed to the top surface of the bottom flange of a wood I-joist at the jobsite (ESR-2552 2008).

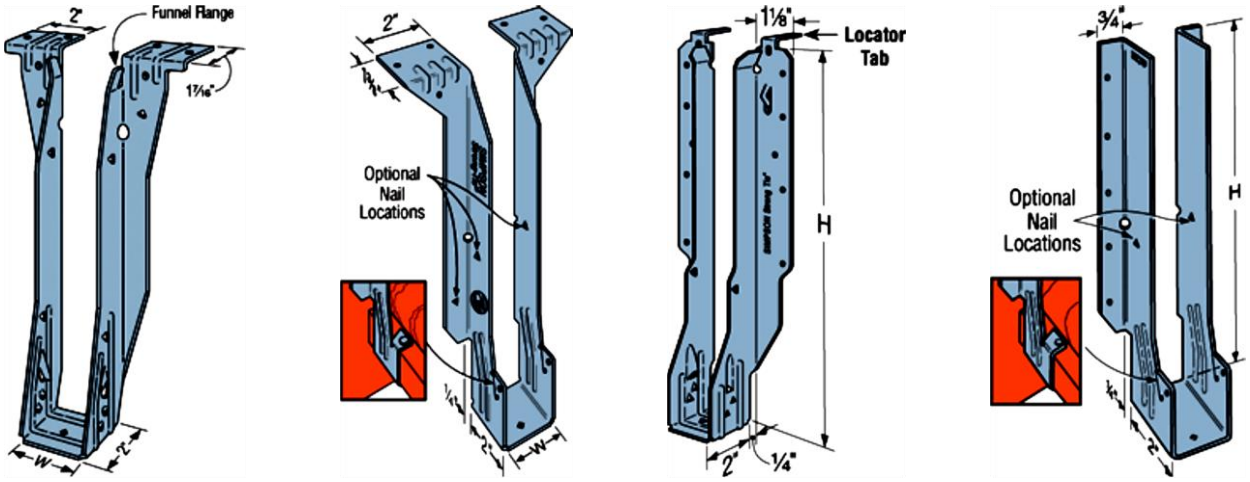

ITS Hanger **ITT Hanger** **IUS Hanger** **IUT Hanger**

Figure 4-2: Wood I-joist hangers used for testing. Simpson Strong-Tie Company, Inc.

4.3: Sample Size

Sample sizes for the two wood I-joist types were determined with Equation 4-1 (ASTM 2005b). The confidence interval was chosen to be 90% for all testing and samples. Static lateral-torsional buckling and dynamic lateral bending testing using five different supported end conditions and three different bracing systems over the same sample of wood I-joists were performed, consequently the population variance as well as the breadth of the tolerable error of Equation 4-1 depended upon of the type of the testing, and thus the sample size was a variable quantity. No values for the population variance and for the tolerable error were found in the literature review for the majority of the testing performed in this research and therefore the sample sizes were calculated using a value for the breadth of the tolerable error corresponding to 80% of the probability distribution. The variance used was an average value from limited data found in WIJMA (2005). Sample size calculations resulted in five wood I-joists for each size. Lateral bending stiffness tests, static and dynamic lateral-torsional buckling tests and torsional rigidity tests were conducted using the same five wood I-joists of each depth. Previous research by Hindman et

al. (2005a), Bamberg (2009) and Timko (2009) have shown no change in mechanical properties from retested wood I-joists, since the wood I-joists were tested within the elastic range of the materials.

$$n_s = \frac{4\sigma^2\left(z_{\frac{\alpha}{2}}\right)^2}{T_e^2} \tag{4-1}$$

Where, n_s is the sample size, σ is the standard deviation of the population, z is the number of standard deviations away from the mean of the normal distribution, α is the probability of committing a Type I error (probability of falsely rejecting the null hypothesis) and T_e is the width of the tolerable error.

4.4: Supported End Conditions

Five different wood I-joist supported end conditions were tested to validate the static lateral-torsional buckling models, the bending motion of the wood I-joists models and the dynamic lateral-torsional buckling models derived in this research. The supported end conditions were: simply supported end condition, ITS hanger, ITT hanger, IUS hanger and IUT hanger fixed end supported conditions. A set of laminated veneer lumber (LVL) platforms mounted on steel stanchions served as the base for the wood I-joist supported end configurations. To allow free rotation of the wood I-joist ends with respect to the principal axes of inertia parallel to the *x*-axis and *y*-axis, the simply supported end condition was manufactured with steel round bars placed at the bottom and laterally of the wood I-joist ends, (Figure 4-3 a). The ITS hanger, ITT hanger, IUS hanger and IUT hanger fixed supported end conditions were constructed by mounting the wood I-joist hangers on the supporting LVL platforms, (Figure 4-3 b). The installation of the wood I-joist hangers was performed following all manufacturer instructions.

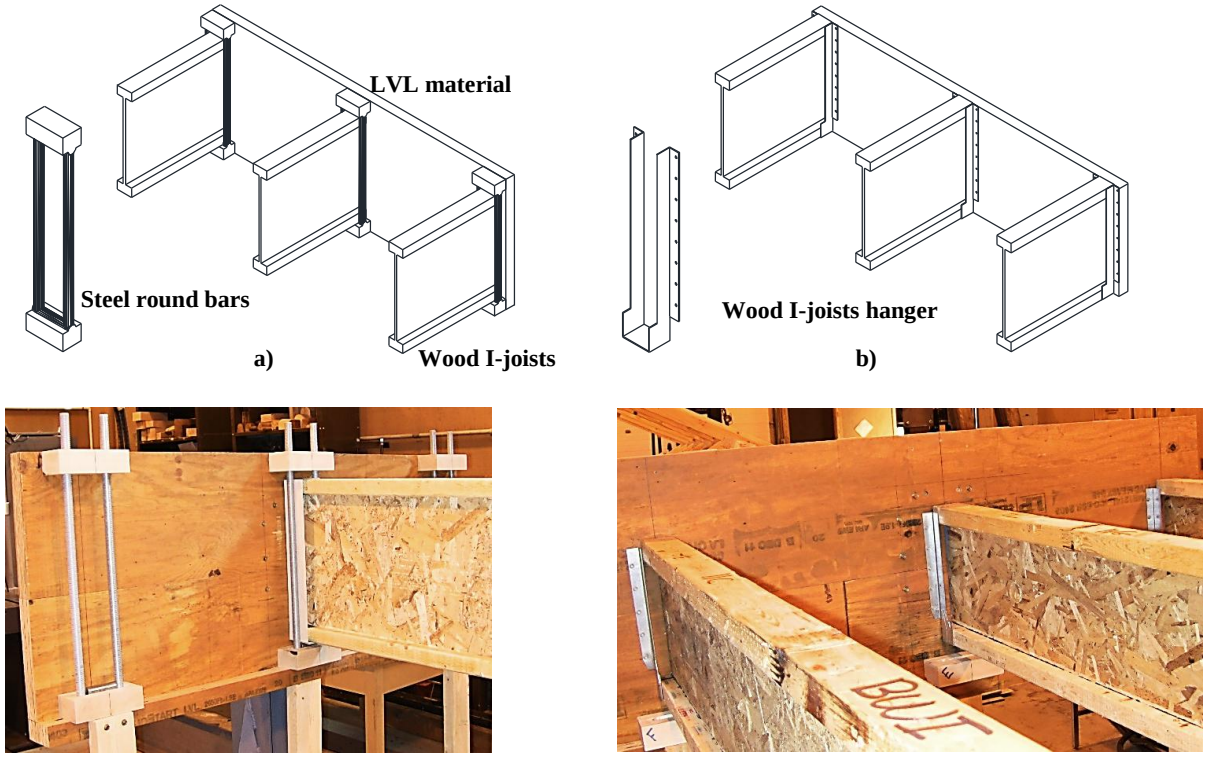

Figure 4-3: End supported platforms a) simply supported end condition and b) hanger supported end condition.

4.5: Bracing Systems

There different bracing systems were tested to validate the static lateral-torsional buckling models, the bending motion of the wood I-joists models and the dynamic lateral-torsional buckling models derived in this research. The bracing systems were: no-bracing, one mid-span brace and two quarter-span braces as shown in Figure 4-4 a), b) and c). Three wood I-joists spaced 24 inches on-center were used to form the bracing system in a lean-on configuration. The bracing system used two "dummy" wood I-joists of the same size and characteristics on either side of the wood I-joist test specimen. Testing for all cases was performed on the wood I-joist located at the middle of the bracing system. No testing was performed in the wood I-joists located at the sides of the bracing system. Steel bracing strands in a cross design scheme were used to brace the wood I-joists as shown in Figure 4-4 d) and e). The steel bracing strands were TB tension bridging for wood I-joists from Simpson Strong-Tie Company, Inc. The TB tension bridging is used to brace wood I-joists and it is fabricated from No. 20 gage galvanized steel (ESR-2608 2008). The steel bracing strands were attached to the top and bottom surfaces of the wood I-joist flanges following the manufacturer instructions as shown in Figure 4-4 d) and e). For a single test the same supported end conditions were applied to all 3 wood I-joists.

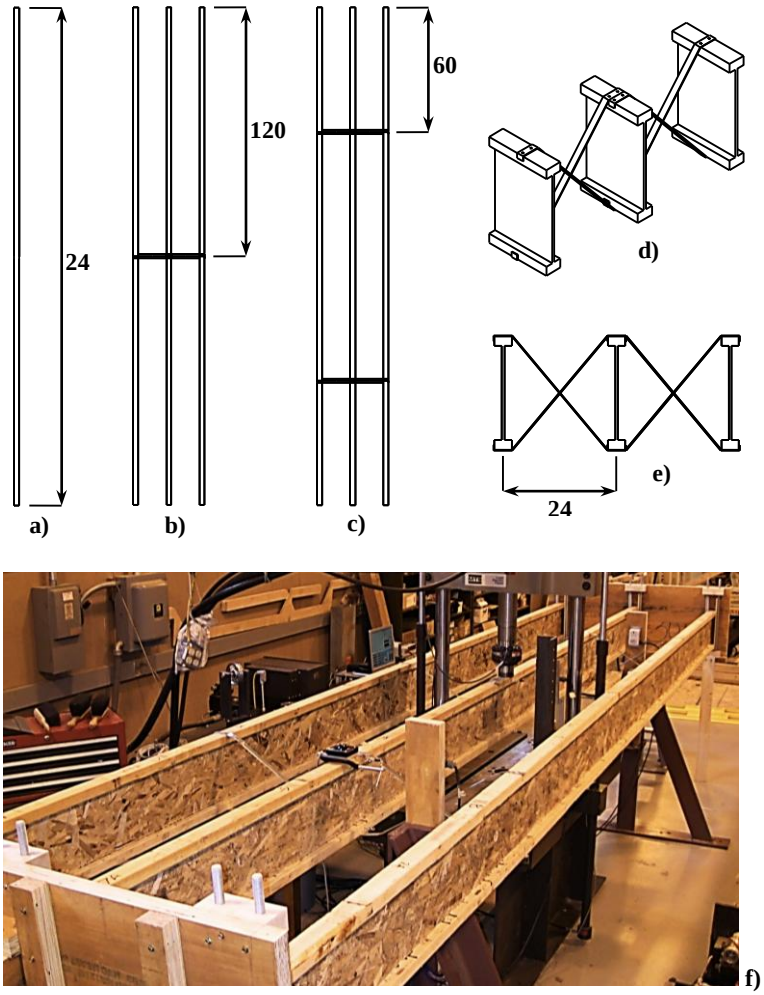

Figure 4-4: Bracing systems, a) no-bracing system, b) one mid-span brace, c) two quarter-span braces, d) bracing isometric view, e) bracing from view and f) photograph showing the bracing system installation.

4.6: Testing Protocol

Testing procedure followed the schematic diagram of Figure 4-5 and Table 4-2. Wood I-joists were received at a length of 288 inches, and then cut into two pieces, 240 inches long and 48 inches long. The 240 inches long specimens were used for the static lateral-torsional buckling tests, the bending motion of the wood I-joist tests and the dynamic lateral-torsional buckling tests, while the 48 inches long specimens were used for the wood I-joist lateral bending stiffness tests. The static lateral-torsional buckling tests, the bending motion of the wood I-joists tests and the dynamic lateral-torsional buckling tests were conducted using all five combinations of supported end conditions, the simply supported condition and the four hanger fixed supported conditions and all three combinations of bracing systems, the no-bracing, the one mid-span brace and the two quarter-span braces.

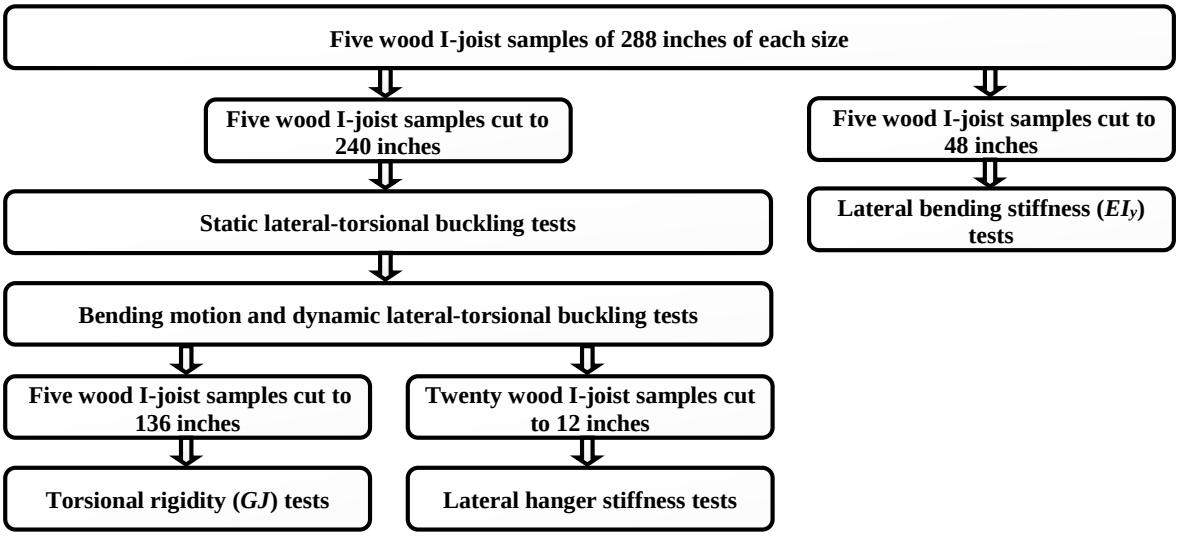

Figure 4-5: Testing protocol.

Table 4-2: Testing Breakdown and Number of Tests.

Static lateral-torsional buckling tests	
• 5 wood I-joist specimens 240 inches long • 2 wood I-joist heights (11 $^{7}/_{8}$ inches and 16 inches) • 5 different supported end conditions (simply supported and four wood I-joist hanger supported) • 3 bracing systems (no-bracing, one mid-span brace and two quarter-span brace)	**Total: 150 tests**
Bending motion and dynamic lateral-torsional buckling tests	
• 5 wood I-joist specimens 240 inches long • 2 wood I-joist heights (11 $^{7}/_{8}$ inches and 16 inches) • 5 different supported end conditions (simply supported and four wood I-joist hanger supported) • 3 bracing systems (no-bracing, one mid-span brace and two quarter-span brace)	**Total: 150 tests**
Torsional rigidity (GJ) tests	
• 5 wood I-joist specimens 136 inches long • 2 wood I-joist heights (11 $^{7}/_{8}$ inches and 16 inches)	**Total: 10 tests**
Lateral wood I-joist hanger stiffness (k) tests	
• 5 wood I-joist specimens 12 inches long • 2 wood I-joist heights (11 7/8 inches and 16 inches) • 4 supported end conditions (four wood I-joist hanger supported)	**Total: 40 tests**
Lateral bending stiffness (EI_y) tests	
• 5 wood I-joist specimens 48 inches long • 2 wood I-joist heights (11 7/8 inches and 16 inches)	**Total: 10 tests**

At the end of the static lateral-torsional buckling tests, the bending motion of the wood I-joist tests and dynamic lateral-torsional buckling tests, the 240 inches long wood I-joist specimens were cut to one piece 64 inches long and four pieces 12 inches long. The 64 inches long wood I-joist specimens were used for the torsional rigidity tests while the 12 inches long wood I-joist specimens were used for the lateral hanger stiffness tests for the four different wood I-joist hangers.

4.7: Lateral Bending Stiffness of the Wood I-Joists

The lateral bending stiffness of the wood I-joists was measured using a three point bending test (Figure 4-6). The length of the wood I-joists was 48 inches, and the span was 40 inches. The lateral bending stiffness EI_y of the wood I-joist was calculated using Equation 4-2.

$$EI_y = \left(\frac{P}{\delta}\right)\frac{L^3}{48} \tag{4-2}$$

Where the term $\frac{P}{\delta}$ is the slope of the load-deflection curve, P is that applied load, δ is the deflection of the wood I-joist at the mid-span and L is the wood I-joist span. Five wood I-joist specimens of each wood I-joist cross section heights were tested for a total of ten tests. A *Student's t* test assuming equal variances and a probability α of a type I error of 0.05 was performed to compare the lateral bending stiffness of the two samples of wood I-joists.

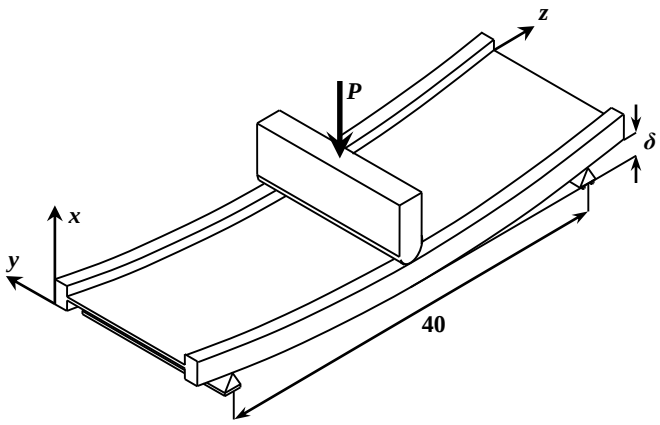

Figure 4-6: Lateral bending stiffness test configuration (inches).

A servo-hydraulic Material Testing System (MTS) 661.20E-01 with a load cell of 5000 lb. capacity and a reported error of less than 1 % (Timko 2009) was used. A separate LVDT with a nominal range of ± 5.0 inches attached to the specimen at the mid-span was used to measure the wood I-joist deflection. Load-deflection data were collected using National Instruments LabVIEW 7.0 software. Loading was applied at constant speed of 0.25 inches per minute. Calculations shown that with this loading speed the lateral bending test should be concluded in less than 16 minutes (ASTM 2005c). The load was applied over the wood I-joist flanges. No load was applied over the wood I-joist web other than that transmitted from the wood I-joist flanges. In the same way the wood I-

joist reactions were supported merely over the wood I-joist flanges. The lateral bending stiffness of the wood I-joists tests were static destructive testing, the load applied to the wood I-joist was removed until the specimen displayed visible failure.

4.8: Torsional Rigidity

The torsional rigidity of the wood I-joists was measured using a torsional stress analyzer. The torsional stress analyzer was previously used for torsional rigidity measurements by Finkenbinder (2007). The torsional stress analyzer generates a torsional moment through the center of the cross-section of the wood I-joist at one of the ends of the wood I-joist while the other end remains rigidly fixed with respect to the floor. Figure 4-7 shows the torsional stress analyzer set-up.

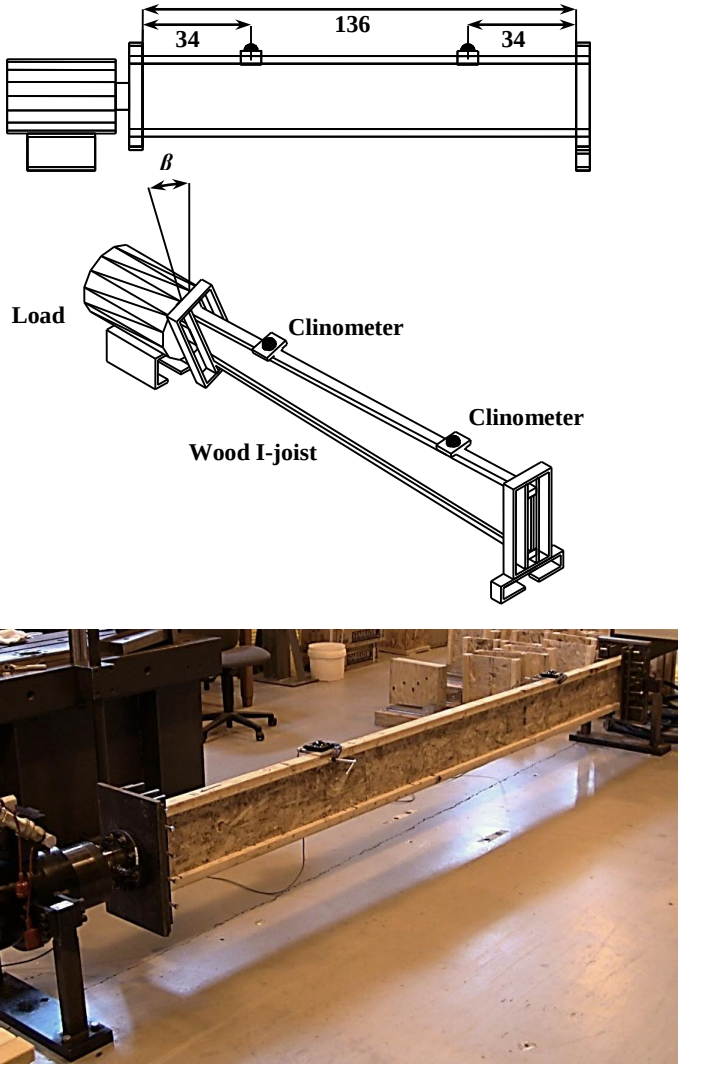

Figure 4-7: Torsional rigidity test configuration (inches).

The torsional rigidity GJ of the wood I-joist was calculated using Equation 4-3. Since Equation 4-3 cannot be solved explicitly for GJ, the Solver Add-in program from Microsoft Office Excel was used. Solver uses the Generalized Reduced Gradient (GRG2) nonlinear optimization algorithm to find the solution. Precision of the solutions was fixed at 0.000001.

$$\frac{T}{\beta} = \frac{GJ}{L}\left(\frac{1}{1-\frac{h}{L}\sqrt{\left(\frac{EI_y}{GJ}\right)}\tanh\left(\frac{L}{h}\sqrt{\frac{GJ}{EI_y}}\right)}\right) \quad (4\text{-}3)$$

Where the term $\frac{T}{\beta}$ is the slope of the torque-angle curve, T is the applied torsional moment, β is the angular displacement, L is the wood I-joist span, h is the wood I-joist height and EI_y is the lateral bending stiffness of the wood I-joist. Five wood I-joist specimens of each cross-sectional height were tested for a total of ten specimens. A *Student's t* test assuming equal variances and a probability α of a type I error of 0.05 was performed to compare the torsional rigidity of the two samples of wood I-joists.

The length of the wood I-joists specimens was 136 inches. The torsional moment was applied at constant speed of 1.00 degrees per minute. Two AccuStar 11/DAS 20 clinometers with a range of ± 20 degrees and a resolution of 0.01 degrees were used to measure the angle of twist. The clinometers were mounted on the top flange of the wood I-joist spaced 34 inches from the wood I-joist ends. Data from the torsional stress analyzer and from the clinometers were collected using National Instruments LabVIEW 7.0 software. A smooth load versus angle of twist curve was obtained and used to calculate the slope of the torque-angle. The load was applied over the wood I-joists flanges. No load was applied over the wood I-joist web other than the transmitted from the wood I-joist flanges. The torsional rigidity of the wood I-joist tests were static destructive testing, the load applied to the wood I-joist was removed until the specimen displayed visible failure.

4.9: Static Lateral-Torsional Buckling Tests

Static lateral-torsional buckling tests were performed using a three point bending test. Loading was applied at the mid-span on the top flange of the wood I-joists (Figure 4-8) at constant speed of 0.16 inches per minute (Timko 2009). A servo-hydraulic MTS 661.20E-01 testing machine with a load cell of 5000 lb. capacity and a reported error of less than 1 % was used. The lateral deflection, the axial deflection and the angle of twist of the wood I-joists at a series of discrete points were measured. The lateral deflections were measured at the top and at the bottom flanges of the wood I-joists using six UniMeasure PA-5-L3M string potentiometers with a measurement range of 5 inches and a reported error of less than 1%. The string potentiometers were placed at the mid-span and at the quarter-span locations as shown in Figure 4-8. The axial deflection was measured using the cross head displacement of the testing machine. The angles of twist were measured at the top flange of the wood I-joists using two AccuStar 11/DAS 20 clinometers with a range of ± 20 degrees and a resolution of 0.01 degrees. The clinometers were placed at the quarter-spans as shown in Figure 4-8. The angle of twist was also calculated by using the differences between the measurements from the string potentiometers placed at the top and at the bottom flanges of the wood I-joist at the same span position. All measurements from the MTS, the string potentiometers and the clinometers were collected using National Instruments LabVIEW 7.0 software. Sets of load versus axial deflection, load versus lateral deflection and load versus angle of twist curves were obtained.

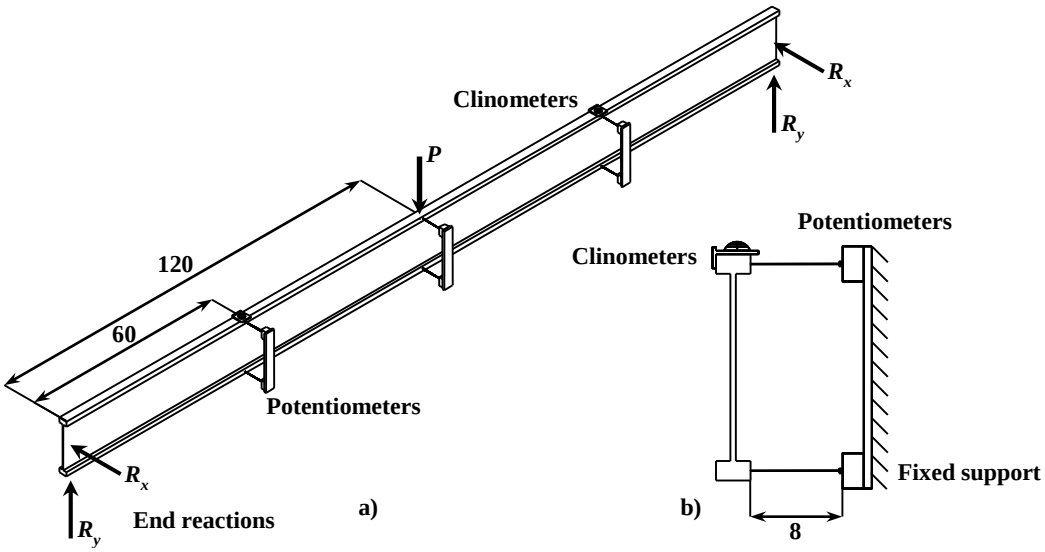

Figure 4-8: Static lateral-torsional buckling test configuration (inches), a) isometric view, b) front view.

The static lateral-torsional buckling tests were performed within the elastic range of the materials, when elastic instability was reached the application of the load was stopped and the test was terminated, thus the static lateral-torsional buckling tests were nondestructive testing. Lateral-torsional buckling instability was assumed to occur when the wood I-joist deflected laterally and twisted. An analysis of the data from the load versus angle of twist compared to the load versus lateral deflection curve and to the load versus axial deflection curve was performed to obtain the critical lateral-torsional buckling load.

Five wood I-joists of each cross-section height were tested for a total of 10 specimens. The length of the wood I-joists was 240 inches. The same five wood I-joists of each cross-section height were tested applying all combination of five different supported end conditions and three different bracing systems totalizing in this way 150 static lateral-torsional buckling tests.

The static lateral-torsional buckling tests conducted on the simply supported end condition with the non-bracing system installed were used to validate Equation 3-6, when a bracing system was installed to the wood I-joists the static lateral-torsional buckling tests were used to validate the application of adjusting Equations 3-30 into Equation 3-6. The static lateral-torsional buckling tests conducted on the hanger fixed end supported condition with the non-bracing system installed were used to validate Equation 3-11, when a bracing system was installed to the wood I-joists the static lateral-torsional buckling tests were used to validate the application of adjusting Equations 3-32 into Equation 3-11.

To investigate possible differences between means from the results of the different theoretical static lateral-torsional buckling models and the static lateral-torsional buckling loads obtained from testing, statistic procedures based on the *Student's t* distribution for paired data were used. In order to appropriately use the *Student's t* procedures an assessment of whether the population has a normal distribution is decisive. The normality of the sample distributions were evaluated by the sample kurtoses and sample skewness values. *Student's t* procedures were chosen since the population variances are unknown, the sample sizes are small (5 samples) and the fact that the *Student's t* distribution provides a reasonable approximation to the distribution when the sample is selected from a population with a mound-shaped distribution (Peck et al. 2007). The null hypotheses used on the *Student's t* comparisons were that the theoretical static lateral-torsional buckling means were equal to the static lateral-torsional buckling loads from testing while the research hypotheses were that the theoretical static lateral-torsional buckling means were not equal to the static lateral-torsional buckling loads from testing. The probability α of a type I error was of 0.05 for all *Student's t* comparisons. The *Student's t* comparisons were performed over the same supported end conditions as well as bracing systems. *Student's t* comparisons between the static lateral-torsional buckling models for the fixed end supported condition and the static lateral-torsional buckling loads obtained from testing for the simply supported end conditions were also performed over the three bracing systems analyzed in this research.

4.10: Dynamic Lateral-Torsional Buckling Tests

The goals of the dynamic lateral-torsional buckling tests were to measure the lateral deflections of the wood I-joists due to bending motion and the critical lateral-torsional buckling position of one individual walking on the wood I-joists. The dynamic lateral-torsional buckling tests were performed using a safety platform to support the wood I-joists. The safety platform was constructed and equipped with all necessary provisions to allow a person to safely walk on the wood I-joists without the possibility of injury. The safety platform was built with two parallel frames along the wood I-joist length, which served as hand rails connected in the transverse direction as shown in Figure 4-9. At the top of the safety platform, a steel I-beam was attached parallel to the wood I-joist length. A movable trolley was attached to the bottom flange of the steel I-beam where a safety lanyard was attached to the participant's safety harness. The trolley allows individuals to walk on the wood I-joists but have a fall arrest system in place at all times. The safety platform is slightly larger than 20 feet long by approximately 5 feet wide.

The individual's weight was recorded at the beginning of the test period. The individual was asked to walk at normal pace and if possible not to use the hand rails except in the event of a fall. The dynamic lateral-torsional buckling test began when the individual started walking from one end of the wood I-joist and finished when the individual reached the opposite end. Since the dynamic lateral-torsional buckling tests are more variable than the static lateral-torsional buckling tests (Timko 2009), three loading repetitions were performed for each test. The average measurements of the three repetitions were used as a single test. Loading was applied through one individual walking on the wood I-joist at normal pace. The individual's footstep frequency f_d was measured by dividing the number of footsteps on the wood I-joist by the time consumed in crossing the wood I-joist. The individual's footstep length was measured by dividing the number of footsteps on the wood I-joist by the wood I-joist length. The individual's footstep frequency f_d was an input parameter to Equation 3-12. The individual's footstep length was used to locate the points of the discrete loading due to the individual's weight.

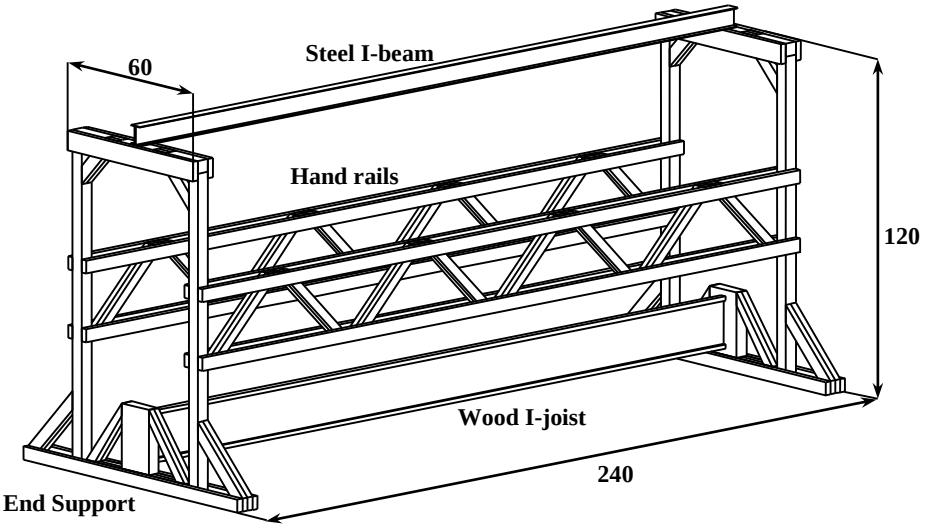

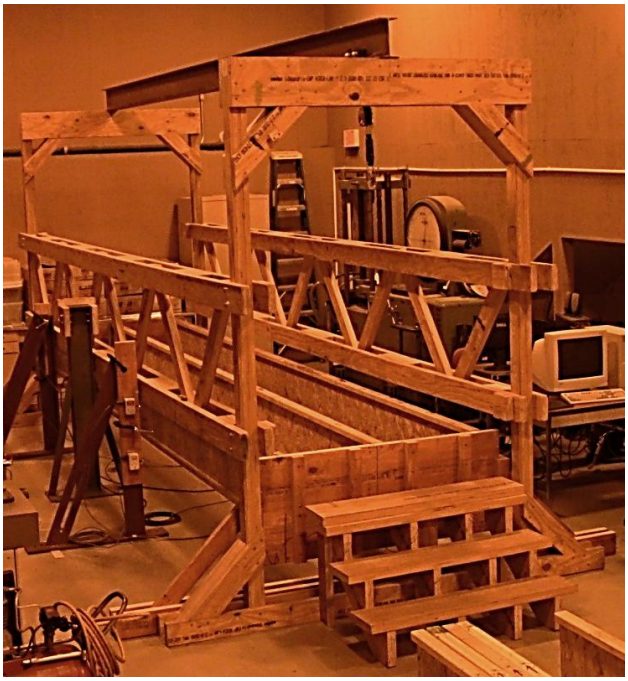

Figure 4-9: Safety platform used in the dynamic lateral-torsional buckling tests (approximate dimensions in inches).

Lateral deflections and angles of twist were measured in the dynamic lateral-torsional buckling tests. Lateral deflections were measured using six string potentiometers placed in the same pattern and positions as they were placed in the static lateral-torsional buckling tests. The angle of twist was calculated using the differences between the measurements from the string potentiometers placed at the top and bottom flanges of the wood I-joist. The use of clinometers in the dynamic lateral-torsional buckling tests was not possible due to the poor response of these devices to the rapid movement that the wood I-joists undergoes when the individual walks on the wood I-joists (Timko 2009). The end support platforms used in the static lateral-torsional buckling tests were also used for the dynamic lateral-torsional buckling tests, but adapted to the safety platform. A Vishay BHL U3SB-A "S" load cell with a 5000 lb. of capacity and an experimental error of 0.02% placed at the bottom flange and at one of the ends of the wood I-joist was used to measure the axial reactions at the end of the wood I-joist induced by the individual walking. The axial reactions were used to calculate the position of the individual walking along the wood I-joist length. Measurements from the string potentiometers and from the load cell were collected using National Instruments LabVIEW 7.0 software. A lateral displacement versus participant position, an axial reaction at the end of the wood I-joist versus participant position and an angle of twist versus participant position curves were obtained. It was assumed that lateral-torsional buckling instability occurred when the wood I-joist laterally deflected and twisted. An analysis of the data from the lateral displacement versus participant position curve compared to the angle of twist versus participant position curve was performed to obtain the critical lateral-torsional buckling position. The data from the dynamic lateral-torsional buckling tests conducted on the simply supported end condition with the non-bracing system installed was used to validate Equation 3-18. When a bracing system was installed to the wood I-joists, the data from the dynamic lateral-torsional buckling tests was used to validate the application of adjusting Equations 3-30 into Equation 3-18. The data from the dynamic lateral-torsional buckling tests conducted on the hanger fixed end supported condition with the non-bracing system installed was used to validate Equation 3-27. When a bracing system was installed to the wood I-joists, the data from the dynamic lateral-torsional buckling tests was used to validate the application of adjusting Equations 3-32 into Equation 3-27.

To investigate possible differences between means from the results of the different theoretical dynamic lateral-torsional buckling models and the dynamic lateral-torsional buckling tests, statistic procedures based on the *Student's t* distribution for paired data were used. The applied *Student's t* procedures followed the same guidelines used in the static lateral-torsional buckling tests. The null hypotheses used on the *Student's t* comparisons were that the theoretical dynamic lateral-torsional buckling means were equal to the dynamic lateral-torsional buckling means from testing while the research hypotheses were that the theoretical dynamic lateral-torsional buckling means were not equal to the dynamic lateral-torsional buckling means from testing. The *Student's t* comparisons were performed over the same supported end conditions as well as bracing systems. *Student's t* comparisons between the dynamic lateral-torsional buckling models for the fixed supported end condition and the dynamic

lateral-torsional buckling means obtained from testing for the simply supported end condition were also performed over the three bracing system analyzed in this research.

4.11: Lateral Hanger Stiffness Tests

The lateral hanger stiffness was investigated using a lever design set-up as shown in Figure 4-10. The hanger was mounted on a rim board following the manufacturer installation instructions. The length of the wood I-joist specimens was of 12 inches.

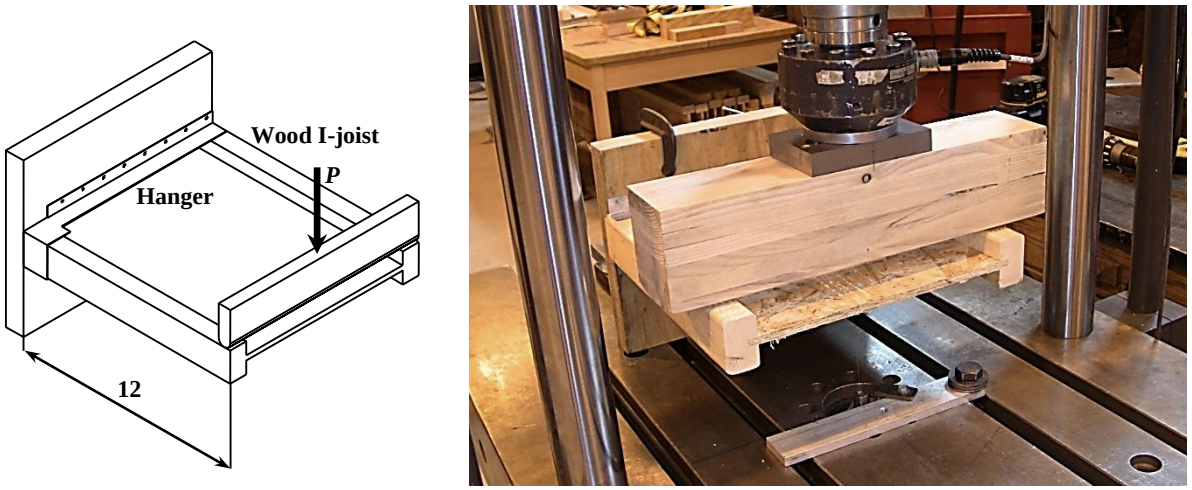

Figure 4-10: Lateral hanger stiffness test configuration (inches).

Loading was applied at one of the wood I-joist ends while the other end was attached to the wood I-joist hanger. A servo-hydraulic MTS 661.20E-01 testing machine with a load cell of 5000 lb. capacity with a reported experimental error of less than 1 % was used. Loading was applied at constant speed of 0.16 inches per minute. This loading speed corresponds to the static lateral-torsional buckling test loading. Testing was designed to measure the stiffness of the wood I-joist hanger, so loading was stopped before a failure was observed. Data were collected using National Instruments LabVIEW 7.0 software. The lateral hanger stiffness k was calculated using Equation 4-4.

$$k = 12B\frac{P}{\gamma} \tag{4-4}$$

Where the term $\frac{P}{\gamma}$ is the slope from the linear elastic portion of the load versus displacement curve, P is the applied load, γ is the induced displacement and B is the wood I-joist hanger bearing constant. The bearing constant was calculated by averaging the halves of the bearing lengths of the two bearing surfaces corresponding to the two wood I-joist flanges (see Figure 4-11). Since Equation 4-4 is multiplied by 12 in. (from the test set-up), the bearing constant is a dimensionless unit. Since the different wood I-joist hangers have different bearing surfaces, a particular bearing constant was used for each type of wood I-joist hanger.

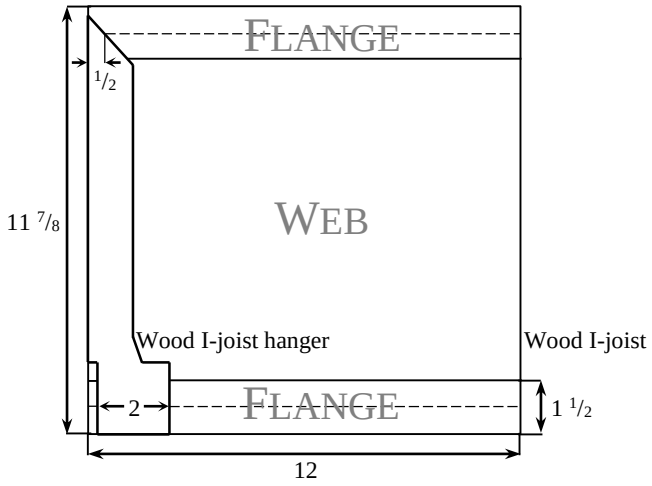

Figure 4-11: Lateral face of a wood I-joist hanger (ITT) showing the bearing lengths (inches).

The top length and the bottom length of the bearing surfaces and the bearing constant that was used to calculate the lateral hanger stiffness for each type of wood I-joist hanger are shown in Table 4-3. Four different wood I-joist hangers were tested: ITS hanger, ITT hanger, IUS hanger and IUT hanger. Five tests were carried out for each of the wood I-joist hangers and for the two wood I-joist cross-section heights used for a total of 40 specimens. To investigate possible differences between the two wood I-joist hanger sizes *Student's t* tests assuming equal variances and a probability α of a type I error of 0.05 were performed for each type of hanger.

Table 4-3: Top and Bottom Lengths of the Bearing Surfaces and the Bearing Constant.

	11 7/8 in. Wood I-Joists Hangers				**16 in. Wood I-Joists Hangers**			
	ITS	ITT	IUS	IUT	ITS	ITT	IUS	IUT
Top Length (in.)	0.625	0.500	0.750	1.250	0.500	0.250	0.750	1.250
Bottom Length (in.)	2.0	2.0	2.0	2.0	2.0	2.5	2.0	2.0
Bearing Constant	**0.656**	**0.625**	**0.688**	**0.813**	**0.625**	**0.688**	**0.688**	**0.813**

4.12: Regression Models

Static lateral-torsional buckling regression models were developed in this research. The goal of the regression models was to simplify the theoretical models previously derived and reduce the number of explanatory variables, especially the variables that need to be determined by testing. To examine the goodness of fit of the static lateral-torsional buckling regression models the following resources were used: analysis of the scatterplots of the response variables versus explanatory variables to inspect for lack of fit, analysis of the residuals plots to inspect for outliers or erroneous observations and for constant variance of the errors, coefficients of determination R^2 and hypotheses testing to inspect for the effects of the individual observations in the lateral-torsional buckling regression models.

The static lateral-torsional buckling regression models were developed considering the static lateral-torsional critical loads as response variables and the intrinsic and geometric properties of the wood I-joists as the

explanatory variables. Equation 4-5 was derived from a rearranged form of Equation 3-11 and is proposed for the static lateral-torsional buckling regression models.

$$P_{cr_i} = \mu_1 \left(EI_{y_i}\right)^{\frac{1}{2}} + \mu_2 h_i \left(EI_{y_i}\right)^{\frac{1}{2}} + \mu_3 h_i \left(EI_{y_i}\left(\frac{k_i}{k_i + EI_{y_i}}\right)\right)^{\frac{1}{2}} + \varepsilon_i \tag{4-5}$$

Where P_{cr_i} is the i^{th} observation of the static critical lateral-torsional buckling load, h_i is the i^{th} observation of the cross-section height of the wood I-joist, EI_{y_i} is the i^{th} observation of the lateral bending stiffness of the wood I-joist, k_i is the i^{th} observation of the lateral bending stiffness of the wood I-joist hanger and ε_i is the i^{th} observation of the random error. The parameters μ_1, μ_2, μ_3 are the coefficients to be determined based on the regression analysis of the numerical data generated in the laboratory. For the simply supported end condition the value of the explanatory variable k_i is taken as infinity, so the values of the terms inside of the parentheses in Equation 4-5 equals one.

The torsional rigidity (GJ) of the wood I-joist was not included in Equation 4-5 since it can be proved that for single elastic, homogeneous and isotropic components (general assumptions used in this research) the torsional rigidity is a linear function of the lateral bending stiffness $\left(EI_y\right)$ of the wood I-joist. The torsional rigidity has a strong collinearity with the lateral bending stiffness and therefore it is not necessary to include both explanatory variables into the regression model. The exclusion of the torsional rigidity in the regression models has the intention of facilitating the calculation of the static critical lateral-torsional buckling load. The length of the wood I-joist in this research is constant, therefore it was not include in Equation 4-5.

In Equation 4-5 the cross-section height of the wood I-joist (h) accounts for the position of the load application with respect to the neutral axis of the wood I-joist. The lateral bending stiffness accounts for the intrinsic and geometric properties of the wood I-joist while the lateral bending stiffness of the wood I-joist hanger (k) accounts for the supported end conditions. For the static lateral-torsional buckling regression models, loading was always applied at the mid-span of the wood I-joist. No direct testing was performed to assess the performance of the bracing systems analyzed in this research. Therefore, three different regression analysis models were obtained from Equation 4-5, one model for the non-bracing system, another model for the one mid-span bracing system and one model more for the two quarter-span bracing system.

5: Results and Discussion

This Chapter includes the analyses of data gathered from experimental testing and the comparison of these experimental data with the corresponding predictions calculated from the theoretical models. Experimental testing measured the lateral bending stiffness and the torsional rigidity of the wood I-joists for use in the static lateral-torsional buckling and in the lateral bending motion theoretical models. The lateral stiffness of four different wood I-joists hangers were measured for assessment of the lateral constraint at the ends of the wood I-joists. Static critical loads were obtained from testing and compared with predicted critical loads from the theoretical models for five different supported end conditions and three different bracing systems. The mass of the wood I-joists, the total time needed to transverse the wood I-joists and the walking frequency were measured for use in the lateral bending motion analyses of the wood I-joists. The maximum lateral displacements measured at the mid-span and at the third quarter-span of the wood I-joists and the position of the individual walking when these maximum lateral displacements took place were obtained from testing and compared with predicted maximum lateral displacements and individual positions by the theoretical models for five different supported end conditions and three different bracing systems. The dynamic lateral-torsional buckling instability was investigated by adding the static lateral-torsional buckling instability to the lateral bending motion of the wood I-joists.

5.1: Lateral Bending Stiffness of the Wood I-Joists

The lateral bending stiffness of the wood I-joists was calculated using Equation 4-2. The slope of the load-deflection curve was taken within the displacement range from 0.1 in. to 0.3 in. as shown in Figure 5-1. This range was chosen in order to avoid initial loading effects due to the attachment of the test specimen with the testing machine and unwanted effects due to yielding of the specimen in the final stages of the test. About 240 points from each test within this range were used to calculate the slope of the line using the linear least squares method. The correlation coefficient of the line inside this range was greater than 0.99 for all tests.

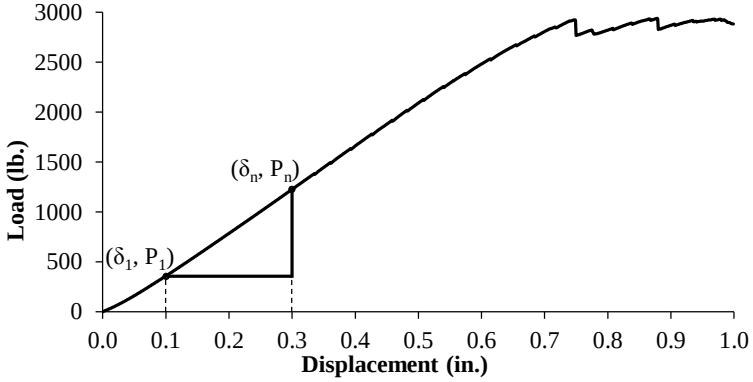

Figure 5-1: Load-displacement curve from the lateral bending stiffness. Test of one 16 in. wood I-joist.

The lateral bending stiffness of the wood I-joists are shown in Table 5-1. The lateral bending stiffness of the 16 in. wood I-joists are 3.97% greater than the lateral bending stiffness of the 11 $^{7}/_{8}$ in. wood I-joists. However, the *Student's t* test (p = 0.4262) concluded that the mean lateral bending stiffness of the 16 in. wood I-joists is not significantly different than the mean lateral bending stiffness of the 11 $^{7}/_{8}$ in. wood I-joists. The variability of the lateral bending stiffness was greater for the 16 in. wood I-joists, this result was most probably due to the larger variability of the moisture content of the 16 in. wood I-joist specimens.

Table 5-1: Lateral Bending Stiffness of the Wood I-Joists.

Sample Size	Lateral Bending Stiffness		Moisture Content	
	EI_y (lb. in.^{2})	*CV* (%)	*MC* (%)	*CV* (%)
11 $^{7}/_{8}$ in. Wood I-Joists	5.79 x 10^6	5.96	8.14	0.992
16 in. Wood I-Joists	6.02 x 10^6	8.30	9.92	3.94

The moisture content of the specimens used for measuring the lateral bending stiffness of the wood I-joists are shown in Table 5-1. The moisture content was calculated using the oven-drying method. The average moisture content of the 16 in. wood I-joists was 1.78% greater compared to the average moisture content of the 11 $^{7}/_{8}$ in. wood I-joists. The variability of the moisture content was greater for the 16 in. wood I-joists. The difference in the average moisture content and in the variability of the moisture content may be due to longer storage of the 11 $^{7}/_{8}$ in. wood I-joists of more than one year before testing while the 16 in. wood I-joists were purchased a few weeks before testing.

5.2: Torsional Rigidity of the Wood I-Joists

The torsional rigidity of the wood I-joists was calculated using Equation 4-3. The lateral bending stiffness of the wood I-joists required by Equation 4-3 were obtained from Table 5-1. The slope of the torque-angular displacement curve was taken within the angular displacement range from 0.04 rad. to 0.12 rad. as displayed in Figure 5-2. This range was chosen in order to avoid initial unwanted loading effects due to the attachment of the test specimen with the testing machine. Approximately 320 points from each test within this angular displacement range were used to calculate the slope of the curves using the linear least squares method. The correlation coefficient of the line inside this range was greater than 0.99 for all torsional rigidity tests.

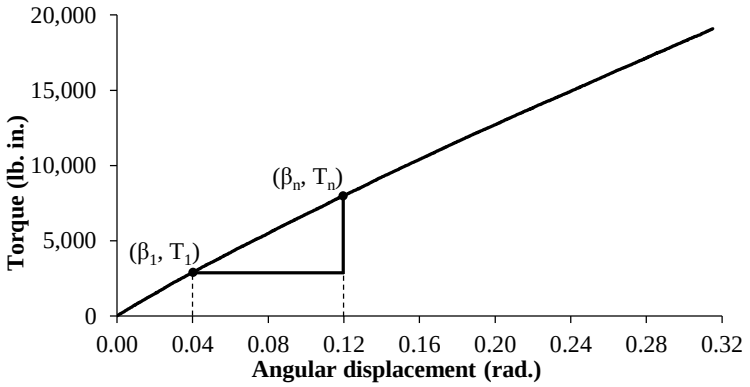

Figure 5-2: Torque-angular displacement curve from the torsional rigidity. Test of one 16 in. wood I-joist.

The torsional rigidity of the wood I-joists are shown in Table 5-2. The torsional rigidity of the 16 in. wood I-joists was 39.3% greater compared to the torsional rigidity of the 11 $^{7}/_{8}$ in. wood I-joists. The *Student's t* test ($p <$ 0.0000) concluded that the mean torsional rigidity of the 16 in. wood I-joists is significantly different than the mean torsional rigidity of the 11 $^{7}/_{8}$ in. wood I-joists. The variability of the torsional rigidity for both wood I-joist samples was smaller compared to the variability of the corresponding lateral bending stiffness.

Table 5-2: Torsional Rigidity of the Wood I-Joists.

Sample Size	Torsional Rigidity		Moisture Content	
	***GJ* (lb. in.^{2})**	***CV* (%)**	***MC* (%)**	***CV* (%)**
11 $^{7}/_{8}$ in. Wood I-Joists	5.01 x 10^6	4.29	11.6	2.26
16 in. Wood I-Joists	6.98 x 10^6	2.52	12.4	3.30

The moisture content of the specimens used for measuring the torsional rigidity of the wood I-joists are shown in Table 5-2. The moisture content was calculated using the oven-drying method. The average moisture content of the 16 in. wood I-joists was 0.80% greater compared to the average moisture content of the 11 $^{7}/_{8}$ in. wood I-joists. The differences in the average moisture content between the lateral bending stiffness samples and the torsional rigidity samples is due to the torsional rigidity tests being performed three months after the lateral bending stiffness tests were performed.

5.3: Lateral Stiffness of the Wood I-Joist Hangers

In investigating the static lateral-torsional buckling instability and the lateral bending motion of the wood I-joists, four different types of wood I-joist hangers for each wood I-joist height were used including two top mount hangers (the ITS and the ITT hangers) and two face mount hangers (the IUS and the IUT hangers). The lateral stiffness of the wood I-joist hangers were calculated using Equation 4-4. The slopes of the load-hanger displacement curves were taken within the hanger displacement range from 0.00 in. to 0.06 in. as shown in Figure 5-3. Approximately 600 points from each test within the corresponding hanger displacement range were used to calculate the slope of the curves using the linear least squares method. The correlation coefficient of the lines inside this range was on average 0.93.

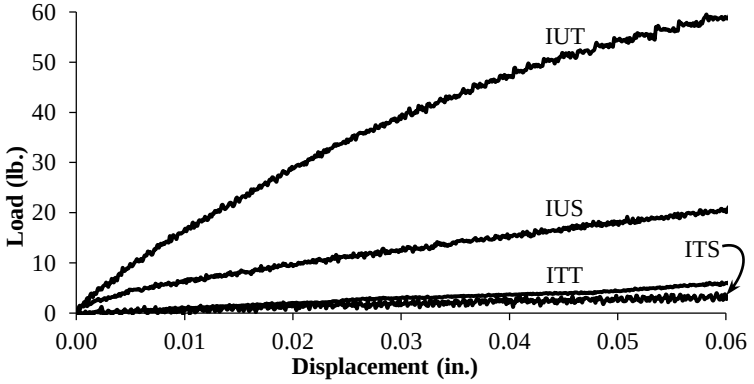

Figure 5-3: Load-hanger displacement curves. Tests of 16 in. wood I-joist hangers.

In Figure 5-3 all wood I-joists hangers demonstrated similar load-displacement behavior. The curvature of the IUT hanger is also present in the IUS, the ITT and the ITS hangers, but not easily observable due to the scale of Figure 5-3. The average lateral stiffness and coefficient of variation values for the wood I-joist hangers are shown in Table 5-3. The ITS and the ITT hangers, both top mount hangers have smaller lateral stiffness values compared to the IUS and the IUT hangers, both face mount hangers. Comparing the stiffness values of the ITS hanger and the ITT hanger, the ITT hanger had greater bearing surface between the hanger and the rim board (see Figure 4-2), especially at the lower part of the hanger, were screws were not used. The bearing surface of the ITT hanger inhibited rotation, preventing lateral hanger displacement.

Table 5-3: Lateral Hanger Stiffness.

Hanger	11 7/8 in. Wood I-Joists Hangers		16 in. Wood I-Joists Hangers	
	k **(lb. / in.)**	***CV*** **(%)**	***k*** **(lb. / in.)**	***CV*** **(%)**
ITS Top mount	58.3	25.0	54.6	47.6
ITT Top mount	111	25.1	289	24.6
IUS Face mount	350	3.80	309	8.96
IUT Face mount	937	7.81	830	6.91

Hanger stiffness differences between the IUS and the IUT hangers may be due to greater bearing surface between the hanger and the wood I-joist specimen for the IUT hanger (approximately 18% greater) compared to the IUS hanger (see Table 4-3 and Figure 4-2). Also because, the 11 7/8 in. IUS hanger was screwed to the rim board approximately 58% of the hanger length while the IUT hanger was screwed to the rim board approximately 73% of the hanger length. For the 16 in. wood I-joist the IUS hanger was screwed to the rim board approximately 69% of the hanger length while the IUT hanger was screwed to the rim board approximately 81% of the hanger length.

The 11 7/8 in. hangers had larger lateral stiffness values compared to the 16 in. hangers, except for the ITT hanger. The 16 in. ITT hangers were die-formed from 16 gage galvanized steel, while all other type of hangers were die-formed from 18 gage galvanized steel. The top mount hangers had larger variability compared to the face mount hangers. When the hangers are laterally loaded, the response of the hanger to the applied load comes from the top flange for the top mount hangers and it comes from both flanges for the face mount hangers.

Testing differences between the ITS top mount hanger and the IUT face mount hanger are shown in Figure 5-4. The bearing surface of the top flange of the wood I-joist is carrying most of the applied load in the ITS hanger while the applied load is more uniformly distributed along the hanger length in the IUT hanger. A large displacement was observed at the bottom flange of the ITS hanger while the displacement in the IUT hanger is approximately constant along the hanger length in the IUT hanger. The photographs were taken approximately under the same load head displacement.

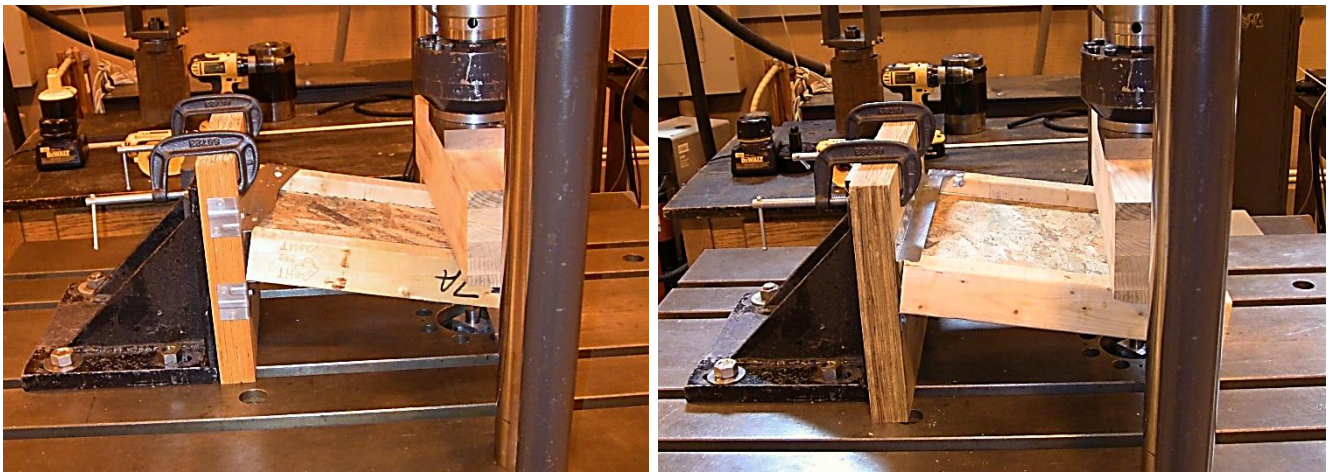

Figure 5-4: Photographs showing the lateral hanger stiffness tests. Left, ITS hanger. Right, IUT hanger.

The *p*-values of the *Student's t* tests comparing the lateral hanger stiffness of the 11 $^{7}/_{8}$ in. hangers to the lateral stiffness of the 16 in. hangers and are shown in Table 5-4. The mean lateral stiffness of the 11 $^{7}/_{8}$ in. ITS hanger was not significantly different compared to the mean lateral stiffness of the 16 in. ITS hanger. The lateral stiffness for the ITS hanger had large variability, especially for the 16 in. wood I-joist hangers (Table 5-3). The mean lateral stiffness of the 11 $^{7}/_{8}$ in. ITT, IUS and IUT hangers were significantly different compared to the mean lateral stiffness of the corresponding 16 in. hangers. Therefore, the size of the hanger should be considered in the lateral hanger stiffness used in the static and dynamic models.

Table 5-4: *Student's t* tests comparing the lateral hanger stiffness of the two wood I-joist hanger sizes.

Hanger	ITS $^{\text{Top mount}}$	ITT $^{\text{Top mount}}$	IUS $^{\text{Face mount}}$	IUT $^{\text{Face mount}}$
***p*-value**	0.7938	0.0008	0.0159	0.0328

5.4: Static Lateral-Torsional Buckling Instability

Static lateral-torsional buckling instability was investigated by testing two different sizes of wood I-joists with five different supported end conditions and three different bracing systems. The main goal of the static buckling instability testing was to obtain the buckling critical loads. Critical loads from testing will be compared with the predicted critical loads from the corresponding theoretical models. Because the theoretical model for the simply supported end condition is less complex than the theoretical model for the hanger stiffness, there is a special interest in how the theoretical model derived for the simply supported end condition predicts the critical loads when wood I-joists hangers are used. Figure 5-5 is a graph of the load-vertical displacement curve of a static lateral-torsional buckling test depicting the critical load. Loading of the wood I-joist demonstrated linear elastic behavior until the critical buckling load (P_{cr}) was reached. After the critical buckling load became constant for increasing displacement. The total time of the static lateral-torsional buckling tests was approximately 6 minutes. After reaching the critical load, the test was continued for approximately 45 seconds to ensure a constant load as shown in Figure 5-5. The static lateral-torsional critical load shown in Figure 5-5 occurred at 1750 lb. with a corresponding vertical displacement of 0.825 in.

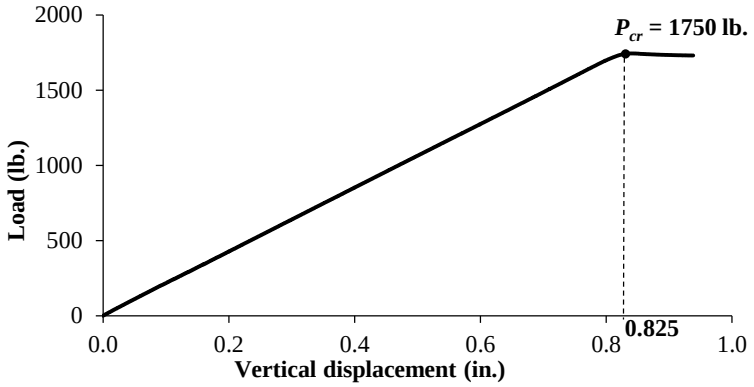

Figure 5-5: Load-vertical displacement curve of the static buckling instability test of one 16 in. wood I-joist.

Figure 5-6 is a graph of the lateral displacement-vertical displacement and the rotation-vertical displacement curves of the static buckling instability test shown in Figure 5-5. The vertical displacement of 0.825 in. is marked on Figures 5-5 a) and b) to illustrate the behavior at buckling. An abrupt increase in the lateral displacement and the rotation of the wood I-joist occurred when the critical load was attained. The total lateral displacement of the wood I-joist was approximately 1.05 in., while the total rotation was approximately 0.117 rad. (6.7 degrees). The displacement and the rotation values were subjective, since the test was ended once the lateral-torsional buckling instability was clearly observed.

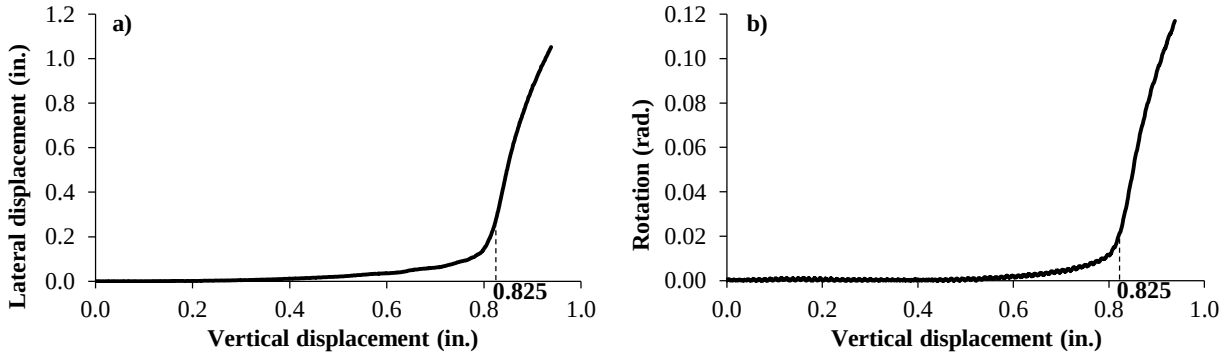

Figure 5-6: a) Lateral displacement-vertical displacement and b) rotation lateral-displacement instability curves.

Figure 5-7 is a graph of the load-lateral displacement and the load-rotation curves of the static buckling instability test shown in Figure 5-5. The lateral displacement and the rotation attained up to the point of the critical load were small compared with the maximum lateral displacement and the rotation observed. Lateral-torsional buckling theory states that the critical load remains constant beyond the point of the critical load. The critical load value of 1750 lb. is marked on Figure 5-7 a) and b). The lateral displacement and rotation of the wood I-joist correlate well with the load measurement observed in the vertical displacement shown in Figure 5-7 a) and b).

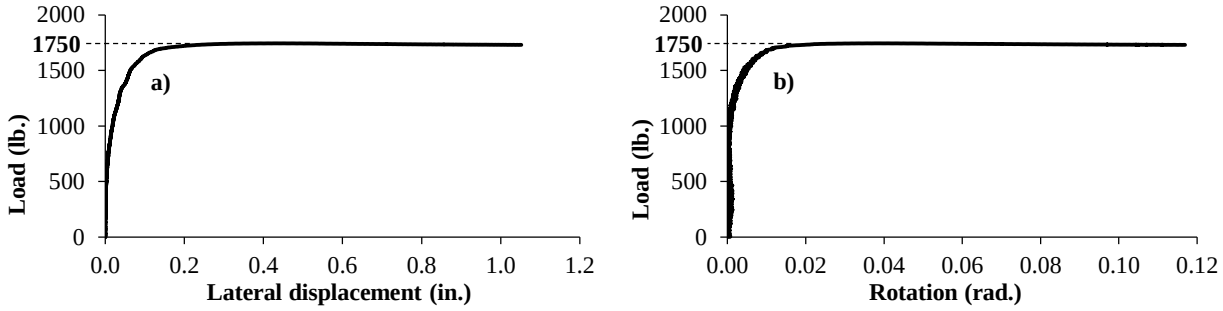

Figure 5-7: a) Load-lateral displacement and b) load-rotation instability curves.

Photographs of the static lateral-torsional buckling instability tests are shown in Figure 5-8. The wood I-joist shown in the photographs pertains to the tests shown in Figures 5-5, 5-6 and 5-7. The photograph on the left is the wood I-joist before loading. The photograph on the right is the wood I-joist after the static lateral-torsional buckling critical load was reached, hence showing wood I-joist instability.

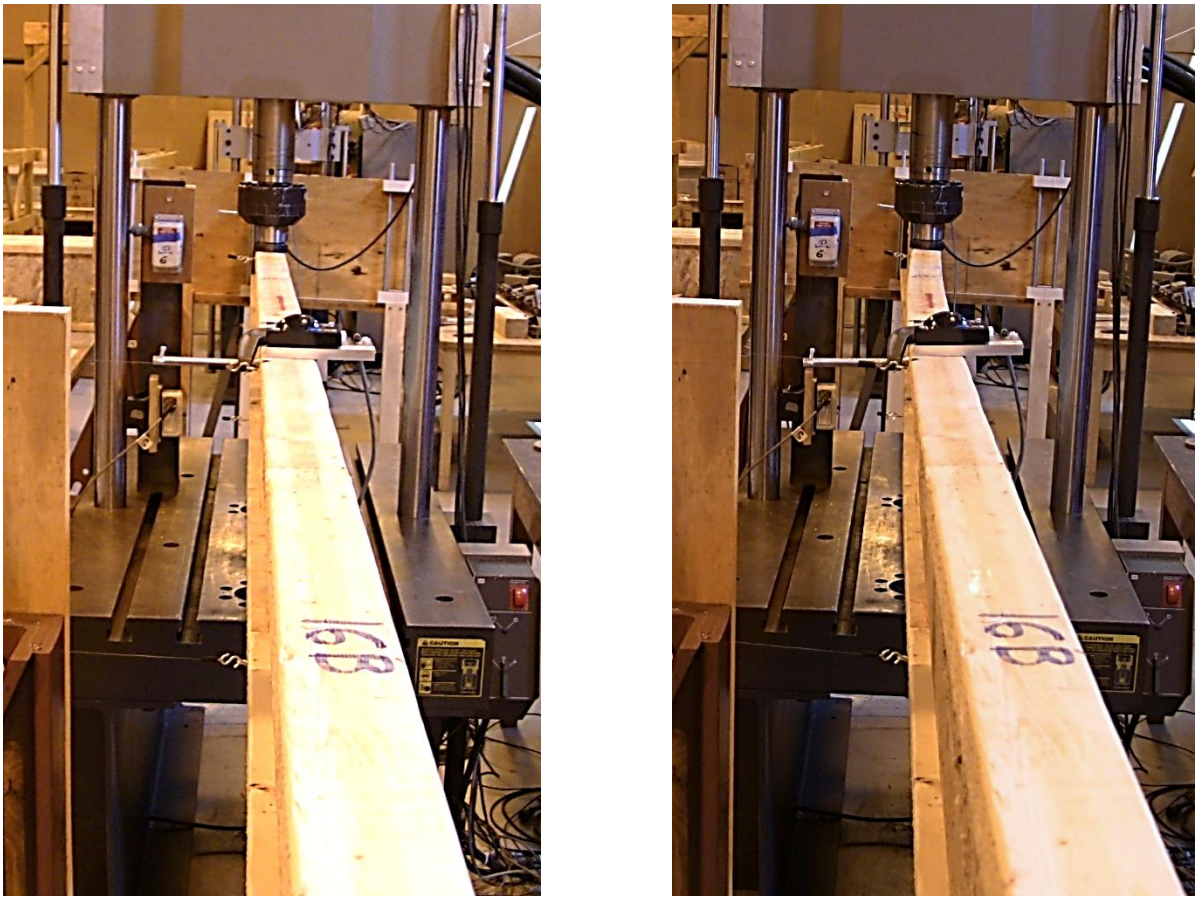

Figure 5-8: Photographs showing the static lateral-torsional buckling instability tests. Left, unloaded wood I-joist. Right, showing buckling instability.

5.4.1: Static Critical Loads for the Non-Bracing System

The theoretical static lateral-torsional buckling critical loads for the non-bracing system were calculated using Equation 3-6 for the simply supported end condition and Equation 3-11 for the hanger supported end conditions.

Static lateral-torsional critical loads (P_{cr}) for the non-bracing system are shown in Table 5-5. The theoretical and testing critical loads obtained from the 16 in. wood I-joists were greater than the corresponding critical loads of the 11 $^{7}/_{8}$ in. wood I-joists. Critical loads from testing were more variable compared to the theoretical critical loads, except for the IUT hanger supported end condition of the 16 in. wood I-joists. The variability value from testing of the IUT hanger supported end condition was the smallest value reported while the theoretical variability value was the second greatest.

Timoshenko (1936) proposed a theoretical model to calculate the static lateral-torsional buckling critical loads for the simply supported end condition in which the warping effects of the I-beams are neglected and the application of the load is at the neutral axis. Using the Timoshenko (1936) model the critical loads for the 11$^{7}/_{8}$ in. wood I-joists were on average 1610 lb. while the critical loads for the 16 in. wood I-joists were on average 1940 lb. The predicted critical loads from the Timoshenko (1936) model of the 11 $^{7}/_{8}$ in. wood I-joists were on average 7.33% greater compared to the critical loads from testing, while the predicted critical loads of the 16 in. wood I-joists were on average 6.01% greater compared to the critical loads from testing. Using the derived model (Equation 3-6), the differences between the predicted critical loads and the critical loads from testing are smaller than those from the Timoshenko (1936) model (Table 5-5). Therefore, the inclusion of warping effects and changes in the load application improved the lateral-torsional buckling critical load predictions.

Table 5-5: Static Critical Loads for the Non-Bracing System.

End Condition	11 $^{7}/_{8}$ in. Wood I-Joists				16 in. Wood I-Joists			
	Testing		Theoretical		Testing		Theoretical	
	P_{cr} (lb.)	CV (%)	P_{cr} (lb.)	CV (%)	P_{cr} (lb.)	CV (%)	P_{cr} (lb.)	CV (%)
Simply Supported	1500	4.35	1570	3.88	1830	10.3	1890	4.54
ITS Hanger	1440	5.27	1430	3.39	1710	5.95	1700	3.70
ITT Hanger	1530	7.13	1490	3.43	1720	7.33	1850	4.25
IUS Hanger	1450	9.76	1550	3.79	1790	12.8	1850	4.21
IUT Hanger	1430	7.48	1560	3.63	1700	4.09	1870	4.31

Percentage differences and *p*-values for the comparisons of the testing and the theoretical critical loads for the non-bracing system are shown in Table 5-6. For the simply supported end condition, the theoretical critical loads were greater compared with the critical loads from testing for both samples of wood I-joists. The theoretical critical loads of the 11 $^{7}/_{8}$ in. wood I-joists were on average 4.67% greater compared to the corresponding critical loads from testing. The theoretical critical loads of the 16 in. wood I-joists were on average 3.28% greater compared to the corresponding critical loads from testing. These differences can be explained from the reduction of the testing critical loads due to eccentricities on the applied loads and/or initial wood I-joists imperfections and deformations. The mean theoretical critical load of the 11 $^{7}/_{8}$ in. wood I-joists was not significantly different than the mean critical load from testing (p = 0.2233). Similarly, the mean theoretical critical load of the 16 in. wood I-joists was not significantly different than the mean critical load from testing (p = 0.5411). The theoretical model

for the simply supported end condition (Equation 3-6) predicted well the static lateral-torsional buckling critical loads.

Table 5-6: Comparison between Testing and Theoretical Critical Loads for the Non-Bracing System.

End Condition	11 7/8 in. Wood I-Joists		16 in. Wood I-Joists	
	Difference (%) [1]	*p*-values	Difference (%) [1]	*p*-values
Simply Supported	4.67	0.2233	3.28	0.5411
ITS Hanger	- 0.69	0.8565	- 0.58	0.8549
ITT Hanger	- 2.61	0.4043	7.56	0.0939
IUS Hanger	6.90	0.1946	3.35	0.5097
IUT Hanger	9.09	0.0533	10.0	0.0282

1 Difference (%) = ((Theoretical/Testing) – 1)100

The critical loads from testing were slightly greater than the theoretical critical loads for both samples of wood I-joists for the ITS hanger supported end condition (Table 5-5). The ITS wood I-joist hangers are able to rotate with respect to the vertical direction in the static lateral-torsional buckling tests. Thus, the ITS hangers are able to accommodate initial wood I-joist deformations as well as eccentricities in the application of the load, which increased the wood I-joist response to the applied load. The mean critical load from testing of the 11 7/8 in. wood I-joists was not significantly different than the mean theoretical critical load (p = 0.8565). Similarly, the mean critical load from testing of the 16 in. wood I-joists was not significantly different than the mean theoretical critical load (p = 0.8549). The critical loads from testing were more variable for both samples of wood I-joists compared with the corresponding theoretical critical loads, similar to the behavior observed for the simply supported end condition. The theoretical model for the hanger supported end condition (Equation 3-11) predicted accurately the static lateral-torsional critical loads when ITS hangers were used.

A Comparison between the theoretical critical loads from the simply supported end condition with the critical loads from testing for the ITS wood I-joist hanger revealed that the theoretical critical loads of the 11 7/8 in. wood I-joists were on average 9.03% greater compared to the corresponding critical loads from testing and the theoretical critical loads of the 16 in. wood I-joists were on average 10.5% greater compared to the corresponding critical loads from testing. The predicted critical loads improved using the theoretical model for the hanger supported end condition (Equation 3-11) rather than the theoretical model for the simply supported end condition (Equation 3-6).

The critical loads from testing of the 11 7/8 in. wood I-joists were 2.61% greater compared to the corresponding theoretical critical loads for the ITT hanger supported end condition (Table 5-6). The 16 in. wood I-joists displayed the opposite behavior, the theoretical critical loads were 7.56% greater than the corresponding theoretical critical loads (Table 5-6). The mean theoretical critical load of the 11 7/8 in. wood I-joists was not significantly different than the mean critical load from testing (p = 0.4043). Similarly, the mean theoretical critical load of the 16 in. wood I-joists was not significantly different than the mean critical load from testing (p = 0.0939). The critical loads from testing were more variable for both samples of wood I-joists compared with the

corresponding theoretical critical loads, similar to the behavior observed for the simply supported and the ITS hanger end supported conditions. The theoretical model for the hanger supported end condition (Equation 3-11) predicted accurately the static lateral-torsional critical loads when ITT hangers were used.

Comparison of the theoretical critical loads from the simply supported end condition with the critical loads from testing for the ITT wood I-joist hanger revealed that the theoretical critical loads of the 11 $^{7}/_{8}$ in. wood I-joists were on average 2.61% greater compared to the corresponding critical loads from testing and that the theoretical critical loads of the 16 in. wood I-joists were on average 9.88% greater compared to the corresponding critical loads from testing. The predicted critical loads improved using the theoretical model for the hanger supported end condition (Equation 3-11) rather than the theoretical model for the simply supported end condition (Equation 3-6).

Student's t tests were also performed comparing the critical loads from testing from the two top mount wood I-joist hangers, the ITS and the ITT hangers. The mean critical load of the ITS hanger of the 11 $^{7}/_{8}$ in. wood I-joists was not significantly different than the mean critical load of the ITT hanger (p = 0.1674). Similarly, the mean critical load of the ITS hanger of the 16 in. wood I-joists was not significantly different than the mean critical load of the ITT hanger (p = 0.8846). Physically the two wood I-joist hangers are similar and the installation and bearing surfaces on the supporting board of both hangers are also comparable.

The theoretical critical loads were greater compared with the critical loads from testing for both samples of wood I-joists for the IUS hanger supported end condition. The theoretical critical loads of the 11 $^{7}/_{8}$ in. wood I-joists were on average 6.90% greater compared to the corresponding critical loads from testing. The theoretical critical loads of the 16 in. wood I-joists were on average 3.35% greater compared to the corresponding critical loads from testing. The mean theoretical critical load of the 11 $^{7}/_{8}$ in. wood I-joists was not significantly different than the mean critical load from testing (p = 0.1946). Similarly, the mean theoretical critical load of the 16 in. wood I-joists was not significantly different than the mean critical load from testing (p = 0.5097). The top mount wood I-joist hangers have the ability to rotate with respect to the vertical axis during the lateral-torsional buckling tests. The face mount wood I-joist hangers are not able to rotate, so these hangers could not accommodate initial wood I-joist deformations and eccentricities in the load application. Consequently, initial deformations of the wood I-joist and/or eccentricities in the load application have greater effects on the lateral-torsional buckling instability when face mount hangers are used compared to top mount hangers. This explains the greater critical loads from testing observed for the IUS hanger compared to the ITS and the ITT hangers. The critical loads from testing were more variable for both samples of wood I-joists compared with the corresponding theoretical critical loads, similar to the behavior observed for the simply supported end condition as well as for the ITS and the ITT hanger supported end conditions. The theoretical model for the hanger supported end condition (Equation 3-11) predicted accurately the static lateral-torsional critical loads when IUS hangers are used.

Comparison of the theoretical critical loads from the simply supported end condition with the critical loads from testing for the IUS wood I-joist hanger revealed that the theoretical critical loads of the 11 $^{7}/_{8}$ in. wood I-joists were on average 8.28% greater compared to the corresponding critical loads from testing and that the theoretical critical loads of the 16 in. wood I-joists were on average 5.59% greater compared to the corresponding critical loads from testing. The predicted critical loads improved using the theoretical model for the hanger supported end condition (Equation 3-11) rather than the theoretical model for the simply supported end condition (Equation 3-6).

The theoretical critical loads of the 11 $^{7}/_{8}$ in. wood I-joists were on average 9.09% greater compared to the corresponding critical loads from testing for the IUT hanger supported end condition. The theoretical critical loads of the 16 in. wood I-joists were on average 10.0% greater compared to the corresponding critical loads from testing. The mean theoretical critical load of the 11 $^{7}/_{8}$ in. wood I-joists was not significantly different than the mean critical load from testing (p = 0.0533). However, the mean theoretical critical load of the 16 in. wood I-joists was significantly different than the mean critical load from testing (p = 0.0282). In testing, the wood I-joists had initial deformations and even though that care was taken in applying the load at the center of the wood I-joist, initial eccentricities in the load application occurred. The IUT hanger was the most restraining hanger with a lateral stiffness more than twice the IUS hanger stiffness value, and several times greater than the top mount wood I-joist hanger stiffness values (Table 5-3). The larger constraint of the IUT hangers prevented wood I-joist reorientations, thus explaining the larger percentage difference compared to the other hanger supported end conditions. As shown in Table 5-5, the critical loads from testing were more variable than the theoretical critical loads for the 11 $^{7}/_{8}$ in. wood I-joists, however the 16 in. wood I-joists displayed the opposite behavior, the theoretical loads were more variable than the critical loads from testing, this partially explains why the *Student's t* test differentiate the theoretical critical loads compared to the critical loads from testing.

Comparison of the theoretical critical loads from the simply supported end condition with the critical loads from testing for the IUT wood I-joist hanger revealed that the theoretical critical loads of the 11 $^{7}/_{8}$ in. wood I-joists were on average 9.79% greater compared to the corresponding critical loads from testing and that the theoretical critical loads of the 16 in. wood I-joists were on average 11.18% greater compared to the corresponding critical loads from testing. The predicted critical loads improved using the theoretical model for the hanger supported end condition (Equation 3-11) rather than the theoretical model for the simply supported end condition (Equation 3-6).

Student's t tests were also performed comparing the critical loads from testing from the two face mount wood I-joist hangers, the IUS and the IUT hangers. The mean critical load of the IUS hanger of the 11 $^{7}/_{8}$ in. wood I-joists was not significantly different than the mean critical load of the IUT hanger (p = 0.5233). Similarly, the mean critical load of the IUS hanger of the 16 in. wood I-joists was not significantly different than the mean critical load of the IUT hanger (p = 0.5120). Physically the two wood I-joist hangers are similar and the installation on the supporting board of both hangers are also comparable.

A theoretical model to calculate the static critical loads for a fixed supported end condition was derived in the Theoretical Models Chapter (Equation 3-18). This model represents a physical boundary of the maximum critical loads that theoretically can be reached. The theoretical critical loads for the fixed supported end condition averaged 1700 lb. for the 11 $^{7}/_{8}$ in. wood I-joists and 2050 lb. for the 16 in. wood I-joists. The theoretical critical loads of the 11 $^{7}/_{8}$ in. wood I-joists were on average 13.33% greater compared to the corresponding critical loads from testing for the simply supported end condition. The theoretical critical loads of the 16 in. wood I-joists were on average 12.02% greater compared to the corresponding critical loads from testing for the simply supported end condition. The simply supported end condition was chosen since it was the end condition with the greatest loads. The mean theoretical critical load of the 11 $^{7}/_{8}$ in. wood I-joists was significantly different than the mean critical load from testing for the simply supported end condition (p = 0.0175). However, the mean theoretical critical load of the 16 in. wood I-joists was not significantly different than the mean critical load from testing for the simply supported end condition (p = 0.0692). The variability of the critical loads of the 16 in. wood I-joists from testing of the simply supported end condition was relatively large, this explains the *Student's t* test result.

5.4.2: Static Critical Loads for the One-Bracing System

A transverse view at the mid-span of the static lateral-torsional buckling testing behavior of the wood I-joists for the one-bracing system is shown in Figure 5-9. The applied load and the braces were placed at the mid-span. Displacements, rotations and deflections shown in the figure represent the testing behavior, rather than the real dimensions of these deformations. The beginning of the test before load was applied and the wood I-joist is in initial position is shown in Figure 5-9 a).

The lateral-torsional buckling configuration of the loaded wood I-joist before the critical load was attained is shown in Figure 5-9 b). A vertical displacement of the loaded wood I-joist is observed with a consequent vertical displacement of the braces attached to the loaded wood I-joist. As the braces of the loaded wood I-joist displaced, the braces attached to the top surface of the loaded wood I-joist buckled and become inactive. The braces attached to the bottom surface of the loaded wood I-joist developed tension forces. These tension forces produced deflection in the top flanges of the braced wood I-joists forcing the braced wood I-joists to displace in the direction of the loaded wood I-joist. Each of the deflected top flange produced a lateral reaction force (F_{JD}) in the opposite direction as shown in Figure 5-9 b). The reaction forces are actually developed in the direction along the braces, but the vertical components of these forces have no effect on the lateral-torsional buckling instability. If the lateral bending stiffness (EI_y) of both top flanges of the braced wood I-joists are equal, then the forces produced at each top flange are also equal. In testing, no lateral displacement was observed on the bottom flanges of the braced wood I-joists due to the tension forces transmitted through the braces.

The lateral-torsional buckling instability of the loaded wood I-joist after the critical load was reached is shown in Figure 5-9 c). In this stage, the bottom flange of the loaded wood I-joist begins to rotate. Since the load head of the testing machine provided lateral constraint, lateral displacement of the loaded wood I-joist was prevented.

When the bottom flange of the loaded wood I-joist begins to rotate, one of the top flanges of one of the braced wood I-joists opposes the rotation (F_R) while the other top flange of the other braced wood I-joist favors the rotation in the same amount but in an opposite direction since the lateral bending stiffness of the top flanges of the braced wood I-joists are equal and this behavior is being developed in the elastic range of the materials. Thus, even after reaching the lateral-torsional buckling instability, the two braced wood I-joists are contributing in the same amount but in opposite directions to the lateral-torsional buckling instability of the loaded wood I-joist. In other words, the braced wood I-joists have no physical contribution on the lateral-torsional buckling instability of the loaded wood I-joist and consequently the static lateral-torsional buckling critical loads for the one-bracing system must be theoretically of the same magnitude than the critical loads for the non-bracing system. The analyses of the static lateral-torsional critical loads of the one-bracing system and the comparison of the one-bracing system to the non-bracing system that follows proved the previous discussion.

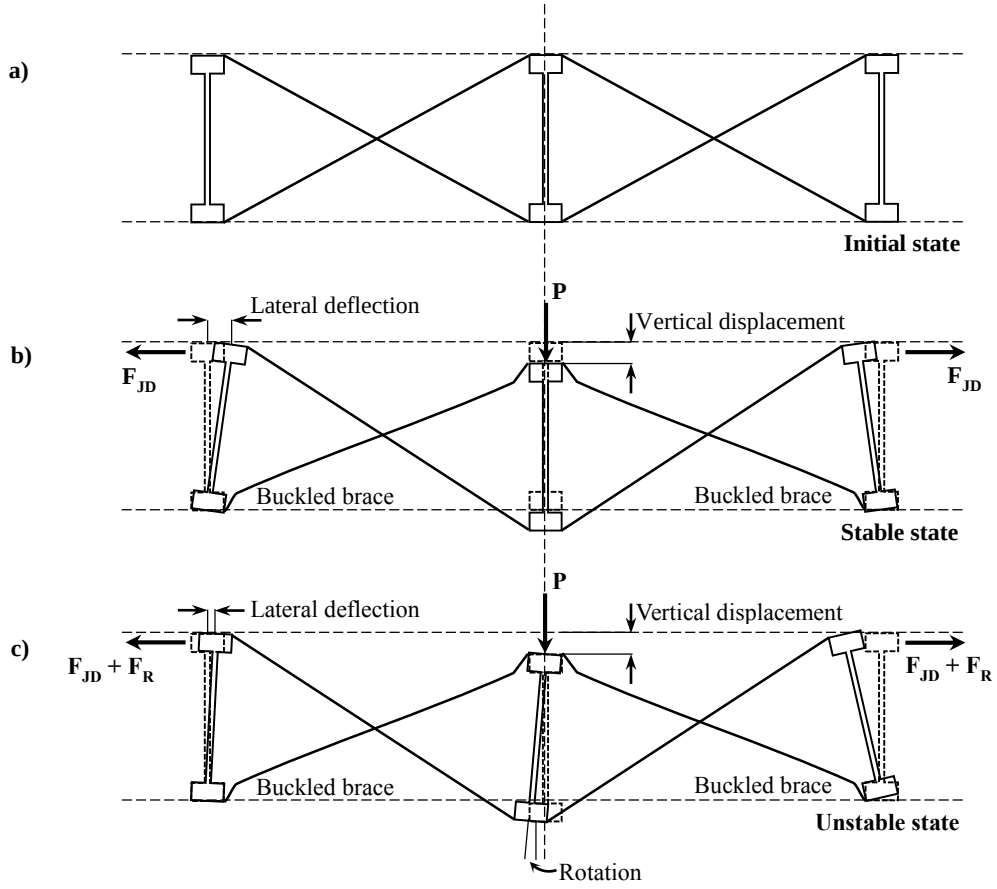

Figure 5-9: Static lateral-torsional buckling testing behavior at the mid-span for the one-bracing system.

The critical loads from testing for the one-bracing system are shown in Table 5-7. Because the same theoretical models apply to the non-braced and one-braced systems, the theoretical critical loads of the one-bracing system are the values in Table 5-5. The critical loads of the simple supported end condition of both sizes of wood I-joists were greater compared to the critical loads of all wood I-joist hangers, which is in agreement with the theoretical models. On average, the top mount wood I-joist hangers of both samples of wood I-joists had slightly greater

critical loads compared to the face mount hangers. This behavior is only possible if the wood I-joist is able to re-orientate itself to accommodate initial imperfections and eccentricities on the applied load. Theoretically, the braces should prevent these re-orientations, demonstrating that the one-bracing system was ineffective. In general, the variability of the critical loads from testing for the one-bracing system (Table 5-7) was smaller compared to the variability of the critical loads from testing for the non-bracing system (Table 5-5). Since the one-bracing tests were performed after the non-bracing tests, any initial eccentricity in the non-bracing tests may have been overcome by the time the one-bracing tests were carried out. *Student's t* tests were performed to compare the critical loads from testing for the non-bracing system to the critical loads from testing for the one-bracing system, and the *p*-values are displayed in Table 5-7. Except for the ITT hanger ($p = 0.0327$) for the 16 in. wood I-joists, the *Student's t* tests concluded that the difference between samples was not significantly different. The percentage differences between the two test configurations are shown in Table 5-7. The ITS hanger and the ITT hanger both top mount hangers reached the greatest percentage difference (6.25% and 3.92% respectively) for both samples of wood I-joists. The one-bracing system had no effects on the lateral-torsional buckling instability, while the top mount hangers were able of reorient to accommodate initial wood I-joist imperfections and eccentricities on the applied load. Therefore, the one-bracing system probably can absorb or reduce the initial wood I-joist imperfections of the attached wood I-joists.

Table 5-7: Static Critical Loads for the One-Bracing System and Testing Non-Bracing vs. One-Bracing Statistics.

End Condition	11 7/8 in. Wood I-Joists				16 in. Wood I-Joists			
	One-Bracing Testing		Non-Bracing vs. One-Bracing		One-Bracing Testing		Non-Bracing vs. One-Bracing	
	P_{cr} (lb.)	*CV* (%)	*p*-values	Difference (%) [1]	P_{cr} (lb.)	*CV* (%)	*p*-values	Difference (%) [1]
Simply Supported	1550	6.41	0.2393	3.33	1800	4.70	0.5878	- 1.64
ITS Hanger	1530	5.34	0.0940	6.25	1760	5.46	0.0536	2.92
ITT Hanger	1470	2.00	0.2755	- 3.92	1770	5.32	0.0327	2.91
IUS Hanger	1470	6.68	0.7771	1.38	1790	9.91	0.9178	0.00
IUT Hanger	1430	2.24	0.9683	0.00	1720	2.03	0.3943	1.18

1 Difference (%) = ((One-bracing/Non-bracing) – 1)100

5.4.3: Static Critical Loads for the Two-Bracing System

A transversal view at one of the quarters-span of the static lateral-torsional buckling testing behavior of the wood I-joists for the two-bracing system is depicted in Figure 5-10. The applied load was at the mid-span while the braces were placed at the quarter-spans. Displacements, rotations and deflections shown in the figure represent the testing behavior, rather than the real dimensions of these deformations. The two first stages in Figure 5-10 a) and b) are the equivalent of the corresponding for the one-bracing system of the previous section. The beginning of the test before loading was applied and the wood I-joist is in its initial position is shown in Figure 5-10 a). The lateral-torsional buckling instability of the loaded wood I-joist before the critical load was attained is shown in Figure 5-10 b).

The lateral-torsional buckling instability of the loaded wood I-joist after the critical load was achieved is shown in Figure 5-10 c). In this stage, the bottom flange of the loaded wood I-joist begins to rotate and to displace laterally. Since the top flange of the wood I-joist in which the load is being applied is attached to buckled braces, this flange is not able to transmit any force. When the bottom flange of the loaded wood I-joist begins to rotate and to displace laterally, this flange develops a force from the rotation (F_R) and a force from the lateral displacement (F_D). One of the top flanges of one of the braced wood I-joists opposes the rotation and the lateral displacement ($F_R + F_D$), while the other top flange of the other wood I-joist favors only the force developed from rotation (F_R). Therefore, the system becomes asymmetric, and has a different behavior compared to the one-bracing system. Consequently, at the moment when wood I-joist reaches the lateral-torsional buckling instability, the two top flanges of the braced wood I-joists are contributing with different reaction forces. The difference of the reaction forces can be taken as approximately ½ of the lateral bending stiffness of one of the braced wood I-joist (the lateral bending stiffness of one of the top flanges of one braced wood I-joist) as discussed in Chapter 3. Subsequently, the static lateral-torsional buckling critical loads for the two-bracing system can be calculated using the adjusted lateral bending stiffness from Equations 3-30 for the simply supported end condition and from Equations 3-32 for the hanger supported end conditions, where the term $\sum_{i=1}^{n} EI_{y_{bi}}$ equals ½ of the wood I-joist lateral bending stiffness.

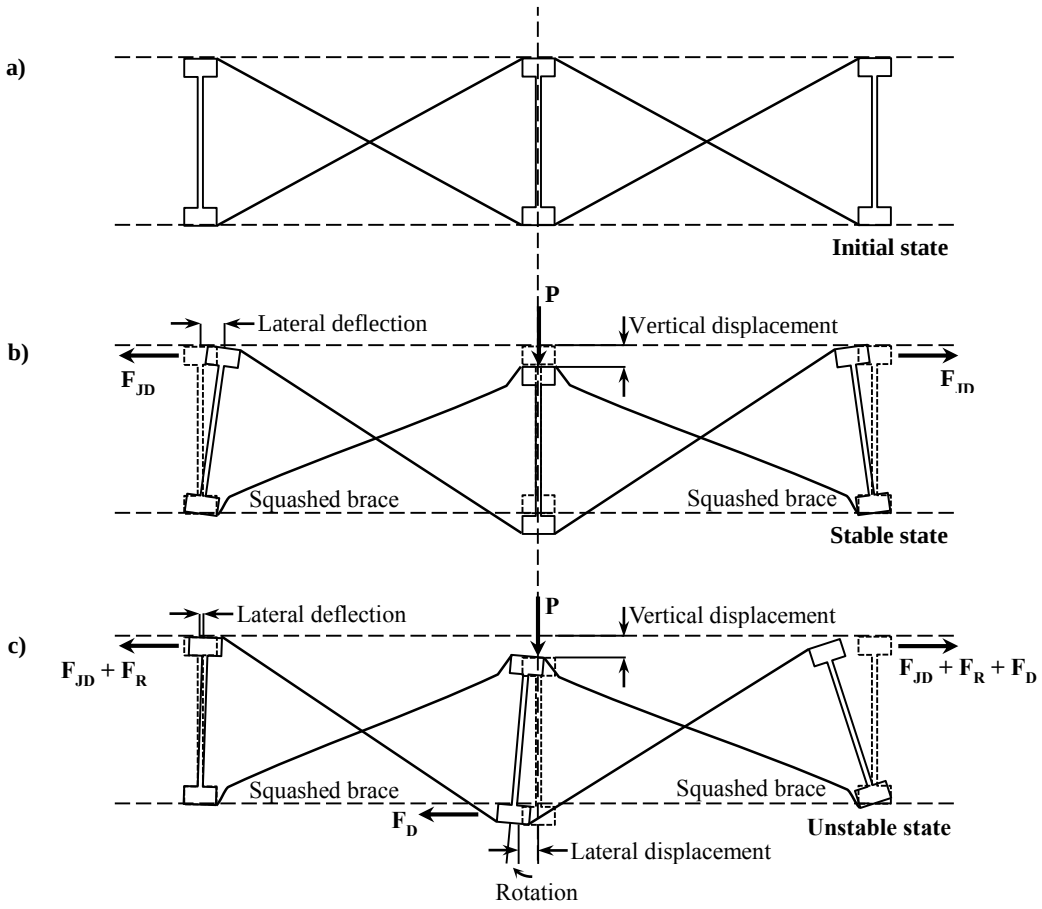

Figure 5-10: Static lateral-torsional buckling testing behavior at the quarter-span for the two-bracing system.

Static lateral-torsional critical loads (P_{cr}) for the two-bracing system are shown in Table 5-8. The theoretical critical loads were calculated using Equation 3-6 for the simply supported end condition and Equation 3-11 for the hanger supported end conditions. The lateral bending stiffness of the wood I-joists was adjusted from the previous analysis using Equation 3-30 for the simply supported end condition and Equation 3-32 for the hanger supported end conditions. The critical loads from testing were in most cases more variable compared to the theoretical critical loads for both sizes of wood I-joists. The variability from testing for the two-bracing system was on average smaller compared to the variability from testing for the non-bracing system.

Table 5-8: Static Critical Loads for the Two-Bracing System.

End Condition	11 7/8 in. Wood I-Joists				16 in. Wood I-Joists			
	Testing		Theoretical		Testing		Theoretical	
	P_{cr} (lb.)	CV (%)	P_{cr} (lb.)	CV (%)	P_{cr} (lb.)	CV (%)	P_{cr} (lb.)	CV (%)
Simply Supported	1710	4.49	1820	3.13	2070	2.96	2180	3.44
ITS Hanger	1660	7.17	1620	2.69	1940	2.81	1920	2.74
ITT Hanger	1760	6.02	1700	3.07	2010	2.83	2130	3.32
IUS Hanger	1620	6.52	1780	3.16	2010	4.68	2130	3.32
IUT Hanger	1720	5.18	1800	3.17	2110	9.12	2160	3.47

Percent differences and *p*-values for the comparisons between the testing and the theoretical critical loads for the two sizes of wood I-joists for the two bracing system are shown in Table 5-9. For the simply supported end condition, the theoretical critical loads of the 11 7/8 in. wood I-joists were on average 6.43% greater compared to the corresponding critical loads from testing, for the 16 in. wood I-joists the theoretical critical loads were on average 5.31% greater compared to the corresponding critical loads from testing. The reduction of the testing loads may be caused by eccentricities of the applied loads and/or initial wood I-joists imperfections and deformations. From the *Student's t* tests, the mean theoretical critical load of the 11 7/8 in. wood I-joists was not significantly different than the mean critical load from testing ($p = 0.1249$). However, the mean theoretical critical load of the 16 in. wood I-joists was significantly different than the mean critical load from testing ($p = 0.0378$). The smaller variability of the critical loads and the percentage difference of the 16 in. wood I-joists explains the results from the *Student's t* test. Differences between the theoretical critical loads and the critical loads from testing for the two-bracing system were somewhat similar to the corresponding differences found for the non-bracing system, concluding that the theoretical bracing model for the simply supported end condition (Equation 3-30) predicted accurately the restraint of the braces of the static lateral-torsional critical loads.

Table 5-9: Comparison between Testing and Theoretical Critical Loads for the Two-Bracing System.

End Condition	11 7/8 in. Wood I-Joists		16 in. Wood I-Joists	
	Difference (%) [1]	*p*-values	Difference (%) [1]	*p*-values
Simply Supported	6.43	0.1249	5.31	0.0378
ITS Hanger	- 2.41	0.6065	- 1.03	0.6155
ITT Hanger	- 3.41	0.4343	5.97	0.0297
IUS Hanger	9.88	0.0739	5.97	0.0752
IUT Hanger	4.65	0.1132	2.37	0.6017

1 Difference (%) = ((Theoretical/Testing) – 1)100

The critical loads from testing were greater 2.41% for the 11 $^{7}/_{8}$ in. wood I-joists and 1.03% for the 16 in. wood I-joists compared with the theoretical critical loads for the ITS hanger supported end condition. The re-orientation capability of the ITS hangers to accommodate initial wood I-joist imperfections and/or eccentricities on the application of the load seems to be retained in the two-bracing configuration system. No re-orientation of the ITS hangers of the braced wood I-joists to the loaded wood I-joist was observed in testing. Since the adjusted lateral bending stiffness of the wood I-joists from the ITS hangers is greater compared with the adjusted lateral bending stiffness for the simply supported end condition, the re-orientation capability of the ITS hanger is implicit in the bracing theoretical model Equation 3-32. From the *Student's t* tests, the mean critical load from testing of the 11 $^{7}/_{8}$ in. wood I-joists was not significantly different than the mean theoretical critical load (p = 0.6065). Similarly, the mean critical load from testing of the 16 in. wood I-joists was not significantly different than the mean theoretical critical load (p = 0.6155). The critical loads from testing were more variable for both sizes of wood I-joists compared with the corresponding theoretical critical loads, equivalent to the behavior observed for the ITS hanger supported end condition of the non-bracing system. Equally to the simply supported end condition, differences between the theoretical critical loads and the critical loads from testing for the two-bracing system were comparatively similar to the corresponding differences found for the non-bracing system. The bracing theoretical model (Equation 3-32) predicted accurately the restraint of the braces of the static lateral-torsional critical loads for the ITS hanger supported end condition.

The critical loads from testing from the ITT hanger supported end condition of the 11 $^{7}/_{8}$ in. wood I-joists were on average 3.41% greater compared to the corresponding theoretical critical loads (Table 5-9). The theoretical critical loads from the ITT hanger supported end condition of the 16 in. wood I-joists were on average 5.97% greater compared to the corresponding critical loads from testing. The mean critical load from testing of the 11 $^{7}/_{8}$ in. wood I-joists was not significantly different than the mean theoretical critical load (p = 0.4343). However, the mean critical load from testing of the 16 in. wood I-joists was significantly different than the mean theoretical critical load (p = 0.0297). The p-values are somewhat similar to the p-values obtained for the corresponding comparisons from the non-bracing system (p = 0.4043 for the 11 $^{7}/_{8}$ in. wood I-joist and p = 0.0939 for the 16 in. wood I-joist). Therefore, it seems that the differences found between the theoretical critical loads and the critical loads from testing are due to the static lateral-torsional buckling tests rather than due to the influence of the bracing system. In other words, the theoretical bracing models predicted the testing behavior well, while the theoretical static lateral-torsional buckling models predicted the testing behavior with the reported differences. The variability of the 11 $^{7}/_{8}$ in. wood I-joists was greater for the critical loads from testing compared to the theoretical critical loads, the variability of the 16 in. wood I-joists depicted the opposite behavior, the theoretical critical loads were more variable compared to the critical loads from testing, this results agree with the results obtained from the *Student's t* tests. Differences between the theoretical critical loads and the critical loads from testing for the two-bracing system were comparatively similar to the corresponding differences found for the non-bracing system. The theoretical bracing model (Equation 3-32) predicted accurately the restraint of the braces of

the static lateral-torsional critical loads for the ITT hanger supported end condition and proved that top mount wood I-joist hangers behaved in a similar way for the two-bracing system than for the non-bracing system.

The theoretical critical loads from the IUS hanger of the 11 $^{7}/_{8}$ in. wood I-joists were on average 9.88% greater compared to the corresponding critical loads from testing. Also, the theoretical critical loads of the 16 in. wood I-joists were on average 5.97% greater compared to the corresponding critical loads from testing. From the *Student's t* tests, the mean critical load from testing of the 11 $^{7}/_{8}$ in. wood I-joists was not significantly different than the mean theoretical critical load (p = 0.0739). Similarly, the mean critical load from testing of the 16 in. wood I-joists was not significantly different than the mean theoretical critical load (p = 0.0752). The bearing surface between the IUS hanger and the top flange of the wood I-joist is smaller compared to the average bearing surface of the other hanger supported end conditions (Table 4-3). The top bearing surface is important for the two-bracing system because the constraining effects of the bracing system are mainly due to the response of the top flanges of the braced wood I-joists, (Figure 5-10). This fact explains partially the relative larger percentage differences between theoretical critical loads and critical loads from testing of the IUS hanger supported end condition. The critical loads from testing were more variable for both samples of wood I-joists compared with the corresponding theoretical critical loads, equivalent to the behavior observed for the IUS hanger supported end condition of the non-bracing system. It seems that the theoretical bracing models do not increase the variability of the critical loads. The bracing theoretical model (Equation 3-32) predicted accurately the restraint of the braces of the static lateral-torsional critical loads for the IUS hanger supported end condition.

The theoretical critical loads of the 11 $^{7}/_{8}$ in. wood I-joists were on average 4.65% greater compared to the corresponding critical loads from testing for the IUT hanger. Also, the theoretical critical loads of the 16 in. wood I-joists were on average 2.37% greater compared to the corresponding critical loads from testing. From the *Student's t* tests, the mean critical load from testing of the 11 $^{7}/_{8}$ in. wood I-joists was not significantly different than the mean theoretical critical load (p = 0.1132). Similarly, the mean critical load from testing of the 16 in. wood I-joists was not significantly different than the mean theoretical critical load (p = 0.6017). The critical loads from testing were more variable for both samples of wood I-joists compared with the corresponding theoretical critical loads. The critical loads from testing of the 16 in. wood I-joists were the most variable, however the percentage difference between the theoretical critical loads and the critical loads from testing was smaller compared with the corresponding percentage difference of the 11 $^{7}/_{8}$ in. wood I-joist. The variability observed did not affect the effectiveness of the theoretical bracing models. The bracing theoretical model (Equation 3-32) predicted accurately the restraint of the braces of the static lateral-torsional critical loads for the IUT hanger supported end condition.

Theoretical models to calculate the bracing system constraint for the static lateral-torsional buckling critical loads for the fixed supported end condition were also derived in the Theoretical Models Chapter (Equations 3-31). The theoretical critical loads for the fixed supported end condition averaged 1910 lb. for the 11 $^{7}/_{8}$ in. wood I-joists and 2300 lb. for the 16 in. wood I-joists. The theoretical critical loads of the 11 $^{7}/_{8}$ in. wood I-joists were on

average 11.70% greater compared to the corresponding critical loads from testing for the simply supported end condition, and 11.11% greater compared to the corresponding critical loads for the simply supported end condition. The simply supported end condition was chosen for comparison since this was the end condition with the greatest loads. From the *Student's t* tests, the mean theoretical critical load of the 11 $^{7}/_{8}$ in. wood I-joists was significantly different than the mean critical load from testing for the simply supported end condition (p = 0.0306), and the mean theoretical critical load of the 16 in. wood I-joists was significantly different than the mean critical load from testing for the simply supported end condition (p = 0.0054). Percentage differences between the theoretical critical loads from the fixed supported end condition and the critical loads from testing for the simply supported end condition for the two-bracing system are somewhat similar to the corresponding differences of the non-bracing system, concluding that the bracing theoretical model (Equation 3-31) predicted accurately the restraint of the braces of the static lateral-torsional critical loads for the fixed supported end condition. The theoretical static lateral-torsional buckling model for the fixed supported end condition effectively predicted critical loads larger than those reached in testing for the simply supported end condition.

5.5: Lateral Bending Motion of the Wood I-Joists

The lateral bending motion was investigated by testing the same samples of wood I-joists, five different supported end conditions and three bracing systems used to measure the static lateral-torsional critical loads. The main goals of the lateral bending motion testing were to measure the maximum lateral displacements of the wood I-joists and to locate the position of the individual walking on the wood I-joists when the maximum lateral displacement occurred. The maximum lateral displacements and the individual position were compared to the predicted maximum lateral displacements and the individual position from the corresponding theoretical models.

Figure 5-11 is a diagram of the positions of the starting and the end points of the lateral bending motion of the wood I-joist test as well as the code for the lateral displacement measurements used in this research. FQT is the position at the top flange of the first quarter-span, FQB is the position at the bottom flange of the first quarter-span, MST is the position at the top flange of the mid-span, MSB is the position at the bottom flange of the mid-span, LQT is the position at the top flange of the last quarter-span and LQB is the position at the bottom flange of the last quarter-span.

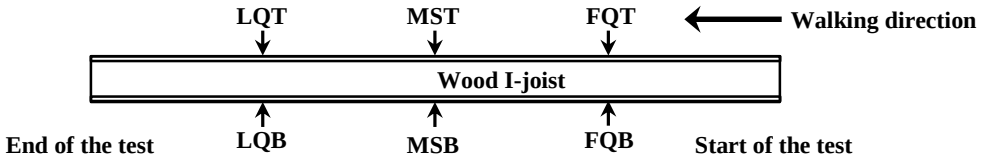

Figure 5-11: Measurement positions of the lateral bending motion testing.

Figure 5-12 is a graph of the lateral displacements of the six measurement positions used in testing (see Figure 5-11). The curves were plotted from the test data of a 16 in. wood I-joist for the simply supported end condition. The order of the curves are as follows, from the outer curve to the inner curve; MST, LQT, FQT, MSB, LQB and

FQB positions. Only five curves can be easily counted in Figure 5-12 since the FQT position and the MSB position were very similar, whit the LQT position slightly greater than MSB position. The lateral displacement versus time curves depicted in Figure 5-12 followed almost the same pattern and this behavior was observed in the majority of the lateral bending motion tests.

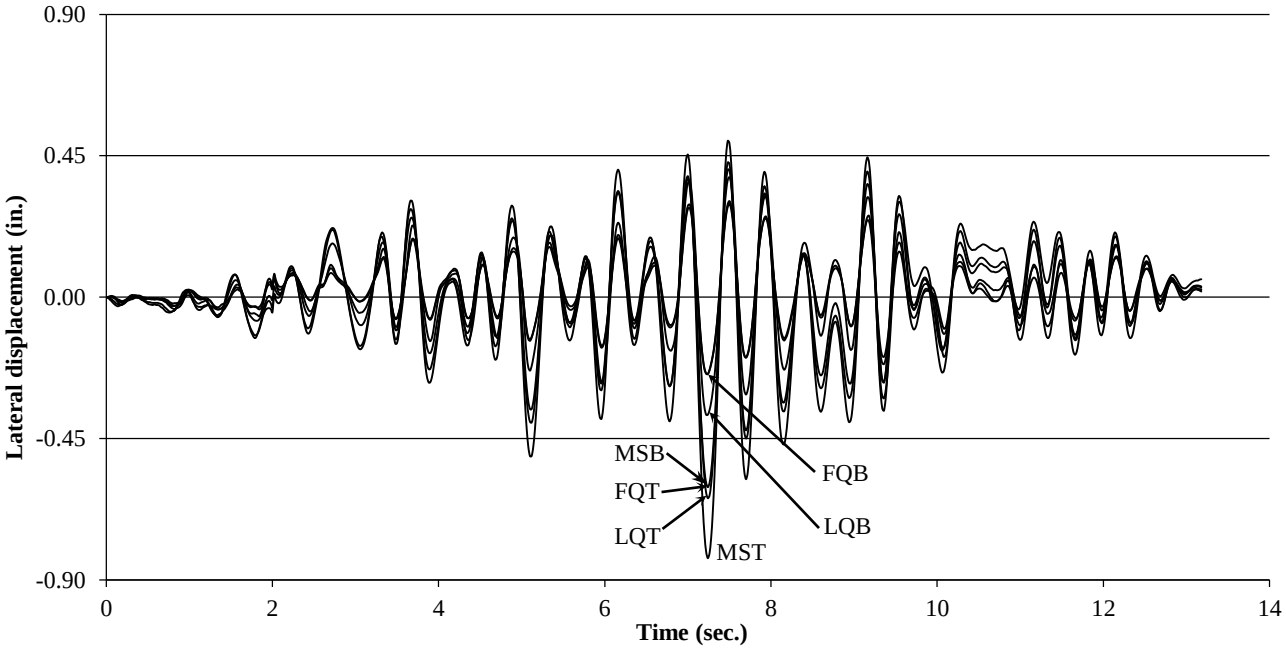

Figure 5-12: Lateral bending motion curves. Test of one 16 in. wood I-joist from the simply supported end condition.

The lateral bending motion of the wood I-joist data demonstrates that this type of testing is highly variable. Factors that added variability to the test included the walking steadiness, alterability in the lateral motion of the wood I-joist due to the walking pattern, difficulty in walking due to the increase of the lateral displacements, and variable step length, especially when the individual walking loses balance due to the wood I-joist movement. The variability in motion can induce a falling feeling in the individual walking causing abrupt changes in the walking pattern. In some cases, the individual stops completely for a few moments. When a falling feeling occurs, the lateral component of the force applied by the individual increases considerably as the human body tries to equilibrate itself.

Because the theoretical models for the lateral bending motion of the wood I-joists were derived considering a constant walking speed, the lateral component of the force and the length of the step were constants, some variations between the wood I-joist behavior observed in testing and the wood I-joist behavior predicted by the theoretical models were expected. However, the main objective of this research was not to mimic the general behavior of the wood I-joist, rather the calculation of the maximum lateral displacement and the position of the individual walking when the maximum lateral displacement occurs. If lateral-torsional buckling instability is attained under the weight of the individual walking, the instability must be at the time of the maximum displacement and at the position of the individual walking.

A comparison between the graphs of the lateral displacement measured at the MST position from the wood I-joist of Figure 5-12 and a graph obtained by plotting the theoretical model Equation 3-18 are shown in Figure 5-13. The maximum lateral displacement (0.811 in.) and the time at which this maximum lateral displacement occurred (7.32 sec.) predicted by the theoretical model were similar to the corresponding maximum lateral displacement (0.831 in.) and the time (7.24 sec.) from the plot from testing. The maximum lateral displacements in Figure 5-13 occurred at the point given by $\sqrt{\frac{L^2-(L-s)^2}{3}}$, but due to the physical characteristics of the testing, this location is close to the mid-span of the wood I-joist. The maximum lateral displacements occurred when the individual walking was standing at 132 in. for the testing plot and at 133 in. for the theoretical model plot.

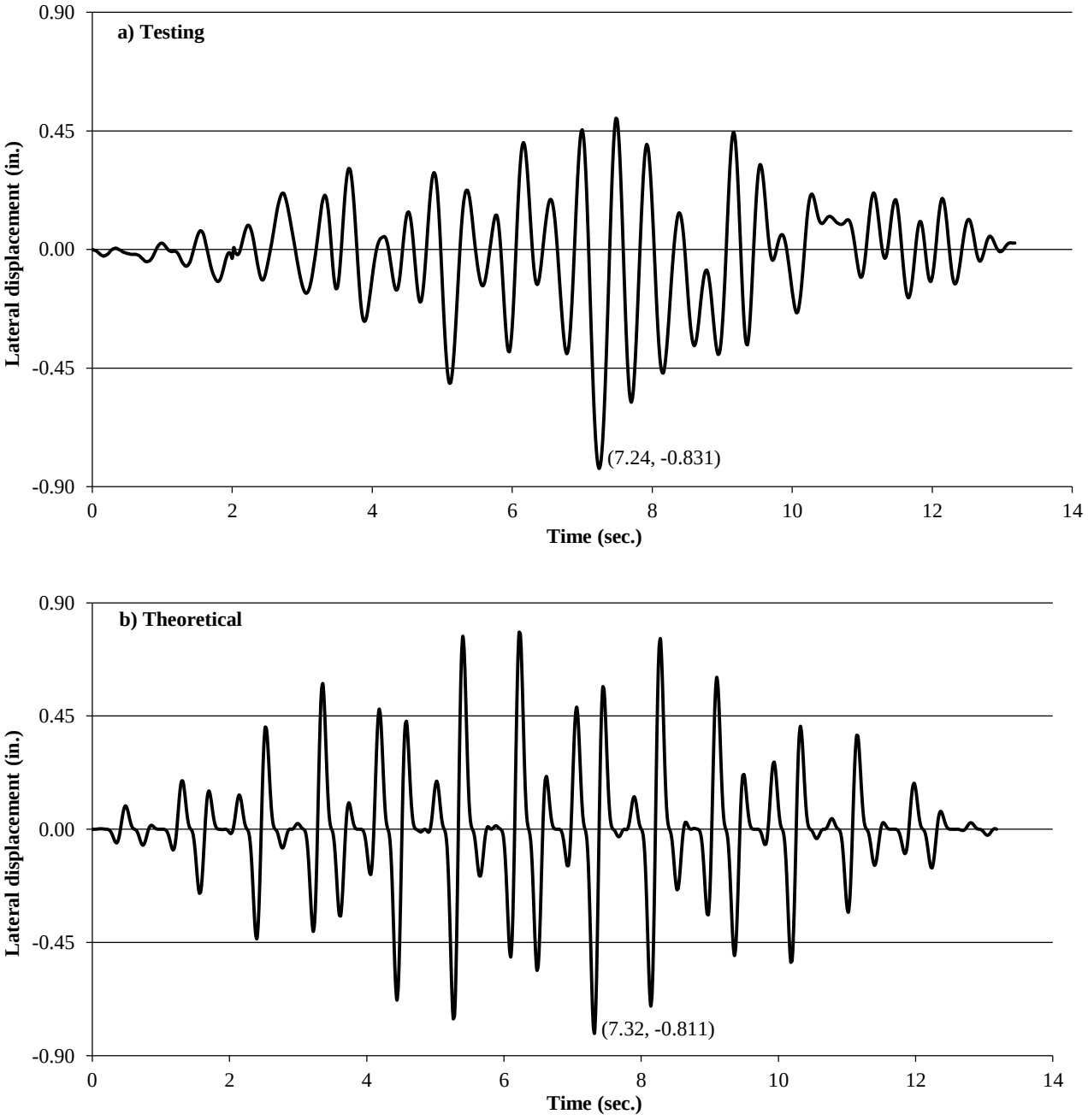

Figure 5-13: Testing and theoretical lateral bending motion curves, a) testing, b) theoretical.

The walking platform for the lateral bending motions tests is shown in the photographs of Figure 5-14. The end supports used in the lateral bending motion tests were the same used in the static lateral-torsional buckling tests. Comparing the photograph from the left with the photograph from the right, it is observed a wood I-joist lateral displacement induced by the lateral component of the force from the participant's weight.

Figure 5-14: Photographs showing the walking platform (left) and a participant walking on a wood I-joists (right).

The descriptive statistics for the walking time (t_T) and walking frequency (f_d) from a total of 150 lateral bending motion tests are displayed in Table 5-10. The standard deviation, kurtosis and skewness of both statistics proved that their samples can be considered as normally distributed. The maximum and minimum values show that no outliers are present. The mean values of 13.2 sec. for the walking time and 1.22 Hz. for the walking frequency will be used as input parameters for all dynamic theoretical models in all subsequent analysis of this research. The mean values are chosen instead of the individual walking times and walking frequencies from each test to overcome difficulties in the application of these parameters in the lateral bending motion theoretical models. If individual values for the walking time and waking frequency are used, closer theoretical values to the testing values are expected. However the testing may be modified to accommodate the theoretical models. Individual values for the walking time and walking frequency instead of the average values increase the number of variables in the dynamic analyses given few opportunities to be compared to the static analyses since in the static testing these variables were not presented.

Table 5-10: Descriptive Statistics for the Walking Time and Walking Frequency.

	Walking Time (t_T)	Walking Frequency (f_d)
Mean	13.2	1.22
Standard Deviation	0.941	0.0533
Kurtosis	- 0.840	- 0.575
Skewness	- 0.831	0.144
Minimum Value	11.3	1.17
Maximum Value	14.1	1.27
Number of Observations	150	150

The mass of the wood I-joist is an input parameter in the lateral bending motion theoretical models. The average mass for the 11 $^7/_8$ in. wood I-joists was 57.4 lb. and for the 16 in. wood I-joists was 66.6 lb. The variability of the mass was very small for both wood I-joist samples, the coefficient of variation for the 11 $^7/_8$ in. wood I-joist was of 1.16% while for the 16 in. wood I-joist it was of 1.30%. The variable mass is not expected to contribute greatly to the overall variability of the further dynamic lateral-torsional buckling analyses. The mass of the 16 in. wood I-joists was measured at a moisture content of approximately 12.4% while the mass of the 11 $^7/_8$ in. wood I-joists was measured at a moisture content of approximately 11.6%, before the lateral bending motion tests were conducted.

5.5.1: Lateral Bending Motion for the Non-Bracing System

The maximum lateral displacements and individual positions at the moment that the maximum lateral displacements occurred for the non-bracing system are shown in Table 5-11. The theoretical maximum lateral displacements and individual positions were calculated using Equation 3-18 for the simply supported end condition, and Equation 3-27 for the hanger supported end conditions. In order to use Equation 3-27, Equation 3-24 must be solved for ψ. Equation 3-24 is a transcendental equation and cannot be solved algebraically to obtain an exact solution. Therefore, a numerical procedure was used to find the solution. Equation 3-27 is very sensitive to the degree of exactness of the variable ψ so the solution was fixed to 1 x 10^{-8}. Equation 3-24 must be solved every time that the lateral bending stiffness of the wood I-joist and/or the lateral stiffness of the wood I-joist hanger change. Equation 3-27 contains a constant A to normalize the system as explained in Section 3.3.3. For the wood I-joist length used in this research an approximate solution for the constant A is $\sqrt{\frac{2\sinh\psi(1+\cosh\psi)}{mL\cosh\psi}}$.

In Table 5-11, the maximum lateral displacements were obtained from the displacement-load curves plotted from data from testing and from the theoretical models. The maximum lateral displacement was the value of the maximum absolute (at each side of the wood I-joist) peak displacement observed on the graph (Figure 5-12). The theoretical maximum lateral displacements were compared to the maximum lateral displacements from testing of the top flanges of the wood I-joists. The top flanges were chosen since the lateral component of the force imposed by the individual walking on the wood I-joist is directly applied to these flanges and observations of the static

lateral-torsional buckling tests noted that the web of the wood I-joist was not able to fully transmit the lateral bending forces of the top flange to the bottom flange. An analysis between the maximum lateral displacements of the top flanges and the maximum lateral displacements of the bottom flanges was also performed after the lateral bending motion of the wood I-joist analyses was completed.

Table 5-11: Maximum Lateral Displacements and Load Positions for the Non-Bracing System.

End Condition	11 7/8 in. Wood I-Joists											
	Testing						Theoretical					
	LQT		MST		Load Position		LQT		MST		Load Position	
	δ (in.)	*CV* (%)	δ (in.)	*CV* (%)	*s* (in.)	*CV* (%)	δ (in.)	*CV* (%)	δ (in.)	*CV* (%)	*s* (in.)	*CV* (%)
Simply Supported	0.787	13.4	1.12	16.8	133	20.2	0.636	4.98	0.900	4.96	122	8.97
ITS Hanger	0.626	9.73	0.907	11.1	132	13.3	0.841	4.64	1.15	4.60	120	13.8
ITT Hanger	0.668	14.6	0.964	17.2	128	6.89	0.763	4.46	1.05	4.59	126	10.4
IUS Hanger	0.776	14.7	1.09	12.7	139	8.25	0.693	7.02	0.958	5.32	120	5.93
IUT Hanger	0.658	26.5	0.922	22.5	129	23.7	0.652	7.75	0.917	7.72	122	10. 2
	16 in. Wood I-Joists											
Simply Supported	0.581	8.38	0.792	7.77	141	9.63	0.612	7.26	0.865	7.25	128	8.29
ITS Hanger	0.555	13.1	0.785	9.62	142	9.04	0.827	5.16	1.13	5.16	123	12.7
ITT Hanger	0.552	12.5	0.772	11.0	144	7.44	0.672	7.47	0.935	7.58	124	4.76
IUS Hanger	0.613	11.7	0.846	8.65	135	7.63	0.658	7.01	0.916	7.13	121	9.50
IUT Hanger	0.688	6.63	0.947	7.45	143	6.46	0.634	7.72	0.891	7.74	123	6.00

Percentage differences and *p*-values for the comparisons between the testing and the theoretical maximum lateral displacements and the load positions for the two sizes of wood I-joists for the non-bracing system are shown in Table 5-12. For the simply supported end condition with the 11 7/8 in. wood I-joists the maximum lateral displacements and individual positions from testing were greater compared to the corresponding theoretical maximum lateral displacements and individual positions. However, for the 16 in. wood I-joists the maximum lateral displacements from testing were smaller compared to the corresponding theoretical maximum lateral displacements (Table 5-12). The difference between the lateral displacements from the theoretical model and from testing may be due to testing performed on the simply supported end condition with the 11 7/8 in. wood I-joists was the first lateral bending motion testing performed. From the *Student's t* tests, the mean theoretical maximum lateral displacements of the 11 7/8 in. wood I-joists were not significantly different than the mean maximum lateral displacements from testing ($p = 0.0683$ at the LQT position and $p = 0.1042$ at the MST position). Similarly, the mean theoretical maximum lateral displacements of the 16 in. wood I-joists were not significantly different than the mean maximum lateral displacements from testing ($p = 0.4452$ at the LQT position and $p = 0.2155$ at the MST position). The mean theoretical load position of the 11 7/8 in. wood I-joists was not significantly different than the mean load position from testing ($p = 0.4382$). However, the mean theoretical load position of the 16 in. wood I-joists was significantly different than the mean load position from testing ($p = 0.0478$). The smaller variability observed in the load position from testing as well as in the theoretical model and the relative

large percentage difference explain the difference between the means of the load position of the 16 in. wood I-joists. The physical difference of the load positions between theoretical and testing of the 16 in. wood I-joists was 13 in. (Table 5-11), this amount is smaller than the average footstep length of the individual walking, concluding that even though the means are significantly different the load position from testing and the theoretical load position were reached by around the same footstep. The testing variability of the maximum lateral displacements and of the load positions were larger compared to the corresponding theoretical variability, similar behavior was observed on average in the static lateral-torsional buckling tests. The theoretical model for the simply supported end condition (Equation 3-18) predicted accurately the maximum lateral displacements due to the loading imposed by an individual walking on the wood I-joist.

Table 5-12: Comparison between Testing and Theoretical Maximum Lateral Displacements and Load Positions for the Non-Bracing System.

End Condition	11 7/8 in. Wood I-Joists					
	LQT		MST		Load Position	
	Difference (%) [1]	*p*-values	Difference (%) [1]	*p*-values	Difference (%) [1]	*p*-values
Simply Supported	- 19.2	0.0684	- 19.6	0.1042	- 6.02	0.4382
ITS Hanger	33.5	0.0028	26.8	0.0093	- 9.09	0.1940
ITT Hanger	14.2	0.0962	8.92	0.3189	- 1.56	0.8301
IUS Hanger	- 10.7	0.2713	-12.1	0.1616	- 13.7	0.0363
IUT Hanger	- 0.912	0.9379	- 0.542	0.9536	- 5.43	0.7156
	16 in. Wood I-Joists					
Simply Supported	5.34	0.4452	9.22	0.2155	- 9.22	0.0478
ITS Hanger	49.0	0.0029	43.9	0.0017	- 13.4	0.0651
ITT Hanger	21.7	0.0807	21.1	0.0753	- 13.9	0.0162
IUS Hanger	7.34	0.3054	8.27	0.2037	- 10.4	0.1763
IUT Hanger	- 7.85	0.1854	- 5.91	0.3280	- 14.0	0.0108

1 Difference (%) = ((Theoretical/Testing) – 1)100

The theoretical maximum lateral displacements were greater than the maximum lateral displacements from testing for both sizes of wood I-joists for the ITS hanger supported end condition. The theoretical maximum lateral displacements of the 11 7/8 in. wood I-joists were on average 33.5% greater at the LQT position and 26.8% greater at the MST position compared to the corresponding maximum lateral displacements from testing. For the 16 in. wood I-joists the maximum lateral displacements were on average 49.0% greater at the LQT position and 43.9% greater at the MST position than the corresponding maximum lateral displacements from testing. From the *Student's t* tests, the mean theoretical maximum lateral displacements of the 11 7/8 in. wood I-joists were significantly different than the mean maximum lateral displacements from testing ($p = 0.0028$ at the LQT position and $p = 0.0093$ at the MST position). Similarly, the mean theoretical maximum lateral displacements of the 16 in. wood I-joists were significantly different than the mean maximum lateral displacements from testing ($p = 0.0029$ at the LQT position and $p = 0.0017$ at the MST position). Statistical results were similar between the two samples of wood I-joists concluding that the ITS hanger supported end condition behaves similarly for the two wood I-

joist heights. The theoretical model assumed that the wood I-joist hanger has a constant lateral stiffness along the entire hanger length, but this behavior was not observed in testing. The hanger had no lateral support at the bottom flange while it was fully supported at the top flange. Since the individual walking on the wood I-joist is applying the lateral force directly at the top flange, the bottom flange has little contribution to the overall wood I-joist lateral bending behavior. Differences between the maximum lateral displacements from testing compared to the corresponding displacements from the theoretical models were greater for the 16 in. wood I-joists than for the 11 $^{7}/_{8}$ in. wood I-joists. The lateral hanger stiffness of the 16 in. wood I-joist was smaller than the lateral hanger stiffness of the 11 $^{7}/_{8}$ in. wood I-joists which contributed to this behavior. The load position from testing were greater compared to the theoretical load position for both sizes of wood I-joists (Table 5-12). The mean theoretical load position of the 11 $^{7}/_{8}$ in. wood I-joists was not significantly different than the mean load position from testing (p = 0.1940). Similarly, the mean theoretical load position of the 16 in. wood I-joists was not significantly different than the mean load position from testing (p = 0.0651). Physically, these results conclude that the predicted load positions and the load positions from testing were reached around the same footstep given by the individual walking.

The maximum lateral displacements and load positions from testing for the ITS hanger supported end condition were also compared to the theoretical maximum lateral displacements and load positions of the simply supported end condition as shown in Table 5-13. The percentage differences of the maximum lateral displacements as well as of the load positions of the two samples of wood I-joists were considerably reduced. In contrast, all p-values were substantially increased especially for the maximum lateral displacements. The theoretical model for the simply supported end condition predicted better the testing maximum lateral displacement of the ITS wood I-joist hanger supported end condition. Reasons include; the applied lateral force from the individual walking was at the top flange of the wood I-joist. The top flange is more constrained than the predicted average value from the theoretical model for the hanger supported end condition.

Table 5-13: Maximum Lateral Displacement and Load Position Comparisons between Testing Hanger Supported End Conditions and the Theoretical Simply Supported End Condition for the Non-Bracing System.

End Condition	11 $^{7}/_{8}$ in. Wood I-Joists					
	LQT		MST		Load Position	
	Difference (%) [1]	p-values	Difference (%) [1]	p-values	Difference (%) [1]	p-values
ITS Hanger	0.952	0.7710	- 0.772	0.9031	- 5.30	0.2377
ITT Hanger	- 4.79	0.5286	- 6.64	0.4500	- 2.34	0.7655
IUS Hanger	- 18.0	0.0670	- 17.4	0.0570	- 10.1	0.1079
IUT Hanger	- 3.34	0.7901	- 2.39	0.8214	- 3.10	0.7334
	16 in. Wood I-Joists					
ITS Hanger	10.3	0.2549	10.2	0.1735	- 9.86	0.1258
ITT Hanger	10.9	0.3001	12.0	0.2201	-11.1	0.0031
IUS Hanger	- 0.163	0.9833	2.25	0.7340	- 5.19	0.4014
IUT Hanger	- 11.0	0.0926	- 8.66	0.1649	- 10.5	0.1180

1 Difference (%) = ((Theoretical/Testing) – 1)100

The theoretical maximum lateral displacements of the ITT hanger supported end condition with the 11 $^{7}/_{8}$ in. wood I-joists were on average 14.2% greater at the LQT position and 8.92% greater at the MST position compared to the corresponding maximum lateral displacements from testing. For the 16 in. wood I-joists the maximum lateral displacements were on average 21.7% greater at the LQT position and 21.1% greater at the MST position than the corresponding maximum lateral displacements from testing. The differences between the maximum lateral displacements from the theoretical model and from testing are explained by the same discussion as the ITS hanger of the previous section since both hangers the ITT and the ITS are top mount hangers. It was stated a constant lateral stiffness along the entire length of the hanger for the theoretical model but not for the tests which were fully supported at the top flange of the wood I-joist where the lateral component of the force imposed by the individual walking was applied. The differences between the theoretical maximum lateral displacements and the maximum lateral displacements from testing are larger for the ITS hanger than for the ITT hanger due to the increase of the lateral hanger stiffness of the ITT hanger (Table 5-3). The load position from testing was greater compared to the theoretical load position for both sizes of wood I-joists (Table 5-12). A similar result was observed in the ITS hanger supported end condition. From the *Student's t* tests, the mean theoretical maximum lateral displacements of the 11 $^{7}/_{8}$ in. wood I-joists were not significantly different than the mean maximum lateral displacements from testing (p = 0.0962 at the LQT position and p = 0.3189 at the MST position). Similarly, the mean theoretical maximum lateral displacements of the 16 in. wood I-joists were not significantly different than the mean maximum lateral displacements from testing (p = 0.0807 at the LQT position and p = 0.0753 at the MST position). Statistical results were similar between the two samples of wood I-joists concluding that the ITS hanger supported end condition behaves similarly for the two wood I-joist heights. As the lateral hanger stiffness increases the theoretical model for the hanger supported end condition shows better maximum lateral displacement predictions. The mean theoretical load position of the 11 $^{7}/_{8}$ in. wood I-joists was not significantly different than the mean load position from testing (p = 0.8301). However, the mean theoretical load position of the 16 in. wood I-joists was significantly different than the mean load position from testing (p = 0.0162). The percentage difference of the load positions of the 16 in. wood I-joists was relatively large (Table 5-12), explaining the *Student's t* test result. The difference between the testing and the theoretical load positions means that the individual walking on the wood I-joists applied greater lateral force beyond the mid-span of the wood I-joists. Reasons include; the participant found some problems in the walking process beyond the mid-span, a falling feeling happened and the participant tried to recover balance and the walking frequency was modified beyond the mid-span and superimposed to the natural movement of the wood I-joist.

The maximum lateral displacements and load positions from testing for the ITT hanger supported end condition were also compared to the theoretical maximum lateral displacements and load positions of the simply supported end condition as shown in Table 5-13. The percentage differences of the maximum lateral displacements of the two samples of wood I-joists were reduced. In contrast, all p-values were increased. The theoretical model for the simply supported end condition better predicted the testing maximum lateral displacements of the ITS wood I-

joist hanger end supported condition. While the prediction of the load positions from either the theoretical model for the simply supported end condition or the theoretical model for the hanger supported end condition is approximately equal.

Student's t tests were also performed comparing the maximum lateral displacements and load positions from testing from the two top mount wood I-joist hangers, the ITS and the ITT hangers. The mean maximum lateral displacements of the ITS hangers of the 11 $^{7}/_{8}$ in. wood I-joists were not significantly different than the mean maximum lateral displacements of the ITT hangers (p = 0.4879 at the LQT position and p = 0.5247 at the MST position). Similarly, the mean maximum lateral displacements of the ITS hangers of the 16 in. wood I-joists were not significantly different than the mean maximum lateral displacements of the ITT hangers (p = 0.9506 at the LQT position and p = 0.8010 at the MST position). The mean load position of the ITS hangers of the 11 $^{7}/_{8}$ in. wood I-joists was not significantly different than the mean load position of the ITT hangers (p = 0.7061). Similarly, the mean load position of the ITS hangers of the 16 in. wood I-joists was not significantly different than the mean load position of the ITT hangers (p = 0.7905). These results are in agreement with the results of the static lateral-torsional buckling tests. Physically the two wood I-joist hangers are similar and the installation and bearing surfaces on the supporting board of both hangers are also comparable.

The test results of the IUS hanger end supported condition show that the maximum lateral displacements from testing were greater (10.7% at the LQT position and 12.1 at the MST position) compared to the theoretical maximum lateral displacements of the 11 $^{7}/_{8}$ in. wood I-joists. However, the results of the 16 in. wood I-joist were the opposite, the theoretical maximum lateral displacements were greater (7.34% at the LQT position and 8.27 at the MST position) compared to the maximum lateral displacements from testing. From the *Student's t* tests, the mean theoretical maximum lateral displacements of the 11 $^{7}/_{8}$ in. wood I-joists were not significantly different than the mean maximum lateral displacements from testing (p = 0.2713 at the LQT position and p = 0.1616 at the MST position). Similarly, the mean theoretical maximum lateral displacements of the 16 in. wood I-joists were not significantly different than the mean maximum lateral displacements from testing (p = 0.3054 at the LQT position and p = 0.2037 at the MST position). Statistical results were similar between the two samples of wood I-joists concluding that the IUS hanger supported end condition behaves similarly for the two wood I-joist heights. The theoretical models for the IUS hanger supported end condition (Equation 3-27) predicted accurately the maximum lateral displacements when IUS hangers are used. The load position from testing were greater compared to the theoretical load position for both samples of wood I-joists (Table 5-12), similar to the result observed in the ITS and ITT hanger supported end conditions as well as in the simply supported end condition. The mean theoretical load position of the 11 $^{7}/_{8}$ in. wood I-joists was significantly different than the mean load position from testing (p = 0.0363), however, the mean theoretical load position of the 16 in. wood I-joists was not significantly different than the mean load position from testing (p = 0.1763). A difference between the testing and the theoretical load positions means that the individual walking on the wood I-joists applied greater lateral force

beyond the mid-span of the wood I-joists. Reasons for the increase in the lateral force were given in the previous paragraph for the ITT hanger supported condition.

The maximum lateral displacements and load positions from testing for the IUS hanger supported end condition were also compared to the theoretical maximum lateral displacements and load positions of the simply supported end condition as shown in Table 5-13. The theoretical model for the hanger supported end condition predicted better the maximum lateral displacements of the 11 $^{7}/_{8}$ in. wood I-joists when IUS hangers are used, however the theoretical model for the simply supported end condition predicted better the maximum lateral displacements of the 16 in. wood I-joists when IUS hangers are used.

The maximum lateral displacements from testing were greater 0.912% at the LQT position and 0.542% at the MST position for the 11 $^{7}/_{8}$ in. wood I-joists, and 7.85% at the LQT position and 5.91% at the MST position for the 16 in. wood I-joists compared to the theoretical maximum lateral displacements of the IUT hanger supported end condition. Percentage differences between testing and theoretical maximum lateral displacements of the IUT hanger were on average the smallest of all wood I-joists hangers. In contrast, the corresponding differences of the ITS hanger were the greatest of all wood I-joists hangers. As the lateral hanger stiffness increases, the theoretical model for the hanger supported end condition improves the maximum lateral displacements predictions. The load position from testing was greater compared to the theoretical load position for both samples of wood I-joists (Table 5-12), a similar result was observed in all other hanger supported end conditions as well as in the simply supported end condition. From the *Student's t* tests, the mean theoretical maximum lateral displacements of the 11 $^{7}/_{8}$ in. wood I-joists were not significantly different than the mean maximum lateral displacements from testing (p = 0.9379 at the LQT position and p = 0.9536 at the MST position). Similarly, the mean theoretical maximum lateral displacements of the 16 in. wood I-joists were not significantly different than the mean maximum lateral displacements from testing (p = 0.1854 at the LQT position and p = 0.3280 at the MST position). The mean theoretical load position of the 11 $^{7}/_{8}$ in. wood I-joists was not significantly different than the mean load position from testing (p = 0.7156). However, the mean theoretical load position of the 16 in. wood I-joists was significantly different than the mean load position from testing (p = 0.0108). A change in the lateral force imposed by the individual walking on the wood I-joist beyond the mid-span of the wood I-joist is the cause of the difference between the predicted and the testing load positions. Reasons that cause a lateral force change were previously discussed for some of the other hanger supported end conditions.

The maximum lateral displacements and load positions from testing for the IUT hanger supported end condition were also compared to the theoretical maximum lateral displacements and load positions of the simply supported end condition as shown in Table 5-13. The percentage differences of the maximum lateral displacements of the two samples of wood I-joists increased. In contrast, all p-values were reduced. The theoretical model for the hanger supported end condition rather than the theoretical model for the simply supported end condition predicted better the testing maximum lateral displacements when IUT wood I-joist hangers are used.

Student's t tests were also performed comparing the maximum lateral displacements and load positions from testing from the two face mount wood I-joist hangers, the IUS and the IUT hangers. The mean maximum lateral displacements of the IUS hangers of the 11 $^{7}/_{8}$ in. wood I-joists were not significantly different than the mean maximum lateral displacements of the IUT hangers (p = 0.1477 at the LQT position and p = 0.1007 at the MST position). However, the mean maximum lateral displacements of the IUS hangers of the 16 in. wood I-joists were significantly different than the mean maximum lateral displacements of the IUT hangers (p = 0.0168 at the LQT position and p = 0.0259 at the MST position). The 16 in. IUS hangers presented different maximum lateral displacements than the 16 in. IUT hangers. Differences between maximum lateral displacements of the IUS hangers compared to the IUT hangers were mainly due to differences in the lateral component of the force imposed by the individual walking. The mean load position of the IUS hangers of the 11 $^{7}/_{8}$ in. wood I-joists was not significantly different than the mean load position of the IUT hangers (p = 0.5237). Similarly, the mean load position of the IUS hangers of the 16 in. wood I-joists was not significantly different than the mean load position of the IUT hangers (p = 0.3508).

A theoretical model to calculate the maximum lateral displacements and load positions for a fixed supported end condition was derived in Chapter 3 (Equation 3-22). This model represents a physical boundary of the smallest maximum lateral displacements than theoretically can be reached. The theoretical maximum lateral displacements for the fixed supported end condition averaged 0.146 in. at the LQT position and 0.187 in. at the MST position for the 11 $^{7}/_{8}$ in. wood I-joists and 0.162 in. at the LQT position and 0.207 at the MST position for the 16 in. wood I-joists. For the 11 $^{7}/_{8}$ in. wood I-joists the maximum lateral displacements from testing of the simply supported end condition were 5.39 times greater at the LQT position and 5.99 times greater at the MST position compared to the theoretical maximum lateral displacements from the fixed supported end condition. For the 16 in. wood I-joists the maximum lateral displacements from testing of the simply supported end condition were 3.59 times greater at the LQT position and 3.83 times greater at the MST position compared to the theoretical maximum lateral displacements from the fixed supported end condition. The simply supported end condition was chosen since this is the end condition with the smallest lateral maximum displacements. The theoretical lateral bending motion model for the fixed end supported condition provided smaller values for the maximum lateral displacements.

5.5.2: Wood I-Joist Rotation for the Non-Bracing System

The top flanges of the wood I-joists underwent greater maximum lateral displacements compared to the maximum lateral displacements of the bottom flanges. Therefore, the wood I-joists experienced some rotation separate from the lateral displacements shown in Figure 5-15. Rotation of the wood I-joist was calculated by the following formula $\beta = \tan^{-1}\left(\frac{d_{tf}-d_{bf}}{2a}\right)$, where d_{tf} is the lateral displacement of the top flange of the wood I-joist, d_{bf} is the lateral displacement of the bottom flange of the wood I-joist, and a is the half of the wood I-joist height.

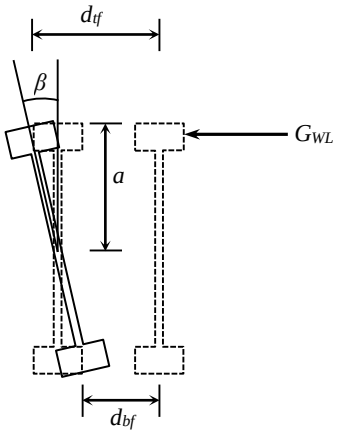

Figure 5-15: Wood I-joist rotation from the lateral bending motion.

The simply supported end condition and the hanger supported end conditions presented similar rotation behaviors for each wood I-joist sample as shown in Table 5-14. For instance, on average the greatest rotation value was observed for the IUS hanger of the 11 $^{7}/_{8}$ in. wood I-joists while for the 16 in. wood I-joists the greatest rotation value was observed for the IUT hanger. The IUS and the IUT hangers are both face mount hangers, so the top mount hangers did not display larger rotations, even though these hangers were not constrained at the bottom. The difference between the maximum and the minimum rotation values was 0.48 degrees for the 11 $^{7}/_{8}$ in. wood I-joists and 0.44 degrees for the 16 in. wood I-joists. Reasons for the differences in rotation include variation in the lateral component of the force applied by the individual walking on the wood I-joist, and the wood I-joist capacity to transmit the lateral displacement of the top flange to the bottom flange.

Table 5-14: Wood I-Joist Rotation from the Lateral Bending Motion Tests of the Non-Bracing System.

Sample	Simply Supported β (Degrees)	ITS Hanger β (Degrees)	ITT Hanger β (Degrees)	IUS Hanger β (Degrees)	IUT Hanger β (Degrees)
11 $^{7}/_{8}$ in. Wood I-Joists	1.82	1.74	1.89	2.22	1.76
16 in. Wood I-Joists	1.20	1.32	1.40	1.41	1.64

Because the wood I-joist rotations between the different supported end conditions were similar, general descriptive statistics were obtained as shown in Table 5-15. The descriptive statistics were calculated for the simply supported and the four hanger end supported conditions of Table A-13 and Table A-14 in the Appendix, totalizing 25 values for each wood I-joist sample. For the 11 $^{7}/_{8}$ in. wood I-joist the average rotation of the wood I-joists was 1.89 degrees while for the 16 in. wood I-joists the average rotation was 1.39 degrees. The standard deviations, kurtoses and skewness for both wood I-joist samples imply that both sizes are approximately normally distributed. The maximum and minimum values of the rotation measurements demonstrated that not outliers were presented in the samples.

Table 5-15: Descriptive Statistics for the Wood I-Joist Rotation from the Lateral Bending Motion of the Non-Bracing System.

	11 7/8 in. Wood I-Joists	16 in. Wood I-Joists
Mean (degrees)	1.89	1.39
Standard Deviation	0.317	0.235
Kurtosis	- 0.427	- 0.331
Skewness	0.397	0.259
Minimum Value	1.29	0.957
Maximum Value	2.49	1.89
Number of Observations	25	25

5.5.3: Lateral Bending Motion for the One-Bracing System

The maximum lateral displacements and individual positions at the moment that the maximum lateral displacements occurred for the one-bracing system are shown in Table 5-16. The theoretical maximum lateral displacements and individual positions were calculated using Equation 3-18 for the simply supported end condition, and Equation 3-27 for the hanger supported end conditions. The influence of the one-bracing system on the wood I-joist lateral bending motion was investigated using Equations 3-30 for the simply supported end condition and Equations 3-32 for the hanger supported end conditions. It was demonstrated previously (see Figure 5-9 and Section 5.3.2) that the one-bracing system had no influence on the static lateral-torsional buckling instability according to the physical characteristics of the particular testing performed in this research. Several differences were observed and are physically explained between the bracing system for the lateral bending motion tests and for the static lateral-torsional buckling tests. The static lateral-torsional buckling instability is a condition of unstable equilibrium meaning that a slight increase in the applied load beyond the critical value will deform the wood I-joist indefinitely. In contrast, the lateral bending motion is a condition of stable equilibrium meaning that a slight increase in the applied load will produce only a slight deformation on the wood I-joist. Therefore, the focus of the static lateral torsional buckling instability is the static equilibrium of the forces at the critical state while the focus of the lateral bending motion is the dynamic equilibrium of the forces. The vertical force applied to the wood I-joist in the lateral bending motion tests was on average approximately 10 times smaller compared with the vertical critical force applied to the wood I-joist in the static lateral-torsional buckling tests. Therefore, the forces that the bracing system must carry were approximately 10 times smaller in the lateral bending motion tests. It was observed that the braces were not able to withstand with the compression forces derived from the static lateral-torsional buckling tests. However the braces were able to withstand with the compression forces derived from the lateral bending motion tests. For instance, the braces were changed for each test in the static lateral-torsional buckling tests because damage occurred. The braces for the lateral bending motion tests were never changed, and the same braces were used every single time for all tests. In the lateral bending motion tests, the wood I-joists moved sideways periodically (Figure 5-12). The braced wood I-joists behaved as springs after the lateral movement was initiated and, consequently, the braces only transmitted forces due to the energy loss in

the wood I-joists by internally friction forces and forces from the increase of the lateral deflection of the loaded wood I-joist. Therefore, the theoretical bracing models for the lateral bending motion were fully applied as stated in Section 3.4.1 for the simply supported end condition and Section 3.4.3 for the hanger supported end conditions.

Table 5-16: Maximum Lateral Displacements and Load Positions for the One-Bracing System.

End Condition	11 7/8 in. Wood I-Joists											
	Testing						Theoretical					
	LQT		MST		Load Position		LQT		MST		Load Position	
	δ (in.)	*CV* (%)	δ (in.)	*CV* (%)	*s* (in.)	*CV* (%)	δ (in.)	*CV* (%)	δ (in.)	*CV* (%)	*s* (in.)	*CV* (%)
Simply Supported	0.279	37.6	0.352	44.3	145	7.99	0.213	2.13	0.301	2.15	125	5.25
ITS Hanger	0.168	5.92	0.207	6.57	146	9.52	0.333	3.89	0.510	3.45	116	17.3
ITT Hanger	0.225	12.1	0.288	17.5	140	9.37	0.311	2.84	0.430	2.70	125	6.10
IUS Hanger	0.221	40.1	0.263	32.9	140	8.61	0.253	2.57	0.347	2.61	125	6.90
IUT Hanger	0.231	29.1	0.294	30.3	138	4.18	0.231	2.45	0.321	2.66	120	8.12
	16 in. Wood I-Joists											
Simply Supported	0.162	17.5	0.194	23.1	140	8.42	0.203	3.32	0.287	3.43	131	5.74
ITS Hanger	0.155	20.2	0.210	19.2	140	15.0	0.319	6.16	0.510	5.10	125	1.79
ITT Hanger	0.149	16.8	0.179	12.9	146	9.47	0.252	3.01	0.345	3.12	122	7.52
IUS Hanger	0.128	13.8	0.171	17.1	129	4.66	0.249	3.76	0.341	3.86	130	5.72
IUT Hanger	0.203	31.6	0.227	25.8	155	5.14	0.225	2.69	0.313	2.53	124	7.53

Percentage differences and *p*-values for the comparisons between the testing and the theoretical maximum lateral displacements and the load positions for the two samples of wood I-joists and for the one-bracing system are shown in Table 5-17. For the simply supported end condition with the 11 7/8 in. wood I-joists the maximum lateral displacements and individual positions from testing were greater compared to the corresponding theoretical maximum lateral displacements and individual positions. However, for the 16 in. wood I-joists the theoretical maximum lateral displacements were greater compared to the corresponding maximum lateral displacements from testing (Table 5-17). From the *Student's t* tests, the mean theoretical maximum lateral displacements of the 11 7/8 in. wood I-joists were not significantly different than the mean maximum lateral displacements from testing ($p = 0.2266$ at the LQT position and $p = 0.5030$ at the MST position). Similarly, the mean theoretical maximum lateral displacement of the 16 in. wood I-joists was not significantly different than the mean maximum lateral displacement from testing at the LQT position ($p = 0.0591$). However, at the MST position the mean theoretical maximum lateral displacement was significantly different than the mean maximum lateral displacement from testing ($p = 0.0156$). The percentage differences between the MST position and the LQT position of the 16 in. wood I-joists are considerably distinctive as the individual walking on the wood I-joists struggled when walking immediately after mid-span. In trying to recover balance the individual induced greater lateral force. This reason may explain the percentage difference of the load positions and the variability of the maximum lateral displacements from testing. The maximum lateral displacements from testing were considerably different between the 11 7/8 in. wood I-joists and the 16 in. wood I-joists while the theoretical maximum lateral displacements were

similar. As the individual walked on the wood I-joist, larger lateral forces were applied to the 11 $^{7}/_{8}$ in. wood I-joists compared to the lateral force applied to the 16 in. wood I-joists. The mean theoretical load position of the 11 $^{7}/_{8}$ in. wood I-joists was significantly different than the mean load position from testing ($p = 0.0128$). However, the mean theoretical load position of the 16 in. wood I-joists was not significantly different than the mean load position from testing ($p = 0.1754$). The difference between the theoretical and the testing load positions of the 11 $^{7}/_{8}$ in. wood I-joists was 18 in. The theoretical model predicted the load position one footstep behind the footstep observed in the tests. The testing variability of the maximum lateral displacements and of the load positions were larger compared to the corresponding theoretical variability (Table 5-16). A similar behavior was observed for the simply supported end condition of the non-bracing system. The bracing theoretical model for the simply supported end condition (Equation 3-30) predicted accurately the constraint in the lateral bending motion tests.

Table 5-17: Comparison between Testing and Theoretical Maximum Lateral Displacements and Load Positions for the One-Bracing System.

End Condition	11 $^{7}/_{8}$ in. Wood I-Joists					
	LQT		MST		Load Position	
	Difference (%) [1]	*p*-values	Difference (%) [1]	*p*-values	Difference (%) [1]	*p*-values
Simply Supported	- 23.7	0.2266	- 14.5	0.5030	- 13.8	0.0128
ITS Hanger	98.2	< 0.0000	146	< 0.0000	- 20. 6	0.0421
ITT Hanger	38.2	0.0029	49.3	0.0041	- 10.7	0.0590
IUS Hanger	14.5	0.4716	31.9	0.0962	- 10.7	0.0863
IUT Hanger	0.00	0.9947	9.18	0.4937	- 13.0	0.0100
	16 in. Wood I-Joists					
Simply Supported	25.3	0.0591	47.9	0.0156	- 6.43	0.1754
ITS Hanger	105	0.0010	143	0.0003	- 10.7	0.1955
ITT Hanger	69.1	0.0009	92.7	0.0001	- 16.4	0.0524
IUS Hanger	94.5	0.0001	99.4	0.0001	0.775	0.8909
IUT Hanger	10.8	0.5043	37.9	0.0417	-20.0	0.0051

1 Difference (%) = ((Theoretical/Testing) – 1)100

The theoretical maximum lateral displacements were greater than the maximum lateral displacements from testing for both samples of wood I-joists for the ITS hanger supported end condition. The theoretical maximum lateral displacements of the 11 $^{7}/_{8}$ in. wood I-joists were on average 98.2% greater at the LQT position and 146% greater at the MST position compared to the corresponding maximum lateral displacements from testing. For the 16 in. wood I-joists the maximum lateral displacements were on average 105% greater at the LQT position and 143% greater at the MST position than the corresponding maximum lateral displacements from testing. From the *Student's t* tests, the mean theoretical maximum lateral displacements of the 11 $^{7}/_{8}$ in. wood I-joists were significantly different than the mean maximum lateral displacements from testing ($p < 0.0000$ at the LQT position and $p < 0.0000$ at the MST position). Similarly, the mean theoretical maximum lateral displacements of the 16 in. wood I-joists were significantly different than the mean maximum lateral displacements from testing ($p = 0.0010$ at the LQT position and $p = 0.0003$ at the MST position). In the ITS hanger supported end condition of the non-

bracing system discussion, the difference between the theoretical and the testing maximum lateral displacements was due to the fact that the theoretical model assumed a constant lateral stiffness along the entire length of the hanger but in the one-bracing testing, this behavior was not observed. In the one-bracing testing, the lateral force imposed by the individual walking was applied at the top flange and this flange was fully constrained. The differences between the theoretical and the testing maximum lateral displacements were larger for the one-bracing system compared to the non-bracing system. The one-bracing system was accounting for the loss of constraint in the six hangers for the three wood I-joists in the system, while the non-bracing system was accounting for the loss of constraint in only two hangers. Percentage differences and statistical results were similar between the two sizes of wood I-joists, concluding that the ITS hanger supported end condition behaved similarly for the two wood I-joist heights when a bracing system at the mid-span of the wood I-joists was used. The percentage differences between the MST position and the LQT position were considerably dissimilar for the two sizes of wood I-joists. A similar result was observed for the simply supported end condition previously discussed. The load position from testing were greater compared to the theoretical load position for both samples of wood I-joists (Table 5-16). The mean theoretical load position of the 11 $^{7}/_{8}$ in. wood I-joists was significantly different than the mean load position from testing (p = 0.0421). However, the mean theoretical load position of the 16 in. wood I-joists was not significantly different than the mean load position from testing (p = 0.1955). The testing and the theoretical load positions of the 11 $^{7}/_{8}$ in. wood I-joists were 30 in. apart or approximately two footsteps of the individual walking on the wood I-joists. The load position from testing of the 11 $^{7}/_{8}$ in. wood I-joists was one of the greatest observed while the theoretical load was one of the smallest, this explains the *Student's t* test outcome.

The theoretical maximum lateral displacements of the ITT hanger supported end condition with the 11 $^{7}/_{8}$ in. wood I-joists were on average 38.2% greater at the LQT position and 49.3% greater at the MST position compared to the corresponding maximum lateral displacements from testing. For the 16 in. wood I-joists the maximum lateral displacements were on average 69.1% greater at the LQT position and 92.7% greater at the MST position than the corresponding maximum lateral displacements from testing. From the *Student's t* tests, the mean theoretical maximum lateral displacements of the 11 $^{7}/_{8}$ in. wood I-joists were significantly different than the mean maximum lateral displacements from testing (p = 0.0029 at the LQT position and p = 0.0041 at the MST position). Similarly, the mean theoretical maximum lateral displacements of the 16 in. wood I-joists were significantly different than the mean maximum lateral displacements from testing (p = 0.0009 at the LQT position and p = 0.0001 at the MST position). Similar to the ITS hanger supported end condition, the differences between the theoretical and the testing maximum lateral displacements of the ITT hanger supported end condition were greater for the one-bracing system compared to the non-bracing system. Again, the one-bracing system was accounting for the loss of constraint in the six hangers for the three wood I-joists in the system, while the non-bracing system was accounting for the loss of constraint in only two hangers. The differences between the theoretical maximum lateral displacements and the maximum lateral displacements from testing were larger for the ITS hanger supported end condition than for the ITT hanger end supported condition, this behavior was due

to the increase of the lateral hanger stiffness of the ITT hanger (Table 5-3). The percentage differences between the theoretical and the testing maximum lateral displacements are larger for the 16 in. wood I-joists compared to the 11 $^{7}/_{8}$ in. wood I-joists. The testing maximum lateral displacements for the 16 in. wood I-joists were considerably smaller, behavior attributed to alterations in the lateral component of the force applied to the wood I-joists by the individual waking. The load position from testing was greater compared to the theoretical load position for both samples of wood I-joists (Table 5-16). A similar result was observed in the ITS hanger supported end condition. The mean theoretical load position of the 11 $^{7}/_{8}$ in. wood I-joists was not significantly different than the mean load position from testing (p = 0.0590). Similarly, the mean theoretical load position of the 16 in. wood I-joists was not significantly different than the mean load position from testing (p = 0.0524). The theoretical and testing load positions were reached approximately at the same footstep given by the individual walking on the wood I-joists.

The test results of the IUS hanger end supported condition show that the theoretical maximum lateral displacements were greater compared to the maximum lateral displacements from testing for both samples of wood I-joists (Table 5-16). From the *Student's t* tests, the mean theoretical maximum lateral displacements of the 11 $^{7}/_{8}$ in. wood I-joists were not significantly different than the mean maximum lateral displacements from testing (p = 0.4716 at the LQT position and p = 0.0962 at the MST position). However, the mean theoretical maximum lateral displacements of the 16 in. wood I-joists were significantly different than the mean maximum lateral displacements from testing (p = 0.0001 at the LQT position and p = 0.0001 at the MST position). The percentage differences between the theoretical and the testing maximum lateral displacements are close to the double for the 16 in. wood I-joists, these difference are even greater than the corresponding of the ITT hanger supported end condition (Table 5-17) previously discussed which theoretically are not possible. These results are mainly due to the testing maximum lateral displacements were considerably small, behavior attributed to a small application of the lateral force to the wood I-joists by the individual walking. For the 11 $^{7}/_{8}$ in. wood I-joists, the percentage differences between the theoretical and the testing maximum lateral displacements are smaller than the corresponding percentage differences for the ITS and the ITT hanger supported end conditions of the one-bracing system, however the corresponding differences are larger compared with the IUS hanger supported end condition of the non-bracing bracing system. The theoretical model of the one-bracing system accounts for the constraint of the six wood I-joist hangers while the theoretical model of the non-bracing system account for the constraint of two wood I-joist hangers. The load positions from testing were greater compared to the theoretical load positions for both sizes of wood I-joists (Table 5-16). Similar to the results observed in the ITS and the ITT hanger supported end conditions as well as in the simply supported end condition, the mean theoretical load position of the 11 $^{7}/_{8}$ in. wood I-joists was not significantly different than the mean load position from testing (p = 0.0863). Similarly, the mean theoretical load position of the 16 in. wood I-joists was not significantly different than the mean load position from testing (p = 0.8909). The predicted and the testing positions of the individual

walking were similar even though that the predicted and the testing maximum lateral displacements of the 16 in. wood I-joists were not similar.

The theoretical maximum lateral displacements were greater compared to the maximum lateral displacements from testing of the IUT hanger supported end condition for both sizes of wood I-joists (Table 5-17). Percentage differences between theoretical and testing maximum lateral displacements of the IUT hanger with the one-bracing system were on average the smallest of all wood I-joists hangers. In contrast, the corresponding differences of the ITS hanger were the greatest of all wood I-joists hangers. Similar results were observed in the non-bracing system (Section 5.5.1). From the *Student's t* tests, the mean theoretical maximum lateral displacements of the 11 $^{7}/_{8}$ in. wood I-joists were not significantly different than the mean maximum lateral displacements from testing (p = 0.9947 at the LQT position and p = 0.4937 at the MST position). Similarly, the mean theoretical maximum lateral displacement of the 16 in. wood I-joists was not significantly different than the mean maximum lateral displacement from testing at the LQT position (p = 0.5043). However, the mean theoretical maximum lateral displacement of the 16 in. wood I-joists was significantly different than the mean maximum lateral displacement from testing at the MST position (p = 0.0417). The mean theoretical load position of the 11 $^{7}/_{8}$ in. wood I-joists was significantly different than the mean load position from testing (p = 0.0100). Similarly, the mean theoretical load position of the 16 in. wood I-joists was significantly different than the mean load position from testing (p = 0.0051). The percentage difference of the load position of the 16 in. wood I-joists was unusual large pointing out evidence of uncommon walking pattern of the individual walking on the wood I-joist. The uncommon walking pattern is the cause of the difference between the predicted and the testing load positions as well as of the difference between the percentage difference of the maximum lateral displacements measured at the LQT and at the MST positions.

Theoretical models to calculate the restraint of a bracing system for the lateral bending motion of the wood I-joists for the fixed supported end condition were derived in the Theoretical Models Chapter (Equations 3-31). The theoretical maximum lateral displacements for the fixed supported end condition averaged 0.0443 in. at the LQT position and 0.0563 in. at the MST position for the 11 $^{7}/_{8}$ in. wood I-joists and 0.0514 in. at the LQT position and 0.0660 at the MST position for the 16 in. wood I-joists. For the 11 $^{7}/_{8}$ in. wood I-joists the maximum lateral displacements from testing of the simply supported end condition were 6.30 times greater at the LQT position and 6.25 times greater at the MST position compared to the theoretical maximum lateral displacements from the fixed supported end condition. For the 16 in. wood I-joists the maximum lateral displacements from testing of the simply supported end condition were 3.15 times greater at the LQT position and 2.94 times greater at the MST position compared to the theoretical maximum lateral displacements from the fixed supported end condition. The simply supported end condition was chosen since it was the end condition with the smallest maximum lateral displacements. Differences between the theoretical maximum lateral displacements of the fixed supported end condition and the maximum lateral displacements from testing for the simply supported end condition were

similar to the corresponding differences observed in the non-bracing system. The bracing theoretical models for the fixed supported end condition accurately predicted the amount of restraint due to the bracing system.

5.5.4: Wood I-Joist Rotation for the One-Bracing System

Rotation of the wood I-joists for the one-bracing system was calculated using the same procedure used for the non-bracing system of Section 5.5.2. Rotation values are shown in Table 5-18. The rotation values of the ITT hanger supported end condition were the smallest for both samples of wood I-joists. The smallest rotation values of the non-bracing system were in the ITS hanger supported end condition for the 11 $^{7}/_{8}$ in. wood I-joist and in the simply supported end condition for the 16 in. wood I-joists. The end supported condition seemed to have little influence on the rotation of the wood I-joists. Variations in the lateral component of the force applied by the individual walking on the wood I-joist, as well as the wood I-joist capacity to transmit the lateral displacement from the top flange to the bottom flange lead to differences in the wood I-joist rotation.

Table 5-18: Wood I-Joist Rotation from the Lateral Bending Motion Tests of the One-Bracing System.

Sample	Simply Supported β (Degrees)	ITS Hanger β (Degrees)	ITT Hanger β (Degrees)	IUS Hanger β (Degrees)	IUT Hanger β (Degrees)
11 $^{7}/_{8}$ in. Wood I-Joists	0.338	0.239	0.227	0.264	0.316
16 in. Wood I-Joists	0.213	0.168	0.154	0.172	0.231

Descriptive statistics for the wood I-joist rotation were calculated for the simply supported end condition and for the four hanger end supported conditions shown in Table 5-19. The maximum lateral displacements at the MST and MSB positions were taken from Table A-15 and Table A-16 in the Appendix, totalizing 25 values for each wood I-joist sample. For the 11 $^{7}/_{8}$ in. wood I-joist, the average rotation of the wood I-joists was 0.276 degrees while for the 16 in. wood I-joists the average rotation was 0.187 degrees. The standard deviations, kurtoses and skewness for both wood I-joist samples imply that both samples are approximately normally distributed. The maximum and minimum values of the rotation measurements demonstrated that no outliers were presented in the samples. The one-bracing system shows larger rotations for the 11 $^{7}/_{8}$ in. wood I-joists compared to the 16 in. wood I-joists, a similar result was observed in the non-bracing system.

Table 5-19: Descriptive Statistics for the Wood I-Joist Rotation from the Lateral Bending Motion of the One-Bracing System.

	11 $^{7}/_{8}$ in. Wood I-Joists	16 in. Wood I-Joists
Mean (degrees)	0.276	0.187
Standard Deviation	0.0875	0.0656
Kurtosis	- 0.0369	0.149
Skewness	0.252	- 0.188
Minimum Value	0.106	0.0358
Maximum Value	0.478	0.326
Number of Observations	25	25

5.5.5: Lateral Bending Motion for the Two-Bracing System

The maximum lateral displacements and individual positions at the moment that the maximum lateral displacements occurred for the two-bracing system are shown in Table 5-20. The theoretical maximum lateral displacements and individual positions were calculated using Equation 3-18 for the simply supported end condition, and Equation 3-27 for the hanger supported end condition. The influence of the two-bracing system on the wood I-joist lateral bending motion was investigated by using Equations 3-30 for the simply supported end condition and Equations 3-32 for the hanger supported end conditions.

Table 5-20: Maximum Lateral Displacements and Load Positions for the Two-Bracing System.

End Condition	11 7/8 in. Wood I-Joists											
	Testing						Theoretical					
	LQT		MST		Load Position		LQT		MST		Load Position	
	δ (in.)	*CV* (%)	δ (in.)	*CV* (%)	*s* (in.)	*CV* (%)	δ (in.)	*CV* (%)	δ (in.)	*CV* (%)	*s* (in.)	*CV* (%)
Simply Supported	0.255	61.4	0.370	59.7	142	10.3	0.271	2.72	0.382	2.71	121	6.99
ITS Hanger	0.154	21.9	0.240	20.3	139	8.62	0.407	2.63	0.593	2.14	120	9.74
ITT Hanger	0.187	15.3	0.290	14.8	140	5.44	0.363	2.07	0.498	1.94	118	10.4
IUS Hanger	0.179	43.2	0.274	39.8	134	7.85	0.306	3.36	0.422	3.47	126	7.74
IUT Hanger	0.215	24.6	0.309	22.2	149	4.14	0.287	2.54	0.401	2.59	117	7.90
	16 in. Wood I-Joists											
Simply Supported	0.124	23.6	0.189	19.7	136	7.51	0.256	4.20	0.362	4.23	125	6.23
ITS Hanger	0.163	14.1	0.241	14.3	142	7.30	0.397	3.57	0.594	2.68	120	1.37
ITT Hanger	0.130	14.9	0.193	25.2	136	5.50	0.303	3.48	0.416	3.54	112	9.22
IUS Hanger	0.130	13.0	0.200	13.8	131	8.32	0.301	3.40	0.414	3.53	112	9.22
IUT Hanger	0.199	14.9	0.292	18.5	138	2.92	0.278	3.37	0.388	3.50	120	9.80

Percentage differences and *p*-values for the comparisons between the testing and the theoretical maximum lateral displacements and the load positions for the two samples of wood I-joists and for the two-bracing system are shown in Table 5-21. For the simply supported end condition, the theoretical maximum lateral displacements were greater compared to the corresponding maximum lateral displacements from testing for both sizes of wood I-joists. From the *Student's t* tests, the mean theoretical maximum lateral displacements of the 11 7/8 in. wood I-joists were not significantly different than the mean maximum lateral displacements from testing ($p = 0.8324$ at the LQT position and $p = 0.9055$ at the MST position). However, the mean theoretical maximum lateral displacements of the 16 in. wood I-joists were significantly different than the mean maximum lateral displacements from testing ($p = 0.0009$ at the LQT position and $p = 0.0009$ at the MST position). The maximum lateral displacements from testing were considerably different between the 11 7/8 in. wood I-joists and the 16 in. wood I-joists while the theoretical maximum lateral displacements were similar. Since the lateral bending stiffness of both samples of wood I-joists are similar, the only explanation is that the individual walking on the wood I-joist applied larger lateral force to the 11 7/8 in. wood I-joists compared to the lateral force applied to the 16 in.

wood I-joists. The mean theoretical load position of the 11 $^{7}/_{8}$ in. wood I-joists was not significantly different than the mean load position from testing (p = 0.0811). Similarly, the mean theoretical load position of the 16 in. wood I-joists was not significantly different than the mean load position from testing (p = 0.1560). The predicted and the testing load positions were reached by around the same footstep given by the individual walking on the wood I-joists.

Table 5-21: Comparison between Testing and Theoretical Maximum Lateral Displacements and Load Positions for the Two-Bracing System.

End Condition	11 $^{7}/_{8}$ in. Wood I-Joists					
	LQT		MST		Load Position	
	Difference (%) [1]	*p*-values	Difference (%) [1]	*p*-values	Difference (%) [1]	*p*-values
Simply Supported	6.27	0.8324	3.24	0.9055	- 14.8	0.0811
ITS Hanger	164	< 0.0000	147	< 0.0000	- 13.7	0.0321
ITT Hanger	94.1	0.0001	71.7	0.0004	- 15.7	0.0270
IUS Hanger	70.9	0.0239	54.0	0.0436	- 5.97	0.3570
IUT Hanger	33.5	0.0340	29.8	0.0360	- 21.5	0.0030
	16 in. Wood I-Joists					
Simply Supported	106	0.0009	91.5	0.0009	- 8.09	0.1560
ITS Hanger	144	0.0001	146	0.0001	- 15.5	0.0071
ITT Hanger	133	0.0001	116	0.0007	- 17.6	0.0042
IUS Hanger	132	< 0.0000	107	0.0001	- 14.5	0.0720
IUT Hanger	39.7	0.0085	32.9	0.0247	- 13.0	0.0403

1 Difference (%) = ((Theoretical/Testing) – 1)100

The theoretical maximum lateral displacements were greater than the maximum lateral displacements from testing for both sizes of wood I-joists for the ITS hanger supported end condition. The theoretical maximum lateral displacements of the 11 $^{7}/_{8}$ in. wood I-joists were on average 164% greater at the LQT position and 147% greater at the MST position compared to the corresponding maximum lateral displacements from testing. For the 16 in. wood I-joists the maximum lateral displacements were on average 144% greater at the LQT position and 146% greater at the MST position than the corresponding maximum lateral displacements from testing. From the *Student's t* tests, the mean theoretical maximum lateral displacements of the 11 $^{7}/_{8}$ in. wood I-joists were significantly different than the mean maximum lateral displacements from testing (p < 0.0000 at the LQT position and p < 0.0000 at the MST position). Similarly, the mean theoretical maximum lateral displacements of the 16 in. wood I-joists were significantly different than the mean maximum lateral displacements from testing (p = 0.0001 at the LQT position and p = 0.0001 at the MST position). Similarly to the one-bracing system, the difference between the theoretical and the testing maximum lateral displacements was due to the theoretical model assuming a constant lateral stiffness along the entire length of the hangers; but in testing this behavior was not observed. In testing the lateral force imposed by the individual walking was applied at the top flange and this flange was fully constrained. Percentage differences between theoretical and testing maximum lateral displacements at the MST position were similar between the one-bracing system and two bracing system demonstrating that the predicted

constraint by the theoretical models worked similarly as the braces were relocated from the mid-span to the quarters-span of the wood I-joists. The load position from testing were greater compared to the theoretical load position for both sizes of wood I-joists (Table 5-21). The mean theoretical load position of the 11 $^{7}/_{8}$ in. wood I-joists was significantly different than the mean load position from testing (p = 0.0321). Similarly, the mean theoretical load position of the 16 in. wood I-joists was significantly different than the mean load position from testing (p = 0.0071). The two bracing system influenced the testing load position displacing it away from the wood I-joist mid-span. In contrast, the predicted load position remained fairly constant through the three bracing systems, explaining the *Student's t* test outcomes.

The theoretical maximum lateral displacements of the ITT hanger supported end condition with the 11 $^{7}/_{8}$ in. wood I-joists were on average 94.1% greater at the LQT position and 71.7% greater at the MST position compared to the corresponding maximum lateral displacements from testing. For the 16 in. wood I-joists the maximum lateral displacements were on average 133% greater at the LQT position and 116% greater at the MST position than the corresponding maximum lateral displacements from testing. From the *Student's t* tests, the mean theoretical maximum lateral displacements of the 11 $^{7}/_{8}$ in. wood I-joists were significantly different than the mean maximum lateral displacements from testing (p = 0.0001 at the LQT position and p = 0.0004 at the MST position). Similarly, the mean theoretical maximum lateral displacements of the 16 in. wood I-joists were significantly different than the mean maximum lateral displacements from testing (p = 0.0001 at the LQT position and p = 0.0007 at the MST position). Differences between the theoretical and the testing maximum lateral displacements were related to the greater stiffness of the wood I-joist hangers compared to the predicted stiffness since the top mount hanger are fully constrain at the top flange of the wood I-joists. The differences between the theoretical and the testing maximum lateral stiffness were smaller for the ITT hanger compared to the ITS hanger. This behavior was attributed to the increase of the lateral hanger stiffness in the theoretical model. Similarly to the ITT hanger supported end condition of the one-bracing system, the differences between the theoretical and the testing maximum lateral displacements are larger for the 16 in. wood I-joists compared to the 11 $^{7}/_{8}$ in. wood I-joists. Results were because the testing maximum lateral displacements of the 16 in. wood I-joists were considerably smaller. Behavior attributed to variations in the lateral component of the force applied to the wood I-joists by the individual waking. The load position from testing were greater compared to the theoretical load position for both sizes of wood I-joists (Table 5-20). A similar result was observed in the ITS hanger supported end condition. The mean theoretical load position of the 11 $^{7}/_{8}$ in. wood I-joists was significantly different than the mean load position from testing (p = 0.0270). Similarly, the mean theoretical load position of the 16 in. wood I-joists was significantly different than the mean load position from testing (p = 0.0042). Similarly to the ITS hanger supported end condition, results concluded that the two bracing system influenced the testing load position displacing it away from the wood I-joist mid-span.

The test results of the IUS hanger end supported condition show that the theoretical maximum lateral displacements were greater compared to the maximum lateral displacements from testing for both sizes of wood

I-joists (Table 5-21). From the *Student's t* tests, the mean theoretical maximum lateral displacements of the 11 $^{7}/_{8}$ in. wood I-joists were significantly different than the mean maximum lateral displacements from testing (p = 0.0239 at the LQT position and p = 0.0436 at the MST position). Similarly, the mean theoretical maximum lateral displacements of the 16 in. wood I-joists were significantly different than the mean maximum lateral displacements from testing (p < 0.0000 at the LQT position and p = 0.0001 at the MST position). The lateral component of the force imposed by the individual walking was constant in the theoretical models. However, results from the one-bracing system and from the two bracing system indicate that the lateral component of the force was in fact reduced. The one-bracing system and the two bracing system increased the stability of the wood I-joists. As the stability of the wood I-joist increased, the lateral component of the force imposed by the individual walking decreased. The load positions from testing were greater compared to the theoretical load positions for both samples of wood I-joists (Table 5-21). Similar results were observed in the ITS and ITT hanger supported end conditions as well as in the simply supported end condition. The mean theoretical load position of the 11 $^{7}/_{8}$ in. wood I-joists was not significantly different than the mean load position from testing (p = 0.3570). Similarly, the mean theoretical load position of the 16 in. wood I-joists was not significantly different than the mean load position from testing (p = 0.0720). The predicted and the testing position of the individual walking was approximately equal even though that the predicted and the testing maximum lateral displacements of the 16 in. wood I-joists were no equal.

The theoretical maximum lateral displacements were greater compared to the maximum lateral displacements from testing of the IUT hanger supported end condition for both samples of wood I-joists (Table 5-21). Percentage differences between theoretical and testing maximum lateral displacements of the IUT hanger with the two-bracing system were on average the smallest of all wood I-joists hangers, in contrast, the corresponding differences of the ITS hanger were the greatest of all wood I-joists hangers. Similar results were observed in the non-bracing system (Section 5.5.1) and in the one-bracing system (Section 5.5.3). The lateral stiffness of the IUT hanger was the greatest observed while the lateral stiffness of the ITS hanger was the smallest (Table 5-3), concluding that as the lateral hanger stiffness increased the theoretical models improved the predicted maximum lateral displacements values. From the *Student's t* tests, the mean theoretical maximum lateral displacements of the 11 $^{7}/_{8}$ in. wood I-joists were significantly different than the mean maximum lateral displacements from testing (p = 0.0340 at the LQT position and p = 0.4937 at the MST position). Similarly, the mean theoretical maximum lateral displacements of the 16 in. wood I-joists were significantly different than the mean maximum lateral displacements from testing (p = 0.0085 at the LQT position and p = 0.0247 at the MST position). Results from the one-bracing system and from the two-bracing system indicate that the lateral component of the force was reduced in the tests, while in the theoretical models the lateral component of the force was constant, affecting the prediction of the maximum lateral displacements. The mean theoretical load position of the 11 $^{7}/_{8}$ in. wood I-joists was significantly different than the mean load position from testing (p = 0.0030). Similarly, the mean theoretical load position of the 16 in. wood I-joists was significantly different than the mean load position from

testing (p = 0.0403). The two bracing system influenced the testing load position displacing it away from the wood I-joists mid-spam, similar results were obtained in the ITS and in the ITT hanger supported end conditions.

The theoretical maximum lateral displacements for the fixed supported end condition averaged 0.0676 in. at the LQT position and 0.0864 in. at the MST position for the 11 $^{7}/_{8}$ in. wood I-joists and 0.0793 in. at the LQT position and 0.101 at the MST position for the 16 in. wood I-joists. For the 11 $^{7}/_{8}$ in. wood I-joists the maximum lateral displacements from testing of the simply supported end condition were 3.77 times greater at the LQT position and 4.28 times greater at the MST position compared to the theoretical maximum lateral displacements from the fixed supported end condition. For the 16 in. wood I-joists the maximum lateral displacements from testing of the simply supported end condition were 1.56 times greater at the LQT position and 1.87 times greater at the MST position compared to the theoretical maximum lateral displacements from the fixed supported end condition. The simply supported end condition was chosen since it was the end condition with the smallest maximum lateral displacements. The bracing theoretical models for the fixed supported end condition accurately predicted smaller values for the maximum lateral displacements of the wood I-joists.

5.5.6: Wood I-Joist Rotation for the Two-Bracing System

Rotation of the wood I-joists for the two-bracing system was calculated using the same procedure for the non-bracing system of Section 5.5.2. Rotation values are shown in Table 5-22. On average the rotation values of the IUT hanger supported end condition were the smallest for the 11 $^{7}/_{8}$ in. wood I-joists, while for the 16 in. wood I-joists the smallest rotation values were for the IUS hanger end supported condition. The smallest rotation values of the non-bracing system were for the ITS hanger supported end condition for the 11 $^{7}/_{8}$ in. wood I-joist and for the simply supported end condition for the 16 in. wood I-joists. The smallest rotation values of the one-bracing system were for the ITT hanger supported end condition for both sizes of wood I-joists. Results concluded that the end supported condition had little influence on the rotation of the wood I-joists. Variations in the lateral component of the force applied by the individual walking on the wood I-joist, as well as the wood I-joist capacity to transmit the lateral displacement from the top flange to the bottom flange lead to differences in the wood I-joist rotation.

Table 5-22: Wood I-Joist Rotation from the Lateral Bending Motion Tests of the Two-Bracing System.

Sample	Simply Supported β (Degrees)	ITS Hanger β (Degrees)	ITT Hanger β (Degrees)	IUS Hanger β (Degrees)	IUT Hanger β (Degrees)
11 $^{7}/_{8}$ in. Wood I-Joists	0.465	0.397	0.530	0.435	0.372
16 in. Wood I-Joists	0.295	0.284	0.266	0.265	0.382

Descriptive statistics for the wood I-joist rotation were calculated for the simply supported end condition and for the four hanger end supported conditions shown in Table 5-23. The maximum lateral displacements at the MST and at the MSB position were taken from Table A-17 and Table A-18 in the Appendix, totalizing 25 values for each wood I-joist sample. For the 11 $^{7}/_{8}$ in. wood I-joist the average rotation of the wood I-joists was 0.440

degrees while for the 16 in. wood I-joists, the average rotation was 0.299 degrees. The wood I-joist rotation for the two-bracing system was slightly greater compared to the wood I-joist rotation for the one-bracing system. The maximum lateral displacements of the two-bracing system were slightly greater compared to the respective displacements of the one-bracing system, a behavior correctly predicted by the theoretical bracing models. The kurtoses of both samples of wood I-joists are different to the kurtoses of the non-bracing and the one-bracing systems, concluding that the two-bracing system provided some constraint that displaced the samples from a normal distribution. This results were also observed in the comparison between the theoretical and the testing load positions of the two-bracing system. The maximum and minimum values of the rotation measurements show that no outliers are present in the samples. The two-bracing system showed greater rotations for the 11 $^{7}/_{8}$ in. wood I-joists compared to the 16 in. wood I-joists, a similar result was observed in the non-bracing and in the one-bracing systems.

Table 5-23: Descriptive Statistics for the Wood I-Joist Rotation from the Lateral Bending Motion of the One-Bracing System.

	11 $^{7}/_{8}$ in. Wood I-Joists	**16 in. Wood I-Joists**
Mean (degrees)	0.440	0.298
Standard Deviation	0.130	0.109
Kurtosis	- 1.13	1.99
Skewness	0.126	0.965
Minimum Value	0.227	0.115
Maximum Value	0.690	0.619
Number of Observations	25	25

The lateral bending motion of the wood I-joists was analyzed in this section. The theoretical model for the simply supported end condition predicted accurately the maximum lateral displacements of both samples of wood I-joists for the non-bracing system. The theoretical model for the hanger supported end condition predicted accurately the maximum lateral displacements of both samples of wood I-joists for the non-bracing system when ITT, IUS and IUT hangers were used. However, the theoretical model provided greater maximum lateral displacements values than the corresponding values obtained from the tests when ITS hangers were used. The smallest lateral hanger stiffness observed in testing was for the ITS hanger. Results concluded that as the lateral hanger stiffness increases the theoretical model for the hanger supported end condition increases the prediction of the maximum lateral displacements.

The differences between the theoretical and the testing maximum lateral displacements increased when a bracing system was used. However, throughout the analysis of the lateral bending motion of this section it was observed that the bracing system increased the stability of the loaded wood I-joists. As the stability of the wood I-joist increased the lateral component of the force imposed by the individual walking reduced. In the theoretical models a constant lateral force was used for all bracing systems. Therefore, the reduction in the performance of the lateral bending motion theoretical models is rather due to the decrease of the lateral component of the force. The one-

bracing system (composed of four braces placed at the mid-span) was more constraining than the two-bracing system (composed of eight braces placed at the quarters-span). This result was accurately predicted by the theoretical bracing models.

5.6: Dynamic Lateral-Torsional Buckling Instability

The static lateral-torsional buckling instability analyses of Section 5.4 and the lateral bending motion analyses of Section 5-5 were used to analyze the dynamic lateral-torsional buckling instability of the wood I-joists. The static lateral-torsional buckling instability theoretical models calculate the critical load at any point along the wood I-joist length. The lateral bending motion theoretical models determine the loaded point at the maximum lateral displacement of the wood I-joist. Therefore, mathematically combining the static lateral-torsional buckling instability model with the lateral bending motion model, the dynamic lateral-torsional buckling critical load can be calculated.

To analyze the dynamic lateral-torsional bucking instability of the wood I-joist, the increase of the critical load when the point of the load application is moved away from the mid-span must be known. Figure 5-16 is the static lateral-torsional buckling instability of the simply supported end condition for the two sizes of wood I-joists. Figure 5-16 was plotted by numerically solving Equation 2-34 with the guidelines from Figure 2-5. Input parameters used to plot Figure 5-16 were average values of the lateral bending stiffness from Table 5-1 and the torsional rigidity from Table 5-2. The minimum values of the critical loads occur at the mid-span of the wood I-joist and increase as the point of the load application is displaced away from the mid-span. Near the mid-span of the wood I-joist, the rise in the critical load is small, while closer to the ends of the wood I-joist, the increase in the critical load becomes asymptotic as shown in Figure 5-16. The increase of the critical load around the mid-span was approximately 3.50 lb. per in. for the 11 $^{7}/_{8}$ in. wood I-joists and approximately 4.20 lb. per in. for the 16 in. wood I-joists.

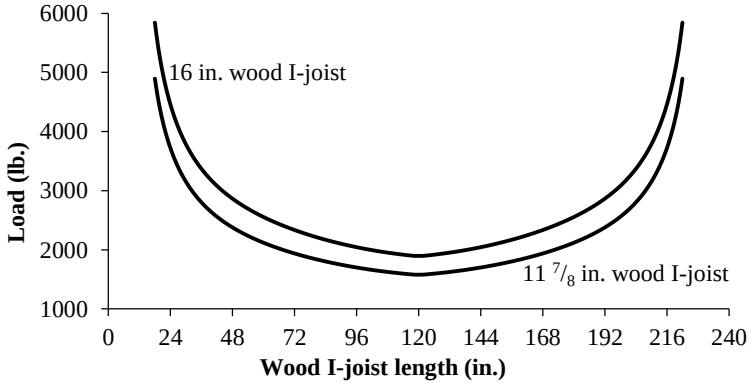

Figure 5-16: Static lateral-torsional critical load behavior along the wood I-joist. Simply supported end condition.

The different end supported conditions analyzed in this research display different behavior in the increase of the static lateral-torsional critical loads when the point of the load application is displaced away from the mid-span of the wood I-joists as shown in Figure 5-17. The graphs were plotted for the interval from 60 in. to 180 in. since

all the theoretical and the testing maximum lateral displacements of the wood I-joists from the lateral bending motion tests of the non-bracing system were obtained inside this interval. The graphs were plotted from Equation 3-10 for the hanger supported end condition and from Equation 2-34 for the simply supported end condition following the guidelines of Figure 2-5. Only the 11 $^{7}/_{8}$ in. wood I-joist samples from the non-bracing system were plotted in Figure 5-17 since the 16 in. wood I-joist samples behaved in a similar manner as well as the one-bracing and the two-bracing systems. In Figure 5-17 the lateral hanger stiffness increases the static lateral-torsional buckling critical load as the load displaced away from the mid-span. The change in the critical load is non-linear with distance rather is increasing at an increasing rate. The change is related to a smaller lateral hanger stiffness of one of the hangers at the ends of the wood I-joist which deforms quicker. In Figure 5-17, as the lateral hanger stiffness increases, the behavior of the graph becomes the behavior of the simply supported end condition graph.

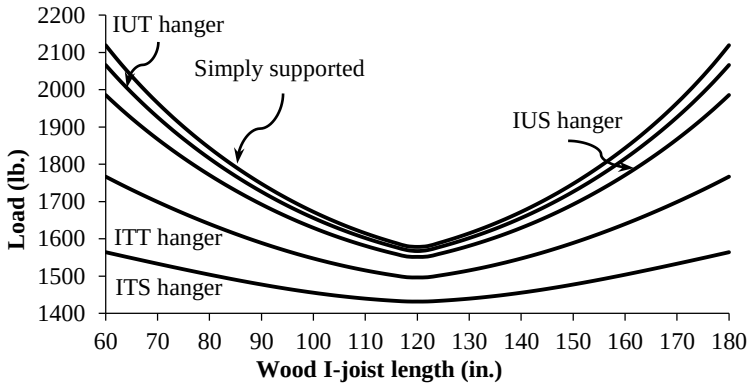

Figure 5-17: Static lateral-torsional critical load behavior along the wood I-joist for the different supported end conditions of the 11 $^{7}/_{8}$ in. wood I-joists.

5.6.1: Reduction of the Lateral-Torsional Buckling Critical Load Due to Initial Lateral Displacements

The lateral-torsional buckling instability is a condition in which only the current instantaneous physical forces of the system are taken into consideration when the system passes from a stable state to an unstable state. Consequently, the only difference between the static lateral-torsional buckling instability and the dynamic lateral-torsional buckling instability is the initial lateral displacement that the wood I-joist presents under the action of the lateral component of the force imposed by the individual walking on the wood I-joist at that particular moment. To calculate the dynamic lateral-torsional buckling instability, it is only necessary to add the work done by the system due to the wood I-joist deflection response to the static lateral-torsional buckling equation. An approximate expression to calculate the work done by the system was calculated by geometric considerations from Figure 2-4, $W_{LD} = \frac{2P\left(x(z,t)\right)^2}{a\sqrt{1-\frac{\left(x(z,t)\right)^2}{a^2}}}$. In this expression, W_{DL} is the work done by the system to produce lateral deflection on the wood I-joist, P is the critical load, $x(z,t)$ is the lateral displacement obtained from Equation 3-18 for the simply supported end condition and Equation 3-27 for the hanger supported end conditions, and a is the vertical distance from the neutral axis to the load application point. The analysis of the work done by the

system expression shows that as the lateral deflection of the wood I-joist increases, the work done by the system increases and consequently the dynamic lateral-torsional critical load decreases.

The reduction of the dynamic lateral-torsional buckling critical load as the wood I-joist lateral deflection increases for the simply supported end condition and the non-bracing system is shown in Figure 5-18. Figure 5-18 was plotted from Equation 2-34 in which the work done by the system when the wood I-joist is laterally deflected was included. The lateral bending stiffness and the torsional rigidity used in Equation 2-34 were the average values of these parameters from Table 5-1 and Table 5-2. The 11 $^{7}/_{8}$ in. wood I-joists reduce critical loads quicker compared to the 16 in. wood I-joists, since the rotation needed to reach lateral-torsional buckling instability is greater for the 16 in. wood I-joists than for the 11 $^{7}/_{8}$ in. wood I-joists due to the increased torsional rigidity.

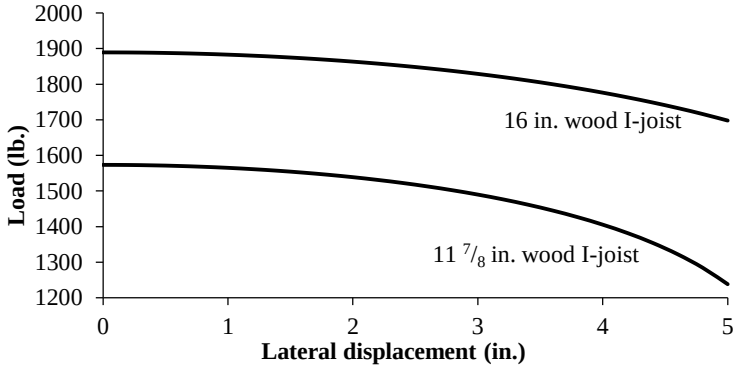

Figure 5-18: Reduction of the critical load versus initial lateral displacement of the wood I-joist. Simply supported end condition.

The reduction of the dynamic lateral-torsional buckling critical load as the initial deflection of the wood I-joist increased for the simply supported end condition compared to the hanger supported end conditions is shown in Figure 5-19. The plots of Figure 5-19 were calculated only for the 11 $^{7}/_{8}$ in. wood I-joists of the non-bracing system, since the 16 in. wood I-joist, the one-bracing and the two bracing systems were similar. The plots in Figure 6-19 were calculated from Equation 2-34 for the simply supported end condition and Equation 3-10 for the hanger end supported condition. In these equations the work done by the system corresponding to the initial wood I-joist deflection was integrated. The lateral bending stiffness and the torsional rigidity were the average values from Table 5-1 and Table 5-2. The reduction of the critical load as the lateral displacement of the wood I-joist increased was greater for the simply supported end condition compared to the hanger supported end conditions as shown in Figure 5-19. The initial lateral displacement of the wood I-joist is partially absorbed by the deformation of the wood I-joist hanger compared to the simply supported end condition which theoretically has not any lateral deformation.

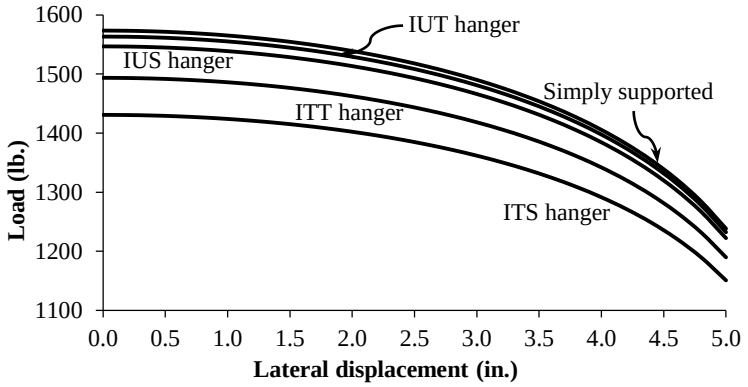

Figure 5-19: Reduction of the critical load versus initial lateral displacement for the different supported end conditions of the 11 $^{7}/_{8}$ in. wood I-joists.

The initial lateral deflection of the wood I-joist due to the lateral component of the force imposed by the individual walking on the wood I-joist had small influence on the dynamic lateral-torsional buckling instability as shown in Figures 5-18 and 5-19. In contrast, the increase of the dynamic lateral-torsional buckling instability due to the displacement of the load away from the mid-span had a greater influence. Therefore, the location along the wood I-joist in which the dynamic lateral-torsional buckling instability can be reached is at the mid-span of the wood I-joist. Calculating the dynamic lateral-torsional buckling critical load is consequently, equivalent to calculating the static lateral-torsional buckling critical load from Equation 3-6, then subtracting the corresponding difference (in pounds-force) from Figure 5-19 according to the corresponding maximum lateral displacement calculated from Equation 3-18 for the simply supported end condition.

5.7: Static Lateral-Torsional Buckling Regression Models

Three static lateral-torsional buckling regression models were developed in this research as explained in Section 4.11 for the non-bracing, the one-bracing and the two-bracing systems. The examination of the statistics of the critical loads obtained from testing for each bracing system was the first step in developing regression models. Once the regression model was calculated, the statistics, the analysis of variance and the parameter estimates of the model were evaluated for goodness of fit of the critical loads. Plots of the standard residuals versus the predicted critical loads were constructed to check for outliers and possible lack of interaction terms of the explanatory variables in the regression model. Plots of the standard residuals versus the predicted loads along with the probability plots were helpful in checking the inclusiveness of the assumptions that the theory behind the regression models must satisfy. Finally, plots of the fitted regression models along with the critical loads obtained from testing were analyzed to verify the agreement of the regression model with the testing data.

5.7.1: Non-Bracing Static Lateral-Torsional Buckling Regression Model

The static lateral-torsional regression model for the non-bracing system was developed by regressing Equation 4-5. The critical loads obtained from testing used to regress the model were obtained from Table A-10 in the Appendix for both the 11 $^{7}/_{8}$ in. wood I-joists and the 16 in. wood I-joists. The lateral bending stiffness of the

wood I-joists were obtained from Table A-1 in the Appendix while the lateral hanger stiffness from Table 5-3. The general statistics of the 50 values of the critical loads used to regress the model are shown in Table 5-24. Since the kurtosis and the skewness of the sample were smaller than one, the critical loads appear to be normally distributed. Thus, standard statistical procedures can be used to develop the regression model. The variability of the sample seems to be large. This effect comes from the fact that both the 11 $^{7}/_{8}$ in. wood I-joists and the 16 in. wood I-joists are being analyzed together (Section 4.12) and the critical loads from both samples were considerably different as previously discussed.

The statistics of the regression model are shown in Table 5-24. The coefficient of determination was 0.993, so the model statistically accounts for at least 99.3% of the variability of the critical loads, with the remaining 0.67% of the variability referred to as random variability from other sources than the explanatory variables. The adjusted coefficient of determination was 0.972, concluding that the penalty for having three terms in the static lateral-torsional buckling regression model is not statistically significant and the three terms provide a good fit of the data to the regression model. The model standard deviation was smaller than the corresponding standard deviation from the critical loads, concluding that a suitable regression model was reached.

Table 5-24: Non-Bracing Regression Model General Statistics.

Critical loads		**Regression model**	
Mean	1610	Coefficient of determination (R^2)	0.993
Standard deviation	192	Adjusted coefficient of determination (R^2_{Ad})	0.972
Kurtosis	0.623	Model standard deviation	137
Skewness	0.749	Number of observations	50
Maximum	2160		
Minimum	1330		

The analysis of variance from the regression model is shown in Table 5-25. Since the *F* value was much larger than the significance *F* (3.24×10^{-50}) there is strong statistical evidence in the data supporting the hypothesis that one or more of the three terms of the static regression model have predictive significance. Because the lateral bending stiffness of the wood I-joists is present in all three terms and the height of the wood I-joists and the lateral hanger stiffness are also used in the model, the obtained regression model is a suitable predictor of the static critical lateral-torsional buckling loads.

Table 5-25: Non-Bracing Regression Model Analysis of Variance.

Resource	**DF**	**Sum of Squares**	**Mean Squares**	***F* Value**	***p*-value**
Regression	3	130×10^6	43.5×10^6	2330	$p < 0.0001$
Residual Error	47	878×10^3	18.7×10^3		
Total	50	131×10^6			

The static lateral-torsional buckling regression model parameter estimates are shown in Table 5-26. The standard errors are small compared to the value of the corresponding coefficients. Therefore, strong statistical evidence exist that there is not significant error in the estimation of these coefficients. The standard errors also confirm that

there are no correlation problems between the different predictors. The *p*-values of the explanatory variables demonstrate strong predictive values on the critical loads. The explanatory variables in the third term have greater *p*-value compared to the other two terms. This *p*-value reflects the large variability of this term since the lateral stiffness of the wood I-joist hanger varied from 54.7 lb. / in. for the ITS hanger of the 16 in. wood I-joists to infinity for the simply supported end conditions. Taking the estimated coefficients from the table into Equation 4-5, the following model is formed to calculate the static buckling critical loads.

$$P_{cr} = 0.315EI_y^{\frac{1}{2}} + 0.0245hEI_y^{\frac{1}{2}} + 0.00210hEI_y^{\frac{1}{2}}\left(\frac{k}{k+EI_y}\right)^{\frac{1}{2}} \quad (5\text{-}1)$$

Table 5-26: Non-Bracing Regression Model Parameter Estimates.

Predictor	Coefficients	Standard Error	*p*-value	95% Confidence Interval
$EI_y^{\frac{1}{2}}$	0.315	0.0545	$p < 0.0001$	$0.205 \leq \mu_1 \leq 0.424$
$hEI_y^{\frac{1}{2}}$	0.0245	0.00387	$p < 0.0001$	$0.0167 \leq \mu_2 \leq 0.0323$
$hEI_y^{\frac{1}{2}}\left(\frac{k}{k+EI_y}\right)^{\frac{1}{2}}$	0.00210	0.00142	0.146	$-0.000755 \leq \mu_3 \leq 0.00495$

Assumptions considered in the developing of the static lateral-torsional buckling regression model included; the errors were expected to equal zero $E(\varepsilon_i) = 0$, the variance of the errors was expected to be constant and the random errors (ε_i) were normally distributed. Since the residuals were the estimates of the random variables, a plot of the residuals versus the predicted value of the critical loads was used to check whether the random errors are actually zero. Studentized standardized residuals were used rather than the typical standardized residual (residuals/model standard deviation) because the mean value of zero and the standard deviation value of one simplified the analyses and further calculations of the regression model. Since the explanatory variable EI_y is present in all three terms of Equation 5-1, and the explanatory variables *h* and *k* enter into the regression model in clusters (for a group of five wood I-joists), the predicted critical loads from Equation 5-1 versus the Studentized residuals were plotted rather than each of the three terms from Equation 5-1 versus the Studentized residuals as shown in Figure 5-20.

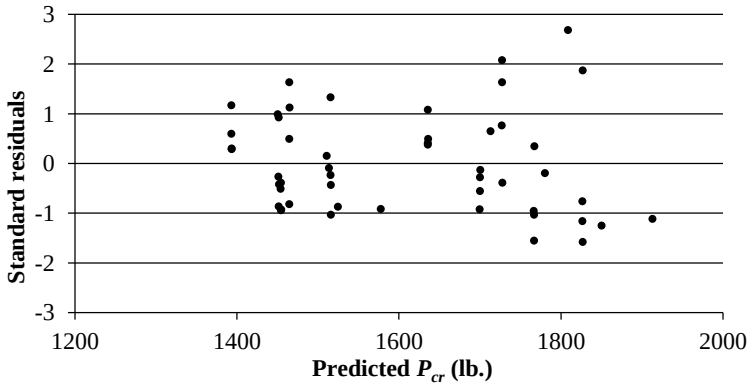

Figure 5-20: Studentized residuals versus the predicted critical load of the non-bracing system.

Extreme values of the standardized residuals were not observed as shown in Figure 5-20. According to Peck et al. (2007) large residuals have an absolute value of three or more. Particular trends to indicate that the static lateral-torsional buckling regression analysis model is not appropriate or is missing additional independent variables were not observed (Figure 5-20). Therefore the proposed linear regression model is considered an adequate model and a nonlinear regression model is not needed. Roughly two groups are formed in Figure 5-20, but this behavior results from the explanatory variable *h*, which was tested at two different levels. The constancy of the variance of the random errors was checked by observation of Figure 5-20. Even though that apparently there is an increase in the dispersion of the Studentized residuals as the predicted critical load increases, this behavior only reflects the fact that the second group on the graph was multiplied by 16 (for the 16 in. wood I-joists) while the first group was multiplied by 11.875 (for the 11 $^{7}/_{8}$ in. wood I-joists), concluding that there is no need to used weighted methods to improve the model.

The normality of the distribution of the random errors were investigated by plotting the Studentized residuals versus the normal quantiles (Figure 5-21). The Studentized residuals approximate a straight line with a correlation coefficient (r) of 0.980, which gives an alpha (α) value of approximately 0.10. According to Peck et al. (2007), this alpha value ascertains that a good normal distribution fit was obtain for the Studentized residuals. The normality of the distribution can also be assessed by the value of the skewness in Figure 5-21, which is approximately 0.1 above the common criterion for an excellent normal distribution fit. The normality of the Studentized residuals assured that the static lateral-torsional buckling model is appropriate since no distorted behavior was observed.

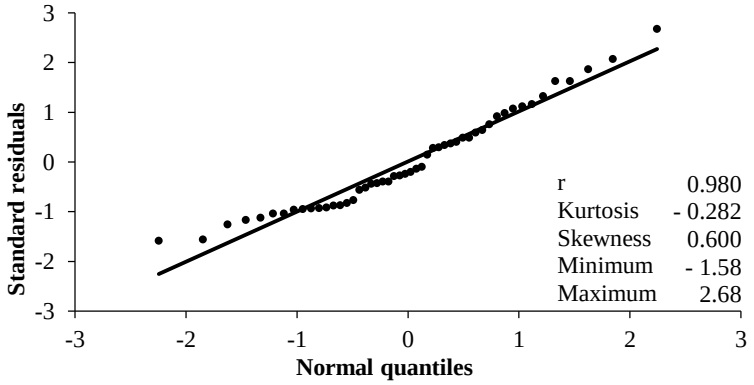

Figure 5-21: Normal probability plot of the Studentized residuals of the non-bracing system.

The static lateral-torsional buckling regression model for the 11 $^{7}/_{8}$ in. wood I-joists and for the 16 in. wood I-joists and the corresponding critical loads obtained from testing for the simply supported end condition are shown in Figure 5-22. The circles and the triangles in the figure represent the critical loads from testing while the lines represent the critical loads from the regression model Equation 5-1. At the beginning of the graph, the difference between the critical loads from the 11 $^{7}/_{8}$ in. wood I-joists and the 16 in. wood I-joists obtained from the regression model is approximately 245 lb. As the lateral bending stiffness of the wood I-joist increases, this difference also increases to approximately 290 lb. at the end of the figure. The same behavior was observed in the critical loads

from testing as previously discussed in the plot of the Studentized residuals versus the predicted critical loads of Figure 5-20. The static lateral-torsional buckling regression models in Figure 5-22 represent accurately the critical loads of the two samples of wood I-joists.

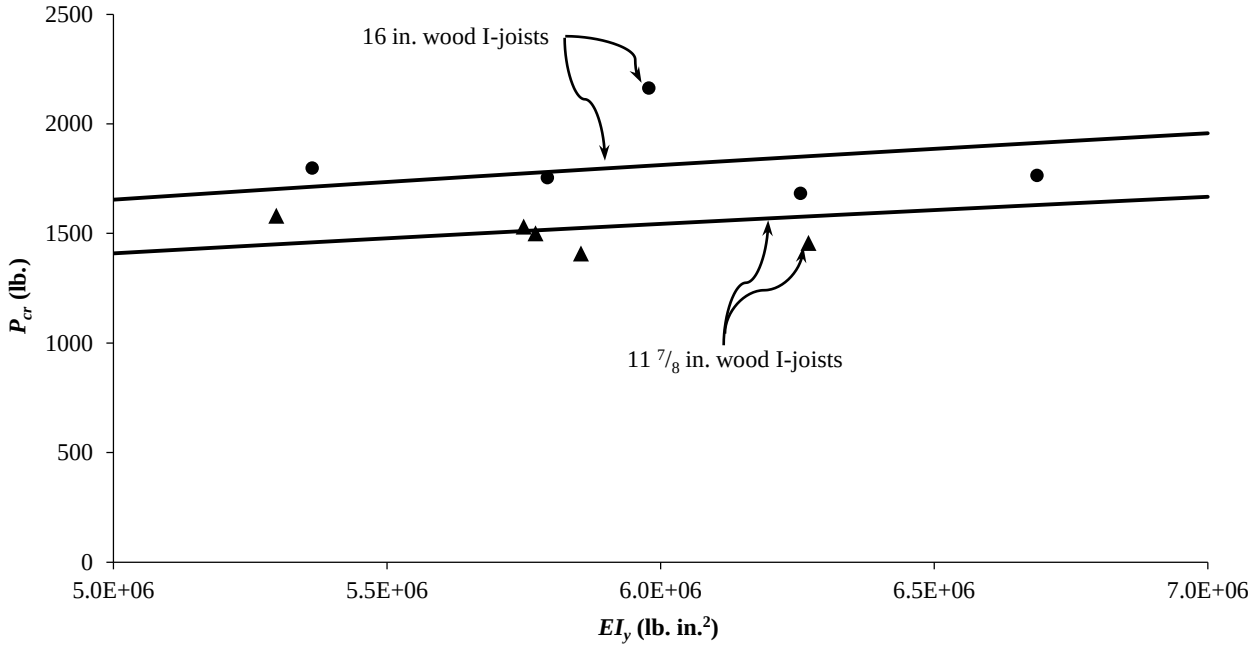

Figure 5-22: Static buckling regression model and the critical loads from testing of the non-bracing system.

5.7.2: One-Bracing Static Lateral-Torsional Buckling Regression Model

The static lateral-torsional regression model for the one-bracing system was developed by following the procedure used for the non-bracing system of the previous section. The critical loads obtained from testing used to regress the model were obtained from Table A-11 in the Appendix for both the 11 $^7/_8$ in. wood I-joists and the 16 in. wood I-joists. The lateral bending stiffness of the wood I-joists were obtained from Table A-1 in the Appendix while the lateral hanger stiffness were obtained from Table 5-3. The general statistics of the 50 values of the critical loads used to regress the model are shown in Table 5-27. Because the absolute values of the kurtosis and the skewness of the sample were smaller than one, the critical loads are assumed to be normally distributed, concluding that standard statistical procedures can be used to develop the regression model. Section 5.4 noted that the critical loads from the non-bracing system must be similar to the critical loads from the one-bracing system, and the statistics from Table 5-24 compared to the statistics from Table 5-27 agree with this behavior. The difference between means from the non-bracing system and the one-bracing system was only 1.24% and the maximum and minimum values were similar.

The statistics of the regression model are shown in Table 5-27. The coefficient of determination was 0.996, slightly greater compared to the corresponding coefficient of determination of the non-bracing system. The adjusted coefficient of determination was 0.975, also slightly larger than the adjusted coefficient of determination of the non-bracing regression model. The adjusted coefficient of determination states that the penalty for having

three terms in the static lateral-torsional buckling regression model is not statistically significant. The model standard deviation is smaller than the corresponding model standard deviation of the non-bracing system regression model. Consequently, the critical loads from testing for the one-bracing system fits the proposed model Equation 4-5 better than the critical loads from testing for the non-bracing system.

Table 5-27: One-Bracing Regression Model General Statistics.

Critical loads		**Regression model**	
Mean	1630	Coefficient of determination (R^2)	0.996
Standard deviation	169	Adjusted coefficient of determination (R^2_{Ad})	0.975
Kurtosis	- 0.641	Model standard deviation	106
Skewness	0.362	Number of observations	50
Maximum	2030		
Minimum	1360		

The analysis of variance from the one-bracing regression model is shown in Table 5-28. The *F* value was much larger than the significance *F* (1.51×10^{-55}), concluding that there is statistical evidence in the data supporting the hypothesis that one or more of the three terms of the static regression model have strong predictive significance. Because the lateral bending stiffness of the wood I-joists is present in all three terms of the regression model and the height of the wood I-joists and the lateral hanger stiffness are also used in the model, the obtained regression model is a suitable predictor of the static critical lateral-torsional buckling loads when the one-bracing system is used.

Table 5-28: One-Bracing Regression Model Analysis of Variance.

Resource	**DF**	**Sum of Squares**	**Mean Squares**	***F* Value**	***p*-value**
Regression	3	133×10^6	44×10^6	3980	$p < 0.0001$
Residual Error	47	525×10^3	11×10^3		
Total	50	134×10^6			

The static lateral-torsional buckling regression model parameter estimates for the one-bracing system are shown in Table 5-29. A comparison between the coefficients of the non-bracing system regression model with the coefficients of the one-bracing system regression model shows that the coefficients for the first and second terms are similar with a difference of 2.86% and 0.41% respectively. However, the difference for the third term (32.1%) is considerably large. Because, the third term of the regression model accounts for the constraint at the ends of the wood I-joists, the one-bracing system was effectively able to balance the influence of the three wood I-joist hangers in the system, even though the expected critical loads did not increase. The standard errors in Table 5-29 are smaller compared to the values of the corresponding coefficients, concluding that strong statistical evidence exists that there is no significant error in the estimation of these coefficients. The standard errors also confirm that there are no correlation problems between the different predictors. The *p*-values of the explanatory variables demonstrated strong predictive values on the critical loads. Similarly to the non-bracing system, the explanatory

variables involved in the third term displayed a higher *p*-value compared to the other two terms, reflecting the large variability as explained in the previous section. The 95% confidence intervals for the estimated coefficients are shown in the last column of Table 5-29. The coefficient of the third term for the non-bracing system regression model was 0.00210 (see Table 5-26), this value falls inside of the 95% confidence interval of the one-bracing system regression model concluding that statistically the non-bracing system regression model is at least 95% equal to the one-bracing system regression model. Taking the estimated coefficients from Table 5-29 into Equation 4-5 the following model is formed to calculate the static buckling critical loads when the one-bracing system is used.

$$P_{cr} = 0.324EI_y^{\frac{1}{2}} + 0.0244hEI_y^{\frac{1}{2}} + 0.00159hEI_y^{\frac{1}{2}}\left(\frac{k}{k+EI_y}\right)^{\frac{1}{2}} \quad (5\text{-}2)$$

Table 5-29: One-Bracing Regression Model Parameter Estimates.

Predictor	Coefficients	Standard Error	*p*-value	95% Confidence Interval
$EI_y^{\frac{1}{2}}$	0.324	0.0422	$p < 0.0001$	$0.239 \leq \mu_1 \leq 0.409$
$hEI_y^{\frac{1}{2}}$	0.0244	0.00299	$p < 0.0001$	$0.0184 \leq \mu_2 \leq 0.0305$
$hEI_y^{\frac{1}{2}}\left(\frac{k}{k+EI_y}\right)^{\frac{1}{2}}$	0.00159	0.00110	0.154	$-0.000616 \leq \mu_3 \leq 0.00380$

The assumption considering that the errors of the regression model must equal zero $E(\varepsilon_i) = 0$ was analyzed by using the techniques of the non-bracing system regression model of the previous section. The predicted critical loads from Equation 5-2 versus the Studentized residuals are shown in Figure 5-23. Extreme values of the standardized residuals were not observed. Particular trends indicating that the one-bracing system regression analysis model was not appropriate or considering missing additional independent variables were not observed. The proposed linear regression model was considered an adequate model and a nonlinear regression model was not required. Similarly to the non-bracing system regression model, two groups of predicted critical loads were observed in Figure 5-23. The constancy of the variance of the random errors was confirmed by analyzing Figure 5-23. Since the behavior of the Studentized standard residuals was very similar to the corresponding non-bracing system regression model, a similar conclusion of a constant variance was obtained.

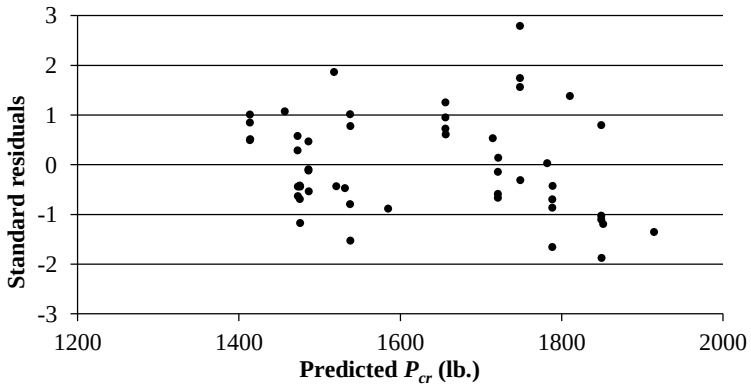

Figure 5-23: Studentized residuals versus the predicted critical load of the one-bracing system.

The normality of the distribution of the random errors were investigated by plotting the Studentized residuals versus the normal quantiles (Figure 5-24). The Studentized residuals approximate a straight line with a correlation coefficient of 0.989, which provides an alpha (α) value of approximately 0.50 and according to Peck et al. (2007), the alpha value ascertains that an excellent normal distribution fit was obtain for the Studentized residuals. The normality of the distribution can also be evaluated by the value of the skewness in Figure 5-24, which is approximately 0.1 below of the common criterion for an excellent normal distribution fit.

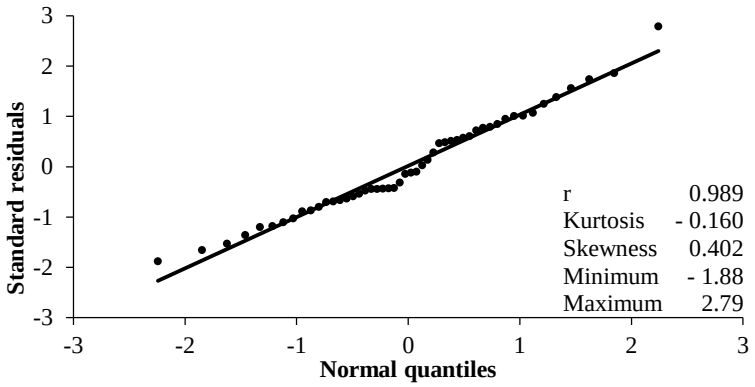

Figure 5-24: Normal probability plot of the Studentized residuals of the one-bracing system.

The static lateral-torsional buckling regression model for the 11 $^{7}/_{8}$ in. wood I-joists and for the 16 in. wood I-joists using the corresponding critical loads obtained from testing for the simply supported end condition are shown in Figure 5-25. The circles and the triangles in the figure represent the critical loads from testing while the lines represent the critical loads from the regression model Equation 5-2. Figure 5-25 was similar to the non-bracing system regression model observed in Figure 5-22, demonstrating that the regression models for the non-bracing and the one-bracing systems are approximately equal.

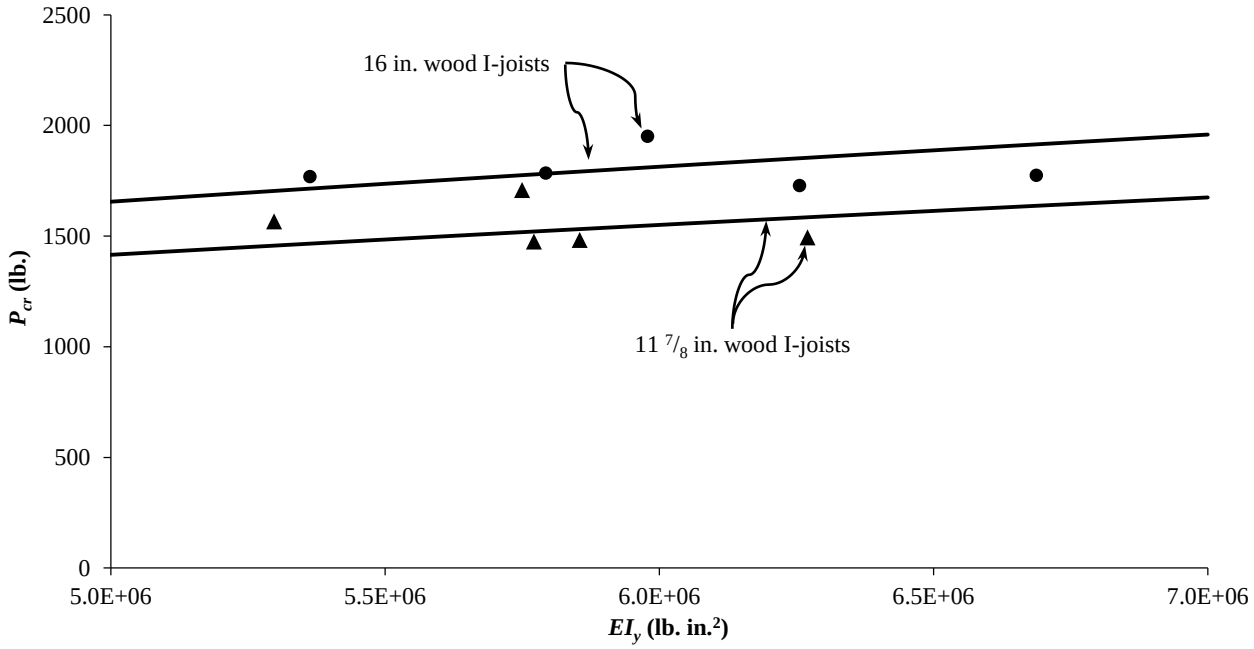

Figure 5-25: Static buckling regression model and the critical loads from testing of the one-bracing system.

5.7.3: Two-Bracing Static Lateral-Torsional Buckling Regression Model

The static lateral-torsional regression model for the two-bracing system was developed using the procedure for the non-bracing system of Section 5.7.1. The critical loads obtained from testing and used to regress the model were obtained from Table A-12 in the Appendix for both the 11 $^{7}/_{8}$ in. wood I-joists and the 16 in. wood I-joists. Because the constraint of the two-bracing system was not directly measured in the tests and also because the main goal of the regression models was to simplify the testing procedures to calculate the lateral-torsional buckling critical loads, the lateral bending stiffness of the wood I-joists used for the two-bracing system regression model were the lateral bending stiffness used for the non-bracing and the one-bracing system regression models rather than the adjusted lateral bending stiffness. Consequently, the constraint induced by the two-bracing system is entered into the regression model as part of the lateral bending stiffness of the wood I-joists. So, the lateral bending stiffness of the wood I-joists were obtained from Table 5-1 in the Appendix while the lateral hanger stiffness were taken from Table 5-3. The general statistics of the 50 values of the critical loads used to regress the two-bracing system model are shown in Table 5-30. The absolute values of the kurtosis and the skewness of the sample are smaller than ½, concluding that the critical loads were normally distributed, so standard statistical procedures can be used to develop the regression model.

The statistics of the regression model are shown in Table 5-30. The coefficient of determination was 0.995 while the adjusted coefficient of determination was 0.973. These coefficients are similar to the corresponding coefficients obtained for the non-bracing system and for the one-bracing system regression models, so the penalty for having three terms on the static lateral-torsional buckling regression model is not statistically significant. The model standard deviation was similar to the corresponding model standard deviation of the non-bracing system regression model. Consequently, the critical loads from testing for the two-bracing system fits the proposed model Equation 4-5 with a similar degree of exactness than the critical loads from testing for the non-bracing system.

Table 5-30: Two-Bracing Regression Model General Statistics.

Critical loads		**Regression model**	
Mean	1860	Coefficient of determination (R^2)	0.995
Standard deviation	199	Adjusted coefficient of determination (R^2_{Ad})	0.973
Kurtosis	- 0.297	Model standard deviation	141
Skewness	0.196	Number of observations	50
Maximum	2400		
Minimum	1480		

The analysis of variance from the two-bracing regression model is shown in Table 5-31. The *F* value in Table 5-31 is much larger than the significance *F* (1.76×10^{-52}) concluding that there is strong statistical evidence in the data supporting the hypothesis that the obtained regression model is a suitable predictor of the static critical lateral-torsional buckling loads when the two-bracing system is used.

Table 5-31: Two-Bracing Regression Model Analysis of Variance.

Resource	DF	Sum of Squares	Mean Squares	*F* Value	*p*-value
Regression	3	174 x 10^6	58.1 x 10^6	2920	p < 0.0001
Residual Error	47	935 x 10^3	19.9 x 10^3		
Total	50	175 x 10^6			

The static lateral-torsional buckling regression model parameter estimates for the two-bracing system are shown in Table 5-32. The coefficients of the first and second terms of the two-bracing system regression model were 11.7% and 19.6% greater compared to the corresponding coefficients of the non-bracing system regression model while the coefficient of the third term of the two-bracing system regression model was 66.7% smaller than the corresponding coefficient of the non-bracing system regression model. The larger difference was acquired in the coefficient of the third term which is the coefficient that accounts by the lateral hanger stiffness, indicating that this explanatory variable had the higher influence on the regression model. This behavior was also observed for both the non-bracing and the one-bracing systems regression models. The standard errors of the coefficients of the first and second terms were smaller compared to the value of the corresponding coefficients, but not the standard error of the coefficient of the third term which was larger, indicating that the coefficients of the first and second terms have strong statistical evidence that there is no significant error in the estimation of these coefficients. The discrepancy in the estimation of the coefficient of the third term is due to the high variability of the lateral hanger stiffness rather than an error in the estimation of this parameter since the coefficient of determination of the regression model is close to one and because the model standard deviation is very small (Table 5-30). Taking the estimated coefficients from the table into Equation 4-5, the following model is formed to calculate the static buckling critical loads when the two-bracing system is used.

$$P_{cr} = 0.352EI_y^{\frac{1}{2}} + 0.0293hEI_y^{\frac{1}{2}} + 0.00126hEI_y^{\frac{1}{2}}\left(\frac{k}{k+EI_y}\right)^{\frac{1}{2}} \quad (5\text{-}3)$$

Table 5-32: Two-Bracing Regression Model Parameter Estimates.

Predictor	Coefficients	Standard Error	*p*-value	95% Confidence Interval
$EI_y^{\frac{1}{2}}$	0.352	0.0562	p < 0.0001	0.239 ≤ μ_1 ≤ 0.466
$hEI_y^{\frac{1}{2}}$	0.0293	0.00399	p < 0.0001	0.0213 ≤ μ_2 ≤ 0.0374
$hEI_y^{\frac{1}{2}}\left(\frac{k}{k+EI_y}\right)^{\frac{1}{2}}$	0.00126	0.00146	0.395	- 0.00169 ≤ μ_3 ≤ 0.00420

The assumption considering that the errors of the regression model must equal zero $E(\varepsilon_i) = 0$ was analyzed by examining the Studentized standard residuals versus the predicted critical loads plot shown in Figure 5-26. One of the residuals was slightly greater than three (3.1), however an analysis of the critical loads obtained from testing does not reveal any specific problems. Particular trends indicating that the two-bracing system regression

analysis model was not appropriate or that additional independent variables were missing were not observed demonstrating that the proposed linear regression model is an adequate model and a nonlinear regression model is not required. A relative constant variance in the random errors are shown in Figure 5-26, so no variation in the prediction ranges of the explanatory variables was expected.

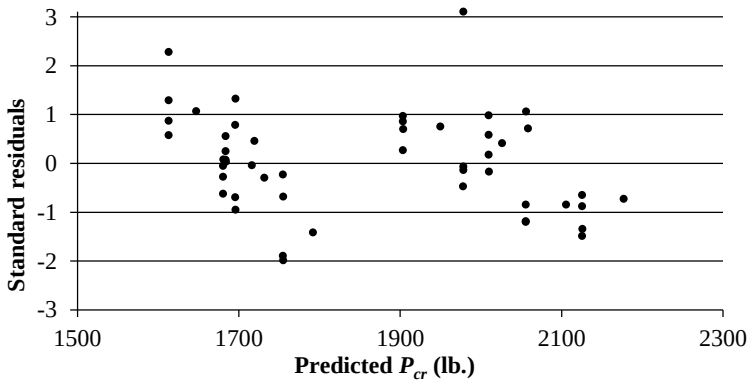

Figure 5-26: Studentized residuals versus the predicted critical load of the two-bracing system.

The normality of the distribution of the random errors was investigated by plotting the Studentized residuals versus the normal quantiles (Figure 5-27). The Studentized residuals approximate a straight line with a correlation coefficient of 0.986, this value of the correlation coefficient gives an alpha (α) value that falls on the range between 0.25 to 0.50 thus according with Peck et al. (2007) this value ascertains that a good normal distribution fit was obtain for the Studentized residuals.

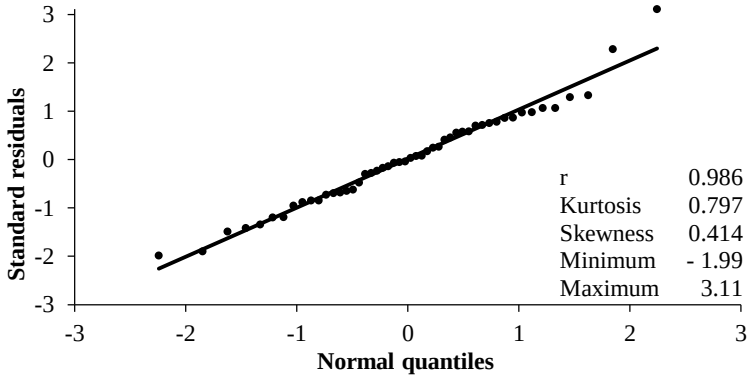

Figure 5-27: Normal probability plot of the Studentized residuals of the two-bracing system.

The static lateral-torsional buckling regression model for the 11 $^{7}/_{8}$ in. wood I-joists and for the 16 in. wood I-joists and the corresponding critical loads obtained from testing for the simply supported end condition are shown in Figure 5-28. The circles and the triangles in the figure represent the critical loads from testing while the lines represent the critical loads from the regression model Equation 5-3. The increase of the critical loads of the 16 in. wood I-joists as the lateral bending stiffness increases with respect to the 11 $^{7}/_{8}$ in. wood I-joists is greater for the two-bracing system regression model compared to the non-bracing system regression model. This behavior results from the increase of the lateral bending stiffness in the three wood I-joists of the system for the two-bracing

system regression model. At the beginning of the graph, the difference between the critical loads from the 11 $^{7}/_{8}$ in. wood I-joists and the 16 in. wood I-joists obtained from the regression model is the approximately 280 lb. As the lateral bending stiffness of the wood I-joist increases, this difference also increases to approximately 335 lb. at the end of the figure.

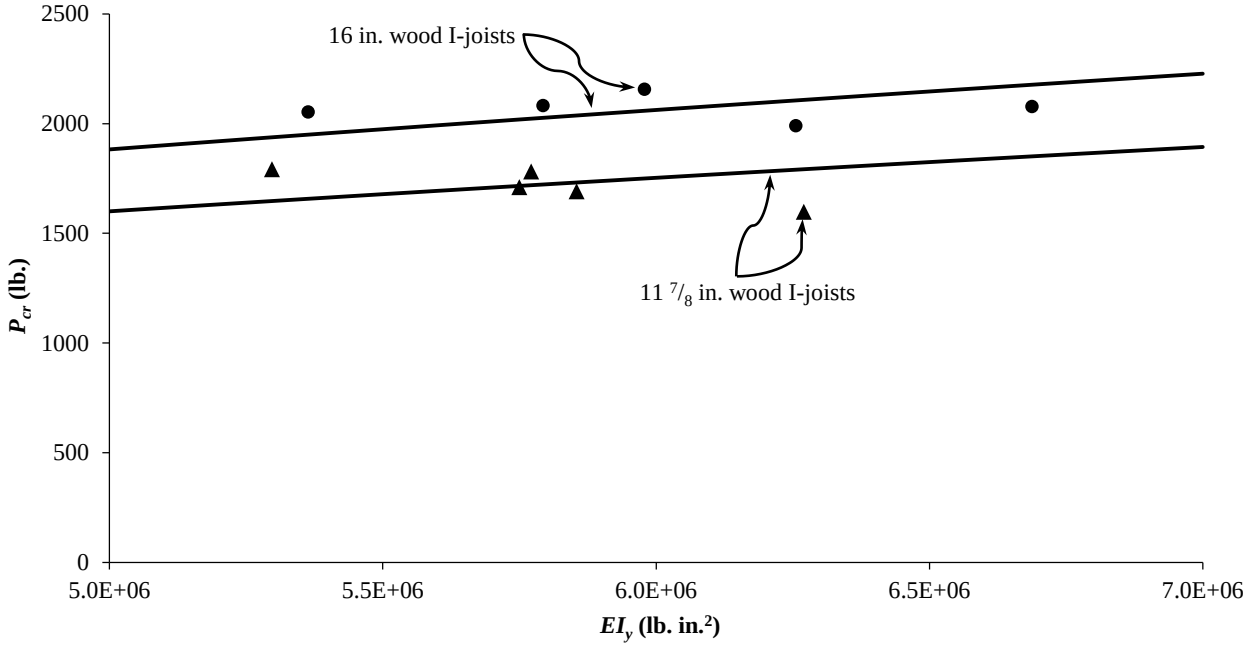

Figure 5-28: Static buckling regression model and the critical loads from testing of the two-bracing system.

A linear regression model for each bracing system was fitted to predict the static lateral-torsional critical loads. The adjusted coefficient of determination was greater than 0.972 for all regression models, concluding an excellent goodness of fit. The lateral bending stiffness of the wood I-joists is used in the three terms of the regression analysis models indicating that this variable is the most important of the variables analyzed in determining the critical loads. The height of the wood is the second most important variable while the lateral hanger stiffness is the less important. However, the variability range of the lateral hanger stiffness was greater than the respective variability ranges of the lateral bending stiffness and the height of the wood I-joist, therefore the lateral hanger stiffness must be accounted for in calculating the static lateral-torsional critical loads. These results agree with the results from the analyses of Section 5.4 of the static lateral-torsional critical loads obtained from testing.

6: Conclusions

The goal of this research was to derive mathematical models to predict the dynamic lateral-torsional buckling instability of wood I-joists loaded by individuals walking. The dynamic lateral-torsional buckling instability was analyzed by linearly combining the static lateral-torsional buckling instability with the dynamic lateral bending of the wood I-joists. Two wood I-joist sizes were used. Five different supported end conditions were tested, a simply supported and four wood I-joist hangers. The difference between the supported end conditions was on the lateral stiffness. The simply supported end condition had a lateral stiffness value of infinity (control). Two top mount and two face mount wood I-joist hangers were tested. Lateral stiffness of the wood I-joist hangers was found to be smaller for the top mount hangers compared to the face mount hangers. Along with the supported end conditions, three bracing systems were investigated, the non-bracing system (control), the one-bracing system and the two-bracing system. The one-bracing system consisted in placing bracing at the mid-span of the wood I-joists. The two-bracing system consisted in placing bracing at each of the quarters-span of the wood I-joists.

A mathematical model was derived to predict the static lateral-torsional buckling critical load for the simply supported end condition. A different mathematical model was derived to predict the static lateral-torsional buckling critical loads for the hanger supported end conditions. To investigate the lateral bending motion of the wood I-joists due to an individual walking, a mathematical model was derived to predict the maximum lateral displacements and individual positions for the simply supported end condition. A different mathematical model was derived to predict the maximum lateral displacements and individual positions for the hanger supported end conditions. Additionally, mathematical models were derived to predict the constraint of a bracing system for both the static lateral-torsional buckling instability and the dynamic lateral bending for the simply supported end condition. Different mathematical models were derived to predict the constraint of a bracing system for both the static lateral-torsional buckling instability and the dynamic lateral bending for the hanger supported end conditions.

- The static lateral-torsional buckling theoretical model for the simply supported end condition predicted accurately the critical loads obtained from testing.
- The static lateral-torsional buckling theoretical model for the hanger supported end condition predicted accurately the critical loads obtained from testing for seven out of eight hanger supported end conditions.
- The static lateral-torsional buckling theoretical model for the hanger supported end condition predicted better the critical loads from testing than the static lateral-torsional buckling theoretical model for the simply supported end condition when wood I-joist hangers were used in the tests.

- As the lateral hanger stiffness increased the theoretical model for the hanger supported end condition approached to the theoretical model for the simply supported end condition and consequently the prediction of the critical loads from both models were approximately equal.
- The static lateral-torsional buckling theoretical model with the theoretical bracing model for the simply supported end condition and the two-bracing system predicted accurately the critical loads obtained from testing for one out of two supported end conditions.
- The static lateral-torsional buckling theoretical model with the theoretical bracing model for the hanger supported end condition and the two-bracing system predicted accurately the critical loads obtained from testing for seven out of eight hanger supported end conditions.
- The lateral bending motion theoretical model for the simply supported end condition predicted accurately the maximum lateral displacements from testing for both samples of wood I-joist and the individual position for one sample of wood I-joists.
- The lateral bending motion theoretical model for the hanger supported end condition predicted accurately the maximum lateral displacements from testing for six out of eight different hanger supported end conditions and predicted accurately the individual positions from testing for five out of eight different supported end conditions.
- Comparisons between the maximum lateral displacements and individual positions from the theoretical model for the simply supported end condition with the theoretical model for the hanger supported end condition concluded that the maximum lateral displacements and individual positions improved when using the theoretical model for the simply supported end condition.
- As the lateral hanger stiffness increased the theoretical model for the hanger supported end condition approached to the theoretical model for the simply supported end condition and consequently the prediction of the maximum lateral displacements from both models were approximately equal.
- The dynamic lateral bending theoretical model with the theoretical bracing model for the simply supported end condition and the one-bracing system predicted accurately the maximum lateral displacements and load positions for one out of two wood I-joist samples.
- The lateral bending motion theoretical model with the theoretical bracing model for the hanger supported end condition and the one-bracing system predicted accurately the maximum lateral displacements for two out of eight different hanger supported end conditions and predicted accurately the individual positions from testing for five out of eight different supported end conditions.
- The lateral bending motion theoretical model with the theoretical bracing model for the simply supported end condition and the two-bracing system predicted accurately the maximum lateral displacements for

both samples of wood I-joists and predicted accurately the individual position for one out of two wood I-joist samples.

- The lateral bending motion theoretical model with the theoretical bracing model for the hanger supported end condition and the two-bracing system did not predicted accurately the maximum lateral displacements for any of eight different hanger supported end conditions but predicted accurately the individual positions from testing for three out of eight different supported end conditions.
- Differences in the lateral component of the force imposed by the individual walking was the main cause of the differences between the theoretical and the testing maximum lateral displacements and individual positions.
- The theoretical bracing models predicted that the one-bracing system is more restrictive than the two-bracing system, results from testing demonstrated agreement with this estimation.
- The smallest critical load was obtained at the mid-span of the wood I-joist. The critical load increased as the load position was displaced away from the mid-span.
- As the lateral hanger stiffness increased the increase of the critical load when displaced away from the wood I-joist mid-span was greater.
- As the initial lateral displacement of the wood I-joists increased the critical load reduced.
- The influence of the initial lateral displacement of the wood I-joist on the lateral-torsional buckling instability depended on the supported end condition.
- As the lateral hanger stiffness increased the reduction of the critical load due to an initial wood I-joist lateral displacement was smaller.
- Static lateral-torsional buckling regression models were fitted for each of the bracing systems using all data for the five different supported end conditions and the two wood I-joist sizes. The goodness of fit was excellent, the adjusted coefficients of determination were above 0.972 for all three models.

6.1: Limitations

The scope of this research is comprised between the following limitations:

- Only two wood I-joist sizes from one manufacture were tested with a common flange, web thickness and constituent materials.
- For the static lateral-torsional buckling instability and lateral bending motion tests, only one wood I-joist length was tested.
- All tests were performed using a sample size of five wood I-joists.
- A single lean-on bracing configuration placed at two different locations on the wood I-joists was used.

- A single type of braces was used in the static lateral-torsional buckling instability and lateral bending motion tests.
- A constant load (individual's weight) was used for all lateral bending motion tests.
- A constant theoretical walking speed and walking frequency were used for all lateral bending motion tests.
- Regression models should be used with caution taking into consideration that only two different wood I-joist sizes and only one wood I-joist length were used.

6.2: Recommendations for Future Work

- Static lateral-torsional buckling instability tests by varying the position of the applied load along the wood I-joist span.
- Combination of the mathematical bracing models with the application of the load away from the mid-span in the static lateral-torsional buckling instability.
- Testing of different span positions of the lean-on bracing system in the wood I-joists as well as different type of braces for inclusion in the current mathematical models.
- Testing of other wood I-joist hangers for inclusion in the current mathematical models.
- Lateral bending motion testing by varying the walking speed and walking frequency of the individual walking on the wood I-joists.
- Understanding the effects of the individual's weight on the response of the wood I-joists in the lateral bending motion testing.
- Because the walking is more stable as the lateral bending stiffness of the wood I-joists increases, testing of the influence of the lateral bending stiffness in the walking pattern is recommended.

Appendix

Table A-1: Lateral Bending Stiffness of the Wood I-Joists.

11 7/8 in. Wood I-Joists		16 in. Wood I-Joists	
I-Joist	**EI_y (lb. in.^{2})**	**I-Joist**	**EI_y (lb. in.^{2})**
E-1	5.85 x 10^6	**S-1**	6.26 x 10^6
E-2	5.30 x 10^6	**S-2**	6.69 x 10^6
E-3	5.77 x 10^6	**S-3**	5.36 x 10^6
E-4	6.27 x 10^6	**S-4**	5.79 x 10^6
E-5	5.75 x 10^6	**S-5**	5.98 x 10^6
Mean	**5.79 x 10^6**	**Mean**	**6.02 x 10^6**

Table A-2: Torsional Rigidity of the Wood I-Joists.

11 7/8 in. Wood I-Joists		16 in. Wood I-Joists	
I-Joist	**GJ (lb. in.^{2})**	**I-Joist**	**GJ (lb. in.^{2})**
E-1	5.18 x 10^6	**S-1**	6.91 x 10^6
E-2	4.80 x 10^6	**S-2**	6.97 x 10^6
E-3	4.94 x 10^6	**S-3**	6.86 x 10^6
E-4	4.84 x 10^6	**S-4**	6.89 x 10^6
E-5	5.29 x 10^6	**S-5**	7.29 x 10^6
Mean	**5.01 x 10^6**	**Mean**	**6.98 x 10^6**

Table A-3: Lateral Wood I-Joist Hanger Stiffness.

Hanger	11 7/8 in. Wood I-Joists Hangers				16 in. Wood I-Joists Hangers			
	ITS k **(lb. / in.)**	**ITT** k **(lb. / in.)**	**IUS** k **(lb. / in.)**	**IUT** k **(lb. / in.)**	**ITS** k **(lb. / in.)**	**ITT** k **(lb. / in.)**	**IUS** k **(lb. / in.)**	**IUT** k **(lb. / in.)**
H-1	46.8	127	336	1050	57.3	344	320	753
H-2	83.5	149	344	886	13.1	205	315	853
H-3	57.1	83.5	369	946	84.7	292	337	903
H-4	52.0	85.2	344	860	63.3	372	308	796
H-5	52.1	111	359	943	54.8	232	263	845
Mean	**58.3**	**111**	**350**	**937**	**54.6**	**289**	**309**	**830**

Table A-4: Wood I-Joist Moisture Content.

11 $^{7}/_{8}$ in. Wood I-joists			16 in. Wood I-joists		
I-Joist	***MC* for EI_y (%)**	***MC* for *GJ* (%)**	**I-Joist**	***MC* for EI_y (%)**	***MC* for *GJ* (%)**
E-1	8.10	11.5	**S-1**	10.3	12.7
E-2	8.18	11.7	**S-2**	10.2	12.8
E-3	8.05	11.5	**S-3**	9.63	12.5
E-4	8.12	11.2	**S-4**	9.53	12.0
E-5	8.26	11.9	**S-5**	10. 7	11.9
Mean	**8.14**	**11.6**	**Mean**	**9.92**	**12.4**

Table A-5: Wood I-Joist Mass.

11 $^{7}/_{8}$ in. Wood I-Joists		16 in. Wood I-Joists	
I-Joist	***m* (lb.)**	**I-Joist**	***m* (lb.)**
E-1	56.7	**S-1**	66.5
E-2	58.3	**S-2**	67.2
E-3	57.6	**S-3**	66.1
E-4	56.8	**S-4**	65.6
E-5	57.6	**S-5**	67.7
Mean	**57.4**	**Mean**	**66.6**

Table A-6: Adjusted Lateral Bending Stiffness for the Static Critical Loads of the Two-Bracing System.

	$EI_{y_{Ad}}$ **(lb. in.^{2})**					
11 $^{7}/_{8}$ in. Wood I-joist	**Simply Supported**	**ITS Hanger**	**ITT Hanger**	**IUS Hanger**	**IUT Hanger**	**Fixed Supported**
E-1	7.84×10^6	7.98×10^6	7.92×10^6	7.87×10^6	7.85×10^6	7.30×10^6
E-2	7.29×10^6	7.41×10^6	7.36×10^6	7.31×10^6	7.30×10^6	6.74×10^6
E-3	7.76×10^6	7.89×10^6	7.84×10^6	7.79×10^6	7.77×10^6	7.22×10^6
E-4	8.26×10^6	8.40×10^6	8.34×10^6	8.29×10^6	8.27×10^6	7.72×10^6
E-5	7.74×10^6	7.87×10^6	7.81×10^6	7.76×10^6	7.75×10^6	7.20×10^6
Mean	**7.78×10^6**	**7.91×10^6**	**7.85×10^6**	**7.80×10^6**	**7.79×10^6**	**7.24×10^6**
16 in. Wood I-joist						
S-1	8.32×10^6	8.48×10^6	8.36×10^6	8.36×10^6	8.33×10^6	7.76×10^6
S-2	8.76×10^6	8.92×10^6	8.79×10^6	8.79×10^6	8.77×10^6	8.19×10^6
S-3	7.43×10^6	7.57×10^6	7.46×10^6	7.46×10^6	7.44×10^6	6.87×10^6
S-4	7.86×10^6	8.01×10^6	7.89×10^6	7.89×10^6	7.87×10^6	7.30×10^6
S-5	8.05×10^6	8.20×10^6	8.08×10^6	8.08×10^6	8.06×10^6	7.48×10^6
Mean	**8.08×10^6**	**8.24×10^6**	**8.12×10^6**	**8.12×10^6**	**8.09×10^6**	**7.52×10^6**

Table A-7: Adjusted Mass and Bending Stiffness for the Lateral Bending Motion of the One-Bracing System.

Simply, Hanger and Fixed Supported End Conditions			Simply, Hanger and Fixed Supported End Conditions		
11 7/8 in. Wood I-Joists	**m_{Ad} (lb.)**	**$EI_{y_{Ad}}$ (lb. in.^{2})**	**16 in. Wood I-Joists**	**m_{Ad} (lb.)**	**$EI_{y_{Ad}}$ (lb. in.^{2})**
E-1	172	1.74 x 10^7	**S-1**	200	1.83 x 10^7
E-2	173	1.69 x 10^7	**S-2**	200	1.87 x 10^7
E-3	172	1.73 x 10^7	**S-3**	199	1.74 x 10^7
E-4	172	1.78 x 10^7	**S-4**	199	1.78 x 10^7
E-5	172	1.73 x 10^7	**S-5**	201	1.80 x 10^7
Mean	**172**	**1.73 x 10^7**	**Mean**	**200**	**1.80 x 10^7**

Table A-8: Adjusted Mass for the Lateral Bending Motion of the Two-Bracing System.

11 7/8 in. Wood I-Joists	**m_{Ad} (lb.)**		**16 in. Wood I-Joists**	**m_{Ad} (lb.)**	
	Simply and Hanger Supported	**Fixed Supported**		**Simply and Hanger Supported**	**Fixed Supported**
E-1	136	114	**S-1**	158	133
E-2	137	116	**S-2**	159	134
E-3	137	115	**S-3**	158	133
E-4	136	114	**S-4**	157	132
E-5	137	115	**S-5**	159	134
Mean	**137**	**115**	**Mean**	**158**	**133**

Table A-9: Adjusted Bending Stiffness for the Lateral Bending Motion of the Two-Bracing System.

	$EI_{y_{Ad}}$ (lb. in.^{2})					
11 7/8 in. Wood I-joist	**Simply Supported**	**ITS Hanger**	**ITT Hanger**	**IUS Hanger**	**IUT Hanger**	**Fixed Supported**
E-1	1.38 x 10^7	1.44 x 10^7	1.41 x 10^7	1.39 x 10^7	1.39 x 10^7	1.16 x 10^7
E-2	1.33 x 10^7	1.37 x 10^7	1.35 x 10^7	1.33 x 10^7	1.33 x 10^7	1.11 x 10^7
E-3	1.37 x 10^7	1.43 x 10^7	1.40 x 10^7	1.38 x 10^7	1.38 x 10^7	1.16 x 10^7
E-4	1.42 x 10^7	1.48 x 10^7	1.46 x 10^7	1.43 x 10^7	1.43 x 10^7	1.21 x 10^7
E-5	1.37 x 10^7	1.42 x 10^7	1.40 x 10^7	1.38 x 10^7	1.37 x 10^7	1.15 x 10^7
Mean	**1.37 x 10^7**	**1.43 x 10^7**	**1.40 x 10^7**	**1.38 x 10^7**	**138 x 10^7**	**1.16 x 10^7**
16 in. Wood I-joist						
S-1	1.46 x 10^7	1.52 x 10^7	1.47 x 10^7	1.47 x 10^7	1.46 x 10^7	1.23 x 10^7
S-2	1.50 x 10^7	1.56 x 10^7	1.51 x 10^7	1.51 x 10^7	1.50 x 10^7	1.27 x 10^7
S-3	1.36 x 10^7	1.42 x 10^7	1.38 x 10^7	1.37 x 10^7	1.37 x 10^7	1.14 x 10^7
S-4	1.41 x 10^7	1.46 x 10^7	1.42 x 10^7	1.42 x 10^7	1.41 x 10^7	1.18 x 10^7
S-5	1.43 x 10^7	1.49 x 10^7	1.44 x 10^7	1.44 x 10^7	1.43 x 10^7	1.20 x 10^7
Mean	**1.43 x 10^7**	**1.49 x 10^7**	**1.44 x 10^7**	**1.44 x 10^7**	**1.43 x 10^7**	**1.20 x 10^7**

Table A-10: Static Lateral-Torsional Critical Loads for the Non-Bracing System.

	11 7/8 in. Wood I-Joists			16 in. Wood I-Joists		
	I-joist	**Testing P_{cr} (lb.)**	**Theoretical P_{cr} (lb.)**	**I-joist**	**Testing P_{cr} (lb.)**	**Theoretical P_{cr} (lb.)**
Simply Supported End Condition	**E-1**	1410	1610	**S-1**	1680	1920
	E-2	1580	1470	**S-2**	1770	1990
	E-3	1500	1560	**S-3**	1800	1770
	E-4	1460	1610	**S-4**	1750	1840
	E-5	1530	1610	**S-5**	2160	1930
	Mean	**1500**	**1570**	**Mean**	**1830**	**1890**
ITS Hanger Supported End Condition	**E-1**	1360	1460	**S-1**	1640	1720
	E-2	1550	1350	**S-2**	1730	1770
	E-3	1390	1420	**S-3**	1780	1610
	E-4	1480	1450	**S-4**	1580	1670
	E-5	1420	1470	**S-5**	1830	1740
	Mean	**1440**	**1430**	**Mean**	**1710**	**1700**
ITT Hanger Supported End Condition	**E-1**	1530	1530	**S-1**	1630	1870
	E-2	1470	1410	**S-2**	1670	1940
	E-3	1400	1480	**S-3**	1690	1740
	E-4	1690	1520	**S-4**	1660	1800
	E-5	1570	1530	**S-5**	1940	1890
	Mean	**1530**	**1490**	**Mean**	**1720**	**1850**
IUS Hanger Supported End Condition	**E-1**	1680	1580	**S-1**	1560	1880
	E-2	1430	1450	**S-2**	2070	1940
	E-3	1330	1530	**S-3**	1690	1740
	E-4	1460	1580	**S-4**	1630	1810
	E-5	1340	1590	**S-5**	2000	1890
	Mean	**1450**	**1550**	**Mean**	**1790**	**1850**
IUT Hanger Supported End Condition	**E-1**	1610	1600	**S-1**	1810	1900
	E-2	1430	1470	**S-2**	1620	1970
	E-3	1330	1550	**S-3**	1700	1760
	E-4	1380	1600	**S-4**	1680	1830
	E-5	1400	1600	**S-5**	1680	1910
	Mean	**1430**	**1560**	**Mean**	**1700**	**1870**
Fixed Supported End Condition	**E-1**	– – – –	1740	**S-1**	– – – –	2080
	E-2	– – – –	1600	**S-2**	– – – –	2160
	E-3	– – – –	1690	**S-3**	– – – –	1920
	E-4	– – – –	1740	**S-4**	– – – –	2000
	E-5	– – – –	1740	**S-5**	– – – –	2090
	Mean	**– – – –**	**1700**	**Mean**	**– – – –**	**2050**

Table A-11: Static Lateral-Torsional Critical Loads for the One-Bracing System.

	11 7/8 in. Wood I-Joists			16 in. Wood I-Joists		
	I-joist	**Testing P_{cr} (lb.)**	**Theoretical P_{cr} (lb.)**	**I-joist**	**Testing P_{cr} (lb.)**	**Theoretical P_{cr} (lb.)**
Simply Supported End Condition	**E-1**	1480	1610	**S-1**	1730	1920
	E-2	1570	1470	**S-2**	1780	1990
	E-3	1480	1560	**S-3**	1770	1770
	E-4	1490	1610	**S-4**	1790	1840
	E-5	1710	1610	**S-5**	1950	1930
	Mean	**1550**	**1570**	**Mean**	**1800**	**1890**
ITS Hanger Supported End Condition	**E-1**	1530	1460	**S-1**	1720	1720
	E-2	1520	1350	**S-2**	1740	1770
	E-3	1410	1420	**S-3**	1780	1610
	E-4	1640	1450	**S-4**	1650	1670
	E-5	1530	1470	**S-5**	1910	1740
	Mean	**1530**	**1430**	**Mean**	**1760**	**1700**
ITT Hanger Supported End Condition	**E-1**	1470	1530	**S-1**	1700	1870
	E-2	1500	1400	**S-2**	1740	1940
	E-3	1430	1480	**S-3**	1750	1740
	E-4	1460	1520	**S-4**	1710	1800
	E-5	1500	1530	**S-5**	1930	1890
	Mean	**1470**	**1490**	**Mean**	**1770**	**1850**
IUS Hanger Supported End Condition	**E-1**	1480	1580	**S-1**	1620	1880
	E-2	1460	1450	**S-2**	1930	1940
	E-3	1360	1530	**S-3**	1730	1740
	E-4	1620	1580	**S-4**	1660	1810
	E-5	1410	1590	**S-5**	2030	1890
	Mean	**1470**	**1540**	**Mean**	**1790**	**1850**
IUT Hanger Supported End Condition	**E-1**	1430	1600	**S-1**	1750	1900
	E-2	1470	1470	**S-2**	1660	1970
	E-3	1430	1550	**S-3**	1720	1760
	E-4	1380	1600	**S-4**	1740	1830
	E-5	1430	1600	**S-5**	1720	1910
	Mean	**1430**	**1560**	**Mean**	**1720**	**1870**
Fixed Supported End Condition	**E-1**	– – – –	1740	**S-1**	– – – –	2080
	E-2	– – – –	1600	**S-2**	– – – –	2160
	E-3	– – – –	1690	**S-3**	– – – –	1920
	E-4	– – – –	1740	**S-4**	– – – –	2000
	E-5	– – – –	1740	**S-5**	– – – –	2090
	Mean	**– – – –**	**1700**	**Mean**	**– – – –**	**2050**

Table A-12: Static Lateral-Torsional Critical Loads for the Two-Bracing System.

	11 7/8 in. Wood I-Joists			16 in. Wood I-Joists		
	I-joist	**Testing P_{cr} (lb.)**	**Theoretical P_{cr} (lb.)**	**I-joist**	**Testing P_{cr} (lb.)**	**Theoretical P_{cr} (lb.)**
Simply Supported End Condition	**E-1**	1690	1860	**S-1**	1990	2200
	E-2	1790	1730	**S-2**	2080	2270
	E-3	1780	1800	**S-3**	2050	2080
	E-4	1600	1840	**S-4**	2080	2140
	E-5	1710	1870	**S-5**	2160	2230
	Mean	**1710**	**1820**	**Mean**	**2070**	**2180**
ITS Hanger Supported End Condition	**E-1**	1600	1650	**S-1**	1890	1930
	E-2	1790	1550	**S-2**	1920	1980
	E-3	1760	1610	**S-3**	1940	1850
	E-4	1500	1630	**S-4**	1910	1890
	E-5	1640	1660	**S-5**	2030	1960
	Mean	**1660**	**1620**	**Mean**	**1940**	**1920**
ITT Hanger Supported End Condition	**E-1**	1800	1740	**S-1**	1940	2150
	E-2	1930	1620	**S-2**	2010	2210
	E-3	1690	1690	**S-3**	2020	2030
	E-4	1720	1720	**S-4**	1970	2090
	E-5	1670	1750	**S-5**	2090	2170
	Mean	**1760**	**1700**	**Mean**	**2010**	**2130**
IUS Hanger Supported End Condition	**E-1**	1570	1820	**S-1**	1890	2150
	E-2	1730	1690	**S-2**	2040	2210
	E-3	1720	1770	**S-3**	2040	2030
	E-4	1480	1800	**S-4**	1960	2090
	E-5	1600	1830	**S-5**	2140	2170
	Mean	**1620**	**1780**	**Mean**	**2010**	**2130**
IUT Hanger Supported End Condition	**E-1**	1880	1840	**S-1**	2200	2180
	E-2	1690	1710	**S-2**	1940	2250
	E-3	1690	1790	**S-3**	2000	2060
	E-4	1660	1830	**S-4**	2400	2120
	E-5	1690	1850	**S-5**	1990	2210
	Mean	**1720**	**1800**	**Mean**	**2110**	**2160**
Fixed Supported End Condition	**E-1**	– – – –	1950	**S-1**	– – – –	2320
	E-2	– – – –	1800	**S-2**	– – – –	2400
	E-3	– – – –	1890	**S-3**	– – – –	2180
	E-4	– – – –	1940	**S-4**	– – – –	2250
	E-5	– – – –	1950	**S-5**	– – – –	2340
	Mean	**– – – –**	**1910**	**Mean**	**– – – –**	**2300**

Table A-13: Lateral Maximum Displacement for the 11 $^{7}/_{8}$ in. Wood I-Joists for the Non-Bracing System.

End Condition	I-Joist	Testing				Theoretical		
		MSB δ (in.)	LQT δ (in.)	MST δ (in.)	Load Position s (in.)	LQT δ (in.)	MST δ (in.)	Load Position s (in.)
Simply Supported	E-1	0.835	0.843	1.20	124	0.631	0.893	126
	E-2	0.521	0.641	0.875	162	0.672	0.950	136
	E-3	0.705	0.766	1.09	106	0.645	0.912	128
	E-4	0.918	0.924	1.38	113	0.586	0.829	106
	E-5	0.719	0.761	1.04	162	0.647	0.915	128
	Mean	**0.740**	**0.787**	**1.12**	**133**	**0.636**	**0.900**	**125**
ITS Hanger Supported	E-1	0.708	0.726	1.05	126	0.834	1.14	103
	E-2	0.461	0.605	0.882	134	0.908	1.24	128
	E-3	0.500	0.565	0.769	153	0.826	1.13	143
	E-4	0.540	0.601	0.902	106	0.805	1.10	118
	E-5	0.523	0.635	0.930	141	0.834	1.14	106
	Mean	**0.546**	**0.63**	**0.907**	**132**	**0.841**	**1.15**	**120**
ITT Hanger Supported	E-1	0.462	0.575	0.814	131	0.732	1.00	136
	E-2	0.676	0.714	1.05	117	0.802	1.10	143
	E-3	0.449	0.554	0.765	128	0.779	1.07	118
	E-4	0.627	0.731	1.04	140	0.723	0.991	113
	E-5	0.648	0.768	1.15	122	0.780	1.07	118
	Mean	**0.572**	**0.668**	**0.964**	**128**	**0.763**	**1.05**	**126**
IUS Hanger Supported	E-1	0.744	0.925	1.26	145	0.666	0.930	128
	E-2	0.487	0.645	0.942	131	0.770	1.03	118
	E-3	0.624	0.708	0.962	129	0.694	0.968	113
	E-4	0.621	0.745	1.10	133	0.640	0.893	126
	E-5	0.680	0.859	1.19	156	0.693	0.968	113
	Mean	**0.631**	**0.776**	**1.09**	**139**	**0.693**	**0.958**	**120**
IUT Hanger Supported	E-1	0.820	0.932	1.21	176	0.657	0.923	111
	E-2	0.665	0.714	1.02	125	0.726	1.02	118
	E-3	0.353	0.482	0.652	136	0.642	0.904	128
	E-4	0.481	0.568	0.874	93	0.584	0.821	141
	E-5	0.473	0.595	0.856	116	0.652	0.917	113
	Mean	**0.558**	**0.658**	**0.922**	**129**	**0.652**	**0.917**	**122**
Fixed Supported	E-1	– – – –	– – – –	– – – –	– – – –	0.108	0.138	129
	E-2	– – – –	– – – –	– – – –	– – – –	0.166	0.212	98.5
	E-3	– – – –	– – – –	– – – –	– – – –	0.143	0.184	125
	E-4	– – – –	– – – –	– – – –	– – – –	0.161	0.207	126
	E-5	– – – –	– – – –	– – – –	– – – –	0.152	0.195	125
	Mean	– – – –	– – – –	– – – –	– – – –	**0.146**	**0.187**	**121**

Table A-14: Lateral Maximum Displacement for the 16 in. Wood I-Joists for the Non-Bracing System.

End Condition	I-Joist	Testing				Theoretical		
		MSB δ (in.)	LQT δ (in.)	MST δ (in.)	Load Position s (in.)	LQT δ (in.)	MST δ (in.)	Load Position s (in.)
Simply Supported	S-1	0.482	0.604	0.850	129	0.577	0.815	133
	S-2	0.495	0.630	0.836	153	0.554	0.784	128
	S-3	0.445	0.602	0.764	159	0.655	0.926	143
	S-4	0.456	0.567	0.813	134	0.647	0.915	118
	S-5	0.408	0.504	0.699	132	0.627	0.886	118
	Mean	**0.457**	**0.581**	**0.792**	**141**	**0.612**	**0.865**	**128**
ITS Hanger Supported	S-1	0.471	0.657	0.891	159	0.798	1.09	128
	S-2	0.426	0.546	0.760	136	0.769	1.05	126
	S-3	0.512	0.578	0.815	135	0.873	1.19	95.8
	S-4	0.361	0.535	0.776	153	0.855	1.17	133
	S-5	0.320	0.457	0.685	129	0.841	1.15	133
	Mean	**0.418**	**0.555**	**0.785**	**142**	**0.827**	**1.13**	**123**
ITT Hanger Supported	S-1	0.362	0.625	0.850	156	0.657	0.913	118
	S-2	0.452	0.619	0.843	147	0.603	0.837	133
	S-3	0.376	0.478	0.644	152	0.740	1.03	126
	S-4	0.359	0.491	0.740	130	0.693	0.965	121
	S-5	0.362	0.548	0.784	137	0.667	0.928	121
	Mean	**0.382**	**0.552**	**0.772**	**144**	**0.672**	**0.935**	**124**
IUS Hanger Supported	S-1	0.513	0.690	0.915	139	0.652	0.907	118
	S-2	0.520	0.644	0.894	137	0.594	0.826	133
	S-3	0.389	0.652	0.878	127	0.724	1.01	128
	S-4	0.440	0.565	0.803	149	0.661	0.921	103
	S-5	0.394	0.514	0.739	123	0.657	0.914	121
	Mean	**0.451**	**0.613**	**0.846**	**135**	**0.658**	**0.916**	**121**
IUT Hanger Supported	S-1	0.484	0.742	1.01	149	0.608	0.855	133
	S-2	0.533	0.702	0.961	137	0.578	0.812	113
	S-3	0.506	0.680	0.910	135	0.709	0.997	126
	S-4	0.543	0.698	1.01	137	0.645	0.906	121
	S-5	0.380	0.617	0.845	156	0.630	0.886	121
	Mean	**0.489**	**0.688**	**0.947**	**143**	**0.634**	**0.891**	**123**
Fixed Supported	S-1	– – – –	– – – –	– – – –	– – – –	0.163	0.208	121
	S-2	– – – –	– – – –	– – – –	– – – –	0.138	0.176	126
	S-3	– – – –	– – – –	– – – –	– – – –	0.188	0.241	113
	S-4	– – – –	– – – –	– – – –	– – – –	0.162	0.208	141
	S-5	– – – –	– – – –	– – – –	– – – –	0.159	0.204	133
	Mean	– – – –	– – – –	– – – –	– – – –	**0.162**	**0.207**	**127**

Table A-15: Lateral Maximum Displacements for the 11 $^{7}/_{8}$ in. Wood I-Joists for the One-Bracing System.

End Condition	I-Joist	Testing				Theoretical		
		MSB δ (in.)	LQT δ (in.)	MST δ (in.)	Load Position s (in.)	LQT δ (in.)	MST δ (in.)	Load Position s (in.)
Simply Supported	E-1	0.300	0.333	0.399	150	0.208	0.294	128
	E-2	0.523	0.429	0.598	135	0.219	0.310	113
	E-3	0.259	0.266	0.311	156	0.214	0.303	128
	E-4	0.170	0.184	0.238	153	0.209	0.296	126
	E-5	0.156	0.182	0.212	130	0.215	0.304	128
	Mean	**0.282**	**0.279**	**0.352**	**145**	**0.213**	**0.301**	**125**
ITS Hanger Supported	E-1	0.177	0.168	0.210	155	0.326	0.501	136
	E-2	0.161	0.168	0.204	123	0.356	0.542	118
	E-3	0.145	0.183	0.226	142	0.326	0.501	95.8
	E-4	0.157	0.163	0.209	154	0.330	0.510	136
	E-5	0.149	0.156	0.188	155	0.327	0.502	95.9
	Mean	**0.158**	**0.168**	**0.207**	**146**	**0.333**	**0.510**	**116**
ITT Hanger Supported	E-1	0.300	0.271	0.367	137	0.313	0.433	128
	E-2	0.247	0.213	0.269	134	0.320	0.441	111
	E-3	0.183	0.203	0.234	126	0.312	0.432	128
	E-4	0.239	0.228	0.303	143	0.296	0.410	128
	E-5	0.237	0.210	0.268	161	0.312	0.432	128
	Mean	**0.241**	**0.225**	**0.288**	**140**	**0.311**	**0.430**	**125**
IUS Hanger Supported	E-1	0.325	0.339	0.371	149	0.251	0.344	136
	E-2	0.261	0.293	0.342	144	0.255	0.350	121
	E-3	0.148	0.174	0.198	153	0.257	0.353	118
	E-4	0.158	0.150	0.200	129	0.242	0.332	133
	E-5	0.147	0.150	0.202	126	0.258	0.354	118
	Mean	**0.208**	**0.221**	**0.263**	**140**	**0.253**	**0.347**	**125**
IUT Hanger Supported	E-1	0.258	0.257	0.341	140	0.232	0.324	113
	E-2	0.336	0.306	0.390	146	0.236	0.330	133
	E-3	0.282	0.270	0.337	138	0.232	0.323	113
	E-4	0.110	0.148	0.178	134	0.221	0.307	128
	E-5	0.156	0.173	0.223	131	0.232	0.323	113
	Mean	**0.228**	**0.231**	**0.294**	**138**	**0.231**	**0.321**	**120**
Fixed Supported	E-1	– – – –	– – – –	– – – –	– – – –	0.0302	0.0382	125
	E-2	– – – –	– – – –	– – – –	– – – –	0.0604	0.0764	118
	E-3	– – – –	– – – –	– – – –	– – – –	0.0433	0.0555	125
	E-4	– – – –	– – – –	– – – –	– – – –	0.0433	0.0555	129
	E-5	– – – –	– – – –	– – – –	– – – –	0.0442	0.0561	125
	Mean	– – – –	– – – –	– – – –	– – – –	**0.0443**	**0.0563**	**124**

Table A-16: Lateral Maximum Displacements for the 16 in. Wood I-Joists for the One-Bracing System.

End Condition	I-Joist	Testing				Theoretical		
		MSB δ (in.)	LQT δ (in.)	MST δ (in.)	Load Position s (in.)	LQT δ (in.)	MST δ (in.)	Load Position s (in.)
Simply Supported	S-1	0.206	0.196	0.268	135	0.196	0.277	133
	S-2	0.126	0.185	0.188	152	0.196	0.277	133
	S-3	0.101	0.130	0.164	133	0.211	0.299	118
	S-4	0.117	0.162	0.194	127	0.207	0.293	136
	S-5	0.121	0.139	0.154	153	0.205	0.290	136
	Mean	**0.134**	**0.162**	**0.194**	**140**	**0.203**	**0.287**	**131**
ITS Hanger Supported	S-1	0.218	0.203	0.259	163	0.297	0.477	126
	S-2	0.167	0.129	0.177	154	0.302	0.491	121
	S-3	0.136	0.151	0.196	143	0.345	0.543	126
	S-4	0.155	0.167	0.246	132	0.327	0.519	126
	S-5	0.139	0.127	0.171	109	0.325	0.519	126
	Mean	**0.163**	**0.155**	**0.210**	**140**	**0.319**	**0.510**	**125**
ITT Hanger Supported	S-1	0.137	0.129	0.163	135	0.252	0.344	126
	S-2	0.146	0.170	0.189	156	0.241	0.329	106
	S-3	0.149	0.181	0.206	156	0.262	0.359	128
	S-4	0.147	0.126	0.189	127	0.255	0.348	126
	S-5	0.101	0.139	0.148	155	0.251	0.344	126
	Mean	**0.136**	**0.149**	**0.179**	**146**	**0.252**	**0.345**	**122**
IUS Hanger Supported	S-1	0.150	0.151	0.210	125	0.246	0.336	126
	S-2	0.100	0.105	0.132	131	0.234	0.320	143
	S-3	0.129	0.130	0.180	121	0.257	0.352	128
	S-4	0.116	0.118	0.176	134	0.255	0.350	126
	S-5	0.118	0.138	0.155	135	0.253	0.346	126
	Mean	**0.123**	**0.128**	**0.171**	**129**	**0.249**	**0.341**	**130**
IUT Hanger Supported	S-1	0.186	0.205	0.253	149	0.218	0.304	121
	S-2	0.244	0.307	0.313	168	0.219	0.305	118
	S-3	0.153	0.196	0.208	157	0.229	0.318	141
	S-4	0.126	0.167	0.202	152	0.231	0.321	121
	S-5	0.103	0.138	0.159	149	0.228	0.317	121
	Mean	**0.162**	**0.203**	**0.227**	**155**	**0.225**	**0.313**	**124**
Fixed Supported	S-1	– – – –	– – – –	– – – –	– – – –	0.0514	0.0654	98.5
	S-2	– – – –	– – – –	– – – –	– – – –	0.0543	0.0693	113
	S-3	– – – –	– – – –	– – – –	– – – –	0.0571	0.0732	126
	S-4	– – – –	– – – –	– – – –	– – – –	0.0470	0.0611	148
	S-5	– – – –	– – – –	– – – –	– – – –	0.0471	0.0611	148
	Mean	– – – –	– – – –	– – – –	– – – –	**0.0514**	**0.0660**	**127**

Table A-17: Lateral Maximum Displacements for the 11 $^{7}/_{8}$ in. Wood I-Joists for the Two-Bracing System.

End Condition	I-Joist	Testing				Theoretical		
		MSB δ (in.)	LQT δ (in.)	MST δ (in.)	Load Position s (in.)	LQT δ (in.)	MST δ (in.)	Load Position s (in.)
Simply Supported	E-1	0.276	0.286	0.392	151	0.267	0.377	111
	E-2	0.609	0.510	0.737	148	0.282	0.398	113
	E-3	0.206	0.209	0.307	140	0.271	0.383	128
	E-4	0.117	0.104	0.164	117	0.262	0.370	126
	E-5	0.162	0.168	0.252	152	0.271	0.384	128
	Mean	**0.274**	**0.255**	**0.370**	**142**	**0.271**	**0.382**	**121**
ITS Hanger Supported	E-1	0.146	0.119	0.206	131	0.407	0.595	111
	E-2	0.183	0.193	0.307	137	0.424	0.614	113
	E-3	0.157	0.157	0.220	159	0.403	0.588	133
	E-4	0.122	0.121	0.192	137	0.395	0.580	111
	E-5	0.179	0.181	0.273	129	0.404	0.590	133
	Mean	**0.157**	**0.154**	**0.240**	**139**	**0.407**	**0.593**	**120**
ITT Hanger Supported	E-1	0.190	0.191	0.288	151	0.359	0.493	106
	E-2	0.192	0.214	0.335	142	0.370	0.506	128
	E-3	0.208	0.211	0.317	135	0.367	0.503	126
	E-4	0.170	0.171	0.289	131	0.352	0.483	103
	E-5	0.142	0.146	0.222	141	0.368	0.504	126
	Mean	**0.180**	**0.187**	**0.290**	**140**	**0.363**	**0.498**	**118**
IUS Hanger Supported	E-1	0.290	0.263	0.398	128	0.307	0.423	133
	E-2	0.089	0.112	0.177	125	0.324	0.447	118
	E-3	0.163	0.151	0.234	126	0.301	0.415	133
	E-4	0.111	0.108	0.177	148	0.299	0.411	113
	E-5	0.264	0.259	0.382	142	0.301	0.414	133
	Mean	**0.183**	**0.179**	**0.274**	**134**	**0.306**	**0.422**	**126**
IUT Hanger Supported	E-1	0.323	0.276	0.387	152	0.280	0.391	113
	E-2	0.241	0.251	0.363	149	0.296	0.414	133
	E-3	0.216	0.198	0.278	155	0.290	0.405	113
	E-4	0.161	0.139	0.215	152	0.279	0.390	111
	E-5	0.218	0.209	0.301	139	0.290	0.406	113
	Mean	**0.232**	**0.215**	**0.309**	**149**	**0.287**	**0.401**	**117**
Fixed Supported	E-1	– – – –	– – – –	– – – –	– – – –	0.0384	0.0481	125
	E-2	– – – –	– – – –	– – – –	– – – –	0.0834	0.106	136
	E-3	– – – –	– – – –	– – – –	– – – –	0.0663	0.0854	125
	E-4	– – – –	– – – –	– – – –	– – – –	0.0810	0.104	128
	E-5	– – – –	– – – –	– – – –	– – – –	0.0691	0.0883	125
	Mean	– – – –	– – – –	– – – –	– – – –	**0.0676**	**0.0864**	**128**

Table A-18: Lateral Maximum Displacements for the 16 in. Wood I-Joists for the Two-Bracing System.

End Condition	I-Joist	Testing				Theoretical		
		MSB δ (in.)	LQT δ (in.)	MST δ (in.)	Load Position s (in.)	LQT δ (in.)	MST δ (in.)	Load Position s (in.)
Simply Supported	S-1	0.123	0.160	0.246	123	0.250	0.353	133
	S-2	0.109	0.122	0.178	139	0.240	0.339	133
	S-3	0.101	0.144	0.193	148	0.265	0.375	121
	S-4	0.093	0.112	0.184	143	0.264	0.373	118
	S-5	0.106	0.084	0.143	129	0.261	0.368	118
	Mean	**0.106**	**0.124**	**0.189**	**136**	**0.256**	**0.362**	**125**
ITS Hanger Supported	S-1	0.175	0.165	0.244	147	0.396	0.595	118
	S-2	0.168	0.160	0.238	126	0.377	0.572	118
	S-3	0.132	0.144	0.204	140	0.417	0.617	121
	S-4	0.133	0.144	0.222	154	0.399	0.594	121
	S-5	0.199	0.200	0.296	142	0.397	0.593	121
	Mean	**0.161**	**0.163**	**0.241**	**142**	**0.397**	**0.594**	**120**
ITT Hanger Supported	S-1	0.133	0.156	0.261	124	0.294	0.403	103
	S-2	0.113	0.109	0.145	142	0.293	0.402	121
	S-3	0.109	0.125	0.173	138	0.319	0.438	126
	S-4	0.133	0.142	0.226	134	0.306	0.420	106
	S-5	0.107	0.116	0.161	142	0.303	0.416	106
	Mean	**0.119**	**0.130**	**0.193**	**136**	**0.303**	**0.416**	**112**
IUS Hanger Supported	S-1	0.144	0.157	0.238	139	0.294	0.404	103
	S-2	0.106	0.114	0.169	134	0.295	0.404	121
	S-3	0.144	0.134	0.198	123	0.319	0.439	126
	S-4	0.123	0.124	0.216	117	0.300	0.412	106
	S-5	0.113	0.120	0.180	143	0.298	0.409	106
	Mean	**0.126**	**0.130**	**0.200**	**131**	**0.301**	**0.414**	**112**
IUT Hanger Supported	S-1	0.154	0.182	0.269	144	0.277	0.386	118
	S-2	0.236	0.242	0.337	135	0.263	0.366	136
	S-3	0.159	0.176	0.234	139	0.287	0.401	103
	S-4	0.188	0.217	0.361	140	0.284	0.396	121
	S-5	0.191	0.176	0.260	134	0.281	0.392	121
	Mean	**0.186**	**0.199**	**0.292**	**138**	**0.278**	**0.388**	**120**
Fixed Supported	S-1	– – – –	– – – –	– – – –	– – – –	0.0796	0.101	106
	S-2	– – – –	– – – –	– – – –	– – – –	0.0789	0.100	128
	S-3	– – – –	– – – –	– – – –	– – – –	0.0905	0.115	118
	S-4	– – – –	– – – –	– – – –	– – – –	0.0736	0.0938	148
	S-5	– – – –	– – – –	– – – –	– – – –	0.0737	0.0939	141
	Mean	– – – –	– – – –	– – – –	– – – –	**0.0793**	**0.101**	**128**

References

American Forest & Paper Association, 1996, Load and Resistance Factor Design (LRFD) Manual for Engineering Wood Construction, AWC, Washington, DC.

American Forest & Paper Association, 1999, "Guideline Wood I-Joists," *Allowable Stress Design (ASD) Manual for Engineered Wood Construction*, AF&PA, Washington, DC.

American Forest & Paper Association, 2003, "Designing for Lateral-Torsional Stability in Wood Members, Technical Report 14," *American Wood Council*, Washington, DC.

American Forest & Paper Association, 2006, "Wood I-joist Awareness Guide", AF&PA Washington, DC.

American Society for Testing and Materials, 2005a, Standard Specification for Evaluation of Structural Composite Lumber Products, ASTM D 5456-03, West Conshohocken, PA.

American Society for Testing and Materials, 2005b, Standard Practice for Evaluating Allowable Properties for Grades of Structural Lumber, ASTM D 2915-03, West Conshohocken, PA.

American Society for Testing and Materials, 2005c, Standard Test Methods of Static Tests of Lumber in Structural Sizes, ASTM D 198-02, West Conshohocken, PA.

Bamberg C.R., 2009, "Lateral Movement of Unbraced Wood Composite I-Joists Exposed to Dynamic Walking Loads," Thesis Submitted to the Faculty of the Virginia Polytechnic Institute and State University, Virginia, U.S. p. 78.

Bažant Z.P., 2000, "2.02 Stability of Elastic, Anelastic, and Disintegrating Structures, and Finite Strain Effects: an Overview," *Comprehensive Structural Integrity*, Vol. 2, pp. 47 – 80.

Bobick T.G., 2004, "Falls through Roof and Floor Openings and Surfaces, Including Skylights: 1992-2000," *Journal of Construction Engineering and Management*, Vol. 130(6), pp. 895 – 907.

Bureau of Labor Statistics, 2011, *National Census of Fatal Occupational Injures in 2010,* United States Department of Labor, Washington, DC.

Burow J.R., Manbeck H.B. and Janowiak J.J., 2006, "Lateral Stability of Composite Wood I-Joists under Concentrated-Load Bending," *Transactions of the ASABE*, Vol. 49(6), pp. 1867 – 1880.

Chen B. and Yura J., 2005, "Structural Bracing," *Handbook of Structural Engineering*, pp. (32) 1–23.

Ebrahimpour A., Hamam A., Sack R.L. and Patten W.N., 1996, "Measuring and Modeling Dynamic Loads Imposed by Moving Crowds," *Journal of Structural Engineering*, Vol. 122(12), pp. 1468 – 1474.

Figueiredo F.P., da Silva J.G.S., de Lima L.R.O., da S. Vellasco P.C.G. and de Andrade S.A.L., 2008, "A Parametric Study of Composite Footbridges under Pedestrian Walking Loads," *Engineering Structures*, Vol. 30, pp. 605 – 615.

Finkenbinder D.E., 2007, "An Experimental Investigation of Structural Composite Lumber Loaded by a Dowel in Perpendicular to Grain Orientation at Yield and Capacity," Thesis Submitted to the Faculty of the Virginia Polytechnic Institute and State University, Virginia, U.S. p. 112.

Gard S.A. and Childress D.S., 2001, "What Determines the Vertical Displacement of the Body During Normal Walking?" American Academy of Orthotists & Prosthetists, Vol. 13(3), pp. 64-67.

Georgia-Pacific Wood Products LLC, 2008, *Wood I Beam™ Joists, Engineered Lumber Residential Guide*, Atlanta, GA., p. 30.

Helwig T.A., Frank K.H. and Yura J.A., 1997, "Lateral-Torsional Buckling of Singly Symmetric I-Beams," *Journal of Structural Engineering*, Vol. 123(9), pp. 1172 – 1179.

Hindman D., Manbeck H.B. and Janowiak J.J., 2005a, "Measurement and prediction of lateral torsional buckling loads of composite wood materials: I-joists sections," *Forest Products Journal*, Vol. 55(10), pp. 43 – 48.

Hindman D., Manbeck H.B. and Janowiak J.J., 2005b, "Torsional Rigidity of Wood Composite I-Joists," *Wood and Fiber Science*, Vol. 37(2), pp. 292 – 303.

Hooley R.F. and Madsen B., 1964, "Lateral Stability of Glued Laminated Beams," *Journal of the Structural Division Proceedings of the American Society of Civil Engineers*, Vol. 90(ST3), pp. 201 – 218.

Huang M.H., Thambiratnam D.P. and Perera N.J., 2007, "Dynamic Performance of Slender Suspension Footbridges under Eccentric Walking Dynamic Loads," *Journal of Sound and Vibration*, Vol. 303, pp. 239 – 254.

Huang X. and Hinze J., 2003, "Analysis of Construction Worker Fall Accidents," *Journal of Construction Engineering and Management*, Vol. 129(3), pp. 262 – 271.

ICC Evaluation Service, Inc., 2008, *Evaluation Report ESR-2552*, p. 13.

ICC Evaluation Service, Inc., 2008, *Evaluation Report ESR-2608*, p. 12.

ICC Evaluation Service, Inc., 2008, *Evaluation Report ESR-2615*, p. 18.

Kirby, P.A. and Nethercot, D.A., 1979, *Design for Structural Stability*, Granada Publishing, Toronto, Ont., p. 162.

Kitipornchai S. and Trahair N.S., 1980, "Buckling Properties of Monosymmetric I-Beams," *Journal of the Structural Division*, Vol. 106(ST5), pp. 941 – 957.

Leichti R.J., Falk R.H., and Laufenberg T.L., 1990, "Prefabricated Wood I-joists: an Industry Overview," *Forest Products Journal*, Vol. 40(3), pp. 15-20.

Leichti R.J., Falk R.H., and Laufenberg T.L., 1990, "Prefabricated Wood Composite I-Beams: A Literature Review," *Wood and Fiber Science*, Vol. 2(1), pp. 62-79.

Lipscomb H.J., Li L. and Dement J.M., 2003, "Falls Among Union Carpenters," *American Journal of Industrial Medicine*, Vol. (44), pp. 148 – 156.

Maljaars J., Stark J.W.B., Steenbergen H.M.G.M. and Abspoel R., 2005, "Lateral-Torsional Buckling Resistance of Coped Beams," *Journal of Constructional Steel Research*, Vol. 61, pp. 1559 – 1575.

Meirovitch L., 2001, *Fundamentals of Vibrations*, McGraw-Hill Companies, Inc., New York, NY, p. 806.

Nakamura S. and Kawasaki T., 2006, "Lateral Vibration of Footbridges by Synchronous Walking," *Journal of Constructional Steel Research*, Vol. 62, pp. 1148 – 1160.

Peck R., Devore J.L. and Olsen C., 2007, *Introduction to Statistics and Data Analysis*, 3rd Edition, Cengage Learning, p. 888.

Pi Y.L. and Trahair N.S., 1992, "Prebuckling Deflections and Lateral Buckling I: Theory," *Journal of Structural Engineering*, Vol. 118(11), pp. 2949 – 2966.

Pi Y.L. and Trahair N.S., 2000, "Distortion and Warping at Beam Supports," *Journal of Structural Engineering*, Vol. 126(11), pp. 1279 – 1287.

Pimentel R.L., Pavic A. and Waldron P., 2001, "Evaluation of Design Requirements for Footbridges Excited by Vertical Forces from Walking," *Canadian Journal Civil Engineering*, Vol. 28, pp. 769 – 777.

Qiao P., Zou G. and Davalos J.F., 2002, "Lateral Buckling of FRP Composite Cantilever Beams," *15th ASCE Engineering Mechanics Conference*, Columbia University, New York, NY.

Roberts T.M., 2002, "Influence of Shear Deformation on Buckling of Pultruded Fiber Reinforced Plastic Profiles," *Journal of Composites for Construction*, Vol. 6(4), pp. 241 – 248.

Singer F.L. and Pytel A., 1980, *Strength of Materials*, Harper & Row Publishers, Inc., New York, p. 560.

Suruda A., Fosbroke D. and Braddee R., 1995, "Fatal Work-Related Falls from Roofs," *Journal of Safety Research*, Vol. 26(1), pp. 1 – 8.

Timko P. 2009, "Finite Element Analysis of Unbraced Structural Wood I-Joists under Construction Loads," Thesis Submitted to the Faculty of the Virginia Polytechnic Institute and State University, Virginia, U.S. p. 57.

Timoshenko S., 1936, *Theory of Elastic Stability*, McGraw-Hill Book Company, Inc., New York and London, p. 518.

United States Department of Agriculture, 1999, *Wood Handbook; Wood as an Engineering Material*, Gen. Tech. Rep. FPL-GTR-113. Madison, WI. U.S., Department of Agriculture, Forest Service, Forest Products Laboratory.

Wang Y.C., El-Khenfas M.A. and Nethercot D.A., 1987, "Lateral-Torsional Buckling of End-Restrained Beams," *Journal of Constructional Steel Research*, Vol. 7, pp. 335 – 362.

Webster T., 2003, "Workplace Falls," *Compensation and Working Conditions*, Washington, DC, pp. 28 – 38.

Wood I-Joist Manufacturers Association, 2005, *Establishing Reaction Capacities for Prefabricated Wood I-Joists*, WIJMA, Madison, WI, p. 11.

Yin S., Corona E. and Ellison M.S., 2004,"Degradation and Buckling of I-Beams under Cyclic Pure Bending," *Journal of Engineering Mechanics*, Vol. 130(7), pp. 809 – 817.

Yu W., 2000, *Cold-Formed Steel Design*, Third Edition, John Wiley & Sons, Inc., United States of America, p. 756.

Zahn J.J., 1984, "Bracing Requirements for Lateral Stability," *Journal of Structural Engineering*, Vol. 110(8), pp. 1786 – 1802.